(2)

Office of Naval Research Technical Final Report

for

Grant N00014-87-J-1218

by

John J. Walsh (813-893-9164)
Department of Marine Science
University of South Florida
140 Seventh Avenue South
St. Petersburg, Florida 33701

With past ONR support from Grant N00014-87-J-1218, we had successfully coupled simple biological models of phytoplankton production (light and nutrient regulation of one size fraction) to time-dependent, 3-dimensional physical models of basin circulation at 25-30 km resolution in the Gulf of Mexico (Walsh et al., 1989). While these coupled models mimicked seasonal cycles of phytoplankton abundance in basin waters, as estimated by changes in chlorophyll stocks, they failed to replicate fluctuations of biological populations within more complex slope and shelf regions.

Accordingly, a more diverse biological model of particle decay within the aphotic zone (3 size classes of phytoplankton, macroaggregates, and zooplankton fecal pellets) was coupled to a static, 2-dimensional model of slope circulation at 0.5 km resolution in the Middle Atlantic Bight (Walsh et al., 1991). By specifying the influx of these particles, both at the shelf-break and from the overlying slope euphotic zone, with variable sinking velocities, the second set of coupled models reproduced seasonal time series of organic carbon caught by moored sediment traps on the slope and rise.

A total of 8 publications were derived from this ONR grant:

Walsh, J.J. (1989) Arctic carbon sinks: present and future. Global Biogeochemical Cycles, 3, 393-411.

Walsh, J.J., D.A. Dieterle, M.B. Meyers, and F.E. Muller-Karger (1989) Nitrogen exchange at the continental margin: a numerical study of the Gulf of Mexico. Progress in Oceanography, 23, 245-301.

Walsh, J.J. (1991) Importance of continental margins in the marine biogeochemical cycling of carbon and nitrogen. Nature, 350, 53-55.

Walsh, J.J., D.A. Dieterle, and J.R. Pribble (1991) Organic debris on the continental margins: a simulation analysis of source and fate. Deep-Sea Research, 38, 805-828.

Muller-Karger, J.J. Walsh, R.H. Evans, and M.B. Meyers. (1991) On the seasonal phytoplankton concentration and sea surface temperature cycles of the Gulf of Mexico as determined by satellites. Journal of Geophysical Research, 96, 12645-12665.

Shuert, P.G. and J.J. Walsh (1992) A time-dependent depth-integrated barotropic physical model of the Bering/Chukchi Seas for use in ecosystem analysis. J. Mar. Syst. 3:141-161.

Walsh, J.J. (1992) Particle export at Cape Hatteras. Continental Shelf Research (in press).

Walsh, J.J., K. L. Carder, and F.E. Muller-Karger (1992) Meridional fluxes of dissolved organic matter in the North Atlantic

Ocean. Journal of Geophysical Research (in press).

Reprints of the 1989-1992 published papers are appended.

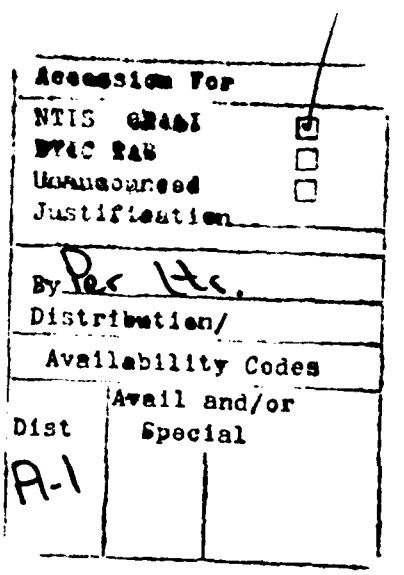

GLOBAL BIOGEOCHEMICAL CYCLES, VOL. 3, NO. 4, PAGES 393-411, DECEMBER 1989

ARCTIC CARBON SINKS: PRESENT AND FUTURE

John J. Walsh

Department of Marine Science, University of South Florida, St. Petersburg

Abstract. Surface air temperatures of the Arctic rose 1.2°-1.5°C from 1880 to 1980, in contrast to a global warming of only 0.4°-0.5°C; since 1980, six of the warmest years in the past century have been observed. Polar enhancement of a temperature rise, induced possibly by anthropogenic release of "greenhouse" gases, CO_2, N_2O, CH_4, and freons, to the atmosphere, is attributed to altered ice/snow albedo at sea level, i.e., melting of sea ice. A 5% decline of sea ice extent in the Arctic and Antarctic from 1979 to 1987 may have resulted in increased light availability within previously ice-covered polar regions. If such a short-term trend were to continue, it might lead to a negative biogeochemical feedback, i.e., enhanced extraction of atmospheric CO_2 during marine photosynthesis. As a consequence of deep vertical mixing in the Antarctic Ocean, however, primary production during the austral summer may have actually declined in response to a reduction in extent of meltwater regions, where stratified water columns allow carbon fixation tenfold that of open water. In contrast, within shallow adjacent seas of the Arctic Ocean, where shelf regions are tenfold larger than those of the Antarctic, the positive global consequences of greenhouse warming at polar latitudes will probably be felt first. Specifically, the Pacific-influenced regions of the Chukchi and East Siberian Seas, where sufficient nutrients and shallow depths prevail, now have annual primary productions of >200 g C m^{-2} yr^{-1}, tenfold that of other high Arctic shelves, and may supply 50% of the carbon respiration demands within the halocline of the deep Canadian and Eurasian basins via brine-mediated runoff. Continued melting of ice in the Arctic could increase by an order of magnitude the present CO_2 sink of $\sim$0.1 x 10^9 t C yr^{-1}.

Paper number 90GB00583.
0886-6236/89/90GB-00583$10.00

INTRODUCTION

The global temperature of surface air increased by 0.4°-0.5°C from 1880 to 1980, while temperatures of Arctic regions ($\sim$64°-90°N) instead rose by as much as 1.2°-1.5°C over this period [Hansen et al., 1983]. After 1980, six of the warmest years in the past century have subsequently been observed (1980, 1981, 1983, 1986, 1987, and 1988), reflecting possible early signs of a "greenhouse" warming of the Earth [Hansen and Lebedeff, 1988]. Initial one-dimensional [Hansen et al., 1981] and then three-dimensional climate models of varying sophistication [Mitchell, 1989] attribute the observed temperature increases to man's accelerated

addition of the greenhouse gases, CO_2, N_2O, CH_4, and freons, to the atmosphere. These climate models simulate the observed polar enhancement of temperature rise by alteration of snow/ice albedos near sea level, since inclusion of realistic Antarctic orography leads to no temperature feedback, i.e., melting of ice, at higher elevations [Manabe and Stouffer, 1980]. Additional parameterization of thermal inversions within the seasonal atmosphere of high latitudes simulates warmer temperatures over winter pack ice [Hansen et al., 1984].

Three times less of the Earth's surface area is now covered with ice sheets than during previous glacial periods, resulting in about a 3% increase of today's ocean volume [Milliman and Emery, 1968]. Melting the rest of the surviving ice sheets would raise sea level by another 70 m, but land-based ice fields have long millennial response times, such that catastrophic deglaciation of the West Antarctic ice sheet is the only probable immediate scenario; over a century, sea level might rise 5-6 m if this austral ice sheet actually melted [Hansen et al., 1981]. A more likely response to a doubling of atmospheric CO_2 and concomitant polar enhancement of >10°C temperature rises by 2035 would be melting of polar pack ice [Hansen et al., 1984]. A subsequent increment of subsurface light within polar seas might then lead to increases of marine primary production and carbon sequestration at high latitudes in response to reduced ice cover [Walsh et al., 1989].

Based on a 15-year satellite survey by the electronically scanning and scanning multifrequency microwave radiometers (ESMR, SMMR) of sea ice cover [Gloersen and Campbell, 1988], the seasonal minima of Arctic sea ice extent in August decreased by ∿5% during 1981-1987, after the initial warm year of 1980. The Okhotsk, Kara, and Barents Seas accounted for most of the total decline of yearly averaged sea ice extent of 23 x 10^3 km^2 yr^{-1} in the Arctic between 1979 and 1986 [Parkinson and Cavalieri, 1989]. As part of a wider global trend since 1972 [Carsey, 1982], the minimum ice extent of the Antarctic ice pack during the austral summer declined by 20% from 1973-1976 to 1979-1987 [Gloersen and Campbell, 1988]. These apparent short-term changes in sea ice extent of polar regions may [Gloersen and Campbell, 1988] or may not [Parkinson and Cavalieri, 1989] be related to a twentieth-century warming trend [Hansen and Lebedeff, 1988].

Since the summer Arctic ice extent is ∿8 x 10^6 km^2, about twice that of the Antarctic minimum, the total amount of increased subsurface light availability within the two polar ecosystems over the last decade may be equivalent, at times of the year when phytoplankton exhibit seasonal bursts of carbon fixation. Incident summer radiation at high latitudes, for example, is greater than at the equator [Holm-Hansen et al., 1977]. If the polar ice packs were to melt, one might expect a similar enhancement of primary production in the Arctic and Antarctic Seas.

Based on a 2-year satellite survey of ocean color (G. Feldman, personal communication, 1989), however, the amount of algal stocks sensed by the coastal zone color scanner (CZCS) during 1978-1980 may be much larger in the Arctic (Plate 1). Extensive regions of >3 μg chlorophyll (chl) L^{-1} were apparently found by the CZCS in the Arctic Mediterranean Seas. Such blooms off Antarctica are restricted to the meltwater regions of the Weddell and Ross Seas [Smith and Nelson, 1985; Smith, 1987; Sullivan et al., 1988].

The gray masks of Plate 1 represent cloud- and ice-covered areas of these polar regions during mainly the respective summer seasons, between November 2, 1978, and May 31, 1980, since CZCS imagery is of dubious quality at solar elevations of <[illegible]° [Barale et al., 1986]. G. Feldman processed the available scenes of the composite images of Plate 1 at Goddard Space Flight Center, using an updated version of the "standard" algorithm [see Gordon et al., 1983; 1988], which may still underestimate higher in situ values of chlorophyll and its degradation products. At Arctic latitudes of the Bering Sea, algal stocks of >1.5 μg chl L^{-1} were previously underestimated by as much as tenfold [Maynard and Clark, 1987], with the original CZCS algorithm [Gordon et al., 1983].

With a third bio-optical algorithm added to the recent calibrations and atmospheric corrections, which does not switch CZCS band ratios at 1.5 μg chl L^{-1} [Gordon et al., 1983], the CZCS imagery only underestimated in situ data in the Bering Sea by a factor of 2 during spring of 1979 and less in 1980 [Müller-Karger et al., 1990]. These recent results imply

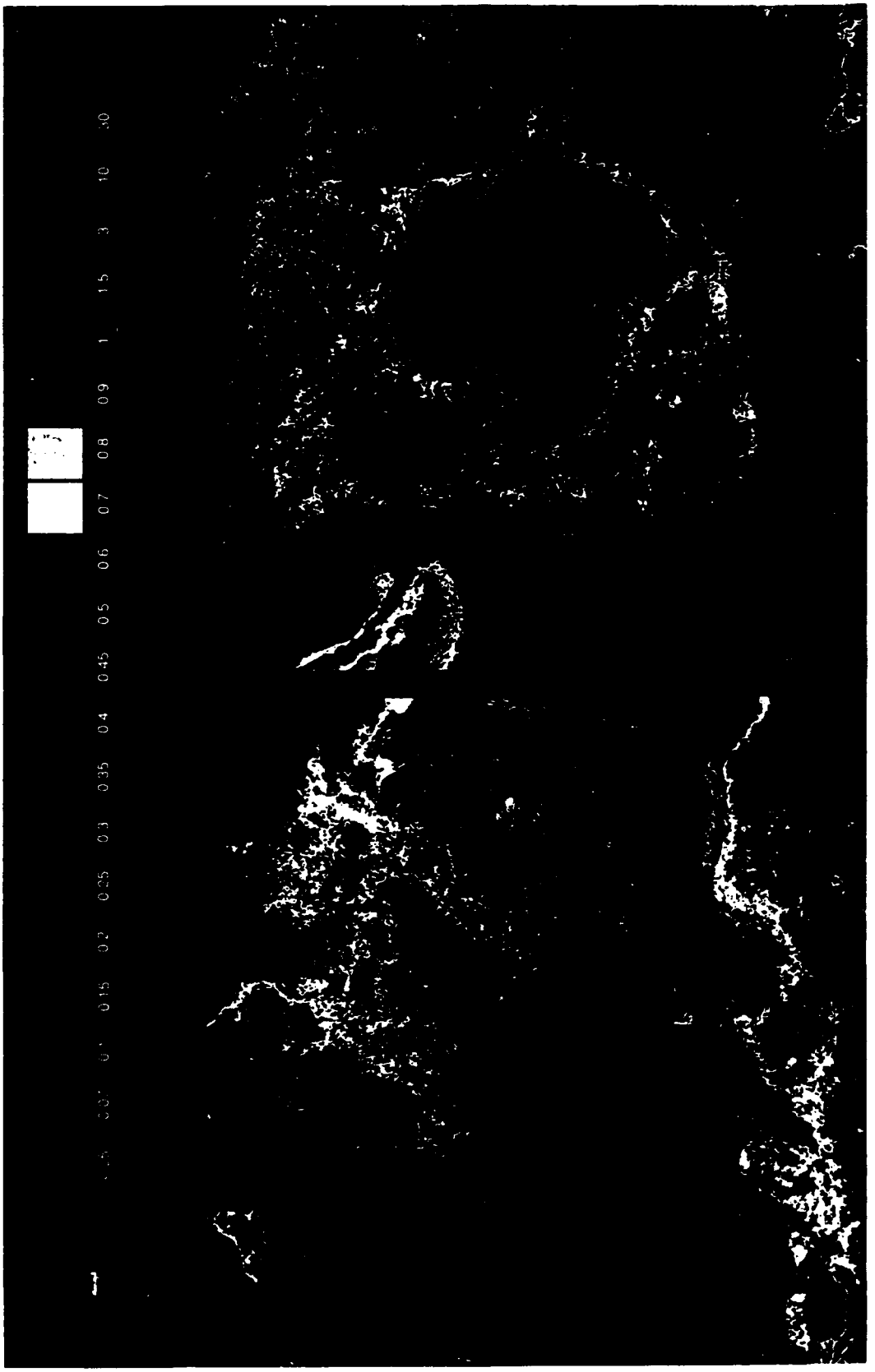

Plate 1. The surface chlorophyll (μg L^{-1}) sensed by the CZCS during November 1978-May 1980 in the Arctic and Antarctic (after G. Feldman, personal communication, 1990).

that extensive chlorophyll values of <1.5 μg chl L^{-1} in the Antarctic may be accurately assessed in Plate 1. If we assume that the relative distributions of color sensed by the CZCS are both accurate at polar latitudes and representative of algal stocks during each summer growing season, what are the present and future implications of phytoplankton photosynthesis for carbon sequestration in the Arctic and Antarctic Seas?

ANTARCTIC RESPONSE

Since ice edge blooms may constitute 67-74% of the annual coastal production of the Weddell and Ross Seas [Smith et al., 1988], in contrast to <10% of the Beaufort and Chukchi Seas [Alexander, 1974; Schell et al., 1982], removal of the freshwater source of stratification may actually lead to a decline of carbon fixation in the Antarctic and an increase in the Arctic. The greater spatial extent of algal blooms (Plate 1) and presumably higher primary production of the Arctic are possibly the result of shallow bottom topography of adjacent continental shelves (Figure 1).

Between 60° and each pole, the Southern Ocean has tenfold less shelf area than the Arctic Ocean [Walsh, 1988]. Within local domains of high light, where freshwater or bottom topography curtail vertical mixing, the shelf regions of the Southern Ocean contain tenfold greater algal stocks than offshore waters [Walsh, 1969; El-Sayed and Turner, 1977; Rakusa-Suszczewski, 1980; El-Sayed and Taguchi, 1981; Fukuchi, 1981; El-Sayed et al., 1983; Fukuchi et al., 1988]. Even under the fast ice of Lutzow-Holm Bay, the integrated chlorophyll biomass is much higher than that of ice-free, deep Antarctic waters [Fukuchi et al., 1985].

Over an austral growing period of at most 120-150 days between November and April [Hart, 1942], average daily productivities in Antarctic coastal waters of 0.1-0.4 g C m^{-2} day^{-1} in the Weddell Sea [El-Sayed and Taguchi, 1981], 0.2-0.9 g C m^{-2} day^{-1} in the Ross Sea [El-Sayed et al., 1983], 0.2 g C m^{-2} day^{-1} in the Scotia Sea [Bodungen et al., 1986], and 0.8-1.1 g C m^{-2} day^{-1} in the Bellingshausen Sea [Bodungen et al., 1986: 1987] yield an annual range of 12-165 g C m^{-2} yr^{-1}. Sediment trap studies at long-term moorings in the Bransfield Strait sector of the Bellingshausen Sea [Wefer et al., 1988] and in the central part of the Weddell Sea [Fischer et al., 1988] suggest growing intervals of just 30-60 days, i.e., annual production of perhaps 3-66 g C m^{-2} yr^{-1}. Similarly, ice edge blooms of phytoplankton within locally stratified meltwaters may only last 1-2 months, depending upon the rate of seasonal ice retreat [Smith et al., 1988].

Despite longer growing periods in the northern regions of the Southern Ocean [Hart, 1942], revised estimates of overall carbon fixation in coastal and open waters suggest a mean of only 16 g C m^{-2} yr^{-1} [Holm-Hansen et al., 1977], since production of offshore waters is 0.02-0.20 g C m^{-2} day^{-1} [Saijo and Kawashima, 1964; El-Sayed and Turner, 1977]. Inclusion of higher mean primary production within marginal ice zones of 0.57-0.96 g C m^{-2} day^{-1} might raise the overall estimate by 60% [Smith et al., 1988], i.e., ~25 g C m^{-2} yr^{-1} for the Southern Ocean, if the ice blooms persist longer than 30 days.

With a paradox of high nutrient content and low primary production [Holm-Hansen, 1985] over the same potential growing period as the Arctic, the low annual carbon fixation of the Southern Ocean is usually attributed to deep mixing in offshore waters [Walsh, 1971; Fogg, 1977; Nemoto and Harrison, 1981; Sakshaug and Holm-Hansen, 1984; Bodungen et al., 1986]. Growth parameters suggest that 50 m may be the depth limit of a surface mixed layer over which Antarctic blooms can develop [Sakshaug and Holm-Hansen, 1984]. In contrast, most of the bottom topography (Figure 2) in the northern Bering Sea and southern Chukchi Sea is <50 m.

Short-term sediment trap studies at the bottom of the euphotic zone in the Bransfield Strait during 1980, 1984, and 1985 [Bodungen et al., 1986; 1987] suggest that 67% of the daily primary production sinks out, i.e., implying a "new" production of the same percentage. Uptake studies of ^{15}N in the Ross, Weddell, and Scotia Seas [Olson, 1980; Holm-Hansen, 1985; Smith et al., 1988] confirm this observation. However, at times, >50% of the daily nitrogen demand of phytoplankton is met by ammonium, implying a significant grazing stress. Nevertheless, grazing of phytoplankton by krill appears to have little control over algal production or abundance in the Southern Ocean [Bodungen, 1986], unlike the role of herbivorous copepods in the Norwegian Sea [Peinert et al., 1987]. Macrozooplankton may consume <5% of the primary production in Antarctic waters [Huntley et al., 1984].

It is possible that microzooplankton

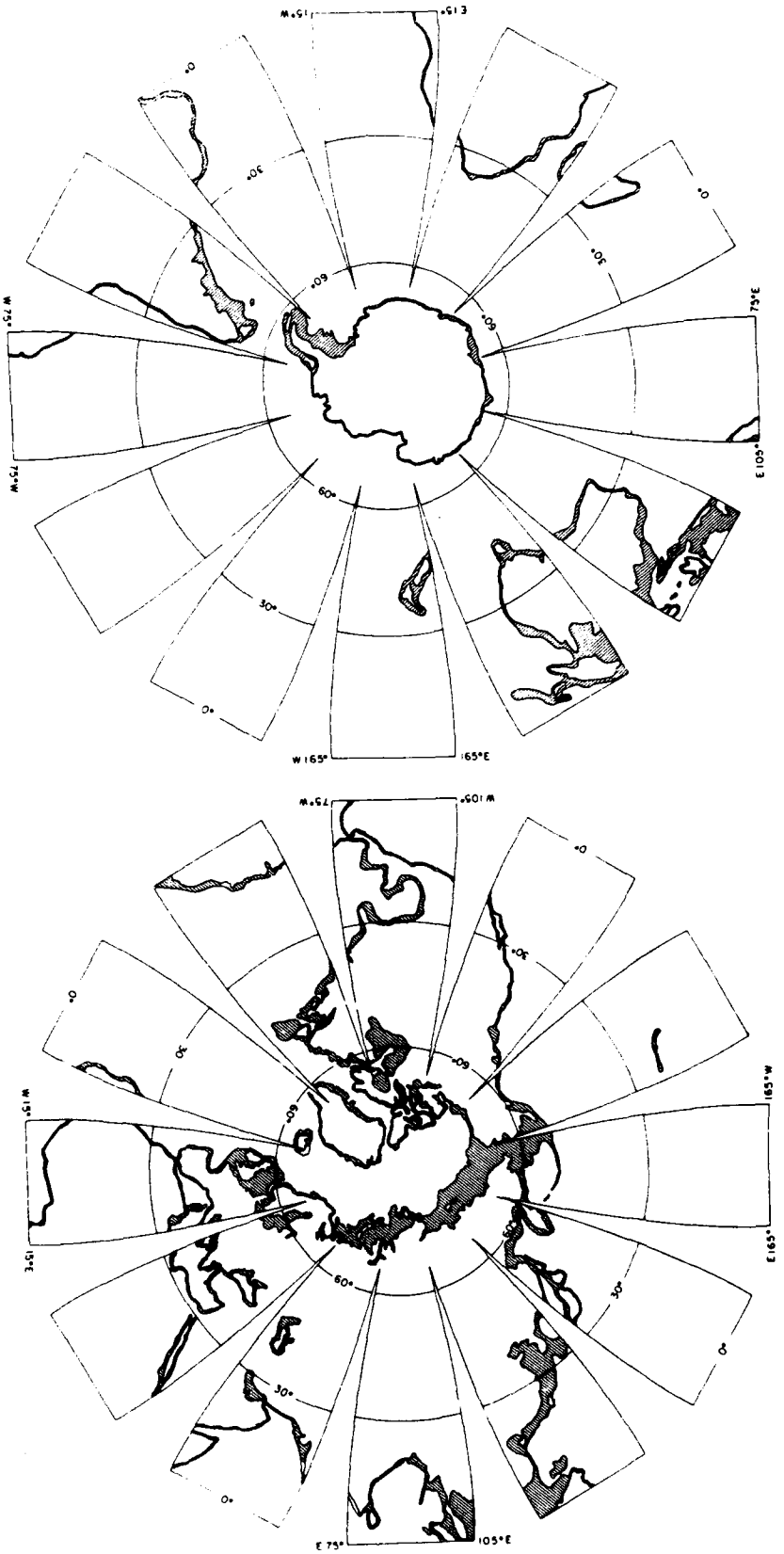

Fig. 1. The distribution of continental shelves (<200 m depth) in the northern and southern hemispheres [after Walsh, 1988].

Fig. 2. The bottom topography (m) of the adjacent shallow seas of the Arctic Ocean [after Walsh et al., 1989].

may crop austral algal blooms [Hewes et al., 1985] in a quasi-steady state, hypothesized originally for the equatorial [Walsh, 1976] and North Pacific [Evans and Parslow, 1985] Oceans, since ∿50% of the phytoplankton biomass in the Antarctic is nanoplankton [Brockel, 1981]. Finally, recent claims of iron limitation in both the North Pacific and Southern Oceans [Martin and Fitzwater, 1988] provide a chemical control mechanism to complement the above physical and biological ones. All three processes may conspire to dampen the response of Antarctic food webs to increased light on seasonal and perhaps decadal time scales. Smith et al. [1988] suggested that the recent reduction in areal extent of meltwater, associated with the Antarctic marginal ice zones, may have resulted in an 11% decrease of annual carbon fixation of the Southern Ocean from 1973 to 1986.

ARCTIC RESPONSE

In contrast, seasonal removal of the ice cover in the Arctic Ocean each year now leads to a total carbon extraction from the atmosphere of ∿18 g C m^{-2} yr^{-1}, which is equivalent to the Antarctic mean [Holm-Hansen et al., 1977] despite the twofold greater extent of pack ice in the northern ecosystem. Within Pacific-influenced regions of the Arctic Ocean, where sufficient nutrients and shallow water columns prevail (Figure 2) throughout the northern growing period of 120-150 days between June and October, the annual production is tenfold (Figure 4). Here the future global biogeochemical impacts of reduced snow/ice albedo may first be felt. The most likely regions are the East Siberian and Chukchi Seas of the Arctic, rather than the Beaufort, Laptev, Kara, Barents, Lincoln, Norwegian, Iceland, Labrador, and Greenland Seas, or those of the Antarctic.

At latitudes of the ice-covered southeastern Bering Sea, the pCO_2 of shelf surface waters in March during the Processes and Resources of the Bering Sea Shelf (PROBES) program was 339 µatm, similar to the overlying atmosphere, but it was reduced to <150 µatm by the end of the spring bloom in June [Codispoti et al., 1986]. Within other waters of the Norwegian-Greenland-Labrador Seas, summer values of 160 µatm are also found, compared to atmospheric values of ∿340 µatm within the winter surface mixed layer of the North Atlantic Ocean [Takahashi et al., 1986]. In contrast, the open waters of the North Pacific Ocean appear to be a net source of CO_2 to the atmosphere [Takahashi et al., 1986], where the seasonal amplitude of primary production is weak [Stephens, 1968]. Similar weak seasonal trends of dissolved CO_2 are found in the nutrient-rich, but presumably light-limited waters south of the Antarctic Convergence, where summer pCO_2 values can be only 35% less than those of the atmosphere [Takahashi et al., 1986].

The annual primary production of the deep basin of the Bering Sea [Taniguchi, 1969; Saino et al., 1979] might be ∿50 g C m^{-2} yr^{-1} over a 150-day growing period, i.e., similar to 85 g C m^{-2} yr^{-1} over 365 days at Station P in the North Pacific [Stephens, 1968]. A combination of ontogenetic migrators [Frost et al., 1983] and microzooplankton [Welschmeyer and Lorenzen, 1985] may consume most of the primary production at Station P and in the deep Bering Sea, but zooplankton consume [Dagg et al., 1982] only 22-42% of the annual carbon fixation on the shallow southeastern Bering Sea shelf [Walsh and McRoy, 1986]. The annual primary production of the southeastern Bering Sea may be only ∿165 g C m^{-2} yr^{-1}, however, because of nutrient depletion at the end of spring [Walsh and McRoy, 1986].

As one proceeds farther north to the Siberian side of the Chukchi Sea, which is continuously supplied with cold, saline and nutrient-rich Anadyr Water of Pacific origin (Figure 3), the annual primary production over 120-150 days is instead 325-360 g C m^{-2} yr^{-1} [Sambrotto et al., 1984; Walsh et al., 1989]. Within nutrient-poor Alaska Coastal Water of riverine and southeastern Bering Sea origin, the annual primary production is instead ∿60 g C m^{-2} yr^{-1} along the Alaskan side of the Chukchi Sea [Walsh et al., 1989].

At the same latitudes in deeper waters of the Iceland, Norwegian, Greenland, and Barents Seas, where destratification and light limitation prevail [Slagstad, 1985], yearly carbon fixation is apparently 40-80 g C m^{-2} yr^{-1} as well [Corlett, 1958; Sokolova and Solov'yeva, 1971; Thordardottir, 1973; Vedernikov and Solov'yeva, 1972; Heimdal, 1983; Smith et al., 1987; Loeng, 1989]. Interannual [Stefansson, 1985] and spatial [Smith et al., 1987] variations of carbon fixation range tenfold within offshore waters as a result of changes in stratification and timing of algal blooms [Skjoldal et al., 1987]. In contrast, little interannual variation of spring bloom onset was observed on the southeastern Bering shelf during the same period [Walsh and McRoy, 1986], while the spring bloom occurred before stratification in nearshore waters of the Barents Sea, where a similar annual production of 150 g C m^{-2} yr^{-1} prevails [Eilertsen et al., 1989].

Daily primary production of >15 g C m^{-2} day^{-1} to <0.5 g C m^{-2} day^{-1} has been measured during July-October in the southern Chukchi Sea, with a temporospatial mean over both Anadyr and Alaska Coastal Waters of 2.4 g C m^{-2} day^{-1} [Walsh et al., 1989]. At such high rates of >15 g C m^{-2} day^{-1} of carbon fixation, neither herbivory nor Fe limitation controls primary production, but instead reduction of light by self-shading of intense algal blooms (>1000 mg chl m^{-2}) limits uptake of CO_2. Expatriots of the southeastern Bering Sea calanoid zooplank-

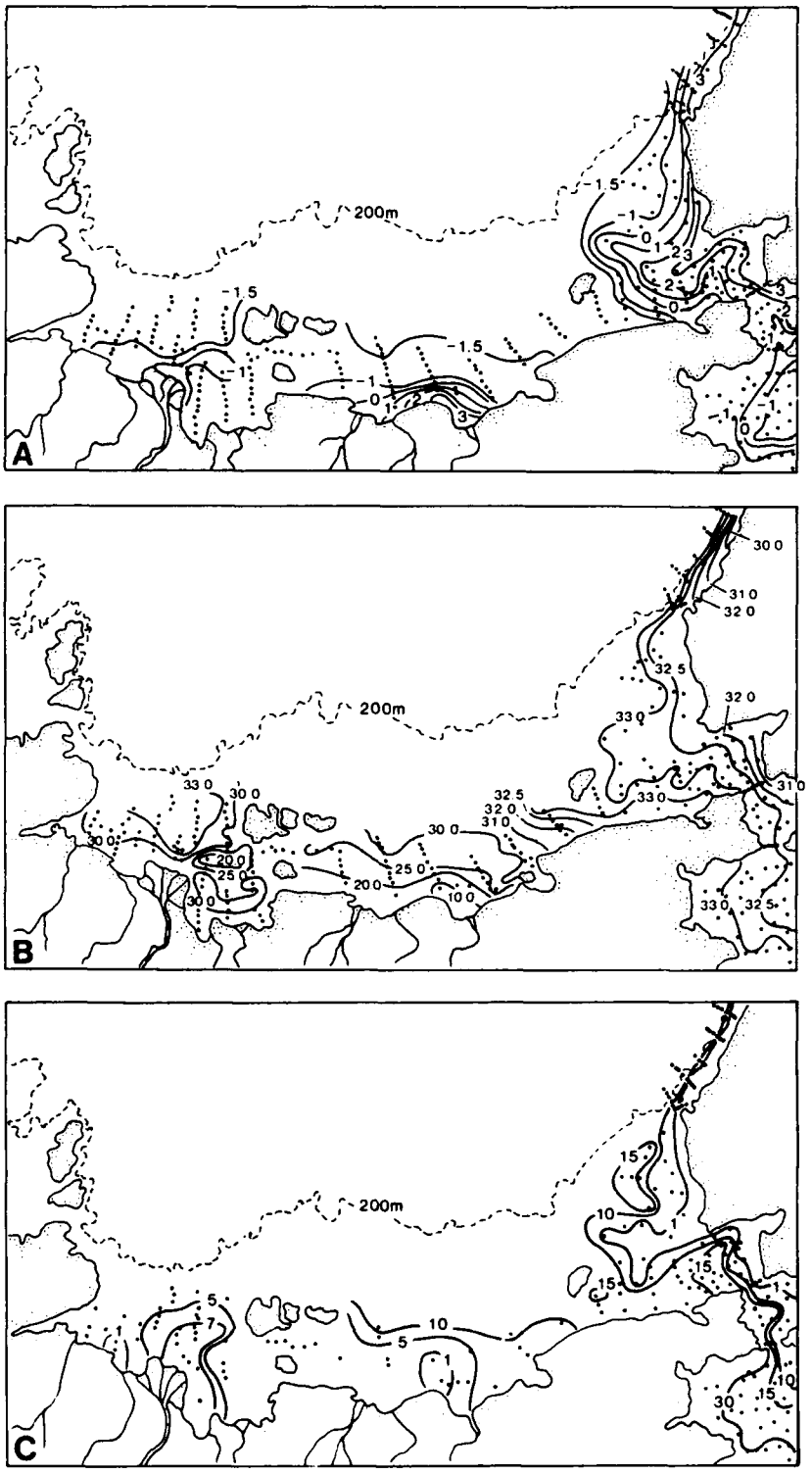

Fig. 3. The composite near-bottom distributions of (a) temperature (°C), (b) salinity (practical salinity units), and (c) nitrate (μg atom L^{-1}) in the Bering, Chukchi, Beaufort, East Siberian, and Laptev Seas during August 1963, 1968, 1969, 1988 and October 1986 [after Codispoti and Richards, 1968; Kinney et al., 1970a; Aagaard et al., 1988; Walsh et al., 1989].

ton community may graze 15% of the primary production within Anadyr Water of the Chukchi Sea, while microzooplankton perhaps remove 8% [Walsh et al., 1989].

Simulation models, which mimic the daily rate of photosynthesis, suggest that 60% of the nitrate introduced by the Bering Slope Current through Anadyr and Shpanberg Straits (Figure 3) is still available for uptake within the northern Chukchi, East Siberian, and Beaufort Seas [Walsh et al., 1989]. As a result of bottom remineralization of particulate matter, the simulated f ratio (new nitrate/total nitrogen production) is 0.6 within the northern Bering Sea and 0.4 in the southern Chukchi Sea, with signals of the recycled nitrogen (>2.5 μg atom NH_4 L^{-1}) measured as far east as the Beaufort Sea [Aagaard et al., 1988]. Neither source of nitrogen leads to large amounts of carbon fixation in the Beaufort Sea, however, with an annual primary production of only 20-40 g C m^{-2} yr^{-1} [Schell et al., 1982; Horner, 1984], as a result of heavy ice cover. Within the deep Arctic basins under the permanent ice pack, the primary production is perhaps even smaller, <1 g C m^{-2} yr^{-1} [Apollonio, 1959; English, 1961].

The primary production of the East Siberian Sea is unknown, although >150% supersaturation of dissolved oxygen has been measured at a depth of ∿10 m in August 1963 southeast of Wrangel Island, compared to 100% at 165°E, near the mouth of the Kolyma River, and 90% at 130°E off the mouth of the Lena River [Codispoti and Richards, 1971]. The same supersaturated O_2 conditions in the Chukchi Sea, for example, have been attributed to intense photosynthesis [Musina and Balysheva, 1960]. During July-August 1968 and 1969 in the Chukchi Sea, >11 mL O_2 L^{-1} was found over the upper 20 m of Anadyr Water near Wrangel Island, compared to <7 mL O_2 L^{-1} observed within unproductive Alaska Coastal Water near Cape Lisburne [Kinney et al., 1970a]. Similarly, only ∿8 mL O_2 L^{-1} was found in Polar Surface Water north of Spitsbergen during July-August 1987 in the Barents Sea [Anderson et al., 1989], where annual oxygen evolution of deeper waters [Loeng, 1989] is 16-25% of that within Anadyr Water.

High primary production, similar to that in the southern Chukchi Sea, presumably led to these east-west gradients of both oxygen evolution and nitrate depletion (Figure 3c) in the East Siberian Sea. The longitudinal gradient of nitrate within bottom water of the inner East Siberian shelf during August-September 1963 [Codispoti and Richards, 1968] in fact declined by an order of magnitude, from as much as 15 μg atom NO_3 L^{-1} south of Wrangel Island at 180°W, to <1 μg atom NO_3 L^{-1} off the Kolyma River at 165°E (Figure 3c). The nitrate/phosphate ratio of the East Siberian Sea is also consistent with a Pacific origin of the bottom water, i.e., Anadyr Water. The phosphate tracer of Pacific water (>2.5 μg atom PO_4 L^{-1}) declines to 0.5-1.0 μg atom PO_4 L^{-1} within bottom waters of the Laptev Sea, presumably reflecting dilution by upwelled Atlantic water [Aagaard et al., 1985] at the shelf break to the west of the New Siberian Islands.

Finally, within surficial sediments of the outer East Siberian shelf, the organic carbon content declines tenfold, from 1-2% dry weight (dw) north of Wrangel Island to 0.2-0.5% dw near the shelf break at 165°E [Romankevich, 1977]. Similarly, another longitudinal gradient of organic carbon in shelf sediments extends eastward, from as much as 1.5% dw off Point Barrow to as little as 0.2% dw within Prudhoe Bay in the Beaufort Sea [Naidu and Hood, 1972]. The boundary of the East Siberian and Laptev Seas at the New Siberian Islands (Figure 2) may thus delineate the maximum westward extent of the Pacific loading of nutrients and organic matter to the Arctic Ocean, while the Beaufort Undercurrent may transfer Pacific nutrients to the western Beaufort Sea.

PRESENT CARBON LOADING

The primary productions of the Laptev and Kara Seas are also unknown, but are probably similar to those of 12-27 g C m^{-2} yr^{-1} within the Canadian Archipelago [Harrison et al., 1982] and the Lincoln Sea [Apollonio, 1980] at the same distances from Bering Strait. The metabolic demands of subsurface water in the Arctic basins provide some constraints on the amount of present carbon fixation within all of these Arctic shelf seas. Recent studies of the nutrients [Jones and Anderson, 1986], radionuclides [Moore and Smith, 1986], and freons [Wallace et al., 1987] in the Arctic Ocean under the CESAR (Canadian Expedition to Study the Alpha Ridge) ice camp, north of Ellesmere Island, have been used to estimate vertical and lateral exchange processes within the deep (>2000 m) Canadian basin (Figure 2).

Advection-diffusion models and the observed distribution of oxygen suggest apparent oxygen utilization (AOU) rates in this basin of an equivalent 4.8-12.7 g C m^{-2} yr^{-1} within the halocline at depths of 55-155 m [Wallace et al., 1987]. Over the whole water column of the CESAR study site, the depth-integrated AOUs indicate a total particulate carbon consumption, or CO_2 evolution, of 5.8-20.6 g C m^{-2} yr^{-1}. In steady state, such AOUs imply "new" production rates of at least the same amount within the euphotic zone of the overlying water if no burial of particulate carbon occurs in the sediments.

Yet the total of new and recycled primary production under the ice pack of the Canadian and Eurasian basins, in terms of carbon fixation, is <1 g C m^{-2} yr^{-1}, with high algal biomass ($\sim$1 μg chl L^{-1}) encountered only during absence of snow cover [English, 1961]. Over the slopes and basins of the Arctic Ocean (5.6 x 10^{12} m^2), the total AOU suggests a carbon input of at least 3.2-11.5 x 10^{13} g C yr^{-1} [Wallace et al., 1987], with at most 2.8 x 10^{12} g C yr^{-1} derived from the new primary production of the overlying water column. A separate analysis of the ice camp data on calcium carbonate dissolution suggests a similar demand of 11.0 x 10^{13} g C yr^{-1} within offshore waters [Anderson et al., 1990], without consideration of burial of organic matter.

The origin of the 100-m-thick halocline of the Arctic basins is thought to be the lateral input of cold, high-salinity water from adjacent shelf regions of open leads and broken ice [Aagaard et al., 1981; Melling and Lewis, 1982; Aagaard et al., 1985]. This annual cascading process might also entrain particulate residues of new production from the seasonally ice-free Arctic shelves. Lateral export of organic matter from the Barents Sea, for example, as a result of winter cooling, has been invoked as the source of a sedimentation pulse within long-term traps moored west of Bear Island in the Norwegian Sea [Honjo et al., 1988].

Partitioned over just the high Arctic shelves (3.4 x 10^{12} m^2), the AOU demand within the interior of the Arctic Ocean implies an import of $\sim$33 g C m^{-2} yr^{-1} from the shallow Chukchi, East Siberian, Laptev, Kara, Barents, Lincoln, and Beaufort Seas to the Eurasian and Canadian basins (Figure 2). This import is perhaps twice that estimated for in situ new production, however, i.e., $\sim$15 g C m^{-2} yr^{-1}, on all Arctic shelves, assuming an f ratio of 0.5 [Harrison et al., 1982; Kristiansen and Lund, 1989; Smith and Kattner, 1989; Walsh et al., 1989] and a total mean production of only 27 g C m^{-2} yr^{-1} [Subba Rao and Platt, 1984].

Consideration of the organic matter fixed south of the Arctic Ocean and carried north through Bering Strait, together with a concomitant Pacific import of new dissolved nitrogen for production on the Chukchi and East Siberian shelves, however, can balance such carbon demands of these polar basins. In this analysis, it is assumed that the net inputs of dissolved and particulate organic carbon to the Arctic Ocean within the West Spitsbergen Current in Fram Strait are negligible, since the transports and particle fluxes here and within the outflowing East Greenland Current are similar [Walsh et al., 1989; Wefer, 1989]. Terrestrial sources and burial of organic matter in shelf and slope sediments are also neglected, such that the export of carbon from Arctic shelves may be underestimated.

It is further assumed that the Pacific nutrient loading is consumed over just about 20% of the broad (up to 900 km wide) Chukchi and East Siberian shelves, extending from 150°W to 150°E over a total area of $\sim$1 x 10^6 km^2. Since the present ice cover is extensive over most of these seas (Figure 4), i.e., close pack ice (70-90% coverage) was found at the northern end of each 1963 Northwind section in the East Siberian and Laptev Seas (Figure 3), significant nutrient uptake within a much smaller region of only 2 x 10^5 km^2 is not an unreasonable assumption. Based on satellite images (Plate 1) [Maynard and Clark, 1987; Müller-Karger et al., 1988], simulation models, previous ^{14}C, oxygen, and nutrient (Figure 3) measurements, and present ice conditions, the spatial pattern of annual carbon fixation in the Bering, Chukchi, Beaufort, and East Siberian Seas is estimated in Figure 4, with respect to the mean location of pack ice during August (dash-dot curve).

Assuming (1) an annual carbon fixation of only 200 g C m^{-2} yr^{-1} over a growing period of 150 days, (2) a C/N ratio of 6, and (3) an f ratio of 0.5, the resultant daily nitrogen uptake in the form of nitrate is 0.11 g NO_3-N m^{-2} day^{-1}. An August 1988 section of nutrients across Bering Strait [Walsh et al., 1989] yielded a mean nitrate concentration of 8 μg atom NO_3 L^{-1}, which together with a transport

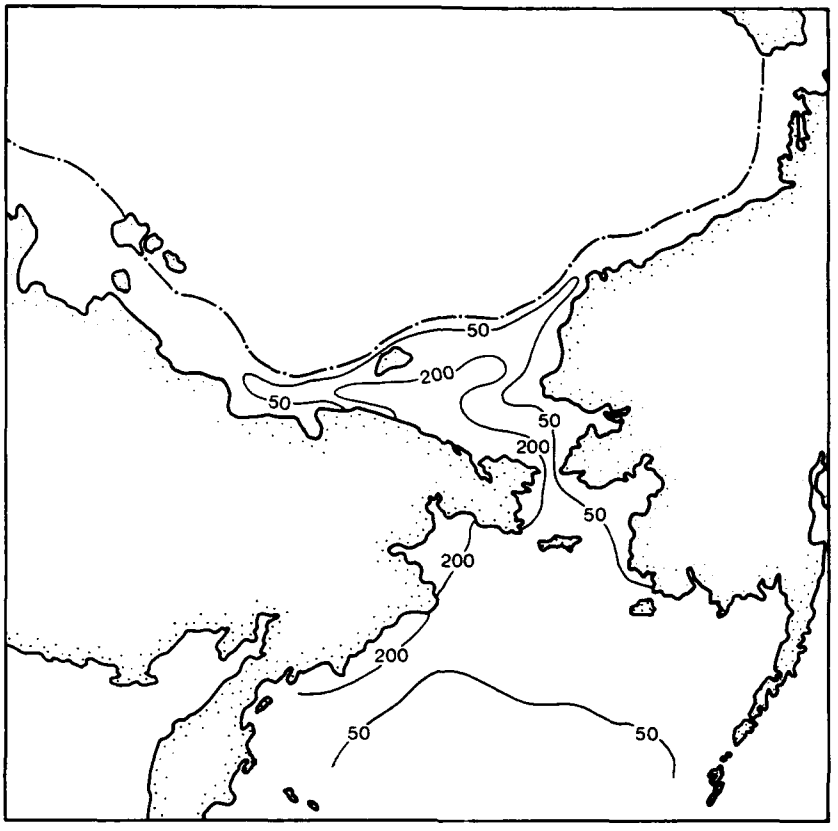

Fig. 4. The estimated annual primary production (g C m^{-2} yr^{-1}) of the Bering, Chukchi, Beaufort, and East Siberian Seas in relation to the distribution of August pack ice [after Taniguchi, 1969; Saino et al., 1979; Schell et al., 1982; Walsh and McRoy, 1986; Müller-Karger et al., 1988; Walsh et al., 1989].

through Bering Strait of ∿1 Sv [Coachman et al., 1975] suggests a summer northward Pacific flux of 112 kg NO_3-N s^{-1} to the Chukchi Sea. In a steady state, where the above phytoplankton uptake just balances the physical supply, this daily nitrate-nitrogen input of 1 x 10^{10} g NO_3-N day^{-1} would be stripped within ∿1 x 10^5 km^2 of the Chukchi Sea, i.e., roughly the area enclosed by the 200 g C m^{-2} yr^{-1} isopleth of Figure 4.

The unutilized nitrate concentrations of 10-15 µg atom NO_3 L^{-1} at the southern edge of the pack ice during August (Figure 3c) presumably reflect winter supplies left behind by the small spring blooms of ice algae; the residence time of water on the Chukchi/East Siberian shelves may be ∿6-12 months (L. Codispoti, L. Coachman, and C. Pease, personal communications, 1990). These algae constitute perhaps 10% of the annual production in the Chukchi [Alexander, 1974] and Beaufort [Schell et al., 1982] Seas. Since longitudinal gradients of nitrate do extend out from Wrangel Island (from 15 to 1 µg atom NO_3 L^{-1}), reflecting additional summer usage of winter stocks, we assume that nutrient supply during the rest of the year (215 days) could at least support an annual production of 125 g C m^{-2} yr^{-1} over another region of ∿1 x 10^5 km^2 extent (Figure 4).

With respect to the AOU demands of the Arctic basin, all of the Pacific import of nitrogen, i.e., nitrate, recycled, or particulate, can be considered a "new" source, since it is exogenous. A mean total production of 1.1 g C m^{-2} day^{-1} for 150 days over 2 x 10^{11} m^2 (Figure 4) thus yields a possible export of 3.3 x 10^{13} g C yr^{-1} of Pacific origin from the East Siberian/Chukchi Seas. This estimate of carbon fixation and export may be low,

because the measured mean primary production during June-September 1985-1987 was 2.4 g C m^{-2} day^{-1} over the southern Chukchi/northern Bering Seas [Walsh et al., 1989].

Additional new production, from upwelled nutrients of interior Arctic Ocean origin at the shelf break of the other high Arctic shelves, might amount to 15 g C m^{-2} yr^{-1}, i.e., ∿10% of the Pacific source (Figure 4) on a unit area basis. The same Atlantic phosphate content of 0.5-1.0 μg atom PO_4 L^{-1}, measured in August-September 1963 at the shelf break of the Laptev Sea [Codispoti and Richards, 1968], was found in October 1986 at the shelf break of the Beaufort Sea [Aagaard et al., 1988], where the initial April nitrate stocks of 2.5 g NO_3-N m^{-2} at the 50-m isobath are stripped by the end of September. Conversion of just this new nitrogen stock to carbon, with a C/N ratio of 6, would yield a new production of 15 g C m^{-2} yr^{-1}, which is available for export to the Canadian Basin. With an f ratio of 0.5, this is similar to a total mean production of 27 g C m^{-2} yr^{-1} estimated for all Arctic shelves [Subba Rao and Platt, 1984], in which the Chukchi Sea was assumed to have an annual production of only 18-28 g C m^{-2} yr^{-1}. Over the much larger area of the rest of the East Siberian, Chukchi, and other high Arctic shelves (3.2×10^{12} m^2), however, this small new production of 15 g C m^{-2} yr^{-1} sums to 4.8×10^{13} g C yr^{-1}.

Import of the combined new shelf production of ∿8.1×10^{13} g C yr^{-1} of both Pacific and Arctic origins could satisfy most of the AOU demands of the Arctic basins. Over the area of the high Arctic basins and shelves (9×10^{12} m^2), an average total carbon fixation of ∿18 g C m^{-2} yr^{-1} is implied, similar to that of the whole Southern Ocean. Inclusion of the annual primary production of 60-80 g C m^{-2} yr^{-1} within low Arctic basins and shelves would lead to a higher overall mean.

An independent assessment of high Arctic metabolic demands has been made, based on mixing models, observed carbonate distribution in the Arctic basins, and the amount of carbon input required for dissolution of calcium carbonate within the halocline. It suggests separate annual inputs of 4.2×10^{13} g C yr^{-1} as terrestrial matter from all Arctic rivers, and of 8.6×10^{13} g C yr^{-1} from new production on these Arctic shelves [Anderson et al., 1990]. We have not considered import of terrestrial organic matter through Bering Strait from the Yukon River, but it is undoubtedly significant. The sediment C/N ratios and their isotopic signatures of $\delta^{13}C$ and $\delta^{15}N$ indicate that >33% of the detrital organic matter on the Alaskan side of the southern Chukchi Sea is of terrestrial origin, in contrast to >67% off the mouth of the Yukon River [Walsh et al., 1989].

Local pockets of high organic carbon are also found within nearshore sediments off the Mackenzie River (Figure 2) in the Beaufort Sea [Pelletier, 1975], off the Lena River in the Laptev Sea [Romankevich, 1977], off the Yenisey and Ob Rivers in the Kara Sea [Kuznetsov, 1976], and off the Pechora River in the Barents Sea [Gorshkova, 1975]. How far across these Arctic shelves the terrestrial organic matter traverses, before burial or conversion to CO_2 occurs, is unknown. Siberian logs, found as driftwood off Greenland, provided evidence of the Transpolar Drift over a century ago [Nansen, 1897]; smaller particles presumably sink closer to the coast.

Within 10 km of the coast, this carbon source from river runoff is equivalent to that of marine primary production between Point Barrow and the Canadian border in the Beaufort Sea [Schell et al., 1982]. Microbial degradation of peat occurs within these coastal waters, but ^{14}C and ^{13}C isotope studies indicate little transfer of terrestrial carbon to the rest of the marine food web [Schell et al., 1982], suggesting that export or dissolution is the major fate of allocthonous carbon. Terrigenous particulate inputs have been detected as deep as 2823 m within the basin of the Greenland Sea [Wefer, 1989].

FUTURE CO_2 SINKS

The role of the Arctic Ocean and adjacent shelves in global carbon budgets has thus far been neglected. Changes in deep-water formation and/or a decline of marine primary production at high latitudes, perhaps as a result of increased light limitation on geological time scales, are suspected to have been important components of atmospheric CO_2 rise, and thus global control of warming trends, begun 15,000 years ago [Knox and McElroy, 1984]. This and other simple four- or five-box models, of a high-latitude ecosystem

embedded within the global oceans [Sarmiento and Toggweiler, 1984; Siegenthaler and Wenk, 1984], ignore the Arctic Ocean, however, assuming that ice cover curtails gaseous exchange between atmosphere and ocean.

More recent three-dimensional models of Pleistocene glacial episodes indicate that atmospheric CO_2 concentrations >250 ppm led to melting of extensive ice sheets covering Scandinavia, the Barents, Kara, and East Siberian Seas, and parts of the Arctic Ocean 14,000 years ago [Lindstrom and MacAyeal, 1989]. Circumvention of the ice cover constraint on CO_2 exchange now mainly occurs by primary production within open waters of the Bering/Chukchi/East Siberian Seas, at the margins of the permanent ice pack in the Arctic Ocean (Plate 1). These Pacific-influenced regions are tenfold more productive than the other Arctic shelves and may produce 50% of the AOU within the ice-covered Arctic Ocean.

Satisfaction of present AOU demands leads to a brine-mediated, shelf input of $\sim 0.1 \times 10^9$ t C yr^{-1} to the halocline of the Eurasian and Canadian Basins, for eventual southward export as mainly dissolved CO_2 via Fram Strait. Partial pressures of carbon dioxide within ice-covered waters of the outflowing East Greenland Current are as much as 20% greater than atmospheric values [Anderson et al., 1990]. In contrast, long-term sediment trap moorings [Wefer, 1989] on the eastern side of Fram Strait, where inflow of the warm West Spitsbergen Current occurs, show the same particulate carbon flux of 0.4 g C m^{-2} yr^{-1} as that caught at similar depth underneath the ice-covered East Greenland Current, extending some 2500 km south of Fram Strait [Foldvik et al., 1988].

In terms of an anthropogenic release of CO_2 of $\sim 5.0 \times 10^9$ t C yr^{-1} to the atmosphere, such a present Arctic sink of CO_2 is small. If continued greenhouse warmings were to melt most of the Arctic ice pack, however, such that a new production of $\sim$150 g C m^{-2} yr^{-1} ensued (Figure 4), a future organic carbon sink of at least 1.4×10^9 t C yr^{-1} might occur here. Eventual sequestration of carbon could then take place within deepwater formation in either the Atlantic or Arctic Oceans [Smethie et al., 1988]. A 2°C increase of air temperature within a coupled ocean-ice model of the Arctic, for example, leads to a seasonal disappearance of sea ice during late summer, in contrast to slight loss of winter ice [Semtner, 1987], i.e., preserving a mechanism for deepwater formation while allowing maximum photosynthesis.

Heating the surface, or altering the salinity budget, would both lead to less ice cover of the Arctic Ocean. With destratification by removal of the vertical salinity gradient of the Arctic Ocean, there is ample heat, of Atlantic origin, stored within the upper 1000 m of the Eurasian and Canadian Basins to melt over 20 m of ice [Aagaard and Coachman, 1975]. If the salinity lid of the smaller Eurasian Basin (Figure 2) were to be destroyed by southward diversion of the Ob and Yenisey Rivers, for example, the halocline within $\sim 1 \times 10^6$ km^2 of this region would be swept south through Fram Strait after 2-3 years [Aagaard and Coachman, 1975].

Release of heat from subsurface Atlantic water, imported by the West Spitsbergen Current, and free convection would then lead to an ice-free area of the deep Arctic Ocean, which is similar to the extent of the productive Chukchi/East Siberian shelves. This sequence would perhaps increase the production of the Eurasian Basin from <1 to >100 g C m^{-2} yr^{-1}, i.e., similar to parts of the Bering and Barents Seas. Continued melting and increased vertical mixing would produce additional CO_2 sinks in the Canadian Basin and adjacent shelves, perhaps summing to a tenfold greater amount than our present estimate.

Surface nitrate concentrations under or near the ice pack in the Canadian Basin [Kinney et al., 1970b], the Beaufort Sea [Aagaard et al., 1988], the Chukchi Sea [Kinney et al., 1970a], and the East Siberian Sea [Codispoti and Richards, 1968] are now ≤ 1 µg atom NO_3 L^{-1}. On the western side of Bering Sea, however, where turbulent mixing prevails [Walsh et al., 1989], surface nitrate stocks of $\sim$15 µg atom NO_3 L^{-1} are instead found under or near the ice pack [Horner and Wencker, 1980]. A reduction in ice cover, river discharge, and vertical stratification would lead to greater fluxes of nutrients, as a result of increased mixing from near-bottom water (Figure 4) to the euphotic zone. In turn, a greater nutrient flux would stimulate primary production over at least the shallow Arctic shelf water column, in contrast to diminished algal fixation in deeper Antarctic waters.

An alternative scenario of continued

inputs of 3300 km^3 yr^{-1} of freshwater discharge [Milliman and Meade, 1983], but removal of just the present ice cover, suggests perhaps a smaller eutrophication of the Arctic. After distillation of fresh water by formation of sea ice, about 900 km^3 yr^{-1} is now added to the Arctic Ocean each year, i.e., ~25% of river runoff [Aagaard and Carmack, 1989]. Following the initial meltwater transient, an ice-free Arctic might thus exhibit a 25% mean reduction in vertical stratification, with greater vertical mixing in the Eurasian Basin, since it now has approximately fourfold less freshwater content than the Canadian Basin [Aagaard and Carmack, 1989]. Greater vertical diffusive fluxes, i.e., more than a 25% increment, might occur on Arctic shelves as well, since they also contain approximately twofold less fresh water than in the Canadian Basin, but they are the direct recipients of river runoff.

Global scenarios of the consequences of a hundredfold increase of primary production at high latitudes lead to declines in both atmospheric CO_2, from 266 ppm to 202 ppm, and "surface" nitrate, from 17.4 μg atom NO_3 L^{-1} to 0.18 μg atom NO_3 L^{-1}, without changes in deepwater formation [Knox and McElroy, 1984]. Such a range of primary production (10.0-0.1 g C m^{-2} day^{-1}) and surface nitrate content [Walsh et al., 1989] now occurs within the inflows of Anadyr and Alaska Coastal Waters on the western and eastern sides of Bering Strait. Removal of additional ice cover would presumably result in similar levels of high production within at least the north Chukchi/East Siberian Seas.

Continued study of this ecosystem is thus clearly warranted to understand both local, i.e., possible Soviet diversion of the Pechora, Ob, and Yenisey Rivers and American fertilization of the drainage basin of the Yukon River, and global amelioration of climatic change within sub-Arctic and Arctic marine ecosystems. The biological consequences of increased light availability in response to a polar enhancement of greenhouse warming will most likely be first observed in the Arctic rather than in the Antarctic.

Acknowledgments. This analysis was supported with funds from NSF grant DPP-B605659, NASA grant NAGW-678, DOE grant DE-FG05-85ER60285, and ONR grant N00014-87-J-1218.

REFERENCES

Aagaard, K., and E. C. Carmack, The role of sea ice and other fresh water in the Arctic circulation, J. Geophys. Res., 94, 14485-14498, 1989.

Aagaard, K., and L. K. Coachman, Toward an ice-free Arctic Ocean, Eos Trans. AGU, 56, 484-486, 1975.

Aagaard, K., L. K. Coachman, and E. C. Carmack, On the halocline of the Arctic Ocean, Deep Sea Res., 28, 529-545, 1981.

Aagaard, K., J. H. Swift, and E. C. Carmack, Thermohaline circulation in the Arctic Mediterranean Seas, J. Geophys. Res., 90, 4833-4846, 1985.

Aagaard, K., C. H. Pease, and S. A. Salo, Beaufort Sea mesoscale circulation study - Preliminary results, NOAA Tech. Memo., ERL PMEL-82, 1-171, 1988.

Alexander, V., Primary productivity regimes of the nearshore Beaufort Sea, with reference to potential roles of ice biota, in The Coast and Shelf of the Beaufort Sea, edited by J. C. Reed and J. E. Sater, pp. 609-632, Arctic Institute of North America, Arlington, Va., 1974.

Anderson, L. G., E. P. Jones, K. P. Koltermann, P. Schlosser, J. H. Swift, and D. W. Wallace, The first oceanographic section across the Nansen Basin in the Arctic Ocean, Deep Sea Res., 36, 475-482, 1989.

Anderson, L. G., D. Dyrssen, and E. P. Jones, An assessment of the transport of atmospheric CO_2 into the Arctic Ocean, J. Geophys. Res., 95, 1703-1711, 1990.

Apollonio, S., Hydrobiological measurements on IGY drifting station Bravo, Natl. Acad. Sci. I.G.Y. Bull. 27, 16-19, 1959.

Apollonio, S., Primary production in Dumbell Bay in the Arctic Ocean, Mar. Biol., 61, 41-51, 1980.

Barale, V., C. R. McClain, and P. Malanotte-Rizzoli, Space and time variability of the surface color field in the northern Adriatic Sea, J. Geophys. Res., 91, 12957-12974, 1986.

Bodungen, B., Phytoplankton growth and krill grazing during spring in the Bransfield Strait, Antarctica--Implications from sediment trap collections, Polar Biol., 6, 153-160, 1986.

Bodungen, B., V. Smetacek, M. M. Tilzer, and B. Zeitzschel, Primary production

and sedimentation during spring in the Antarctic Peninsula region, Deep Sea Res., 33, 177-194, 1986.

Bodungen, B., G. Fischer, E. M. Nothig, and G. Wefer, Sedimentation of krill faeces during spring development of phytoplankton in Bransfield Strait, Antarctica, in Particle Flux in the Ocean, edited by E. T. Degens et al., Mitt. Geol. Palaeontol. Inst. Univ. Hamburg, 62, 149-164, 1987.

Brockel, K., The importance of nanno-plankton within the Antarctic ecosystem, Kiel. Meeresforsch. Sonderh., 5, 61-67, 1981.

Carsey, F. D., Arctic sea ice distribution at the end of summer 1973-1976 from satellite microwave data, J. Geophys. Res., 87, 5809-5835, 1982.

Coachman, L. K., K. Aagaard, and R. B. Tripp, Bering Strait: The Regional Oceanography, pp. 1-172, University of Washington Press, Seattle, 1975.

Codispoti, L. A., and F. A. Richards, Micronutrient distributions in the East Siberian and Laptev Seas during summer 1963, Arctic, 21, 67-83, 1968.

Codispoti, L. A., and F. A. Richards, Oxygen supersaturation in the Chukchi and East Siberian Seas, Deep Sea Res., 18, 341-351, 1971.

Codispoti, L. A., G. E. Friedrich, and D. W. Hood, Variability in the inorganic carbon system over the southeastern Bering Sea shelf during spring 1980 and spring-summer 1981, Cont. Shelf Res., 5, 133-160, 1986.

Corlett, C., Measurements of primary production in the western Barents Sea, Rapp. P. V. Reun. Cons. Perm. Int. Explor. Mer, 144, 76-78, 1958.

Dagg, M. J., J. Vidal, T. E. Whitledge, R. L. Iverson, and J. J. Goering, The feeding, respiration, and excretion of zooplankton in the Bering Sea during a spring bloom, Deep Sea Res., 29, 45-64, 1982.

Eilertsen, H. C., J. P. Taasen, and J. M. Weslawski, Phytoplankton studies in the fjords of West Spitzbergen: Physical environment and production in spring and summer, J. Plankton Res., 11, 1245-1260, 1989.

El-Sayed, S. Z., and S. Taguchi, Primary production and standing crop of phyto-plankton along the ice-edge in the Weddell Sea, Deep Sea Res., 28, 1017-1032, 1981.

El-Sayed, S. Z., and J. T. Turner, Productivity of the Antarctic and tropical/subtropical regions: A comparative study, in Polar Oceans, edited by M. J. Dunbar, pp. 463-503, Arctic Institute of North America, Calgary, Alberta, 1977.

El-Sayed, S. Z., D. C. Biggs, and O. Holm-Hansen, Phytoplankton standing crop, primary productivity, and near-surface nitrogenous nutrient fields in the Ross Sea, Antarctica, Deep Sea Res., 30, 871-886, 1983.

English, T. S., Some biological oceanographic observations in the central north Polar Sea, Drift Station Alpha, 1957-58, Res. Pap. 13, pp. 1-80, Arctic Inst. of North Am., Arlington, Virginia, 1961.

Evans, G. T., and J. S. Parslow, A model of annual plankton cycles, Biol. Oceanogr., 3, 327-347, 1985.

Fischer, G., D. Futterer, R. Gersonde, S. Honjo, D. Ostermann, and G. Wefer, Seasonal variability of particle flux in the Weddell Sea and its relation to ice cover, Nature, 335, 426-428, 1988.

Fogg, G. E., Aquatic primary production in the Antarctic, Philos. Trans. R. Soc. London, Ser. B, 279, 27-38, 1977.

Foldvik, A., K. Aagaard, and T. Torreson, On the velocity field of the East Greenland Current, Deep Sea Res., 35, 1335-1354, 1988.

Frost, B. W., M. R. Landry, and R. P. Hassett, Feeding behavior of large calanoid copepods Neocalanus cristatus and N. plumchrus from the subarctic Pacific Ocean, Deep Sea Res., 30, 1-14, 1983.

Fukuchi, M., Phytoplankton chlorophyll stocks in the Antarctic Ocean, J. Oceanogr. Soc. Jpn., 36, 73-84, 1981.

Fukuchi, M., A. Tanimura, and H. Ohtsuka, Marine biological and oceanographical investigations in Lützow-Holm Bay, Antarctica, in Antarctic Nutrient Cycles and Food Webs, edited by W. R. Siegfried et al., pp. 52-59, Springer-Verlag, New York, 1985.

Fukuchi, M., H. Hattori, H. Sasaki, and T. Hoshiai, A phytoplankton bloom and associated processes observed with a long-term moored system in Antarctic waters, Mar. Ecol. Prog. Ser., 45, 279-288, 1988.

Gloersen, P., and W. J. Campbell, Variations in the Arctic, Antarctic, and global sea ice covers during 1978-1987 as observed with the Nimbus 7 scanning multichannel microwave radiometer, J. Geophys. Res., 93, 10666-10674, 1988.

Gordon, H. R., D. K. Clark, J. W. Brown, O. B. Brown, R. H. Evans, and W. W. Broenkow, Phytoplankton pigment concentrations in the Middle Atlantic Bight: Comparison of ship determinations and CZCS estimates, Appl. Opt., 22, 20-35, 1983.

Gordon, H. R., O. B. Brown, R. H. Evans, J. W. Brown, R. C. Smith, K. S. Baker, and D. K. Clark, A semianalytical radiance model of ocean color, J. Geophys. Res., 93, 10909-10924, 1988.

Gorshkova, T. I., Organic Matter in the Present Shelf Sediments of the Northern USSR Seas (in Russian), pp. 1-45, Nauka, Moscow, 1975.

Hansen, J., and S. Lebedeff, Global surface air temperatures: Update through 1987, Geophys. Res. Lett., 15, 323-326, 1988.

Hansen, J., D. Johnson, A. Lacis, S. Lebedeff, P. Lee, D. Rind, and G. Russell, Climate impact of increasing atmospheric carbon dioxide, Science, 213, 957-966, 1981.

Hansen, J., D. Johnson, A. Lacis, S. Lebedeff, P. Lee, D. Rind, and G. Russell, Climatic effects of atmospheric carbon dioxide, Science, 220, 874-875, 1983.

Hansen, J., A. Lacis, D. Rind, G. Russell, P. Stone, I. Fung, R. Ruedy, and J. Lerner, Climate sensitivity: Analysis of feedback mechanisms, in Climate Process and Climate Sensitivity, Geophys. Monogr. Ser., vol. 29, edited by J. E. Hansen and T. Takahashi, pp. 130-163, AGU, Washington, D. C., 1984.

Harrison, W. G., T. Platt, and B. Irwin, Primary production and nutrient assimilation by natural phytoplankton of the eastern Canadian Arctic, Can. J. Fish. Aquat. Sci., 39, 335-345, 1982.

Hart, T. J., Phytoplankton periodicity in Antarctic surface waters, Discovery Rep., 21, 261-356, 1942.

Heimdal, B. R., Phytoplankton and nutrients in the waters northwest of Spitsbergen in the autumn of 1979, J. Plankton Res., 5, 901-918, 1983.

Hewes, C. D., O. Holm-Hansen, and E. Sakshaug, Alternate carbon pathways at lower trophic levels in the Antarctic food web, in Antarctic Nutrient Cycles and Food Webs, edited by W. R. Siegfried et al., pp. 271-276, Springer-Verlag, New York, 1985.

Holm-Hansen, O., Nutrient cycles in Antarctic marine ecosystems, in Antarctic Nutrient Cycles and Food Webs, edited by W. R. Siegfried et al., pp. 6-10, Springer-Verlag, New York, 1985.

Holm-Hansen, O., S. Z. El-Sayed, G. A. Franceschini, and R. L. Cuhel, Primary production and the factors controlling phytoplankton growth in the Southern Ocean, in Adaptation Within the Antarctic Ecosystem, edited by G. A. Llano, pp. 11-50, Gulf, Houston, Tex., 1977.

Honjo, S., S. J. Manganini, and G. Wefer, Annual particle flux and a winter outburst of sedimentation in the northern Norwegian Sea, Deep Sea Res., 35, 1223-1234, 1988.

Horner, R. A., Phytoplankton abundance, chlorophyll a, and primary productivity in the western Beaufort Sea, in The Alaskan Beaufort Sea, edited by P. W. Barnes et al., pp. 295-310, Academic, San Diego, Calif., 1984.

Horner, R. A., and D. L. Wencker, Plankton studies in the Bering Sea: CGC Polar Sea, 17 April - 6 May 1978, Annu. Rep. 03-78-B01-6, pp. 275-349, Alaska Outer Continental Shelf Environmental Assessment Program, Bureau of Land Management, Anchorage, Alaska, 1980.

Huntley, M., V. Marin, P. Sykes, and R. Rohan, Antarctic Salps II, Trophodynamics in the Scotia Sea and Bransfield Strait, 1983-84, Eos Trans. AGU, 65, 922-923, 1984.

Jones, E. P., and L. G. Anderson, On the origin of the chemical properties of the Arctic Ocean halocline, J. Geophys. Res., 91, 10759-10767, 1986.

Kinney, D. J., D. C. Burrell, M. E. Arhelger, T. C. Loder, and D. W. Hood, Chukchi Sea data report: USCGC Northwind, July-August 1968; USCGC Staten Island, July-August 1969, Rep. Univ. Alaska Inst. Mar. Sci., R-70-23, 1-305, 1970a.

Kinney, D. J., M. E. Arhelger, and D. C. Burrell, Chemical characteristics of water masses in the Amerasian Basin of the Arctic Ocean, J. Geophys. Res., 75, 4097-4104, 1970b.

Knox, F., and M. B. McElroy, Changes in atmospheric CO_2: Influence of the marine biota at high latitude, J. Geophys. Res., 89, 4629-4637, 1984.

Kristiansen, S., and B. A. Lund, Nitrogen cycling in the Barents Sea, I, Uptake of nitrogen in the water column, Deep Sea Res., 36, 255-268, 1989.

Kuznetsov, A. P., Bottom Fauna of the USSR

Fringing Seas (in Russian), pp. 1-10, Shirshov Institute of Oceanography, Moscow, 1976.

Lindstrom, R. D., and D. R. MacAyeal, Scandinavian, Siberian, and Arctic Ocean glaciation: Effect of Holocene atmospheric CO_2 variations, Science, 245, 628-631, 1989.

Loeng, H., Ecological features of the Barents Sea, in Proceedings of the Sixth Conference of the Comite Arctique International 13-15 May 1985, edited by L. Rey and V. Alexander, pp. 327-364, E. J. Brill, Leiden, Netherlands, 1989.

Manabe, S., and R. J. Stouffer, Sensitivity of a global climate model to an increase in the CO_2 concentration in the atmosphere, J. Geophys. Res., 85, 5529-5554, 1980.

Martin, J. M., and S. E. Fitzwater, Iron deficiency limits phytoplankton growth in the north-east Pacific subarctic, Nature, 321, 341-343, 1988.

Maynard, N. G., and D. K. Clark, Satellite color observations of spring blooming in Bering Sea shelf waters during the ice edge retreat in 1980, J. Geophys. Res., 92, 7127-7139, 1987.

Melling, H., and E. L. Lewis, Shelf drainage flows in the Beaufort Sea and their effect on the Arctic Ocean pycnocline, Deep Sea Res., 29, 967-985, 1982.

Milliman, J. D., and K. O. Emery, Sea levels during the past 35,000 years, Science, 162, 1121-1123, 1968.

Milliman, J. D., and R. H. Meade, World-wide delivery of river sediment to the oceans, J. Geol., 91, 1-21, 1983.

Mitchell, J. F., The "greenhouse" effect and climate change, Rev. Geophys., 27, 115-139, 1989.

Moore, R. M., and J. N. Smith, Disequilibria between ^{226}Ra, ^{210}Pb, and ^{210}Po in the Arctic Ocean and the implications for chemical modification of the Pacific water inflow, Earth Planet. Sci. Lett., 77, 285-292, 1986.

Müller-Karger, F. E., C. R. McClain, and G. C. Ray, Phytoplankton productivity, in Bering, Chukchi and Beaufort Seas Coastal and Ocean Zones Strategic Assessment, Data Atlas, map 2.2, NOAA, National Ocean Service, Strategic Assessment Branch, Washington, D. C., 1988.

Müller-Karger, F. E., C. R. McClain, R. N. Sambrotto, and G. C. Ray, A comparison of ship and CZCS-mapped distribution of phytoplankton in the southeastern Bering Sea, J. Geophys. Res., in press, 1990.

Musina, A. A., and E. V. Balysheva, Hydrochemical features of Arctic Seas (in Russian), Khim. Morya, 10, 61-68, 1960.

Naidu, A. S., and D. W. Hood, Chemical composition of bottom sediments of the Beaufort Sea, Arctic Ocean, Rep. 135, Inst. of Mar. Sci., Fairbanks, Alaska, 1972.

Nansen, F., Farthest North, p. 22, Harper, New York, 1897.

Nemoto, T., and G. Harrison, High latitude ecosystems, in Analysis of Marine Ecosystems, edited by A. R. Longhurst, pp. 95-126, Academic, San Diego, Calif., 1981.

Olson, R. J., Nitrate and ammonium uptake in Antarctic waters, Limnol. Oceanogr., 25, 1064-1074, 1980.

Parkinson, C. L., and D. J. Cavalieri, Arctic sea ice 1973-1987: Seasonal, regional, and interannual variability, J. Geophys. Res., 94, 14499-14523, 1989.

Peinert, R., V. Bathmann, B. Bodungen, and T. Noji, The impact of grazing on spring phytoplankton growth and sedimentation in the Norwegian Current, in Particle Flux in the Ocean, edited by E. T. Degens et al., Mitt. Geol. Palaeontol. Inst. Univ. Hamburg, 62, 149-164, 1987.

Pelletier, B. R., Sediment dispersal in the southern Beaufort Sea, Tech. Rep. 25a, Geol. Surv. of Can., Ottawa, Canada, 1975.

Rakusa-Suszczewski, S., The role of nearshore research in gaining an understanding of the functioning of Antarctic ecosystems, Pol. Arch. Hydrobiol., 27, 229-233, 1980.

Romankevich, E. A., Geochemistry of Organic Matter in the Ocean (in Russian), pp. 1-256, Nauka, Moscow, 1977.

Saijo, Y., and T. Kawashima, Primary production in the Antarctic Ocean, J. Oceanogr. Soc. Jpn., 19, 190-196, 1964.

Saino, T., K. Miyata, and A. Hattori, Primary productivity in the Bering and Chukchi Seas and in the northern North Pacific in 1978 summer, Bull. Plankton Soc. Jpn., 26, 96-103, 1979.

Sakshaug, E., and O. Holm-Hansen, Factors governing pelagic production in polar oceans, in Marine Phytoplankton and Productivity, edited by L. Bolis and R. Gilles, pp. 1-17, Springer-Verlag, New York, 1984.

Sambrotto, R. N., J. J. Goering, and C. P. McRoy, Large yearly production of phytoplankton in the western Bering Strait, Science, 225, 1147-1150, 1984.

Sarmiento, J. L., and J. R. Toggweiler, A new model for the role of the oceans in determining atmospheric pCO_2, Nature, 308, 621-624, 1984.

Schell, D. M., P. J. Ziemann, D. M. Parrish, K. H. Dunton, and E. J. Brown, Food web and nutrient dynamics in nearshore Alaskan Beaufort Sea waters, NOAA contract 3-S-022-56 RU 537, pp. 1-185, Inst. of Water Res., Univ. Alaska, Fairbanks, 1982.

Semtner, A. J., A numerical study of sea ice and ocean circulation in the Arctic, J. Phys. Oceanogr., 17, 1077-1099, 1987.

Siegenthaler, U., and T. Wenk, Rapid atmospheric CO_2 variations and oceanic circulation, Nature, 308, 624-626, 1984.

Skjoldal, H. R., A. Hassel, F. Rey, and H. Loeng, Spring phytoplankton development and zooplankton reproduction in the central Barents Sea in the period 1979-1984, in Dynamics of Commercial Fish Stocks in the Barents Sea, edited by H. Loeng, pp. 59-89, Institute of Marine Research, Bergen, Norway, 1987.

Slagstad, D., A model of phytoplankton in the marginal sea-ice zone of the Barents Sea, in Marine Biology of Polar Regions and Effects of Stress on Marine Organisms, edited by J. S. Gray and M. E. Christiansen, pp. 35-48, John Wiley, New York, 1985.

Smethie, W. M., D. W. Chipman, J. H. Swift, and K. P. Koltermann, Chlorofluoromethanes in the Arctic mediterranean seas: Evidence for formation of bottom water in the Eurasian Basin and deep-water exchange through Fram Strait, Deep Sea Res., 35, 347-369, 1988.

Smith, W. O., and D. M. Nelson, Phytoplankton blooms provided by a receding ice edge in the Ross Sea: Spatial coherence with the density fields, Science, 227, 163-166, 1985.

Smith, W. O., M. E. Baumann, D. L. Wilson, and L. Aletsee, Phytoplankton biomass and productivity in the marginal ice zone of the Fram Strait during summer 1984, J. Geophys. Res., 92, 6777-6786, 1987.

Smith, W. O., Phytoplankton dynamics in marginal ice zones, Oceanogr. Mar. Biol., 25, 11-38, 1987.

Smith, W. O., and G. Kattner, Inorganic nitrogen uptake by phytoplankton in the marginal ice zone of the Fram Strait, Rapp. P. V. Reun. Cons. Int. Explor. Mer, 188, 90-97, 1989.

Smith, W. O., N. K. Keene, and J. C. Comiso, Interannual variability in estimated primary productivity of the Antarctic marginal ice zone, in Antarctic Ocean and Resources Variability, edited by D. Sahrhage, pp. 131-139, Springer-Verlag, New York, 1988.

Sokolova, S. A., and A. A. Solov'yeva, Primary production in Dal'nezelenetskaya Bay (Murman Coast) in 1967, Oceanology, Engl. Transl., 11, 386-395, 1971.

Stefansson, V., Oceanographic variations in recent decades and their impact on the fertility of the Iceland Sea, in North Atlantic Deep Water Formation, edited by T. Bennett et al., NASA Conf. Publ., 2367, 19-22, 1985.

Stephens, K., Data Record. Primary production data from the northeast Pacific Ocean, January 1966 to December 1967, Rep. Sci. Fish. Res. Board. Can., 957, 1968.

Subba Rao, D. V., and T. Platt, Primary production of Arctic waters, Polar Biol., 3, 191-201, 1984.

Sullivan, C. W., C. R. McClain, J. C. Comiso, and W. O. Smith, Phytoplankton standing crops within an Antarctic ice edge assessed by satellite remote sensing, J. Geophys. Res., 93, 12487-12498, 1988.

Takahashi, T., J. Goddard, S. Sutherland, D. W. Chipman, and C. C. Breeze, Seasonal and geographic variability of carbon dioxide sink/source in the oceanic areas: Observations in the North Pacific and Equatorial Pacific Ocean, 1984-86 and global summary, Tech. Rep. MRETTA 19X-89675C, pp. 1-52, Dep. of Energy, Oak Ridge, Tenn., 1986.

Taniguchi, A., Regional variations of surface primary production in the Bering Sea in summer and the vertical stability of water affecting the production, Bull. Fac. Fish Hokkaido Univ., 20, 169-179, 1969.

Thordardottir, T., Successive measurements of primary production and composition of phytoplankton at two stations west of Iceland, Nor. J. Bot., 20, 257-270, 1973

Vedernikov, V. I., and A. A. Solov'yeva, Primary production and chlorophyll in the coastal waters of the Barents Sea, Oceanology, Engl. Transl., 12, 559-565, 1972.

Wallace, D. W., R. M. Moore, and E. P. Jones, Ventilation of the Arctic

Ocean cold halocline: Rates of diapycnal and isopycnal transport, oxygen utilization, and primary production inferred using chlorofluoromethane distribution, Deep Sea Res., 34, 1957-1980, 1987.

Walsh, J. J., Vertical distribution of Antarctic phytoplankton, II, A comparison of phytoplankton standing crops in the Southern Ocean with that of the Florida Straits, Limnol. Oceanogr., 14, 86-94, 1969.

Walsh, J. J., Relative importance of habitat variables in predicting the distribution of phytoplankton at the ecotone of the Antarctic upwelling ecosystem, Ecol. Monogr., 41, 291-309, 1971.

Walsh, J. J., Herbivory as a factor in patterns of nutrient utilization in the sea, Limnol. Oceanogr., 21, 1-13, 1976.

Walsh, J. J., On the Nature of Continental Shelves, pp. 1-520, Academic, San Diego, Calif., 1988.

Walsh, J. J., and C. P. McRoy, Ecosystem analysis in the southeastern Bering Sea, Cont. Shelf Res., 5, 259-288, 1986.

Walsh, J. J., C. P. McRoy, L. K. Coachman, J. J. Goering, J. J. Nihoul, T. E. Whitledge, T. H. Blackburn, P. L. Parker, C. D. Wirick, P. G. Shuert, J. M. Grebmeier, A. M. Springer, R. D. Tripp, D. Hansell, S. Djenidi, E. Deleersnijder, K. Henriksen, B. A. Lund, P. Andersen, F. E. Müller-Karger, and K. Dean, Carbon and nitrogen cycling within the Bering/Chukchi Seas: Source regions for organic matter effecting AOU demands of the Arctic Ocean, Prog. Oceanogr., 22, 279-361, 1989.

Wefer, G., Particle flux in the ocean: Effects of episodic production, in Productivity of the Ocean: Past and Present, edited by W. H. Berger et al., pp. 139-154, John Wiley, New York, 1989.

Wefer, G., G. Fischer, D. Futterer, and R. Gersonde, Seasonal particle flux in the Bransfield Strait (Antarctica), Deep Sea Res., 35, 891-898, 1988.

Welschmeyer, N. A., and C. J. Lorenzen, Chlorophyll budgets: Zooplankton grazing and phytoplankton growth in a temperate fjord and the central Pacific gyres, Limnol. Oceanogr., 30, 1-21, 1985.

J. J. Walsh, Department of Marine Science, University of South Florida, 140 Seventh Avenue South, St. Petersburg, FL 33701.

(Received September 1, 1989;
revised March 1, 1990;
accepted March 5, 1990.)

Prog. Oceanog. Vol. 23, pp. 245- 301, 1989.
Printed in Great Britain.

0079 - 6611/89 $0.00 + .50

Nitrogen exchange at the continental margin: A numerical study of the Gulf of Mexico

JOHN J. WALSH, DWIGHT A. DIETERLE, MARK B. MEYERS
and FRANK E. MÜLLER-KARGER

Department of Marine Science, University of South Florida, 140 Seventh Avenue South, St. Petersburg, Florida 33701, U. S. A.

Abstract— A two-layered baroclinic circulation model and a 21-layered biochemical model are used to explore the consequences of Loop Current-induced upwelling and terrestrial eutrophication on "new" production within the Gulf of Mexico. During a quasi-annual penetration and eddy-shedding cycle of the Loop Current, the simulated seasonal changes of incident radiation, wind stress, and surface mixed layer depth induce an annual cycle of algal biomass that corresponds to *in situ* and satellite time series of chlorophyll. The simulated nitrate fields match those of shipboard surveys, while fallout of particulate matter approximates that caught in sediment traps and accumulating in bottom sediments. Assuming an f ratio of 0.06-0.12, the total primary production of the Gulf of Mexico might be 105-210g C $m^{-2}y^{-1}$ in the absence of anthropogenic nutrient loadings, i.e. 2-3 fold that of oligotrophic regions not impacted by western boundary currents. Less than 25% of the nitrogen effluent of the Mississippi River may be stored in bottom sediments, with most of this input dispersed in dissolved form beneath the pycnocline, after remineralization of particulate detritus within several production cycles derived from riverine loading. At a sinking rate of 3m d^{-1}, however, sufficient phytodetritus survives oxidation in the water column to balance estimates of bottom metabolism and burial at the margins.

CONTENTS

1. INTRODUCTION

The major nitrogen sources for the Gulf of Mexico are advection of nitrate in through Yucatan Strait, nitrogen fixation by cyanobacteria, and river discharge of sewage and fertilizers. Similarly, the significant nitrogen sinks for the Gulf of Mexico are presumably advection of water out

through Florida Strait, denitrification by other bacteria, and burial of organic matter. Rainfall, dry deposition, and exchange of nitrous oxide are considered to be small sources and sinks of nitrogen, compared to the above processes. To explore the consequences of altered fluxes of nitrogen across the oceanic, atmospheric, and terrestrial boundaries of the Gulf of Mexico (Fig.1), we combined a 2-layered model of water motion with a 21-layered model of nutrient cycling in the basin.

Such coupled models require specification of boundary conditions of flow, dissolved nitrogen, and particulate matter; but synoptic nitrate, current, and plankton data from both the Yucatan and Florida Straits are scarce. During January 1952, two sections were taken across these Straits by the R/V *Alaska* (Fig.2) within 5-6 days of each other. To construct consistent depth profiles of nitrate distribution from the NODC files on this cruise, we deleted 20 apparently spurious observations from the available 136 measurements of NO_3 at these 11 stations (Fig.3). The questionable data indicated a local decline of NO_3 with depth, before encountering the subsurface maximum of 30-40μg-at $NO_3 \ell^{-1}$ at depths of 500-1000m (Fig.3), i.e. just below the oxygen minimum layer and within the salinity minimum of Antarctic Intermediate Water.

The edited 1952 data set displays the same vertical structure of NO_3 within Yucatan Strait (Fig.3a) as subsequently observed 20-25 years later during October 1972 (BERBERIAN and STARR, 1978) and July 1977 (FURNAS and SMAYDA, 1987). A more recent nutrient data set, taken across

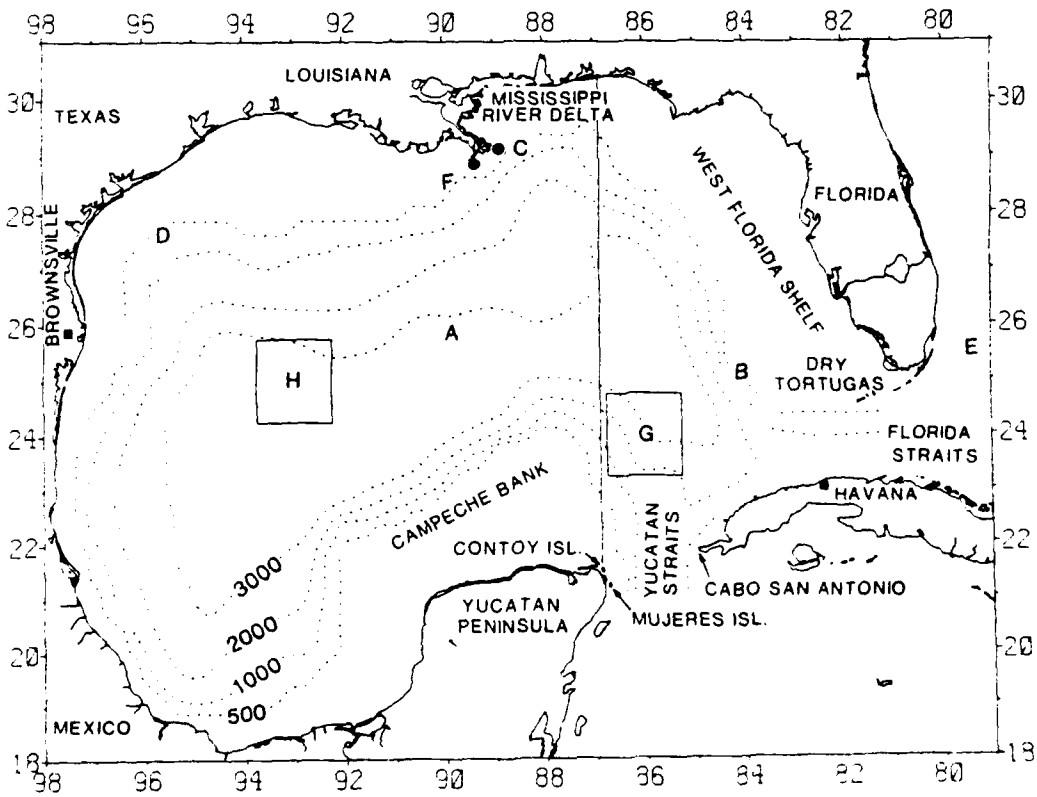

FIG. 1. Locations of a latitudinal section of the circulation model, of anthropogenic sources of nitrogen (●), and of simulated time series from both the biological model (E) and from the coupled physical/biological models (A-D), with respect to shipboard (F) and aggregated satellite (G-H) data in the Gulf of Mexico.

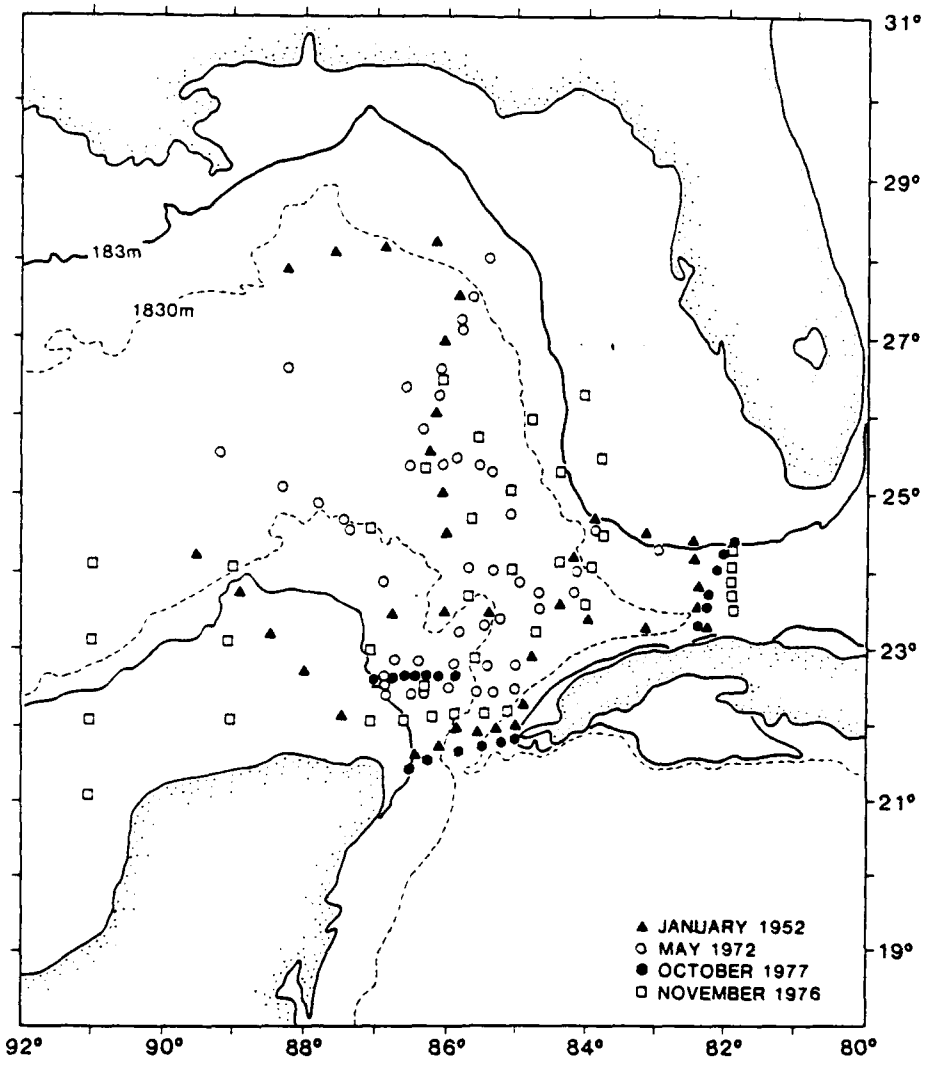

FIG. 2. Station location of nutrient surveys within the eastern Gulf of Mexico during January 1952 (▲), May 1972 (○), November 1976 (⊐), and October 1977(●).

Yucatan and Florida Straits during November 1976 and October 1977 (G. BERBERIAN, personal communication; MAUL, THOMAS and NELSEN, 1979) by R/V *Researcher* (Fig.2), provides a further quality check on our editing of the 1952 data. Autoanalyzer determination of nitrate distribution from the 1976-1977 frozen samples (G. BERBERIAN, personal communication) provided similar subsurface maxima of >35 μg-at NO_3 ℓ^{-1} at the same depths (Figs 4-5) of the 1952 sections (Fig.3), while impoverished nitrate stocks (<1 μg-at NO_3 ℓ^{-1}) were found in the euphotic zone of mid-strait stations, sampled 25 years apart (Figs 3-5). We did not use nutrient data from the *Researcher* sampling of the western Gulf in October 1976, however, when poor nutrient standards on a

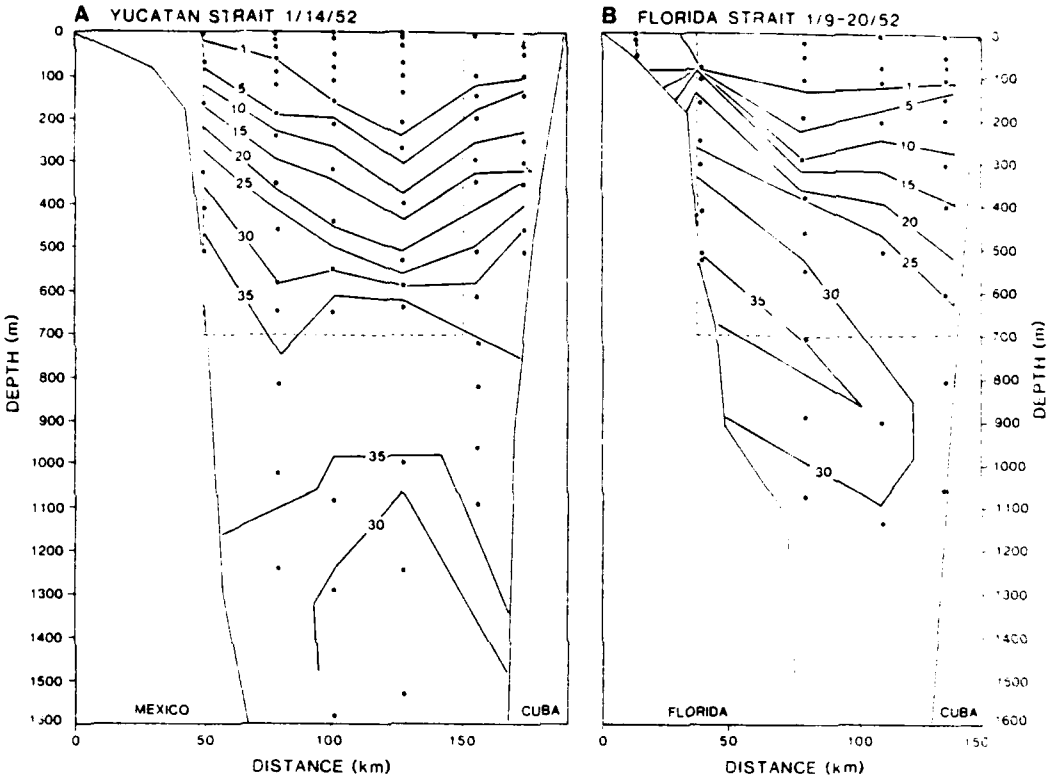

FIG.3. Nitrate distribution (μg-at ℓ^{-1}) within the upper 1600m during (A) January 14, 1952 in Yucatan Strait and (B) January 19-20, 1952 in Florida Strait. The dotted regions delimit the flux calculations of Table 1.

separate leg of the cruise evidently led to erroneously high nitrate values within the subsurface maxima.

1.1. *Flow*

At a sill depth of 768m in the eastern part of Florida Strait, efflux of nitrogen must be restricted to the upper half of the water column, sampled upstream and north of Havana within the deeper part of this channel on 19-20 January 1952, 14 November 1976 and 29 October 1977 (Figs 3b-5b). During May 1972,13 direct measurements of the Florida Current, south of Key West, suggested a mean eastward flow of $21.4 \times 10^6 m^3 s^{-1}$(Sv). This average includes both the baroclinic and barotropic components of transport in the Florida Strait above a σ_t surface of 27.0, i.e. above depths of 160-460m near respectively Florida and Cuba (BROOKS and NIILER, 1975). The 1972 dropsonde transects terminated at 35km north of Havana, however, perhaps missing a significant part of the eastward transport. The 25μg-at ℓ^{-1} isopleths of nitrate in Figs 3b-5b approximated the $27.0\sigma_t$ interfaces of these 1952, 1976 and 1977 sections. At these times, the nitrate profiles of the nearshore *Alaska* (Fig.3b) and *Researcher* (Fig.4b) stations were taken within ~10km of Havana on the Cuban coast, where the $27.0\sigma_t$ layer was deeper at depths of 600-620m.

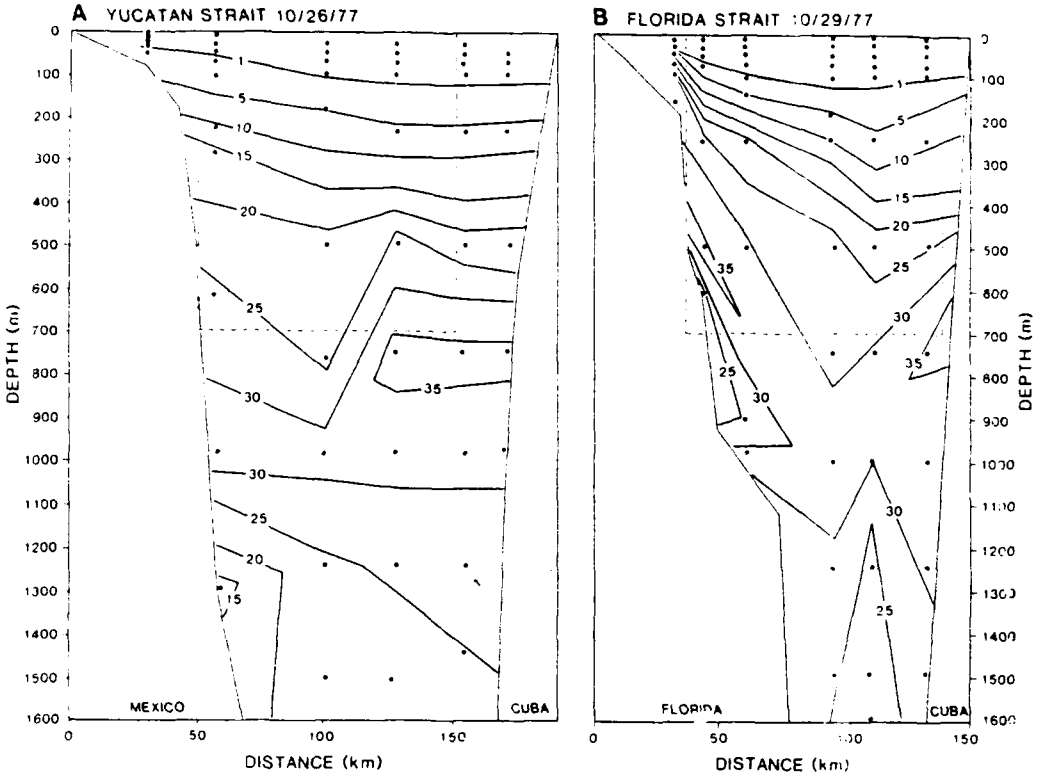

FIG.4. Nitrate distribution (μg-at ℓ^{-1}) within the upper 1600m during (A) October 26, 1977 in Yucatan Strait and (B) October 29 1977 in Florida Strait. The dotted regions delimit the flux calculations of Table 1.

Recalculation (MAUL, 1978) of the baroclinic contribution to flow in the Florida Strait above 700m and closer to Cuba during March 1938 (MONTGOMERY, 1941), suggests a geostrophic transport of 22.8Sv. But 27% of the flow was then located within 23km of the Cuban coast. Another 7.2Sv of eastward transport occurred between 700m and 1200m, where this flow was sampled by a station taken 7km north of Havana in 1938 (MONTGOMERY, 1941). Presumably some of this deeper flow in the western part of Florida Strait did not exit above the shallow sill to the east. Additional complexities of transport in this strait are flow reversals, for example, with shallow westward flow observed south of Key West in March 1938 (MONTGOMERY, 1941), March 1962 (HOFMANN and WORLEY, 1986) and May 1972 (BROOKS and NIILER, 1975).

In a series of monthly hydrographic transects, taken between August 1972 and September 1973 from the 50m isobath off Key West to 22km north of Cuba, the eastward geostrophic transport above 700m varied from 12.4 to 29.0Sv, with a mean of 19.5Sv (MAUL, 1978). Resident Gulf of Mexico water (NOWLIN and MCLELLAN, 1967), i.e. not water of immediate Yucatan or Caribbean origin (WÜST, 1964) and also termed Continental Edge Water (WENNEKENS, 1959), exits Florida Strait in varying amounts (Fig.6). It constituted as much as 8.3Sv of the monthly geostrophic transport through Florida Strait in 1972-73, with a mean flux of 2.7Sv, i.e. 14% of the outflow (MAUL, 1978). When the precursor of the Florida Current, e.g. the Loop Current, penetrates farther north into the Gulf of Mexico from Yucatan Strait, displacing resident waters, the outflow of Continental Edge Water increases along the northern wall of the Florida Strait (MAUL, 1977, 1978).

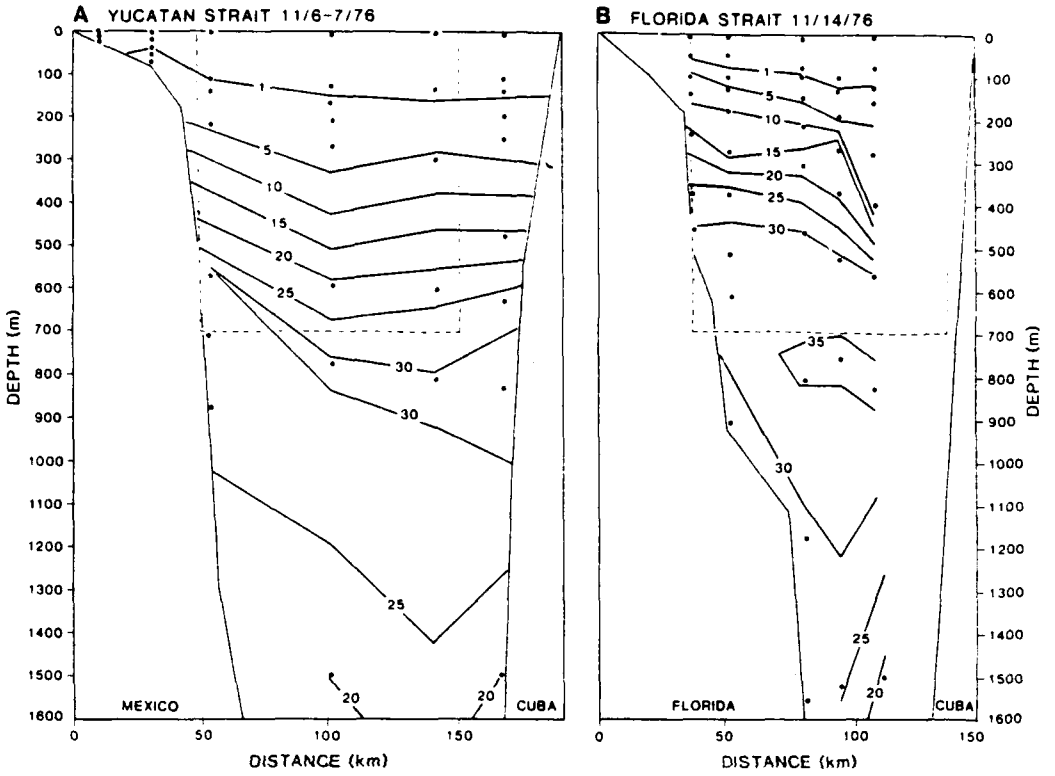

FIG.5. Nitrate distribution (μg-at ℓ^{-1}) within the upper 1600m during (A) November 6-7, 1976 in Yucatan Strait and (B) November 14, 1976 in Florida Strait.

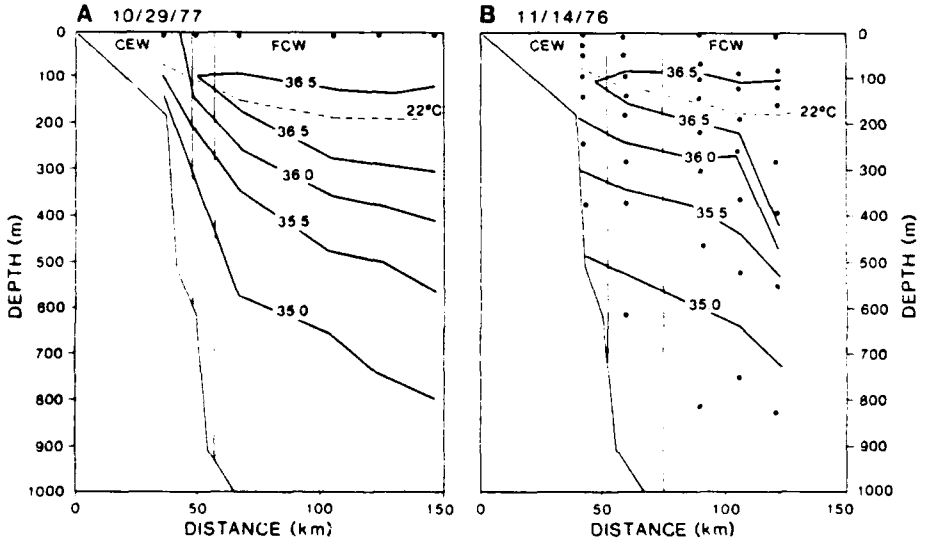

FIG.6. The depth of the 22°C isotherm in relation to both salinity fields and boundaries of Continental Edge Water and of Florida Current Water within Florida Strait during (A) October 29, 1977 and (B) November 14, 1976.

The precursor of the Loop Current in the Gulf of Mexico is termed the Yucatan Current when this western boundary flow is south of and within Yucatan Strait. Measurements of surface flow and hydrographic transects in May 1972 suggested a northward transport above the $27.0\sigma_t$ interface of 22.3Sv within the Yucatan Current between Isla Mujeres, Mexico, and Cabo San Antonio, Cuba (MOLINARI and YAGER, 1977). Similarly 24.0Sv of northward transport were found above this interface within 6 crossings of the Loop Current, taken north of Yucatan Strait in the same experiment (MORRISON and NOWLIN, 1977). The depths of the $27.0\sigma_t$ surface in Yucatan Strait ranged from 300m near Mexico to 600m near Cuba in 1952 and 1977, and were again mainly coincident with the 25μg-at NO_3 ℓ^{-1} isopleths of Figs 3a and 4a.

Southward counterflow has been observed both at greater depths and to the east within Yucatan Strait (GORDON, 1967; HANSEN and MOLINARI, 1979). Between Contoy Island, Mexico, and Cabo San Antonio, Cuba, for example, the geostrophic transport within the upper 700m in Yucatan Strait varied from 17.5 to 31.1Sv between August 1972 and September 1973, with a mean of 25.4Sv (MAUL, 1978). With such variance of the transport of water in and out of the Gulf of Mexico, three daily realizations of the nitrate fields within the Yucatan (Figs 3a-5a) and Florida (Figs 3b-5b) Straits provide only a departure point for possible assessment of the oceanic boundary fluxes of nitrogen.

1.2. *Dissolved nitrogen*

To provide a perspective on the following numerical results, however, we computed the flux of nitrogen in the form of nitrate through Yucatan and Florida Straits. We assume an average transport of 30Sv within the upper 700m of equivalent 97km-long portions (the dotted regions) of the sections made during 14-20 January 1952 (Fig.3) and 26-29 October 1977 (Fig.4). The 1976 section in Florida Strait (Fig.5b) was not taken close enough to the Cuban coast to allow a third calculation. To estimate these fluxes, we measured the area between each set of NO_3 isopleths, e.g. 0 and 1μg-at NO_3 ℓ^{-1}, of Figs 3 and 4 with a planimeter. We then multiplied the mean nitrogen content (μg-at x 14) of each nitrate layer by a mean flow of 44cm s^{-1} to yield the flux estimates of Table 1.

A total of 7.0×10^3kg NO_3-N s^{-1} entered the Gulf of Mexico via Yucatan Strait on 14 January 1952, with an efflux of 7.5×10^3kg NO_3-N s^{-1} through Florida Strait on 19-20 January 1952, i.e. an increment of 7%. Similarly, a nitrogen influx of 6.0×10^3kg NO_3-N s^{-1} on 26 October 1977 and an efflux of 7.1×10^3kg NO_3-N s^{-1} on 29 October 1977 suggests a larger nitrogen increment of 18% between surface layers of the Yucatan and Florida Straits. Within the uncertainties of smoothing the nutrient data and of estimating the width, depth, and speed of the Yucatan and Florida Currents, the above scenario may or may not indicate a net nutrient loss from the Gulf of Mexico.

The mean salinities of the 8 *Alaska* stations within the upper 700m of Fig. 3 were 35.98psu for the 42 discrete bottle samples taken during 1952 in Florida Strait, and 35.94psu for the 46 samples taken ~400km upstream in Yucatan Strait. They suggest little addition of estuarine water to the Atlantic Ocean from the Gulf of Mexico at the time of these sections. The increased salt and nutrient contents of the 1952 surface layer (<700m) of the Florida Current, compared to the Yucatan Current (Fig.3), instead suggest that upwelling occurred during the mean transit time of about 10 days from Yucatan Strait (i.e. over a distance of ~500km at a speed of 44cm s^{-1}).

However, the mean salinities of 8 comparable *Researcher* stations within the upper 700m of Fig.4 were 35.85psu for the 150 CSTD samples taken during 1977 in Florida Strait, compared to 35.99psu for 143 samples in Yucatan Strait. The larger increase of nitrate stocks between Florida

TABLE 1. Nitrogen flux through the upper 700 m of Yucatan and Florida Straits during 14–20 January 1952/ 26–29 October 1977

Nitrate layer (μg-at NO_3 ℓ^{-1})	Average N content (mg NO_3-N m^{-3})	Layer area (10^4 m^2)	Unit nitrogen stock (kg NO_3-N m^{-1})	Mean flow (m s^{-1})	Nitrogen flux (10^3 kg NO_3-N s^{-1})
Yucatan Strait:					
0–1	7	13.52/10.52	94.64/73.64	0.44	0.04/0.03
1–5	42	6.76/8.26	283.92/346.92	0.44	0.13/0.15
5–10	105	5.41/6.01	568.05/631.05	0.44	0.25/0.28
10–15	175	6.08/7.51	1064.00/1314.25	0.44	0.47/0.58
15–20	245	8.11/9.01	1986.95/2207.25	0.44	0.87/0.97
20–25	315	4.73/17.28	1489.95/5443.20	0.44	0.66/2.40
25–30	385	7.44/6.76	2864.40/2602.60	0.44	1.26/1.15
30–35	455	8.79/2.25	3999.45/1023.75	0.44	1.76/0.45
35–40	525	6.76/0.00	3549.00/0.00	0.44	1.56/0.00
Total:		67.60/67.60	15900.36/13642.66		7.00/6.01
Florida Strait:					
0–1	7	10.82/11.14	75.74/77.98	0.44	0.03/0.03
1–5	42	5.41/6.69	227.22/280.98	0.44	0.10/0.12
5–10	105	6.08/6.69	638.40/702.45	0.44	0.28/0.31
10–15	175	5.41/4.46	946.75/780.50	0.44	0.42/0.34
15–20	245	6.08/5.20	1489.60/1274.00	0.44	0.66/0.56
20–25	315	6.76/8.17	2129.40/2573.55	0.44	0.94/1.13
25–30	385	14.20/15.60	5467.00/6006.00	0.44	2.41/2.64
30–35	455	9.46/8.91	4304.30/4054.05	0.44	1.89/1.78
35–40	525	3.38/0.74	1774.50/388.50	0.44	0.78/0.17
Total:		67.60/67.60	17052.91/16138.01		7.51/7.08

and Yucatan Straits in 1977 was instead associated with a freshening of surface waters. From a much larger data base, MAUL (1978) determined that the Yucatan Current has 0.05psu higher salinity than the Florida Current, with both being as much as 0.40psu saltier than Continental Edge Water at a temperature of 22°C.

The lower salt content of Continental Edge Water is derived from either upwelling of Antarctic Intermediate Water (Fig.6) or from land runoff. Higher nutrients can similarly result from either coastal discharge or upwelling at the cyclonic edge of these western boundary currents (Figs 3 and 4). Note that, while the depth integral of NO_3-N over the upper 700m only increased 7-18% (Table 1) between the 1952 and 1977 sections across Yucatan Strait and those across Florida Strait, the vertical structure of NO_3 changed significantly. For example, the 5-15μg-at NO_3 ℓ^{-1} isopleths were all grouped at or above the 100m depth on the Florida shelf-break, compared to deeper levels off Mexico, while the 20μg-at NO_3 ℓ^{-1} isopleth was found at depths of 80-140m off Florida (Figs 3a-4a), compared to depths of 220-380m near Mexico (Figs 3b-4b).

The average depth change in the latter isopleth suggests continued upwelling, at perhaps 20m d^{-1}, if the water flowed directly northeast at 44cm s^{-1} over 500km within the successive Yucatan, Loop, and Florida Currents. Northward excursions of the Loop Current into the Gulf of Mexico would increase the time over which upwelling occurs, thereby decreasing the estimate of upward movement. The depth of the 22°C isotherm can be used (LEIPPER, 1970; MAUL, 1977, 1978) to demarcate the boundaries of the respective Yucatan, Loop and Florida Currents (>100m) with resident Gulf of Mexico water, where the nearshore, shallower depth (<100m) of this isotherm at their cyclonic edge reflects the upwelling process as well.

A plot of the depths of the 22°C isotherm during the 1952 cruise of the R/V *Alaska*, suggests that the Loop Current penetrated to 24°30'N (Fig.7), implying minimal occupation of the Florida Strait by Continental Edge Water at this time (MAUL, 1978). As in May 1972 (MERRELL, MORRISON, NOWLIN, MOLINARI, BROOKS and YAGER, 1978), there appears to be a previously-shed anticyclonic eddy just to the northwest of the Loop Current during January 1952 (Fig.7). Synoptic infrared imagery of surface temperature gradients from the NOAA VHRR suggests that the Loop Current had similarly penetrated to only 24°30'N on 28 October 1977, compared to 28°N between 14 October 1976 and 4 December 1976 (VUKOVICH, CRISSMAN, BUSHNELL and KING, 1979). With a large northward excursion, the inclined front between Loop Current and resident Gulf of Mexico water extended over 1500km between Yucatan and Florida Straits in the fall of 1976, compared to ~500km in the fall of 1977.

Over a longer travel distance of ~1500km for water parcels observed in the 6-7 and 14 November 1976 sections across Yucatan and Florida Straits (Fig.5), an upward movement of the 20μg-at NO_3 ℓ^{-1} isopleth, from respectively 440m off Mexico to 280m off Florida, implies an upwelling velocity of only ~5m d^{-1}. A decline in the upwelling rate, from 20 to 5m d^{-1}, and increase of residence time, from 10 to 30 days, would allow phytoplankton to take up more of the upwelled nitrate within the euphotic zone at the cyclonic edge of these currents. Note that both the 1 and 5μg-at ℓ^{-1} isopleths of nitrate have the same slope, between depths of 100 and 200m in the middle of Florida Strait, during October 1977 (Fig.4b) and November 1976 (Fig.5b). Near the shelf-break, however, the 5μg-at NO_3 ℓ^{-1} isopleth is at 60m depth in 1977, compared to 100m depth in 1976, presumably as a result of enhanced nutrient uptake within the lower part of the >100m euphotic zone during 1976. Within the deeper aphotic zone, increased upwelling during 1977 led to a shoaling of other isopleths, e.g. the 10, 15 and 20μg-at NO_3 ℓ^{-1} (Fig.4b), previously found ~120m deeper on the upper slope in 1976 (Fig.5b).

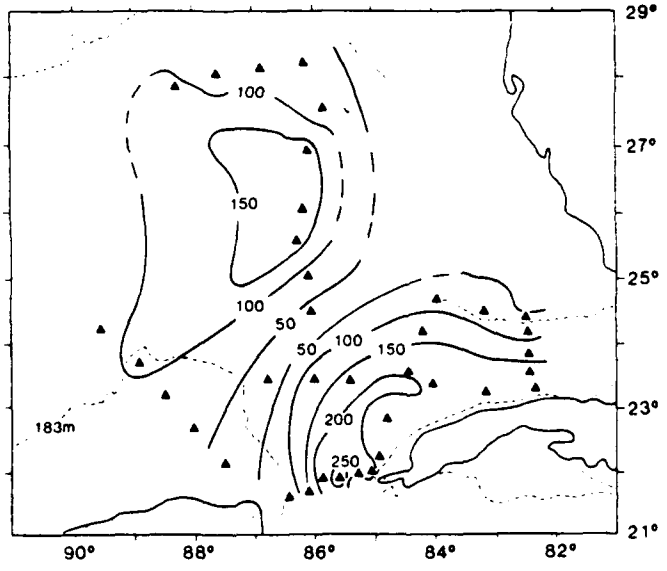

FIG.7. The depth of the 22°C isotherm within the eastern Gulf of Mexico during January 1952.

The rates of upwelling and nutrient uptake in Florida Strait, as well as the lateral extent of Continental Edge Water, appear to be affected by the extent of northward penetration of the Loop Current into the Gulf of Mexico. Using water type criteria of Continental Edge Water, as the 22°C isotherm ≤100m depth, and of Florida Current Water, as 36.70psu salinity at 22°C (MAUL, 1978), the respective locations of these water types in Florida Strait are shown in Fig. 6, before (Fig.6a) and during (Fig.6b) an excursion of the Loop Current into the Gulf of Mexico. When the Loop Current flows directly into Florida Strait, the Florida Current Water is located 49km south of the US coast, with isopleths of salinity sharply inclined shoreward (Fig.6a). The 25 μg-at ℓ^{-1} isopleth of nitrate coincides with the 35.5psu isopleth of salinity (Fig.4b). With a northward intrusion of the Loop Current, the Florida Current Water is instead located 65km south of the coast, with the strongest vertical gradient of salinity found at mid-channel (Fig.6b), similar to the nitrate structure (Fig.5b).

Depression of nearshore upwelling at the Florida Keys during intrusions of the Loop Current and greater export of Continental Edge Water, with possible offshore and/or upstream shifts in loci of nutrient input, are the local result of southward movement of the Dry Tortugas meander (VUKOVICH and MAUL, 1985). During northward penetration of the Loop Current, sporadic upwelling also occurs along the West Florida shelf, until southerly retreat of the Current and/or shedding of an anticyclonic eddy. In the western half of the Gulf of Mexico, these shed eddies may induce further upwelling at the Texas-Mexican shelf-break. Based on salinity budgets, about 10% of the transport of the inflowing Yucatan Current is annually exchanged with resident water in the Gulf of Mexico via the Loop Current upwelling and eddy shedding (MAUL, 1978). From Table 1, this exchange rate suggests that about 700kg NO_3-N s^{-1} may be supplied at the oceanic boundary of the Gulf.

1.3. *Particulate matter*

Part or all of the oceanic nitrate input must fuel the primary production of the interior basin and shelves of the Gulf of Mexico. Assuming a maximal nitrate concentration of 150mg-at m^{-3} and a mean flow of $1.8 \times 10^4 m^3 s^{-1}$ for the Mississippi River (WALSH, ROWE, IVERSON and MCROY, 1981), an equivalent anthropogenic terrestrial flux of nitrogen to the Gulf might be as much as 38kg NO_3-N s^{-1}, i.e. ~5% of the oceanic source. Finally, applying open-ocean nitrogen fixation rates of 16.1-32.3kg N $km^{-2} y^{-1}$ (CAPONE and CARPENTER, 1982; FOGG, 1982) over the surface area of the Gulf ($1.53 \times 10^6 km^2$), a possible atmospheric nitrogen input to the Gulf might be only 1-2kg NO_3-N s^{-1}.

Because the atmospheric input of nitrogen is small (~<1%), compared to oceanic and terrestrial inputs of nitrogen to the Gulf of Mexico, we ignored N_2 fixation by cyanobacteria in our calculations. Redistribution of the oceanic and terrestrial boundary inputs of nitrogen of 738kg NO_3-N s^{-1} within the interior of the Gulf over the life cycle of a Loop Current intrusion, their possible loss to the sediments and atmosphere via burial and N_2 evasion, as well as their possible export to the Atlantic Ocean are the subjects of our simulation models.

The burial and denitrification losses of nitrogen in the Gulf of Mexico can be constrained *a priori* from the abundance of organic-rich sediments, their porosity, C/N ratio, and sedimentation rates. Using values of organic carbon (%dw) measured in surficial sediments over the last 30 years (STETSON and TRASK, 1953; TRASK, 1953; SCHOLL, 1963; UPSHAW, CREATH and BROOKS, 1966; VASILEV and TORIN, 1969; HATHAWAY, 1971; ROWE and MENZEL, 1971; ARMSTRONG, 1974; GEARING, 1975; GEARING, GEARING, LYTLE and LYTLE, 1976; HEDGES and PARKER, 1976; BERRYHILL, 1977; SUSIO, 1977; ESE and LGL, 1975; LGL, 1986), we constructed a composite (Fig.8) of the

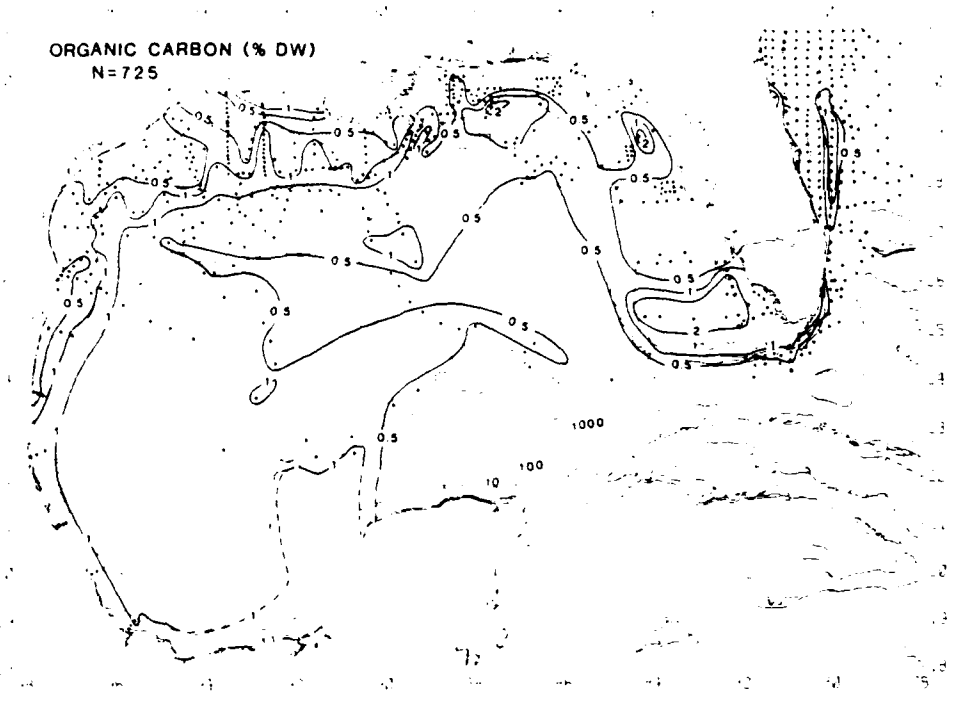

FIG.8. The composite distribution of organic carbon (%dw) within surficial sediments of the Gulf of Mexico over the last 30 years.

distribution of organic matter in recent sediments of the Gulf. Typically, regions of 1-2% organic carbon have C/N ratios of 6/1, whereas those of 0.5-1.0% carbon have higher C/N ratios of 10/1 (WALSH, 1983), reflecting increased remineralization and lower accumulation rates, since the $\delta^{13}C$ signature of these sediments is mainly marine (HEDGES and PARKER, 1976; GEARING, PLUCKER and PARKER, 1977).

The burial rate of organic matter on a unit area basis can then be obtained (MULLER and SUESS, 1979) from

$$A = S \cdot G \cdot C \cdot N/C \cdot (1 - P) \quad (1)$$

where A is the accumulation rate of nitrogen in the sediment (g N $cm^{-2}y^{-1}$); S is the sedimentation rate (cm y^{-1}); G is the specific gravity of sediment (2.6g cc^{-1}); C is the % dw carbon content (more frequently measured); N/C is the ratio of nitrogen and carbon within the surviving organic matter of the sediment; and P is the porosity, providing an estimate of the volume of water within the sediment column. At the shelf-break off the Mississippi River Delta, sedimentation rates as high as 1.0cm y^{-1} have been observed near the 100m isobath (SHOKES, 1976; PARKER, 1977), but more typical rates in other shelf and slope regions are 0.01-0.10cm y^{-1} (WALSH, PREMUZIC, GAFFNEY, ROWE, HARBOTTLE, STOENNER, BALSAM, BETZER and MACKO, 1985).

Using a specific gravity of 2.6g cc^{-1}, a porosity of 0.8, a sedimentation rate of 0.10cm y^{-1}, a N/C ratio of 0.17, and a mean carbon content of 1.5% dw for the area ($0.24 \times 10^{12} m^2$) enclosed by the 1.0% dw isopleth of sediment carbon (Fig.8), as well as a rate of 0.01cm y^{-1}, a ratio of 0.10, and a mean content of 0.75% dw for the area ($0.70 \times 10^{12} m^2$) enclosed by the 0.5%-1.0% isopleths

(Fig.8), we obtain a hypothetical Gulf burial rate, from eq.(1) and Fig. 8, of 3.5 x 10^8kg N y^{-1}. We assume that "new" nitrogen, in the form of either nitrate or anthropogenic input (EPPLEY and PETERSON, 1980; WALSH, 1983), sets the limit for export of nitrogen fixed in the Gulf's euphotic zone. Such a burial estimate then implies, in a steady state, that at least 3.5 x 10^8kg NO_3-N y^{-1} must be supplied to the overlying water column, without consideration of either shunts of recycled nitrogen (ammonium, urea, amino acids), or of gaseous losses of nitrogen (N_2).

Assuming a denitrification rate of 1.1 x 10^3kg N $km^{-2}y^{-1}$ (CHRISTENSEN, 1981; HAINES, ATLAS, GRIFFITHS and MORITA, 1981) for the richer carbon (>1% dw) sediments of the outer shelf and upper slope of the Gulf of Mexico, the area (0.24 x $10^6$$km^2$) enclosed by the 1.0% isopleth of carbon (Fig.8) yields an estimated N_2 loss to the atmosphere of 2.6 x 10^8kg N y^{-1}. On an annual basis, the above estimated rate of nitrogen fixation of atmospheric N_2 in surface waters of the Gulf by cyanobacteria is evidently much lower, 2.5-5.0 x 10^7kg N y^{-1}, implying a net loss of nitrogen gas from the Gulf to the local atmosphere. Man's fixation of atmospheric nitrogen for fertilizer, its leaching from fields into the drainage basin of the Mississippi River, as well as addition of sewage as another by-product of agricultural activities, lead, however, to a circuitous return from the global atmosphere of 8.5 x 10^8kg N y^{-1} within the mean plume of the Mississippi River.

A total mean nitrogen input of 738kg NO_3-N s^{-1} to the Gulf of Mexico, or 231 x 10^8kg N y^{-1}, from the oceanic and terrestrial boundaries appears to more than offset a combined loss of perhaps 6 x 10^8kg N y^{-1} from our preliminary estimates of the burial of organic nitrogen and evasion of N_2. We have thus far not included possible export of nitrogen via the Florida Strait. Also, our estimate of the oceanic input of nitrate to the southern Gulf of Mexico is a depth integral over 700m, which may not all be utilized by phytoplankton, nor by the rest of the food web.

For example, low near-surface chlorophyll concentrations of 0.10-0.15 μg chl ℓ^{-1} resulted in a 1% light depth of 115m during an intrusion of the Loop Current in early February 1981 (ORTNER, FERGUSON, PIOTROWICZ, CHESAL, BERBERIAN and PALUMBO, 1984). During this study, the nitrate content of the euphotic zone within the Loop Current was <0.4 μg-at NO_3 ℓ^{-1}. Even after local wind forcing, the depth of the 3 μg-at $NO_3\ell^{-1}$ isopleth only shoaled from 240m to 140m within the center of the Loop Current. This is in contrast to nutrient conditions at the cyclonic edge of these western boundary currents, where 20 μg-at $NO_3\ell^{-1}$ are found at this same depth near the Florida shelf-break (Fig.3b).

Conversion of the oceanic input of nitrate by organisms to organic nitrogen and N_2 would thus be enhanced by upwelling, in addition to diffusion supply to the euphotic zone. Such a kinetic energy supplement is not required for consumption of the terrestrial input of nitrogen which occurs within a low-salinity lens at the surface of the northern Gulf of Mexico. Our assumptions about the factors controlling the biochemical conversion process of nitrate uptake, i.e. light and nutrient limitation, upwelling velocities, vertical mixing, and horizontal dispersion, are discussed in the next section.

2. METHODS

2.1. *Circulation formulation*

Initial barotropic simulations of western boundary currents, e.g. the Loop Current (PASKAUSKY and REID, 1972), the Kuroshio (O'BRIEN, 1971) and the Gulf Stream (HOLLAND and HIRSCHMAN, 1972), underestimated their transports of respectively 30, 90 and 150Sv by about 30-90%.

Addition of baroclinicity and realistic bottom topography to numerical models generates larger transports, e.g. 81Sv for the Gulf Stream (HOLLAND and HIRSCHMAN, 1972). Use of large horizontal eddy viscosities on grids of poor spatial resolution over whole ocean or basin domains, however, damps the nonlinear acceleration terms of the Navier-Stokes equations. The models then lead to smaller transports, for example, of 60Sv within the Gulf Stream (COX, 1975). The large horizontal viscosities over these grids of world ocean models (BRYAN and COX, 1972; COX, 1975) are also unable to resolve the formation of mesoscale eddies, shed from these western boundary currents by latitudinal variation of the Coriolis term (HULBURT and THOMPSON, 1980).

The simplest baroclinic formulation of flow within these currents is a "reduced gravity" model, which assumes no motion in the lower part of a two-layered ocean. Early (STOMMEL, 1965) and more recent (CSANADY and HAMILTON, 1988) analytical studies of the Gulf Stream, as well as numerical studies of the Loop Current (HULBURT and THOMPSON, 1980), invoked such oversimplification of time-invariant buoyancy fluxes within a stratified water column. The most complex baroclinic models of western boundary currents utilize 16-21 layers to approximate the vertical structure of density and associated time-dependent thermodynamics, vertical mixing, and advection within the Loop Current (BLUMBERG and MELLOR, 1985) and the Gulf Stream (BLUMBERG and MELLOR, 1983). These models did not resolve eddy shedding from the Loop Current, however. To provide an initial assessment of the consequences of nutrient injection by western boundary currents, we thus employed a simple baroclinic circulation model which was still capable of shedding eddies.

Of particular interest in our present study was the shedding of cyclonic eddies (VUKOVICH and MAUL, 1985), which induces upwelling here and in the South Atlantic Bight (ATKINSON, MENZEL and BUSH, 1985), as opposed to the anticyclonic, warm core eddies (ELLIOTT, 1982) within the Gulf of Mexico. Lateral movement of a western boundary current and/or wind stress can also induce upwelling at the shelf-break. Eddy-resolving simulation models of this region require small grid spacing (10-25km), and associated low viscosities (1-10 x $10^6 cm^2 s^{-1}$). With appropriate parameterization, they allow formation of cyclonic eddies both at the shoreward wall of the Loop Current in the eastern Gulf and as part of an eddy pair in the western Gulf (HULBURT and THOMPSON, 1980; BLUMBERG and MELLOR, 1985; WALLCRAFT, 1986).

Natural boundary conditions for simulating the circulation, in which these eddies are embedded, within the Gulf of Mexico might be the time-dependent influx of the order of ~30Sv through Yucatan Strait and an outflow of about the same magnitude through Florida Strait. The cycle of northward penetration of the Loop Current into the eastern Gulf of Mexico, release of an anticyclonic eddy, and southward retreat, may have less of periodic signal than originally hypothesized (MAUL, 1977), however. There is evidently a seasonal amplitude of 4.1Sv for the Florida Current off Miami from 7 years of observations made during 1964-1970, when a mean transport of 29.5Sv was found (NIILER and RICHARDSON, 1973). A similar seasonal signal of the Loop Current may be masked upstream by counterflows within Yucatan Strait, since most of the continuity requirement of a Loop Current intrusion may be met by outflow of Yucatan Bottom Water south through this Strait (MAUL, 1978).

HULBURT and THOMPSON (1980), as well as WALLCRAFT (1986), were able to produce quasi-annual cycles of Loop Current penetration and eddy shedding, however, with time-invariant boundary conditions of flow within Yucatan and Florida Straits. We have adopted their approach, using a steady input through Yucatan Strait of a transport of 20Sv above, and 10Sv below, an initial interface (pycnocline) depth of 200m, embedded in a two-layered model of constant densities, ρ_1 and ρ_2. This interface is impermeable. The Boussinesq approximation is used and

a mean density, ρ_0, replaces ρ_1 or ρ_2, except for the buoyancy term described below by eq.(8).

In a cartesian coordinate system (x,y,z), with z positive upwards and t denoting time, the vertically-integrated equations for the flow (u,v) within each layer are:

$$\frac{\partial U_i}{\partial t} + \frac{\partial (U_i u_i)}{\partial x} + \frac{\partial (V_i u_i)}{\partial y} = fV_i - h_i \frac{\partial P_i}{\partial x} + \frac{(\tau_i^x - \tau_{i+1}^x)}{\rho_0} + K_i h_i \nabla^2 u_i \tag{2}$$

$$\frac{\partial V_i}{\partial t} + \frac{\partial (U_i v_i)}{\partial x} + \frac{\partial (V_i v_i)}{\partial y} = -fU_i - h_i \frac{\partial P_i}{\partial y} + \frac{(\tau_i^y - \tau_{i+1}^y)}{\rho_0} + K_i h_i \nabla^2 v_i \tag{3}$$

and

$$\frac{\partial h_i}{\partial t} = -\frac{\partial U_i}{\partial x} - \frac{\partial V_i}{\partial y} \tag{4}$$

where the index, i=1,2 indicates the upper and lower layers of the model. The variable u_i is the x (positive to the east) component of the velocity, v_i is the y (positive to the north) component, h_i is the thickness, and $U_i = u_i h_i$, $V_i = v_i h_i$ are the depth-integrated transports in each layer.

The pressure gradient term of eq.(2) [and similarly for eq.(3)] is defined additionally (HULBURT and THOMPSON, 1980) by

$$\frac{\partial P_1}{\partial x} = g \frac{\partial \eta}{\partial x} \tag{5}$$

and

$$\frac{\partial P_2}{\partial x} = g \frac{\partial \eta}{\partial x} - g' \frac{\partial h_1}{\partial x} \tag{6}$$

where g is the acceleration as a result of gravity, η is the sea surface elevation, and g′ is the reduced gravity, or buoyancy effect. Without stratification of the water column, $\partial P_1/\partial x = \partial P_2/\partial x$, and the circulation model is barotropic. The free surface, η, is defined by

$$\eta = h_1 + h_2 - D \tag{7}$$

where D is the local depth. The baroclinic shear of the model is incorporated in the reduced gravity term as

$$g' = g(\rho_2 - \rho_1)/\rho_0 \tag{8}$$

which we set to 3cm s^{-2}.

The Coriolis parameter, f, is assumed to vary with latitude. We follow the β-plane approximation of

$$f = f_0 + \beta(Y - Y_0) \tag{9}$$

Using a central latitude of 24.5°N, f_0 is 6.03 x $10^{-5} s^{-1}$ and β is 2.08 x $10^{-13} cm^{-1} s^{-1}$.

The stress terms, $\tau_i^{x,y}$ of this type of Lagrangian model (O'BRIEN and HULBURT, 1972) lead to numerical instabilities, if the interface depth either surfaces or intersects the bottom. Wind stress, for example, generates rapid upwelling in this Gulf of Mexico model, with consequent abortion of the numerical solution as the upper layer approaches zero thickness (WALLCRAFT, 1986). In the circulation model, both wind stress and interfacial stresses are thus ignored; wind forcing is considered in the vertical mixing term of the biological model, however.

The bottom stress is defined in quadratic form by

$$\tau^x = \rho_0 c q u_2 \tag{10}$$

$$\tau^y = \rho_0 c q v_2 \tag{11}$$

where $q = (u_2^2 + v_2^2)^{1/2}$ and c is a drag coefficient of 2.0×10^{-3}. To avoid intersection of the interface depth with the bottom, a minimum bottom depth, D, of 500m was assumed for the continental shelf regions. Other bottom topography was digitized from NOS Chart 411 and smoothed to eliminate small-scale features (Fig.1).

The last term on the right hand side of eqs.(2) and (3) represents horizontal mixing of momentum, where $\nabla^2 = \partial^2()/\partial x^2 + \partial^2()/\partial y^2$ is the Laplacian operator and $K_x = K_y = 2.5 \times 10^6 cm^2 s^{-1}$ are the horizontal eddy viscosities. Our formulation differs somewhat from HULBURT and THOMPSON (1980), because we use the Laplacian of the horizontal velocities, rather than the transports, to simulate the horizontal mixing processes. A full derivation of this term is given by THOMPSON (1974).

The computational grid for the two-layered circulation model involves a horizontal resolution of 1/4° x 1/4°. Such spatial resolution yields a rectangular grid increment in the x-dimension of 25.4km and of 27.8km in the y-dimension. The model grid covers the entire Gulf to avoid specification of other open boundary conditions, besides those of Yucatan and Florida Straits. The inflow port has a 175km width across Yucatan Strait and the outflow port is 125km wide across Florida Strait. The land boundaries of the models were chosen to conform to the coastlines of the Gulf (Fig.1).

At these coastal boundaries, a no-flow constraint was imposed on the velocity component normal to the shore. Use of the Laplacian horizontal friction term, i.e. MUNK (1950), in eqs. (2)-(3) requires the tangential component of the flow to also be specified at the coast. A simple method, parameterizing vorticity generation at solid boundaries, is the no-slip boundary condition. The no-slip condition is achieved by assigning an equivalent velocity, at each boundary grid point, of opposite sign to that of the tangential component (HOLLAND and LIN, 1975).

A steady northward flow, with a quadratic profile in the upper layer and uniform flow in the lower layer, was prescribed at the inflow open boundary of Yucatan Strait. Outflow through Florida Strait was constrained to match the volume inflow from Yucatan Strait, in a manner similar to HULBURT and THOMPSON (1980), i.e. the latitudinal pressure gradient of eq.(2) is assumed constant along the outflow boundary. It is determined by imposing the constraint that the outflow of water in each layer must match the corresponding inflow from Yucatan Strait. In addition, the tangential component of the flow was set to zero for grid points just outside the inflow and outflow ports.

2.2. *Vertical mixing*

As a result of the impermeable nature of the interface between the two layers of the model, complex formulations of wind stress, heat flux, and vertical stratification have been added to

simulate vertical mixing of momentum and temperature (THOMPSON, 1974; O'BRIEN and HEBURN, 1983). Similarly, without a term for description of nutrient exchange across this interface, no renewal of nitrogen would occur in the upper layer, except for river discharge and remineralization. Uncertainties in the actual wind curl (WALLCRAFT, 1986) and heat flux (ETTER, 1983) within the Gulf of Mexico, together with a poor resolution of vertical stratification within a two-layered circulation model preclude a complex description of vertical mixing for use in the companion biological model.

We instead prescribed an empirical depth profile of the vertical eddy diffusivity, K_z, over the upper layer of the circulation model as additional input to the twenty-layer biological model, which is nestled in this upper part of the water column. At the depth of the interface, i.e., $z_1 = h_1 - \eta$, K_z is taken to be $0.1 cm^2 s^{-1}$, reflecting low turbulent mixing of nutrients across the pycnocline (EPPLEY, RENGER and HARRISON, 1979; KING and DEVOL, 1979). Within the surface mixed layer, K_z is much greater, with variation of both K_z and the mixed layer depth, h_m, at time scales ranging from wind events to seasons.

Using a one-dimensional model of time-dependent, wind-induced mixing (NIILER, 1975) and a turbulence closure scheme (MELLOR and YAMADA, 1974), a K_z of $188.0 cm^2 s^{-1}$ can be calculated for a 44m thick surface mixed layer of weak vertical stratification ($0.4\sigma_t$ $50m^{-1}$) after ~9hr of wind forcing at $10m\ s^{-1}$ (WROBLEWSKI and RICHMAN, 1987). A day after cessation of the simulated wind impulse in their model, K_z had declined to $22.0 cm^2 s^{-1}$, however. Since exogenous factors of the biological model change at the 30 day time scale (Table 2), we chose to average over such wind events using field estimates of mean wind stress and the thickness of the surface mixed layer.

TABLE 2. The monthly wind stress and photosynthetically active radiation (PAR) at the sea surface, in relation to the vertical eddy diffusivity and depth of mixed layer in the simulated Gulf of Mexico

	τ (dyne cm^{-2})	K_0 ($cm^2\ s^{-1}$)	h_m at 25.5°N, 40.5°W (m)	Maximum I_0 (1200 h) at 25° N (μEin $cm^{-2}\ h^{-1}$)
Jan	0.61	49	100	731
Feb	0.62	50	93	827
Mar	0.72	58	86	930
Apr	0.77	62	62	997
May	0.69	56	41	1016
Jun	0.59	48	24	1016
Jul	0.42	34	24	1016
Aug	0.32	26	24	1005
Sep	0.56	45	45	956
Oct	0.81	66	48	860
Nov	0.77	62	59	752
Dec	0.70	57	78	696

A surface mixed layer of 50m thickness ($\leq \Delta\, 0.13\sigma_t$ criterion), measured at the *Researcher* stations within Florida Strait near the end of October 1977, for example, is quite similar to a climatological monthly average of 48m thickness (Table 2) for October in the middle of the Atlantic Ocean at 25.5°N, 40.5°W (LEVITUS, 1982). The mixed layer depths, h_m, in January at the *Alaska* stations within the eastern Gulf of Mexico (Fig.2) were also similar to those of the mid-Atlantic, while the *Alaminos* stations in May suggested shallower depths than the climatological mean (Table 2). Finally, a compilation of these and other temperature data over the whole Gulf (>0.5 x 10^6 stations prior to 1979) yields a seasonal cycle of vertical temperature structure (Fig.11a of BLUMBERG and MELLOR, 1985), which confirms our assumed seasonal cycle of the depth of the surface mixed layer.

From monthly estimates (>1 x 10^6 observations) of wind stress on a 1° square grid of the Gulf of Mexico, the area-averaged wind stress vector (Fig.3a of BLUMBERG and MELLOR, 1985) was used to obtain the magnitude of the surface wind stress, τ, in Table 2. A number of relationships (SVERDRUP, JOHNSON and FLEMING, 1942; MUNK and ANDERSON, 1948; CSANADY, 1976; KULLENBERG, 1976), have been derived for estimation of the vertical eddy viscosity within the mixed layer, K_0, from the surface wind stress. Using dye experiments and classical Ekman theory (KULLENBERG, 1976), the early estimates of K_0 have been reduced by an order of magnitude to

$$K_0 = \rho_a c_a \tau \, (\rho_0^2 \zeta^2 f)^{-1} \tag{12}$$

where ρ_a and ρ_0 are the densities of air and seawater, c_a is another drag coefficient, and ζ is a proportionality constant. Assuming values of 1.23 x 10^{-3} for ρ_a, 1.0 for ρ_0, 1.3 x 10^{-3} for c_a, and 1.8 x 10^{-2} for ζ, eq.(12) reduces to

$$K_0 = 4.9 \times 10^{-3}\, \tau / f \tag{13}$$

which is identical to the relationship of CSANADY (1976). Using eq.(13), the wind stresses in Table 2, and the value of the Coriolis parameter at 24.5°N, we computed monthly entries for K_0 (Table 2).The monthly wind stress, vertical eddy coefficient, and mixed layer depth range from respective maxima of 0.81 dynes cm^{-2}, 66$cm^2 s^{-1}$, and 100m to minima of 0.32 dynes cm^{-2}, 26$cm^2 s^{-1}$, and 24m (Table 2).

The vertical profile of K_z is completed by assuming an exponential decay, from the uniform monthly value in the surface mixed layer, K_0, to the smaller value of 0.1$cm^2 s^{-1}$ at the interface, K_f, described by

$$K_z(z) = K_0 e^{b(|z| - h_m)} \tag{14}$$

where h_m is the depth of the mixed layer, b is log $(K_f/K_0)/(z_1-h_m)$, and z_1 is the interface depth. The overall shape of our K_z profile with depth is similar to the Richardson number-dependent profiles calculated by HAMILTON and RATTRAY (1978).

The depth of the interface, $z_1 = h_1 - \eta$, varied over time and space from 100 to 400m in separate runs of the circulation model. Therefore, a vertical resolution of 20 levels for the biological model over h_1 insured that at least the K_z of the topmost layer reflected the value of K_0 during each time step. The 21st layer of the biological model extended over h_2, the lower layer of the circulation model. The value of K_z over each of the 20 depth intervals of the upper water column was the average over each respective depth integral, similar to the following calculations for estimation of the *in situ* light field.

2.3. *Biochemical formulation*

With both upwelling/downwelling motion of the interface between layers and vertical mixing within the upper layer of the physical model, phytoplankton, M, experience large temporal and spatial changes in the gradients of light, I, and nutrient, N, over the domains of the coupled biological/physical models. Since little ammonium, urea, or even chlorophyll data exist for the Gulf, our validation data consist mainly of dissolved nitrate in the water column (Fig.2), particulate carbon in the sediment (Fig.8), and satellite estimates of pigment within the first optical depth (Figs 26 and 27). Accordingly, we chose to model the "new" production of the system, employing nitrate as the nutrient state variable, N.

The tempo-spatial distributions of nitrate (μg-at NO_3 ℓ^{-1}) can be described on an Eulerian grid by

$$\frac{\partial N}{\partial t} = -u\frac{\partial N}{\partial x} - v\frac{\partial N}{\partial y} - w\frac{\partial N}{\partial z} + \frac{\partial}{\partial z}K_z\frac{\partial N}{\partial z} - aMs^{-1} + oMs^{-1} \qquad (15)$$

where u and v are the depth-averaged flows of the upper layer of the physical model, as calculated from eqs.(2)-(4). The third term is the vertical advection of nitrate, which does not appear explicitly in the Lagrangian formulation of eq.(18). The horizontal eddy diffusivities, K_x and K_y of eqs.(2)-(3) are ignored, since the advective terms are much larger than the diffusive terms in the horizontal dispersion of nitrate. The vertical eddy diffusivity, K_z, is obtained at each grid point by the procedure described above. The fifth term of eq.(15) is the uptake of nitrogen by phytoplankton, expanded in the more complex expression of eq.(20), where s = 1.68 relates either pigment formation (μg ℓ^{-1} h^{-1}) to nitrogen uptake (μg-at $\ell^{-1}h^{-1}$), or pigment degradation during nitrification, assuming a C/chl ratio of 50/1 and a C/N ratio by weight of 6/1. The last term of eq.(15) is nitrification in the water column, where o = 0.0050-0.0025d^{-1} are the remineralization rates of phytoplankton within respectively the upper and lower layers of the circulation model.

Phytoplankton biomass (μg chl ℓ^{-1}), M, in the simulated Gulf of Mexico is similarly described by

$$\frac{\partial M}{\partial t} = -u\frac{\partial M}{\partial x} - v\frac{\partial M}{\partial y} - w\frac{\partial M}{\partial z} + \frac{\partial}{\partial z}K_z\frac{\partial M}{\partial z} + aM - w_s\frac{\partial M}{\partial z} - oM \qquad (16)$$

where the first four terms have been defined. The last two terms are the sinking and oxidative losses of phytoplankton. In steady state, the sinking loss should be equivalent to the supply of "new" production, i.e., river discharge within the first two terms of eq.(15), and vertical input within the fourth term of eq.(15). Oxidation in the model will result in some recycling of particulate nitrogen (ammonification and nitrification) within the upper and lower layers.

Decomposition of organic matter within the open ocean eventually liberates CO_2 and NO_3 from sinking particles, forming the nitrate subsurface maximum at 500-1000m (recall Figs 3-5). In the Pacific Ocean, the particulate carbon and nitrogen fluxes at a depth of 1000m are 10% of those at 100m (MARTIN, KNAUER, KARL and BROENKOW, 1987). At sinking velocities, w_s, of 10m d^{-1} for large phytoplankton and 100m d^{-1} for fecal pellets, the mean daily decomposition rates, o, of falling particles over the 900m depth interval would be respectively 0.01 and 0.10d^{-1}.

Sinking rates of phytoplankton may accelerate during nutrient depletion (CULLEN and EPPLEY, 1981; BIENFANG, SZYPER and LAWS, 1983) and cell aggregation (SMETACEK, 1985), or decelerate during particle decomposition (CSANADY, 1986), however. During formulation of the initial conditions of the biological model, we thus explored a range in both sinking and decomposition rates of eq.(16) — a rate of 3m d^{-1} was chosen. Such a sinking rate of 3m d^{-1} over h_1 and h_2 layer thickness of 100m and 800m, together with upper and lower layer decomposition rates of 0.0050-0.0025d $^{-1}$ to simulate the increased refractory nature of organic matter in the aphotic zone (BERGER, FISCHER, LAI and WU, 1987), yield, for example, a survival rate of 16.7% for phytoplankton at a depth of 900m after 300 days in the model. Under certain situations, however, much higher sinking rates of 30-300m d^{-1} may prevail for aggregated picoplankton (LOCHTE and TURLEY, 1988).

Since the circulation model is a Lagrangian formulation with depth, the vertical velocity, w, is not an explicit term of eqs.(18)-(19). Transformation of eqs.(15)-(16) into the vertical coordinate of the circulation model by

$$\phi = (z - \eta)/h_1 \tag{17}$$

leads to

$$\frac{\partial h_1 N}{\partial t} = -\frac{\partial h_1 uN}{\partial x} - \frac{\partial h_1 vN}{\partial y} + \frac{1}{h_1^2}\frac{\partial}{\partial \phi} K_z \frac{\partial h_1 N}{\partial \phi} + h_1(-aMs^{-1} + oMs^{-1}) \tag{18}$$

and

$$\frac{\partial h_1 M}{\partial t} = -\frac{\partial h_1 uM}{\partial x} - \frac{\partial h_1 vM}{\partial y} + \frac{1}{h_1^2}\frac{\partial}{\partial \phi} K_z \frac{\partial h_1 M}{\partial \phi} - \frac{w_s}{h_1}\frac{\partial h_1 M}{\partial \phi} + h_1(aM + oM) \tag{19}$$

where η and h_1 were previously defined as the sea surface elevation and the thickness of the upper layer.

The movement of the depth of interface, $z_1 = h_1 - \eta$, is recorded in eqs.(18)-(19) by the changing vertical gradients of nitrate and chlorophyll at each grid point and time step, with respect to both the nitrate boundary condition at the pycnocline and the light regime at the surface. The sinking and decomposition terms of eq.(16) are also computed over h_2, the lower layer of the circulation model, to allow input of the surviving particles to the sea floor of the model. The circulation field of the lower layer is not applied to particles within h_2, i.e. the sinking debris falls in place after passing through the interface. The biological model thus consists of 20 layers within the upper layer of the circulation model and 1 additional layer of sinking, oxidizing particles within the stationary lower layer of this coupled physical-biological model.

The effects of temperature, light, and recycled nitrogen on algal growth are expressed in the fifth term of eq.(16) by

$$a = \mu_T \tanh\left[\alpha \frac{chl}{C} I(z)\mu_T^{-1}\right]\chi \tag{20}$$

where μ_T is the maximum, carbon-specific growth rate of phytoplankton, taken here as 4 cell

divisions d^{-1} for a temperature of 25°C (EPPLEY, 1972). This is an exponential growth rate of $0.12 h^{-1}$ over a 24 hour day, and is adjusted to the simulated photoperiod. We have not corrected this maximum growth rate for lower temperatures with depth or season.

The hyperbolic tangent function of light (PLATT and JASSBY, 1976) in eq.(20) does not contain a photoinhibition effect, as did our previous model of the Mid-Atlantic shelf (WALSH, DIETERLE and MEYERS, 1988a). Since most of the nitrate-based, "new" production would take place at depth in the deeper water column of the Gulf of Mexico model, however, we assumed that depression of algal growth by photoinhibition would be minimal. At the surface of the mouth of the Mississippi River, self-shading by phytoplankton in eq.(21) was similarly considered to be more important than photoinhibition.

The initial slope, α, of the general photosynthesis-light relationship (WALSH, 1988) in eq.(20) is taken to be 0.132 $\mu g\ C\ \mu g\ chl^{-1}\ hr^{-1}/\mu Ein\ cm^{-2}\ hr^{-1}$ (JASSBY and PLATT, 1976; PLATT and JASSBY, 1976; MALONE and NEALE, 1981). This parameter can be considered as the product of the maximum photon efficiency and the chlorophyll-specific, light absorption cross-section of the algal cell (BANNISTER and WEIDEMANN, 1984; GEIDER and OSBORNE, 1986). The latter property of the algal population is considered in the depth dependence of the *in situ* light field.

At depth, variation of light is effected by extinction as a result of water, k_w, absorption as a result of chlorophyll, k_m, and scattering as a result of particulates (including phytoplankton) over an average cosine light path. These processes are parameterized by

$$I(z) = I_0\, e^{-1.33\left[k_w z + k_m \int_0^z M(z)\, dz\right]} \tag{21}$$

Towards the blue end of the spectrum of photosynthetically-active radiation (PAR), the diffuse attenuation coefficient for water is taken as $k_w = 0.03 m^{-1}$. The spectral average of chlorophyll-specific absorption for an open-ocean community of phytoplankton in the Pacific is $k_m = 0.055$ $(mg\ chl)^{-1} m^2$ (K. CARDER, personal communication).

We assume this value typifies the algal communities of the Gulf of Mexico and multiply the product of this coefficient and the chlorophyll biomass by an average cosine value of 1/0.75 to obtain the diffuse attenuation coefficient of phytoplankton in our model. Using the chlorophyll biomass from a depth profile taken within the Loop Current by EL-SAYED and TREES (1980) and eq.(21), we obtained a 1% light depth, at the bottom of the conventional euphotic zone, of 88.5m, which is similar to their secchi-disk estimated value within ±5m. To include growth and nutrient uptake at the 0.1% light depths, we integrated "new" production down to the depth of the interface.

Because the coupled physical-biological models explore the consequences of an annual cycle of Loop Current dominated Gulf of Mexico circulation, seasonal changes in the surface light intensity and in photoperiod are included as biological forcings. The surface mean daily irradiance ($\bar{I}_0$) was determined at 25°N from the Smithsonian Meteorological Tables (REED, 1977):

$$\bar{I}_0 = \frac{1}{24} \int_{t=0}^{24} I_0(t)\, dt \tag{22}$$

Additionally, it was assumed that 43% of the total radiation is photosynthetically available radiation (PAR) and that the conversion factor from the tabulated values of joule $m^{-2} s^{-1}$ to $\mu Ein\ m^{-2} s^{-1}$ is 4.13 (MOREL and SMITH, 1977).

Daily photoperiod values (ℓ), in hours, were determined using the relationship of solar elevation angle, e, to tabulated values of the daily declination angle, ω at 25°N (e.g. KIRK, 1983):

$$\sin(e) = \sin(25°)\sin(\omega) + \cos(25°)\cos(\omega)\cos(n) \tag{23}$$

where n is the hour angle difference from local solar noon (15°h $^{-1}$); ℓ is derived from this by setting e=0, solving for n, and then multiplying by 2 for the number of daylight hours. Sunrise, $\lambda = (12\text{-}0.5\ell$).

Apportioning the daily mean PAR over the photoperiod for a given day is done assuming a sinusoidal relationship:

$$I_0(t) = I_m \sin^3[\pi(t-\lambda)\ell^{-1}] \tag{24}$$

where I_m is the solar noon maximum PAR value, found from the daily mean PAR by:

$$I_m = 24\,\bar{I}_0\left[\int_{t=\lambda}^{\lambda+\ell} \sin^3[\pi(t-\lambda)\ell^{-1}]\,dt\right]^{-1} \tag{25}$$

The monthly averages of I_m are presented in Table 2 as an index of the seasonal variation of light forcing in our coupled models.

The last formulation of our models is the nitrogen dependence, χ, of this daily light-regulated growth of phytoplankton. In contrast to our model of the uncoupled spring food chain of the continental shelf ecosystem off New York (WALSH *et al.*, 1988a), we assume here that nitrogen is not limiting the individual growth of a phytoplankton cell, i.e. there is no Michaelis-Menten expression for nutrient uptake in the present model. At a growth rate of 4 cell divisions d $^{-1}$, we assume that an individual algal cell is instead growing maximally on recycled nitrogen (GOLDMAN, MCCARTHY and PEAVEY, 1979), before consumption by a herbivore within a tightly coupled picoplankton-protozoan-bacterial food web (AZAM, FENCHEL, FIELD, GRAY, MEYER-REED and THINGSTAD, 1983). Nitrogen instead limits the amount of primary production, with the supply of new nitrogen determining the flux of possible export from the euphotic zone. The last term of eq.(20), χ, thus defines the oligotrophic nature of the nutrient dynamics of the Gulf of Mexico, where as much as 90% of the nitrogen demand of daily primary production may be met by dissolved ammonium, urea, and amino acids (EPPLEY and PETERSON, 1980).

In a model of new production, we must differentiate between the algal biomass grown on oceanic NO_3 and river effluent, i.e. N of eq.(18), and that synthesized from the recycled sources of nitrogen, by using χ, the ratio of new to total nitrogen uptake by the phytoplankton. This ratio can be expressed as a fraction of the ambient new nitrogen (PLATT and HARRISON, 1985) by:

$$\chi = \chi_m[1 - e^{-(\theta N \chi_m^{-1})}] \tag{26}$$

where $\chi_m = 0.83$ is the maximum ratio, i.e. assuming a minimal recycled production of 17%.

A nitrate concentration of 10μg-at NO_3 ℓ^{-1} at the interface depth yields a χ of 0.83 in a region where uptake of "new" nitrogen will be negligible as a result of light limitation. Near the mouth

of the Mississippi River, uptake of new nitrogen will be the largest, however, where both light and nitrogen are abundant. Our value of $\theta = 0.74 m^3 mg\text{-}at^{-1}$ simulates a subtropical oceanic habitat (LEWIS, HARRISON, OAKEY, HEBERT and PLATT, 1986), compared to $5.48 m^3 mg\text{-}at^{-1}$ for coastal waters (PLATT and HARRISON, 1985). As another unitless fraction, eq.(26) replaces our prior formulation of

$$\chi = \frac{N}{k_N + N} \tag{27}$$

where k_N was a half-saturation constant of this Michaelis-Menten expression for nutrient limitation (WALSH *et al.*, 1988a).

2.4. *Numerical techniques*

Solutions to eqs.(2)-(4) and (18)-(19) are obtained numerically, using finite-difference approximations to their time and space derivatives. The numerical scheme for eqs.(2)-(4) is similar to that of HULBURT and THOMPSON (1980), except that our time differencing is fully explicit. The scheme for eqs.(18)-(19) consists of a semi-implicit Crank-Nicholson method for the vertical mixing terms and an explicit, forward-in-time method for the remaining terms.

A staggered grid system is used for both the physical and biological models, with the state variables of layer thickness, h_i, pressure, P_i, nutrient, N, and phytoplankton, M, positioned in the center of each grid cell. The horizontal velocity component, u_i, is instead placed one-half grid increment to the east and west of each cell center, while v_i is located one-half grid increment to the north and south. Similarly, the vertical transfer processes, effected by K_z and w_s, are positioned one-half grid increment above and below the centroid of each of the 20 vertical cells.

The lateral boundaries of the models are drawn through either u or v points, where the appropriate normal velocity component is zero. Similar to eqs.(2)-(4), the flux boundary conditions for eqs.(18) and (19) then consist of zero orthogonal transfer of nitrogen and chlorophyll along the solid land-sea boundaries. Input of nitrogen from the Mississippi River is simulated as a continuous release into the three upper layers (~25m) of each of the two cells of the biological model, immediately adjacent to its mouth (the • of Fig.1), at a rate of 4.86×10^{12} g-at N h^{-1}. Instantaneous mixing of the river effluent is assumed over the changing volumes of these surface layers at each time step. The other import of nitrate and chlorophyll through Yucatan Strait involves the product of the boundary inflows with changing depth profiles of NO_3 and chlorophyll. The dissolved and particulate fluxes through the outflow port of Florida Strait are instead self-determined, using an upstream differencing formulation, which requires no external information (WALSH, 1988).

The fluxes at the surface of the sea are defined as

$$K_z \frac{\partial N}{\partial \phi} = K_z \frac{\partial M}{\partial \phi} = w_s M = 0 \tag{28}$$

At the bottom of the upper layer of the circulation model, i.e. the twentieth layer of the biological model, the time-invariant boundary conditions are $N_b = 10 \mu g\text{-}at\ NO_3\ \ell^{-1}$ and again $K_z \partial M/\partial \phi = 0$. As in the case of export through Florida Strait, the vertical particulate flux, as a result of sinking through the interface to the sediments, is self-determined, using our upstream formulation of the finite-difference equations at the boundaries.

The finite difference forms of eqs.(2)-(4) involved a central difference operator in space and time (e.g. HULBURT and THOMPSON, 1980; WALSH, 1988). To avoid numerical instabilities of this technique (HALTINER, 1971), the horizontal turbulence terms of eqs.(2)-(3) were evaluated at a prior time step to that of the other terms. The use of this leap-frog scheme can also lead to decoupling of the numerical solution at odd and even time steps (e.g. O'BRIEN, 1986). Euler's backward scheme (HALTINER, 1971) was thus employed for two consecutive time steps, at intervals of 900 time steps, to prevent this time splitting.

Our time step of the circulation model was determined by the Courant, Freidricks, Lewy (CFL) stability condition (O'BRIEN, 1986) of

$$\Delta t \leqslant \frac{1}{2}\left[\gamma^2\left(\frac{1}{\Delta x^2}+\frac{1}{\Delta y^2}\right)\right]^{-1/2} \tag{29}$$

where γ is the phase speed of the free surface gravity wave. With $\gamma = \sqrt{gD}$, where $D = h_1+h_2$ is the total depth in the model, and using a maximum depth of 3800m, eq.(29) leads to a time step of ~50 sec. A time step of 48 sec was consequently used over a duration of 3y to simulate penetration and shedding of eddies by the Loop Current.

Within the biochemical model, an upstream finite difference scheme is used for the advective terms of eqs.(18)-(19), following SMOLARKIEWICZ (1983). This scheme can be written, using eq.(18), as:

$$(h_{i,j}N_{i,j})^{t+\Delta t} - (h_{i,j}N_{i,j})^{t} = -[F(N^t_{i,j}, N^t_{i+1,j}, U^t_{i+1/2,j}) - F(N^t_{i-1,j}, N^t_{i,j}, U^t_{i-1/2,j})]\frac{\Delta t}{2\Delta x}$$

$$-[F(N^t_{i,j}, N^t_{i,j+1}, V^t_{i,j+1/2}) - F(N^t_{i,j-1}, N^t_{i,j}, V^t_{i,j-1/2})]\frac{\Delta t}{2\Delta y}$$

where (30)

$$U_{i\pm1/2,j} = u_{i\pm1/2,j}\left(\frac{h_{i,j}+h_{i\pm1,j}}{2}\right)$$

and

$$V_{i,j\pm1/2} = v_{i,j\pm1/2}\left(\frac{h_{i,j}+h_{i,j\pm1}}{2}\right)$$

The subscripts i and j are grid indices in the x and y directions respectively, while the superscripts, t and t+Δt, denote time levels. The general form of the operator F() is

$$F(N_{i,j}, N_{i+1,j}, U) = [(U + |U|)N_{i,j} + (U - |U|)N_{i+1,j}] \tag{31}$$

Although this first-order scheme introduces strong implicit diffusion, it is transportive, the phase errors are relatively small, it conserves mass, and is economical to use. The CFL stability condition for this scheme is

$$\Delta t \leqslant \frac{1}{2}\left(\frac{u^2_{i+1/2,j}}{\Delta x^2}+\frac{v^2_{i,j+1/2}}{\Delta y^2}\right)^{-1/2} \tag{32}$$

This is easily satisfied with a time step of 1h for maximum velocities of 1m s^{-1}.

The Von Neumann stability condition for the vertical mixing terms in eqs.(18) and (19) is, however,

$$\Delta t \leqslant \frac{\Delta z^2}{2K_z} \tag{33}$$

A maximum value for K_z of 66cm^{2}s^{-1} (Table 2), and the smallest Δz of 5m, suggests a time step of ~0.5h. To remove this time restriction, a semi-implicit Crank-Nicholson (O'BRIEN, 1986) method was employed for these terms.

It consists of

$$(h_{1i,j}N_{i,j,k})^{t+\Delta t} = (h_{1i,j}N_{i,j,k})^t + \frac{1}{\bar{h}^2_{1i,j}\Delta\phi}\,[K^t_{i,j,k-1/2}(\bar{N}_{i,j,k-1} - \bar{N}_{i,j,k}) - K^t_{i,j,k+1/2}(\bar{N}_{i,j,k} - \bar{N}_{i,j,k+1})] \tag{34}$$

where

$$\bar{N}_{i,j,k} = \frac{[(h_{1i,j}N_{i,j,k})^{t+\Delta t} + (h_{1i,j}N_{i,j,k})^t]}{2},$$

and

$$\bar{h}_1 = (h_1^t + h_1^{t+\Delta t})/2.$$

Here k is the grid index in the vertical dimension, with k=1 being the topmost layer of the model. Equation (34), with appropriate boundary conditions, reduces to a tridiagonal matrix, which can be solved using standard methods (WALSH *et al.*, 1988a).

The no-flux boundary conditions are incorporated in the model by assigning the values of N and M at fictitious exterior points to equal those just inside a particular boundary. The lower boundary value of N is incorporated using a one-sided, second order approximation for the first derivatives of N at the interface depth. This becomes

$$\frac{\partial N}{\partial \phi} \simeq \frac{1}{3\Delta\phi}\,(-8N_b + 9N_{b-1} - N_{b-2}) \tag{35}$$

where N_b is the value of N at the interface, and N_{b-1}, N_{b-2} are $1/2\Delta\phi$ and $3/2\Delta\phi$ above the interface depth. The remaining terms of eqs.(18)-(19) were approximated using an explicit, forward-in-time procedure (WALSH, 1988).

Consequently, numerical solutions of eqs.(18)-(19) were obtained with a time step of 1h over a duration of 1y within the coupled physical/biological models. The output of the third year results of the circulation model was the time-dependent circulation field of the biological model. Interpolating between the monthly entries of K_o and I_o in Table 2, the values of vertical mixing and incident radiation were changed hourly, while the flow field was updated daily. The initial conditions of algal biomass and nitrate were derived from steady-state solutions of the one-dimensional, depth-dependent form of eqs.(18)-(19) for the month of May (Table 2). Day 0 of the coupled biological/physical models is thus May 1.

2.5. *CZCS imagery*

To provide an additional check on the validity of our calculation, time series of Coastal Zone Color Scanner (CZCS)images were compiled for two 3.5 x 10^4km^2 areas of the eastern (Location G of Fig.1) and western (Location H) Gulf of Mexico, as well as over the whole basin (MÜLLER-KARGER, WALSH, DIETERLE and EVANS, 1988). Briefly, synoptic estimates of the concentration of pigments in surface waters of the Gulf were obtained from approximately 300 individual scenes between January 1979 and July 1982. This preliminary CZCS time series consists of pigment concentrations derived from ratios of the blue (443nm) or blue-green (520nm) water-leaving radiances to the green radiance (550nm) — see GORDON, BROWN, EVANS, BROWN, SMITH, BAKER and CLARKE, 1988, and references therein. The pigment estimates are actually the concentration of chlorophyll a, phaeopigments, and dissolved organic matter.

The CZCS data were first processed at 1/16 of their original 1km spatial resolution by OTIS BROWN and BOB EVANS at the University of Miami. These pigment concentrations were then binned spatially into 20km x 20km squares, with 30 day composites based on congruent images, mapped to a cylindrical equidistant projection — see Fig. 26 as an example. A time series of the arithmetic means of the monthly pigment concentrations are then presented in Fig. 27 for three areas of interest: the entire Gulf of Mexico, an eastern region centered at 24°N, 86°W, and a western one centered at 25°N, 93°W.

These CZCS spatial composites and time series provided an estimate of the average pigment concentration within the first optical depth of the water column (at most 10m). Thus, we compared these satellite estimates with results of the model by taking the arithmetic mean each day at noon of the simulated chlorophyll concentration of the first layer over the same spatial domains. Shipboard validation data of these chlorophyll fields are available from cruises taken during February 1980 and 1981 (EL-SAYED and TREES, 1980; ORTNER *et al.*, 1984).

3. RESULTS

After formulation of the initial states and boundary conditions, the time-dependent inputs of N, as a result of circulation and river discharge, were either accumulated in the water column as N and M, remineralized, or transferred to the sediments as sinking losses of M. The phytoplankton, M, are not consumed by herbivores, since neither grazing pressure, nor metazoan excretion, are explicit processes of eqs.(18)-(19) for estimation of "new" production. Accordingly, fecal pellets do not exit the simulated water column. The coupled physical-biological models nevertheless provide an enormous 3-dimensional array of numbers, varying from 2-21 layers at 2193 active grid points over time steps of 48-3600s for 1-3y of simulated time. To digest our results and their implications, we present them in three sections: 2-dimensional output of the circulation model, 1-dimensional output of the biological model, and 3-dimensional output of the coupled physical-biological models. Locations of representative time series are shown in Fig.1.

3.1. *Circulation model*

Integration of eqs.(2)-(4) was performed over 1080 days of simulated time (Fig.9), assuming an initial state of no motion throughout the basin. Inflow across Yucatan Strait was increased linearly for a period of 30 days to a value of 30Sv. After this spinup, the circulation patterns exhibit a cycle of intrusion, westward bending, and finally eddy separation of the Loop Current in the Gulf. This is similar to the numerical results of HULBURT and THOMPSON (1980) and to the physical

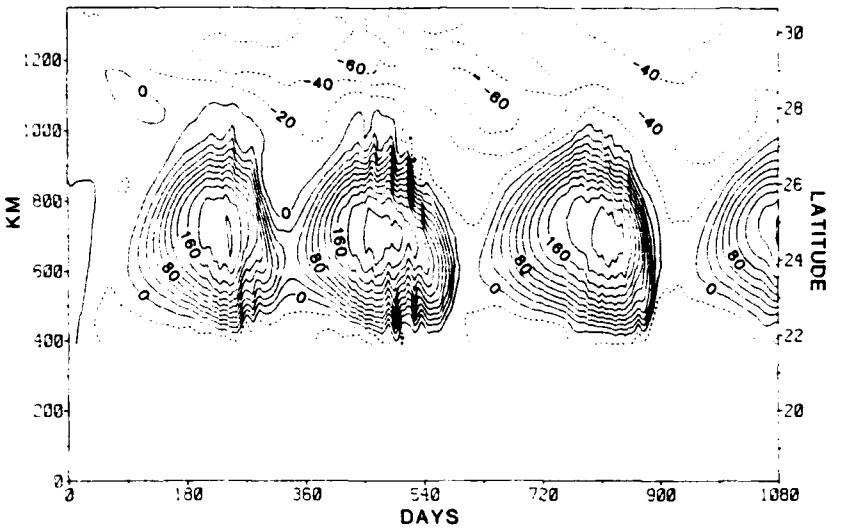

FIG.9. Interannual variation in pycnocline height across a north-south section of the Gulf of Mexico, between the Yucatan peninsula and Pensacola, Florida - see Fig.1.

results of SUGIMOTO and ICHIYE (1988). Flows of ~90cm s^{-1} were calculated for individual snapshots of the Loop Current and its anticyclonic eddies, while weaker currents of <10cm s^{-1} were associated with cyclonic eddies at the margins of the basin (Fig.10a).

Figure 9 is a plot of the relative pycnocline depth as a function of time along a north-south section, 40km west of the inflow port (see Fig.1 for location), over the 1080 days of simulated time. The pycnoclines in this and following figures are plotted as the deviation of the pycnocline from its initial position at 200m, with positive values indicating a deeper pycnocline as a result of downwelling. The negative values of Fig. 9 denote upwelling on Campeche Bank and the northwest Florida shelf. Figure 9 also shows approximately 3-1/2 cycles of Loop Current penetration and eddy shedding, with an average period of 309 days. Our near annual cycle of the simulated Loop Current conforms to mean hydrographic (ELLIOTT, 1982) and satellite (AUER, 1987) estimates of an annual cycle of major eddy formation by the Loop Current.

A look at one such cycle, beginning at day 10 of the third annual event (Fig.9), is shown in Figs 10b and 11. The pycnocline displacement field in Fig. 10b shows the Loop Current with minimal penetration into the Gulf, similar to field observations in January 1952 (Fig.5) and May 1972 (Fig.15a). An anticyclonic eddy is centered just north of Campeche Bank; the eddy had detached from the Loop Current approximately 10 days earlier. The shape of this initial eddy is elliptical (Fig.10b), becoming more so (Fig.11b), as it approached the Mexican coast (KIRWAN, LEWIS, INDEST, REINERSMAN and QUINTERO, 1988). Using the distance between speed maxima, V_m of Fig.10a, this recently-shed eddy had a north-south diameter of 232km and an east-west diameter of 354km. ELLIOTT (1982) found rms radii of 183km in a study of three anticyclones formed in 1966-1967, while AUER (1987) reported a mean initial diameter of 307km in his study of 1981-1985 Loop Current rings.

HULBURT and THOMPSON (1980) suggest that a typical north-south diameter for Loop Current eddies should be of the order $d = \sqrt{V_m/\beta} \simeq 225$km, if a value of $V_m = 1$m s^{-1} is used, where β is defined in eq.(9). The upper layer velocity field (Fig.10a) shows the dominant circulation

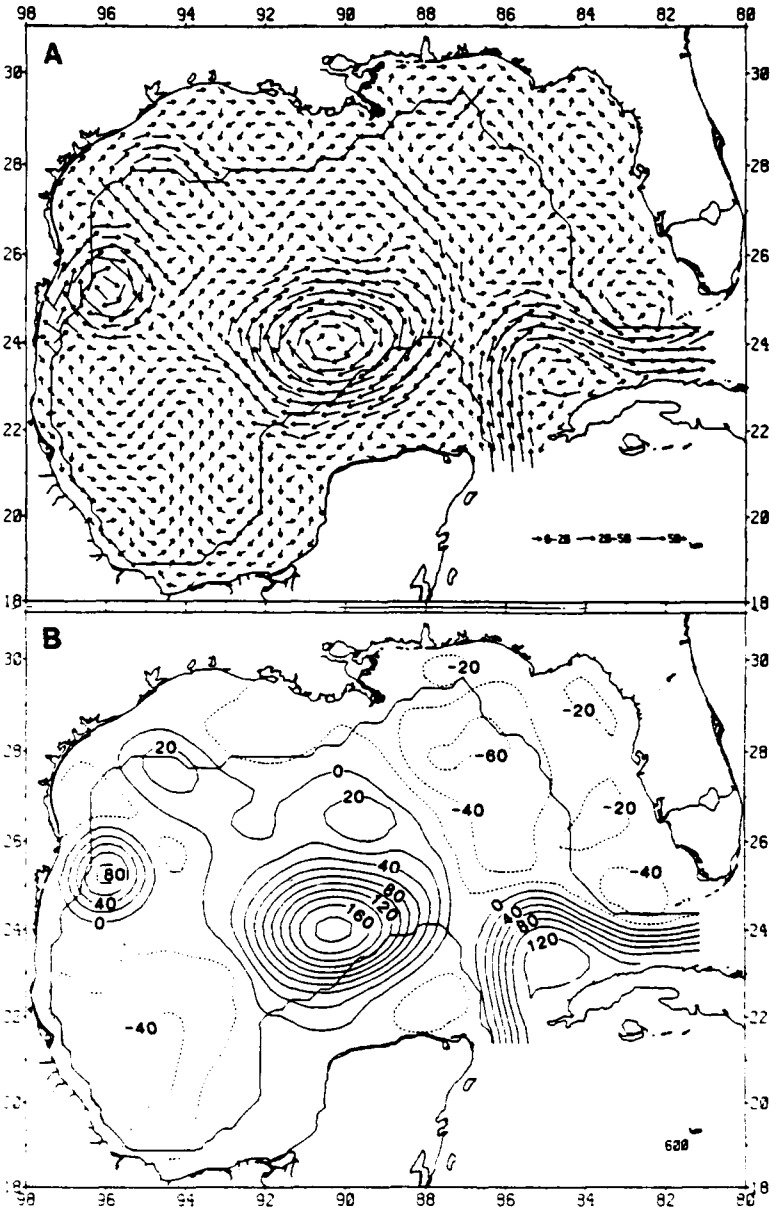

FIG. 10. The distribution of (A) surface currents in relation to (B) pycnocline height within the Gulf of Mexico during day 10 of the third penetration cycle of the Loop Current (see Fig.9).

patterns associated with the Loop Current and its newly formed anticyclonic eddy. A fairly strong anticyclonic cell is also evident along the Texas-Mexican coastline. This additional cell is a remnant of an eddy spawned during the second penetration cycle of the Loop Current (Fig.9). Simulated currents within the Loop Current and the Campeche Bank anticyclonic eddy reach speeds of 90cm s^{-1}, similar to HULBURT and THOMPSON's (1980) formulation of a trajectory of

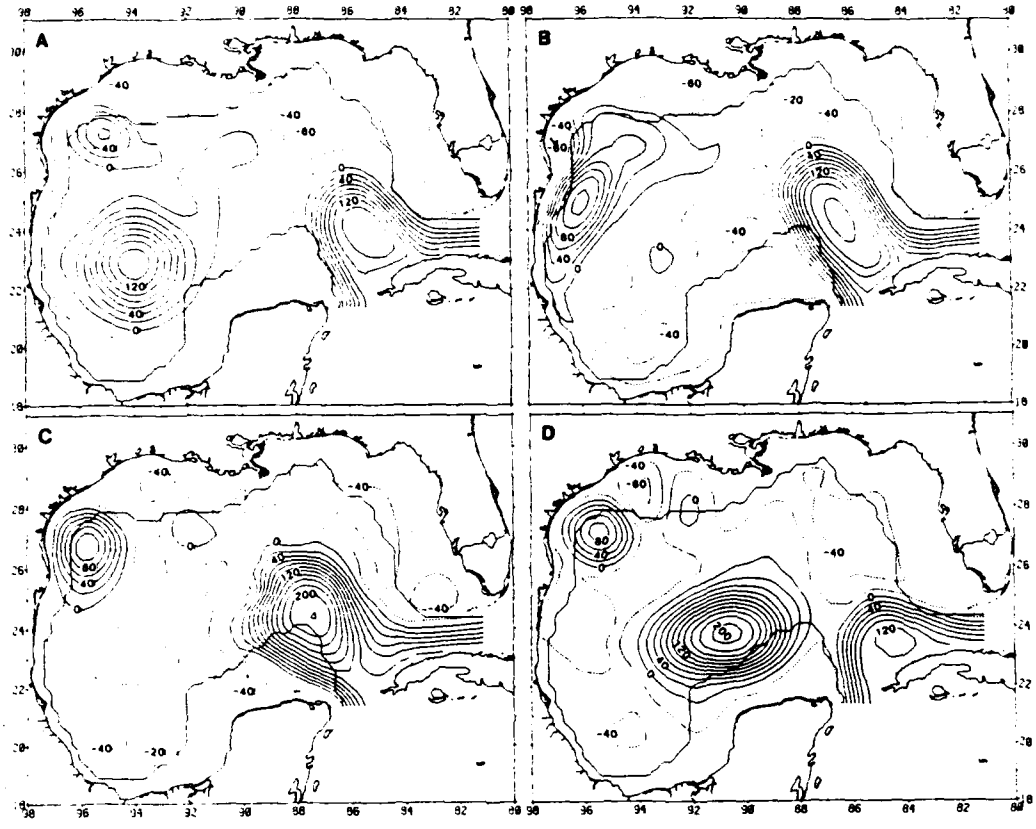

FIG. 11. Annual variation of pycnocline height within the Gulf of Mexico on days (A) 90, (B) 170, (C) 250 and (D) 330 during a penetration cycle of the Loop Current.

constant absolute vorticity. These simulated flows are also in accord with near-surface geostrophic speeds of ~100cm s $^{-1}$ calculated by NOWLIN and HUBERTZ (1972) from hydrographic observations of both the Loop Current and an anticyclonic eddy.

Figure 11 shows subsequent pycnocline displacement fields at 80-day intervals from day 10 of the third penetration cycle (Fig. 10b); the associated currents are shown in Fig. 20. At day 90, the Loop Current has penetrated approximately 150km farther into the Gulf, with the pycnocline deepening to 340m in the center of the Loop (Fig. 11a). The anticyclonic eddy, previously located north of Campeche Bank, moved 350km west-southwest to the northern part of the Bay of Campeche. This movement corresponds to a translation speed of ~5cm s $^{-1}$, similar to observations of 4-6cm s $^{-1}$ for 1980-1985 Loop Current rings (AUER, 1976; KIRWAN *et al.*, 1988). This motion also corresponds to the nondispersive internal Rossby wave speed, c, approximated by $c = \beta g' h_1 / f^2$, where all terms are previously defined, if a value of $h_1 = 300$m is used.

By day 170 (Fig. 11b), the Loop Current is near its maximum northern penetration into the Gulf, reaching 27°N, if the zero isopleth of the pycnocline displacement field is used. Within the center of the Loop Current, the pycnocline has been further depressed to a depth of 380m, the same

displacement as the center of the shed eddy on day 10 (Fig.10b). Also, with westward movement no longer possible, the eddy previously in the Bay of Campeche has moved north to a position off the continental slope southeast of Brownsville, Texas, similar to observations of rings in 1980 and 1982 (KIRWAN *et al.*, 1988).

By day 250 (Fig.11c), this eddy has moved to the northwestern corner of the Gulf. With the shelf turning eastward there, the eddy can move no farther and slowly dissipates (Fig.11d). During its sojourn across the western Gulf of Mexico, the depressed center of the anticyclonic eddy rose from a depth of 380m on day 10 (Fig.10b) to 280m on day 330 (Fig.11d), yielding apparent upwelling rates of 0.3-0.4m d^{-1}. Comparable upwelling rates of ~1m d^{-1} occur within decaying warm core rings of the Gulf Stream (FRANKS, WROBLEWSKI and FLIERL, 1986). Thus, the anticyclonic rings of the Loop Current may be loci of enhanced production in the oligotrophic western Gulf of Mexico.

Back in the eastern Gulf of Mexico, the Loop Current has moved westward a total distance of approximately 100km by day 250 (Fig.11c), with the closed center taking on a more circular shape. Several small waves can be seen on the eastern wall of the simulated Current, preceding the separation of the next anticyclonic ring. These have also been inferred from satellite imagery and hydrography (VUKOVICH and MAUL, 1985). Satellite temperature data in October and December 1976 (VUKOVICH *et al.*, 1979) were used to estimate the northward extension of the Loop Current in November 1976 (Fig.12a), which is similar to day 250 of the simulation (Fig.11c). Note the inferred wave at the cyclonic edge of the Loop Current, demarcated by the 100m depth of the 22°C isotherm during the *Researcher* cruise (Fig.12a).

By day 330 (Fig.11d) the penetration cycle of the Loop Current is complete. The Loop Current, having extended farther to the west, has shed another eddy and retreated, leaving a circulation pattern very similar to that seen on day 10 (Fig.10b). The areal extent of 40m upward displacement of the pycnocline at the west Florida shelf-break is minimal under this situation, compared to more northward penetration of the Loop Current (Figs11a, 11b and 11c). If light and wind forcing were minimal at this time as well, we might expect little primary production or export to the sediments. Since the shedding cycle of the Loop Current varies interannually from 4 to 16 months between generation events (AUER, 1987), however, we must first sort out the seasonal effects of incident radiation and vertical mixing on algal growth, before introducing the additional complexity of upwelling and downwelling events.

3.2. *Biological model*

A monthly time series of temperature, phosphate, and chlorophyll was collected during 1960 (ALEXANDER, STEELE and CORCORAN, 1962) in 800m of water on the eastern side of the Florida Current (25°33'N, 79°25'W) near Cat Cay, Bahamas (Location E of Fig.1), where upwelling, as a result of cyclonic eddies, should be minimal. The depth of the 22°C isotherm (recall Fig.7) remained at 165-175m throughout this time series, except for June 1960, when an upward vertical displacement of 25m occurred. The 19°C isotherm moved up 60m that month to a depth of 140m.

Concomitantly, a subsurface chlorophyll maximum of >0.5μg chl ℓ^{-1} and phosphate depletion occurred in June 1960. We deleted the data from this month in Figs 13b and 14b, in a comparison of the seasonal results from the biological model, where we held the depths of the interface constant at respectively 200m (Figs 13a and 14a) and 100m (Figs13c and 14c). Using a Redfield dissolved N/P ratio of 15/1, we also converted their phosphate data of the aphotic zone to equivalent nitrate concentrations in Fig. 14b.

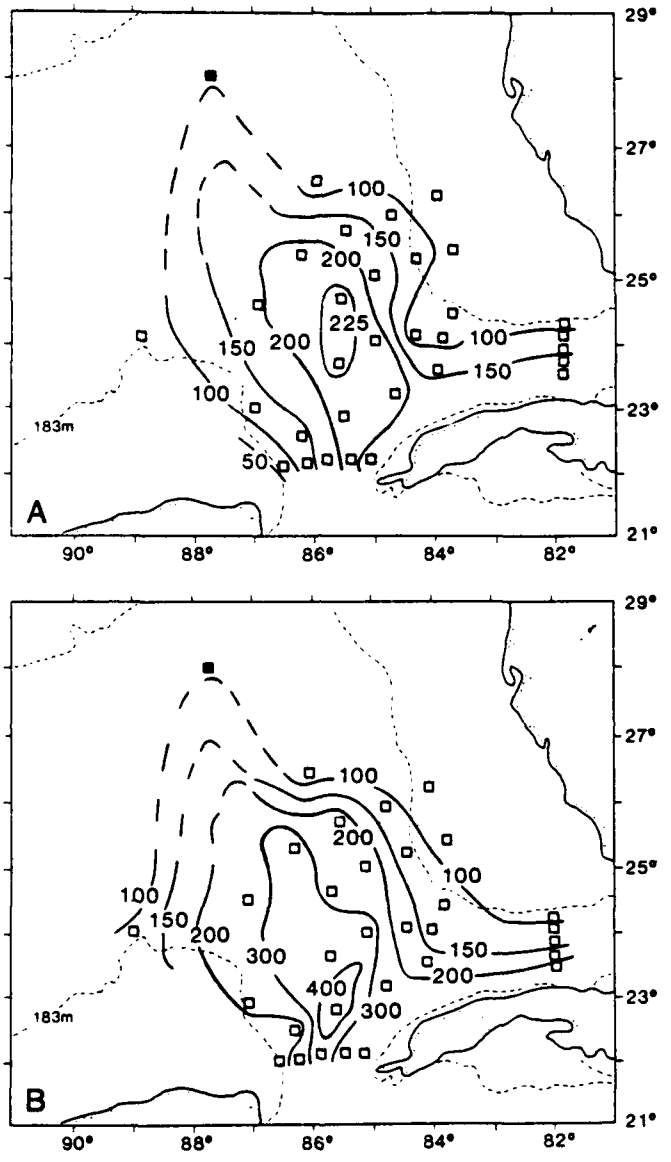

FIG. 12. The depths of (A) the 22°C isotherm and (B) the 5 μg-at ℓ^{-1} isopleth of nitrate within the eastern Gulf of Mexico during November 1976, based on shipboard and satellite (■) data.

Surface chlorophyll concentrations of 0.30 μg ℓ^{-1} in January and 0.03 μg ℓ^{-1} in August off Cat Cay (Fig. 13b) are reproduced by the model, when the interface depth is held constant at 200m (Fig. 13a). Concordance of model and field results of the temporal change in algal biomass implies that the minimum chlorophyll concentration of ~0.03 μg chl ℓ^{-1} is the "steady-state" result of grazing and growth from recycled nitrogen. Addition of new nitrogen as nitrate by vertical mixing in the model, modified by eq. (26), leads to observed increases of algal biomass, which are not grazed, but available for export instead to the aphotic zone, demarcated by the dotted lines in Figs 13a and 13c.

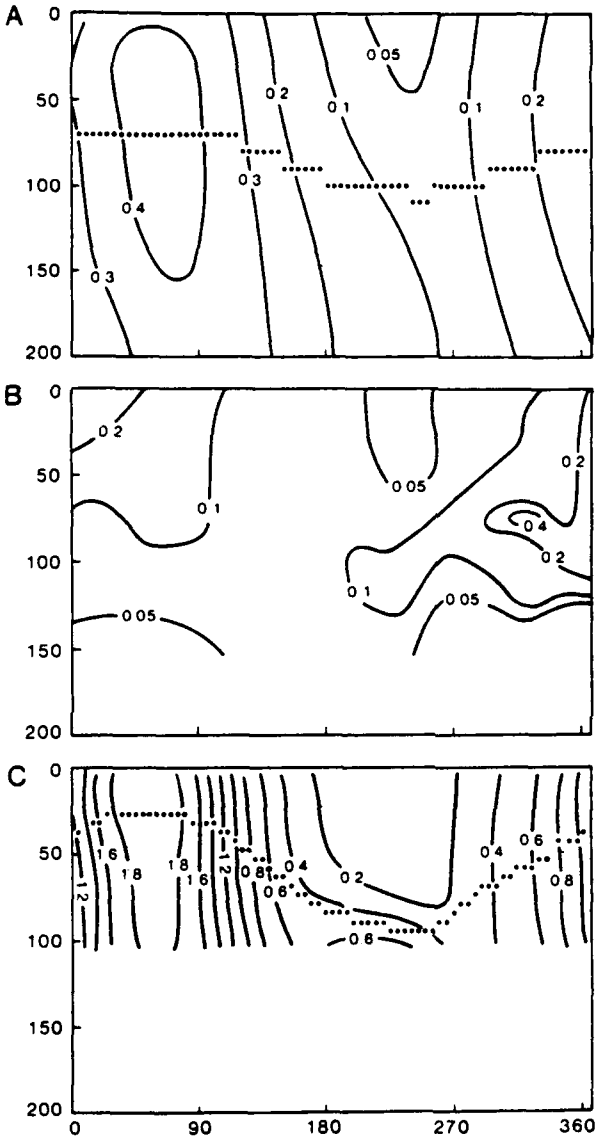

FIG. 13. Annual variation of chlorophyll both in the simulated Gulf of Mexico, when the pycnocline depth is held constant at (A) 200m and (C) 100m and in (B) the Florida Current off the Bahamas; the euphotic zone depth is denoted by (●).

Subsurface chlorophyll maxima of 0.4μg ℓ^{-1} (Fig.13b) are also reproduced by the model (Fig.13a), but with poor phasing between observation and theory. Such discrepancy in the timing of midwater chlorophyll maxima may reflect inadequate sampling of the water column, both with bottle casts in 1960, and with vertical resolution of mixing in the model. For example, the mean depths of the 1.5μg-at NO_3 ℓ^{-1} isopleth of nitrate, averaged over the year, are equivalent, ~160m, in the 200m case of the model (Fig.14a) and off Cat Cay (Fig.14b). The apparent vertical excursion of the surrogate 1.5μg-at NO_3 ℓ^{-1} isopleth from depths of >200m to 125m off Cat Cay

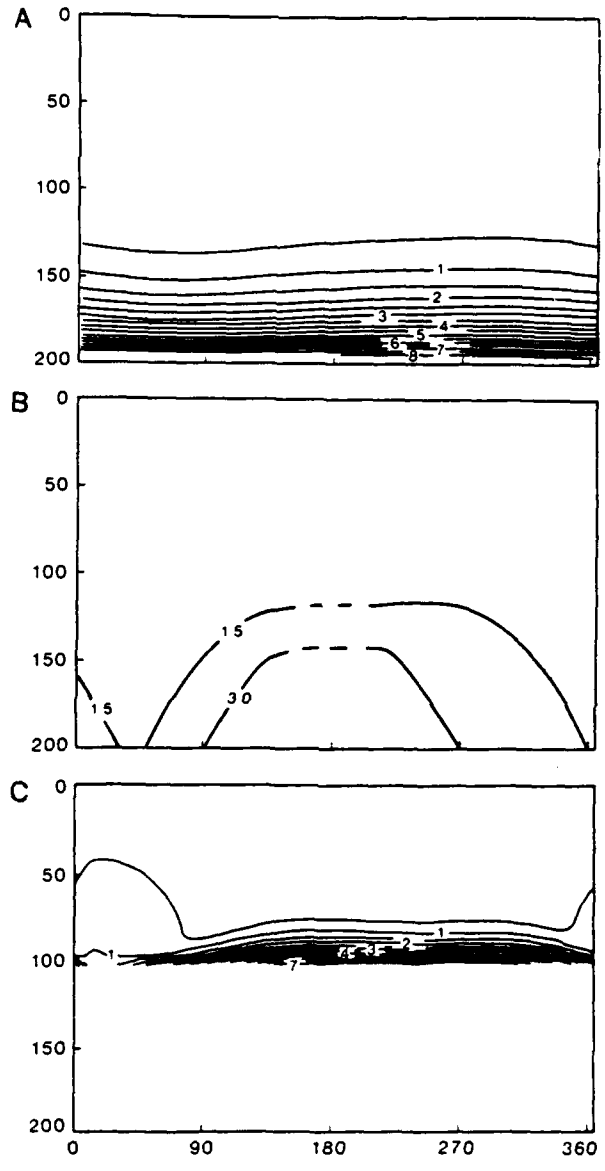

FIG. 14. Annual variation of surrogate nitrate (N/P = 15/1) both in the simulated Gulf of Mexico, when the pycnocline depth is held constant at (A) 200m and (C) 100m and in (B) the Florida Current off the Bahamas.

(Fig. 14b) may reflect a time-dependent flux of nitrate across the pycnocline of the real ocean. In the model, the cross-pycnocline flux was held constant in these initial cases.

Upward movement of the model's interface depth, e.g. Figs 13c and 14c, allows greater nitrate concentration at shallower depths (Fig. 14c). A stronger seasonal signal in the depth of the

0.5μg-at NO_3 ℓ^{-1} isopleth results from increased phytoplankton activity within the euphotic zone. When the depth of the interface is held constant at 100m in this second case, however, the seasonal cycle of simulated algal biomass (Fig.13c) continues to reflect the change of the mixed layer depth from 100m in January to 24m in August, rather than the opposite seasonal variation of light, which is never less than a maximum daylight value of 696μEin $cm^{-2}h^{-1}$ (Table 2).

With greater nitrate concentrations at the bottom of the euphotic zone in the second case (Fig.14c), the simulated chlorophyll stocks increase about fivefold (Fig.13c) over those of the first case (Fig.13a). The seasonal cycle of the depth of the euphotic zone is also more pronounced, ranging from 25m to 100m. The annual sinking loss of algal biomass across the pycnocline in the first case of a 200m interface depth was 0.2g chl $m^{-2}y^{-1}$, compared to the much higher value of 1.0g chl $m^{-2}y^{-1}$ after upward movement of the pycnocline to a constant depth of 100m in the model. Using a range in C/chl ratio of 50/1 to 100/1 for living phytoplankton and detritus in the Florida Current (STEELE, 1964), these annual inputs to the aphotic zone represent respective carbon fluxes of 10-20 and 50-100g C $m^{-2}y^{-1}$.

About 160 miles farther north of the Cat Cay time series (Figs13b and14b), a sediment trap was moored at 660m near 27°42'N,78°54'W during June, 1977 (HINGA, SIEBURTH and HEATH, 1979).Upwelling in the water column above this trap on the eastern side of the Florida Current near Walker's Cay,Bahamas, should be minimal. The flux of particulate organic carbon estimated at this sediment trap was 14.4mg C $m^{-2}d^{-1}$, or 5.2g C $m^{-2}y^{-1}$, compared to 10-20g C $m^{-2}y^{-1}$ exiting the euphotic zone of the biological model, where the interface depth is held constant at 200m (Figs13a and 14a). Assuming a constant C/N ratio of 10/1 for particulate matter in the low carbon sediments on the upper slope of this region (Fig.8), the equivalent nitrogen fluxes at 200m in the model and 660m in the sea are 1-2 and 0.5g N $m^{-2}y^{-1}$. The observed C/N ratio of the trapped particulate matter was 46/1, indicating significant remineralization of presumably slow sinking organic matter within the water column.

Another sediment trap mooring at a depth of 1345m on the slope off Myrtle Beach, South Carolina, at 33°30'N,76°15'W (HINGA *et al.*, 1979), yielded 29.8mg C $m^{-2}d^{-1}$ or 10.8 g C $m^{-2}y^{-1}$. Despite the greater descent, the surviving particulate matter had a lower C/N ratio of 23/1. The higher flux of carbon at greater depth may represent active transport by diel migrators (ANGEL, 1989) here and unsampled off the Bahamas. Alternatively, this mooring was located both near the western edge of the Florida Current, where cyclonic eddy-induced upwelling is expected (LEE, ATKINSON and LEGECKIS, 1981), and downstream of the Charleston Bump, where topographic upwelling also prevails (BANE and DEWAR, 1988). Using a generalized depth-flux relationship (MARTIN *et al.* 1987), we obtain possible fluxes of 21.6g C $m^{-2}y^{-1}$ at 660m and 86.4g C $m^{-2}y^{-1}$ at 100m in the water column above the trap at 1345m. With the model's interface depth held constant at 100m in the second case (Fig.13c), reflecting increased upwelling, the predicted flux of 50-100g C $m^{-2}y^{-1}$ at a depth of 100m is similar to that extrapolated from the field data off South Carolina.

We thus expect two sources of variance in the results of the coupled physical/biological models: temporal as a result of seasonal vertical mixing effected by wind, and spatial as a result of upwelling effected by the Loop Current. For example, the nitrate flux across the pycnocline into the 20th layer of the biological model ranges from 0.1 to 0.6g-at $NO_3m^{-2}y^{-1}$ in respectively the 200m and 100m cases of constant interface depth (Figs 14a and 14c). The former case is similar to microscale velocity shear estimates of a nitrate flux of 0.05 g-at $NO_3m^{-2}y^{-1}$ into the euphotic zone southeast of the Azores (LEWIS *et al.*, 1986), where mesoscale eddies are less energetic (STOMMEL, 1987). In another study (FASHAM, PLATT, IRWIN and JONES,1985) southwest of the Azore Islands, a similar low flux of 0.03g-at $NO_3m^{-2}y^{-1}$ was obtained. The latter case of

the model, however, is equivalent to ^{3}He estimates of a nitrate flux of 0.6g-at $NO_3 m^{-2} y^{-1}$ into the euphotic zone off Bermuda (JENKINS, 1988), where mesoscale upwelling events (WOODS, 1988) may be the major supply mechanism.

If the biological model is run for a year with a constant interface depth of 400m, however, i.e. in the center of an anticyclonic eddy,the nitrate flux into the 20th layer is only 0.05g-at NO_3 $m^{-2} y^{-1}$; the simulated depth profile of nitrate then also approximates the field observations south of the Azores (FASHAM *et al.*, 1987; LEWIS *et al.*, 1986). In this third case of the model, the winter maximum of algal biomass was tenfold less than that of the second case of a 100m interface depth (Fig.14c), while the seasonal variation was about threefold, from >0.15μg ℓ^{-1} in January to <0.05μg ℓ^{-1} in August. Upward movement of the interface depth from 400m to 100m thus leads to the same range of algal biomass variation as that effected by seasonal changes in wind forcing and vertical mixing (Table 2), when the interface depth is held constant at 200m.

To distinguish between the biochemical consequences of the annual cycle of wind forcing and the subannual periodicity (~310 days) of the Loop Current penetration and eddy shedding, we ran three cases of the coupled physical/biological model. Over the same cycle of Loop Current advance and retreat discussed in the first section of our results, the biological response to this time-dependent nutrient addition was explored with (1) a constant K_o and h_m of 50cm^{2}s^{-1} and 100m, i.e. January; (2) a constant K_o and h_m of 25cm^{2}s^{-1} and 25m, i.e. August; and (3) the monthly variation in both parameters using the values of Table 2. The April and November mixed layer depths and vertical eddy diffusivities are the same (Table 2), for example, such that the observed nitrate fields of early May 1972 (Fig.15b) and November 1976 (Fig.12b) reflect absence and presence of the Loop Current in the eastern Gulf of Mexico, rather than seasonal changes in vertical mixing. If the vertical mixing regimes of January or August were operative, however, the biological utilization rates would be different from those under April or November conditions.

3.3. *Physical-biological models*

The biological model is initialized using the circulation field on day 10 of the third cycle of Loop Current penetration (Fig.10), and a May 1 value (Table 2) for daily incident radiation. For the seasonal wind mixing cases, May 1 values were used for the mixed-layer depth and eddy viscosity as well. Day 170 of the coupled physical/biological models thus represents October 8 in terms of daily incident radiation, mixed-layer depth, and eddy viscosity for the two seasonal wind mixing cases (Fig.16a,b). In the winter and summer cases of constant mixing, however, day 170 instead represents January (Fig.16c) and August (Fig.16d) mixing regimes, coupled to October light conditions.

Without nutrient input from the Mississippi River, the simulated nitrate on day 170 of the first seasonal case (Fig.16a) matches the observed nitrate distribution within the Loop Current during November 1976 (Fig.12b). The 5μg-at ℓ^{-1} isopleth of NO_3 is found at >300m depths within the cores of the simulated (Fig.16a) and observed (Fig.12b) Loop Current, but at <150m depths at the shelf break off the Yucatan Peninsula and West Florida. Nitrogen from the Mississippi River stimulates phytoplankton growth in the second seasonal case of the model (Fig.17b), such that little nitrate is found on the Louisiana shelf (Fig.16b); otherwise the nitrate fields on day 170 of these two seasonal mixing cases are identical (Figs 16a,b). The contour levels of Fig. 17 are 0.05, 0.10, 0.25, 0.50, 1, 2, 3, 4, and 5μg chl ℓ^{-1}.

The depth of the surface mixed layer in January is twice that of October (Table 2), however, such that the January mixing case leads to greater nutrient uptake (Fig.16c) and algal standing stock (Fig.17c) than the seasonal October cases (Figs 16a,b and 17a,b). The 5μg-at ℓ^{-1} isopleth

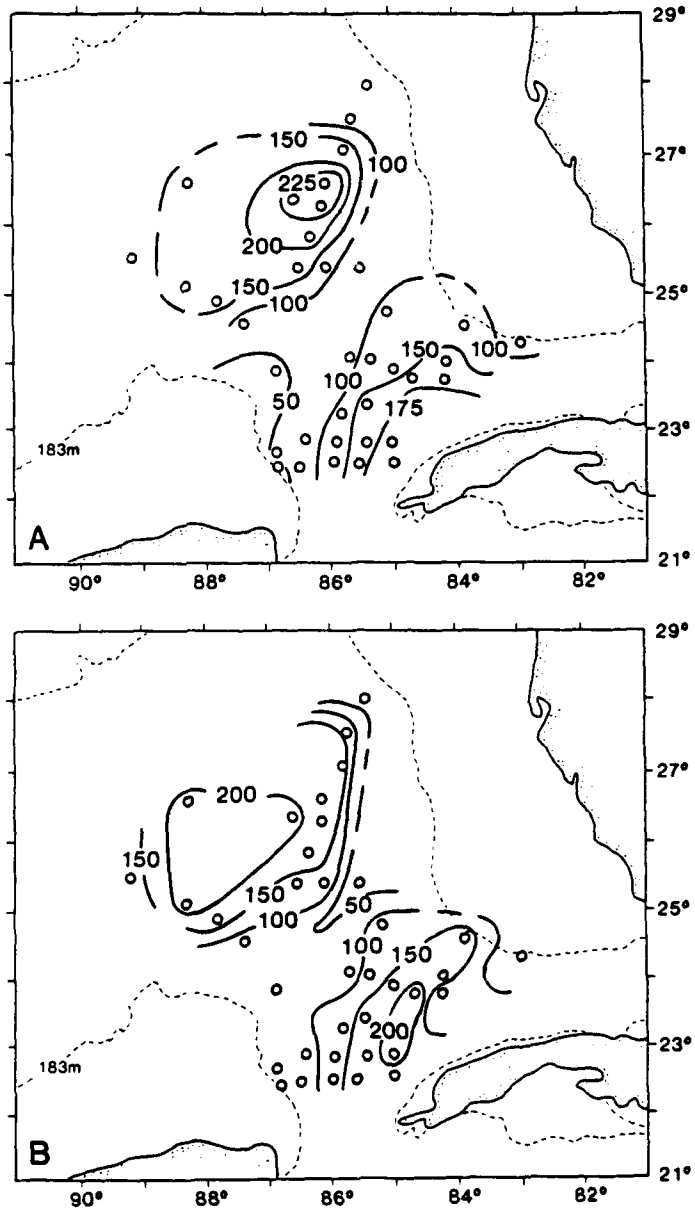

FIG.15. The depths of (A) the 22°C isotherm and (B) the 5 μg-at ℓ^{-1} isopleth of nitrate within the eastern Gulf of Mexico during May 1972, based on shipboard data.

of the January case on day 170 is found deeper within the Loop Current, within the previously-shed anticyclonic rings off Mexico, and on the West Florida shelf (Fig.16c), while 2- to 3-fold greater chlorophyll concentrations are simulated at the surface of the model (Fig.17c).

In contrast, the August depth of the surface mixed layer is half that of October (Table 2), such that the August mixing case leads to smaller nutrient uptake (Fig.16d) and algal standing stock

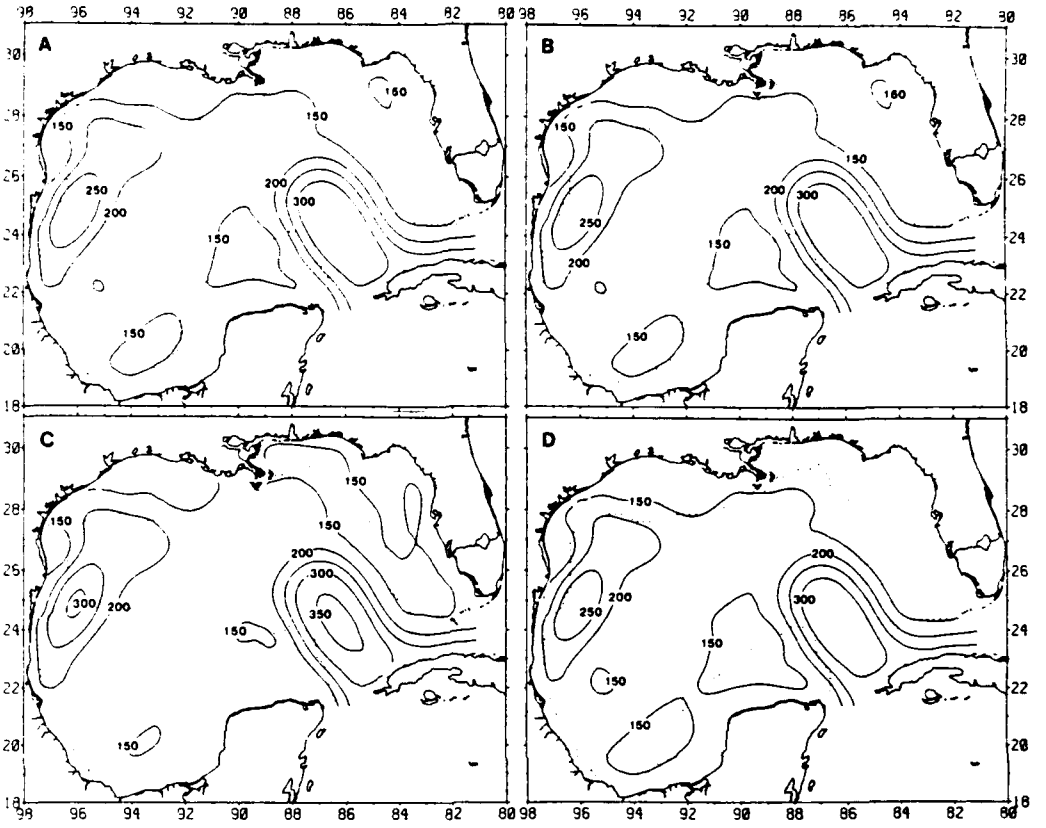

FIG. 16. The depth of the 5 μg-at ℓ^{-1} isopleth of nitrate within the Gulf of Mexico on day 170 when the simulated Loop Current is at 27°N, under (A) seasonal wind forcing (Table 2), (B) seasonal wind forcing and Mississippi River effluent, (C) January mixing and River, (D) August mixing and River.

(Fig.17d) than the seasonal October cases (Figs 16a,b and 17a,b). The regions of the simulated Gulf of Mexico on day 170, where the depth of the 5 μg-at ℓ^{-1} isopleth of nitrate is shallower than 150m, are more extensive in the August case (Fig.16d), while half the amount of chlorophyll is found in the Loop Current and its rings (Fig.17d). The observed distribution of surface chlorophyll in Florida Strait during October-November is ~0.1 μg chl ℓ^{-1} (Fig.13b), similar to only the seasonal mixing cases (Fig.17a,b), suggesting that the time-invariant January (Fig.17c) and August (Fig.17d) mixing cases are unrealistic.

For example, day 330 in our coupled physical/biological simulation represents March 17, when the depth of the surface mixed layer is 86m, similar to that in January, but almost 4-fold that of August (Table 2). The simulated nitrate fields of the seasonal wind mixing cases (Fig.18a,b) and the January case on day 330 (Fig.18c) then more closely resemble each other than either the August case (Fig.18d) or May observations (Fig.15b), when the mixed layer depth is at 41m (Table 2). The rest of our discussion is thus restricted to the results of the second seasonal mixing case, i.e. with inclusion of anthropogenic nutrients from the Mississippi River.

Day 90 of the seasonal mixing case with Mississippi River effluent (Fig.19a) represents July 20, when the depth of the surface mixed layer is the same as in August (Table 2). The surface eddy

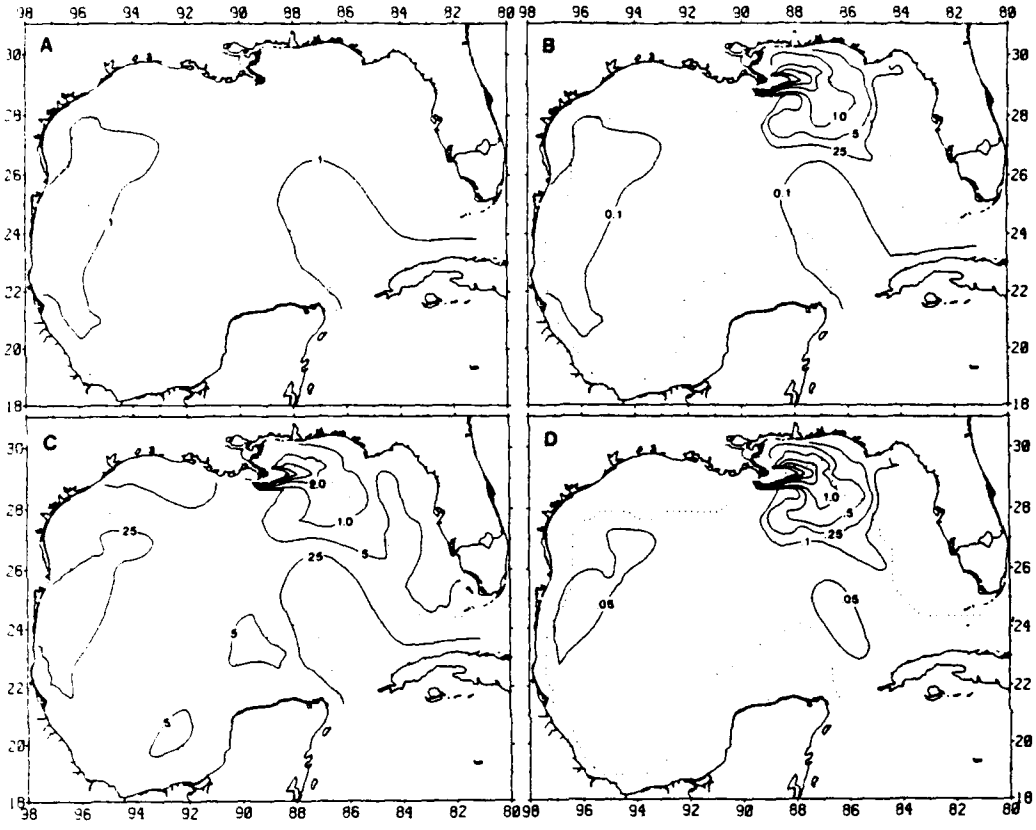

FIG.17. The distribution of surface chlorophyll within the Gulf of Mexico on day 170 when the simulated Loop Current is at 27°N, under (A) seasonal wind forcing (Table 2), (B) seasonal wind forcing and Mississippi River effluent, (C) January mixing and River, and (D) August mixing and River.

viscosity of July is larger than August, however, such that the surface chlorophyll within the Loop Current and the western Gulf of Mexico is slightly higher on day 90 of the seasonal case (Fig.19a), compared to day 170 of the time-invariant August case (Fig.17d). Although the Loop Current had penetrated ~150km north into the Gulf of Mexico at this time (Fig.11b), the vertical exchange processes were too weak on day 90 to allow a surface signal of enhanced chlorophyll abundance at the cyclonic edges of the western boundary current.

By day 170, i.e. October 8, the Loop Current had reached 27°N (Fig.11c), the surface mixed layer had deepened twofold (Table 2), and the cyclonic edges of the Loop Current were demarcated by the 0.1 μg chl ℓ^{-1} isopleths at the surface in the eastern Gulf of Mexico (Fig.19b). As a result of strong southeastward flow, e.g. day 170 (Fig.20b), along the shelf-break, from the mouth of the Mississippi River to off Tampa Bay [in contrast to days 10 (Fig.10a) and 90 (Fig.20a)], the 1.0 μg chl ℓ^{-1} isopleth of the Mississippi phytoplankton plume had also moved southeast 100km along the shelf-break between day 90 (Fig.19a) and day 170 (Fig.19b). Within the western Gulf, the cyclonic edges of the shed eddy (Fig.11b, Fig.20b) were similarly demarcated by the 0.1 μg chl ℓ^{-1} isopleth (Fig.19b).

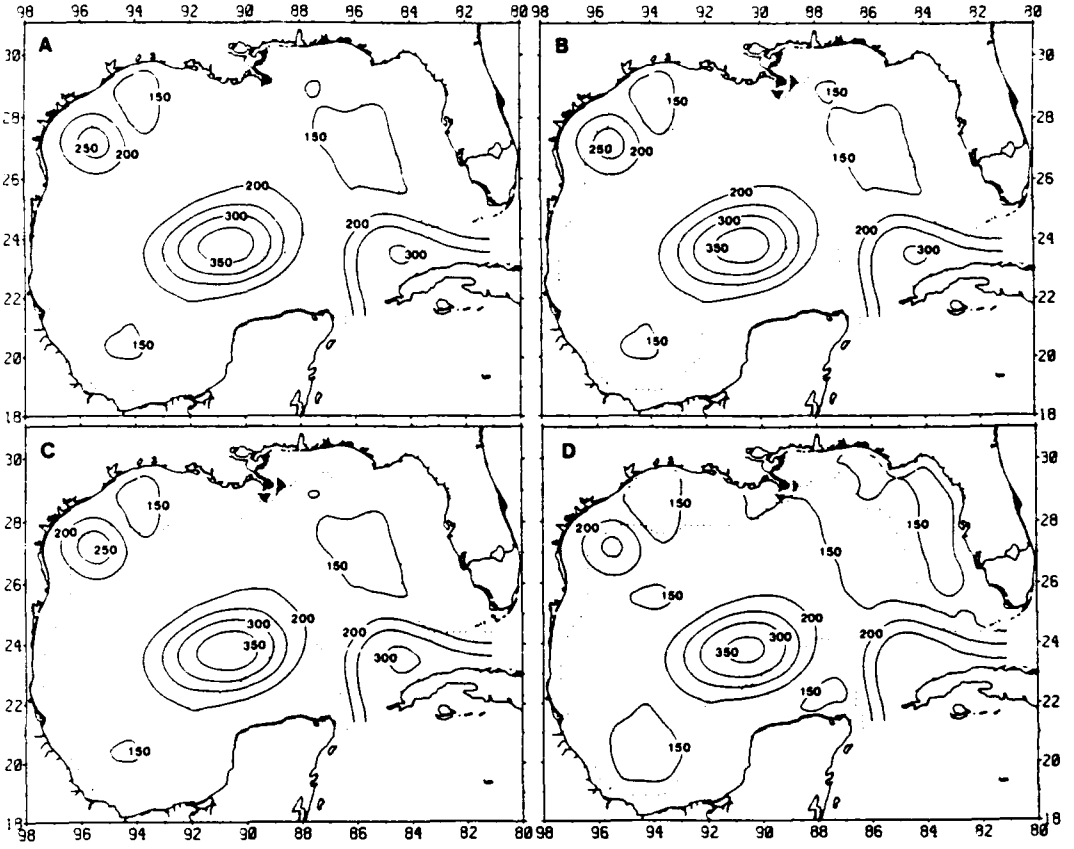

FIG. 18. The depth of the 5μg-at ℓ^{-1} isopleth of nitrate within the Gulf of Mexico on day 330 when the simulated Loop Current is at 25°N, under (A) seasonal wind forcing (Table 2), (B) seasonal wind forcing and Mississippi River effluent, (C) January mixing and River, (D) August mixing and River.

Over the next 80 days, the depth of the surface mixed layer reached its seasonal maximum, yielding surface concentrations of 0.3-0.4μg chl ℓ^{-1} (Fig. 19c) on day 250, or December 27, at the edge of the calving Loop Current and within the cyclonic circulation cells in the Bay of Campeche and on the west Texas shelf (Figs 11c, 20c). Continued southeastward flow at the shelf-break below Tampa Bay (Fig. 20c) advected the 1μg chl ℓ^{-1} isopleth associated with the Mississippi River plume, another 100km to the southeast between day 170 (Fig. 19b) and day 250 (Fig. 19c). Boluses of fresh water (ATKINSON and WALLACE, 1975), escaped buoys (SCHROEDER, DINNEL, WISEMAN and MERRELL, 1987), red-tide trajectories (MURPHY, STEIDINGER, ROBERTS, WILLIAMS and JOLLEY, 1975), and CZCS imagery (TREES, 1985) all support this simulated southeastward export of surface waters along the west Florida shelf-break.

By day 330, or March 17, an anticyclonic eddy of the Loop Current had shed and offshore flows prevailed west of Tampa Bay (Figs 11d, 20d). As a consequence, the 1μg chl ℓ^{-1} isopleth retreated ~250km to the northwest (Fig. 19d), suggesting a seasonal modulation of estuarine export from the Gulf of Mexico. Continued deep mixing within the surface layer (Table 2) led to lower nutrient (Figs 18b, 21a) and higher chlorophyll (Fig. 19d) concentrations of 0.4-0.5μg chl ℓ^{-1} on day 330 at the cyclonic edges of the shriveled Loop Current and recently-shed eddy. This surface signature of the combination of wind mixing and upwelling is reflected at depth in the

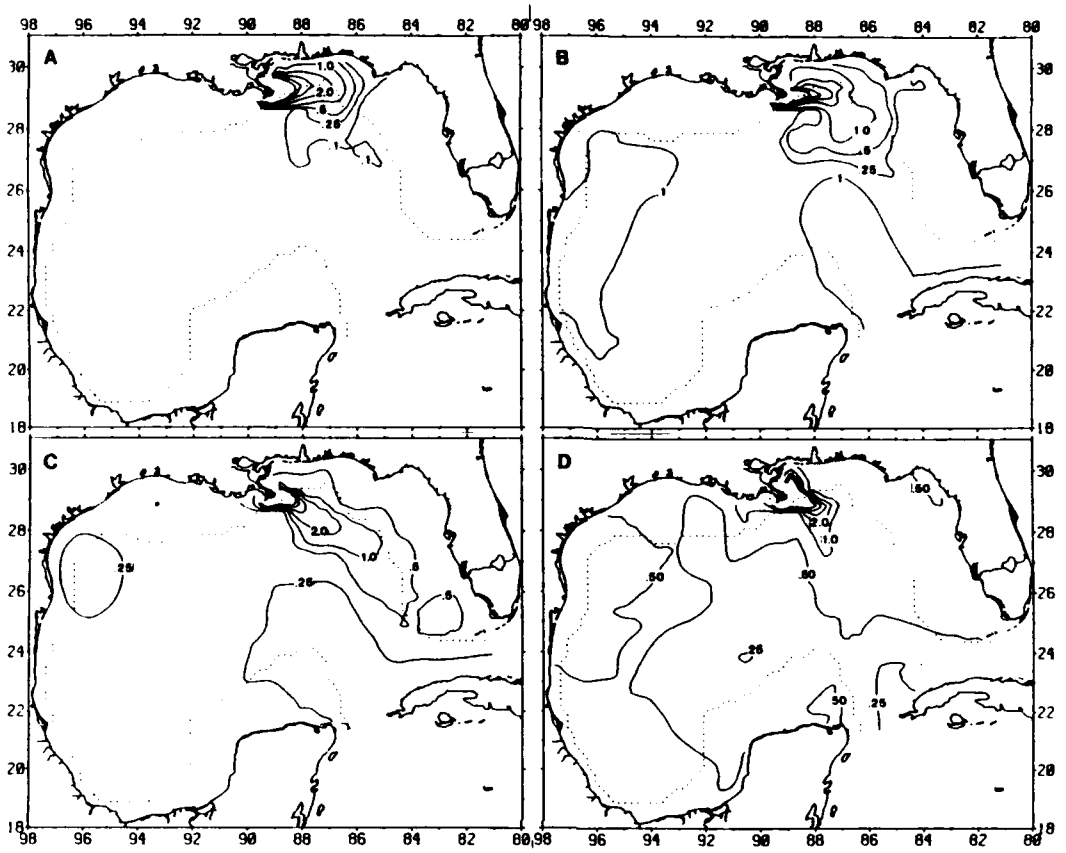

FIG. 19. Annual variation of surface chlorophyll within the Gulf of Mexico under seasonal wind forcing (Table 2) and Mississippi River effluent on days (A) 90, (B) 170, (C) 250 and (D) 330 during a penetration cycle of the Loop Current.

model as well, with 0.5μg chl ℓ^{-1} found near 150m within the central part of the Gulf of Mexico for days 315-330 (Fig.22a).

More detailed time series of nitrate (Fig.21) and chlorophyll (Fig.22) over the upper 20 layers of the coupled physical/biological models are shown for 4 representative areas (Table 3) of the central Gulf of Mexico and the shelf-break off west Florida, Louisiana, and Texas (Locations A,B,C, and D of Fig.1). The central Gulf time series at 25°53'N, 89°53'W, for example, shows little impact of the Loop Current until day 225 (Fig. 21a). With westward movement of the Current between days 170 (Fig.11b) and 250 (Fig.11c), the depth of the 2μg-at ℓ^{-1} isopleth of nitrate (Fig.21a) dropped below 150m on day 225, while the interface depth (shown as a dashed line in Figs 21 and 22) was then >200m. Separation of the anticyclonic eddy and its southwestward movement by day 330 (Fig.11d) resulted in shoaling of the depths of both the 2μg-at NO_3 ℓ^{-1} isopleth and the interface as early as day 295 (Figs 21a, 22a).

The highest concentrations of chlorophyll in the central Gulf were simulated during the presence of the Loop Current (Fig.22a), however. These results imply that the depth of the surface mixed layer (Table 2) was more important than a 45-day downwelling episode of less nutrient availability within the core of the Loop Current. In this region of the Gulf, the annual nitrate input of 132.6mg-at $m^{-2}y^{-1}$ and a remineralization of 56.7mg-at $m^{-2}y^{-1}$ produced a mean standing crop

TABLE 3. Annual nitrate fluxes, mean chloropyll content, "new" primary production, remineralization, and sinking losses within 4 regions of the Gulf of Mexico under (A) seasonal wind mixing and no Mississippi discharge (M), compared to Mississippi discharge with (B) seasonal, (C) winter and (D) summer vertical mixing regimes

	Central Gulf (25°53'N,89°53'W)	West Florida (25°8'N,84°8'W)	Louisiana (29°8'N,88°23'W)	Texas (27°38'N,95°38'W)
Nitrate input to upper layer (mg-at m^{-2} yr^{-1})				
A. Seasonal	132.6	160.8	188.4	119.3
B. Seasonal + M	132.6	159.5	176.9	119.3
C. Winter + M	195.2	242.0	289.0	175.9
D. Summer + M	99.8	115.0	124.8	90.8
Chlorophyll content of upper layer (mg m^{-2})				
A. Seasonal	51.5	51.6	53.8	55.5
B. Seasonal + M	52.1	58.8	479.9	55.5
C. Winter + M	69.7	78.3	477.8	73.3
D. Summer + M	26.5	31.5	482.8	26.3
Primary production of upper layer (g C m^{-2} yr^{-1})				
A. Seasonal	19.0	26.6	26.2	15.6
B. Seasonal + M	19.1	27.7	332.4	15.6
C. Winter + M	24.7	36.1	318.1	21.2
D. Summer + M	11.3	16.1	284.6	8.8
Particle export of upper layer (mg chl m^{-2} yr^{-1})				
A. Seasonal	254.2	294.8	363.0	247.2
B. Seasonal + M	257.9	350.7	1497.0	247.4
C. Winter + M	352.9	453.8	1827.7	337.7
D. Summer + M	174.5	249.6	1103.0	157.5
Particle export of lower layer (mg chl m^{-2} yr^{-1})				
A. Seasonal	27.5	158.8	190.9	141.8
B. Seasonal + M	28.0	185.7	723.7	141.8
C. Winter + M	44.9	267.2	955.3	214.7
D. Summer + M	22.7	144.6	545.6	100.5
Remineralization of upper layer (mg-at m^{-2} yr^{-1})				
A. Seasonal	56.2	56.3	58.6	60.5
B. Seasonal + M	56.7	64.1	522.4	60.5
C. Winter + M	76.0	85.3	520.2	79.9
D. Summer + M	28.9	34.4	525.7	28.7

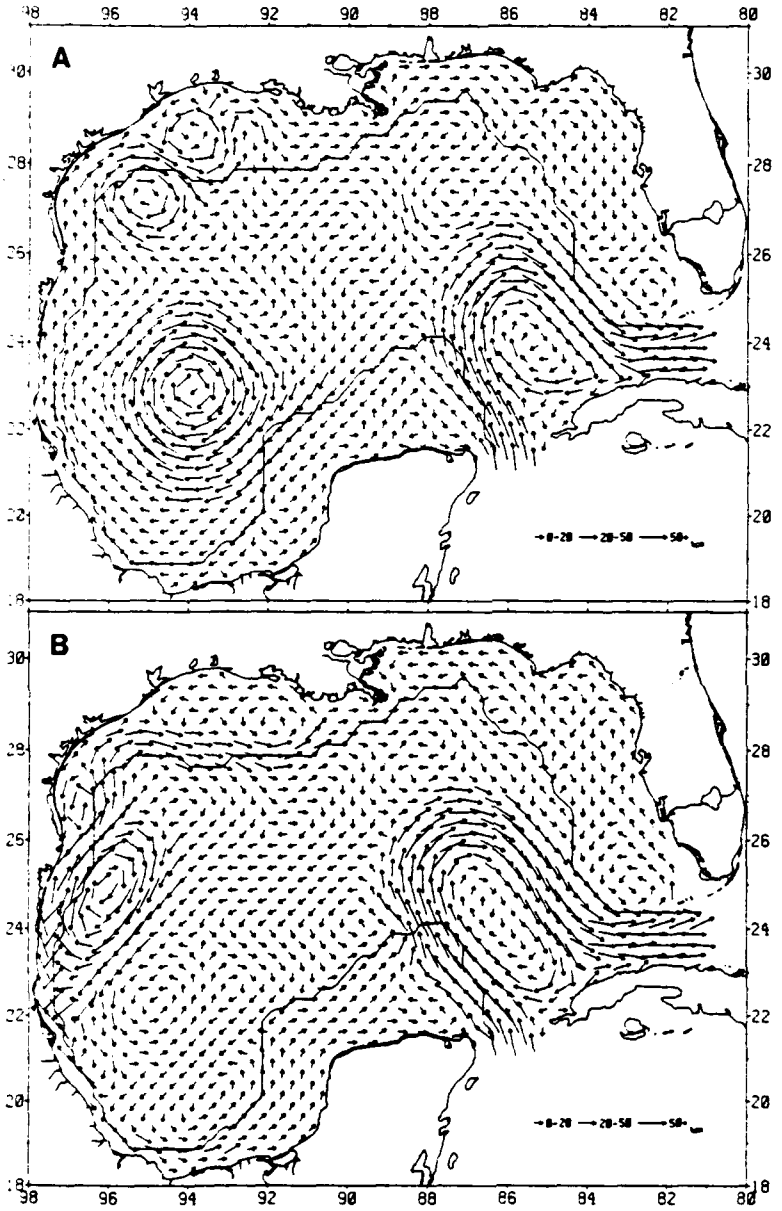

FIG.20 (A and B). Annual variation of currents within the surface layer of the circulation model on days (A) 90 and (B) 170 during a penetration cycle of the Loop Current.

of 52.1mg chl m^{-2} over an average upper layer of 174m extent, containing a 1% light depth of 81.7m, a "new" primary production of 19.1g C $m^{-2}y^{-1}$ (assuming a C/chl ratio of 50/1), and an export at the interface depth of 257.9mg chl $m^{-2}y^{-1}$ after partial decomposition of the sinking phytodetritus (Table 3).

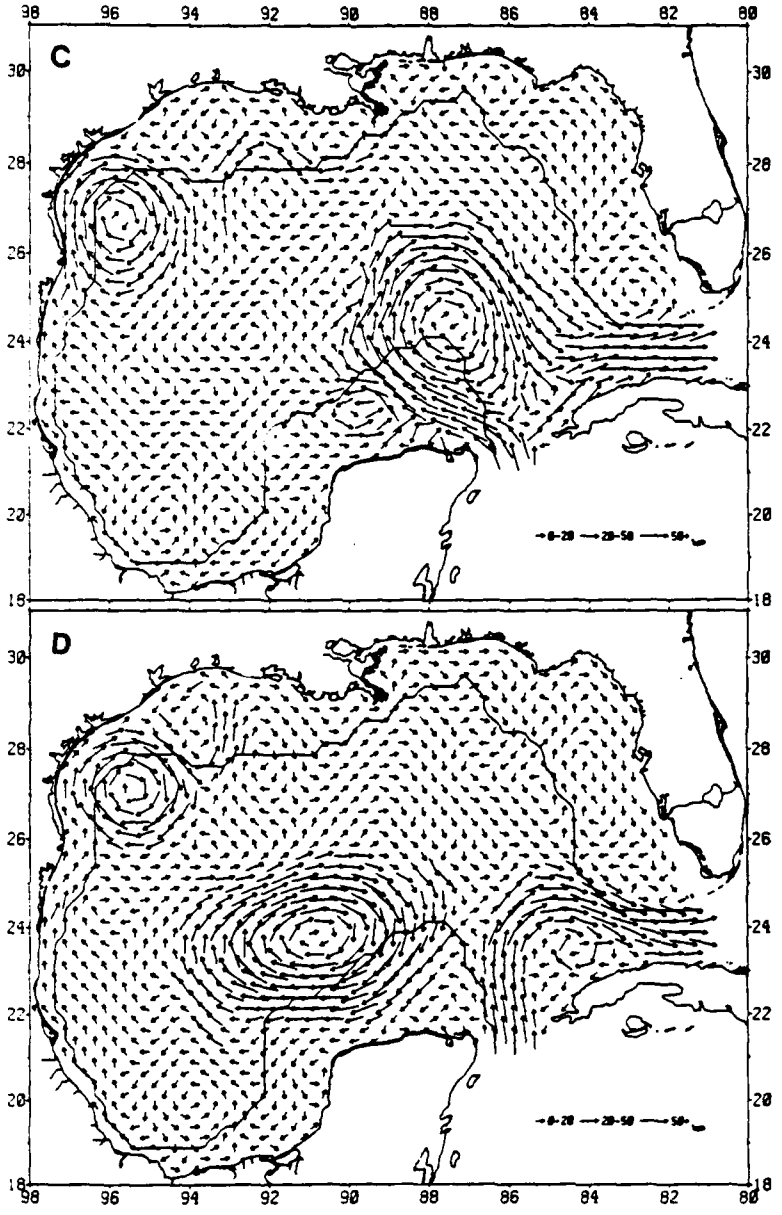

FIG.20(C and D). Annual variation of currents within the surface layer of the circulation model on days (C) 250 and (D) 330 during a penetration cycle of the Loop Current.

Farther to the east at 25°8'N, 84°8'W above the Florida shelf-break (Fig.1), only the cyclonic impact of the simulated Loop Current was observed (Fig.21b). The depth of the 2μg-at ℓ^{-1} isopleth of nitrate was always <150m, shoaling to 125m between days 165 and 235, while the interface depth remained above 200m throughout the year (Fig.22b). A nitrate input of 159.5mg-

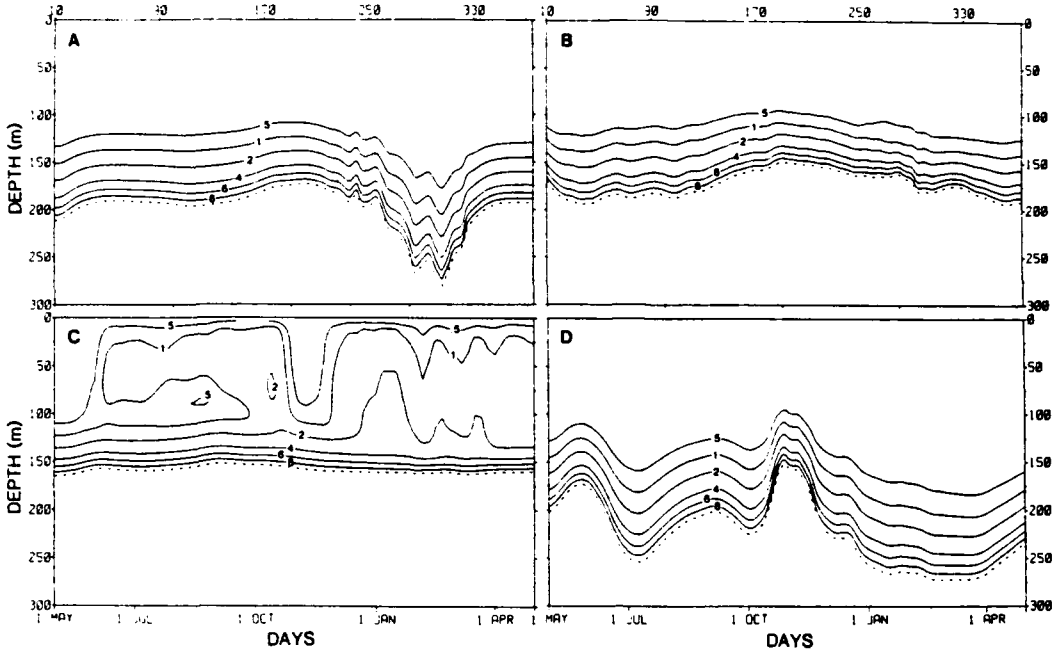

FIG.21. Annual variation of nitrate under seasonal wind forcing (Table 2) and Mississippi River effluent in (A) the central Gulf of Mexico, and at the edge of (B) the west Florida, (C) the Louisiana, and (D) the Texas shelves.

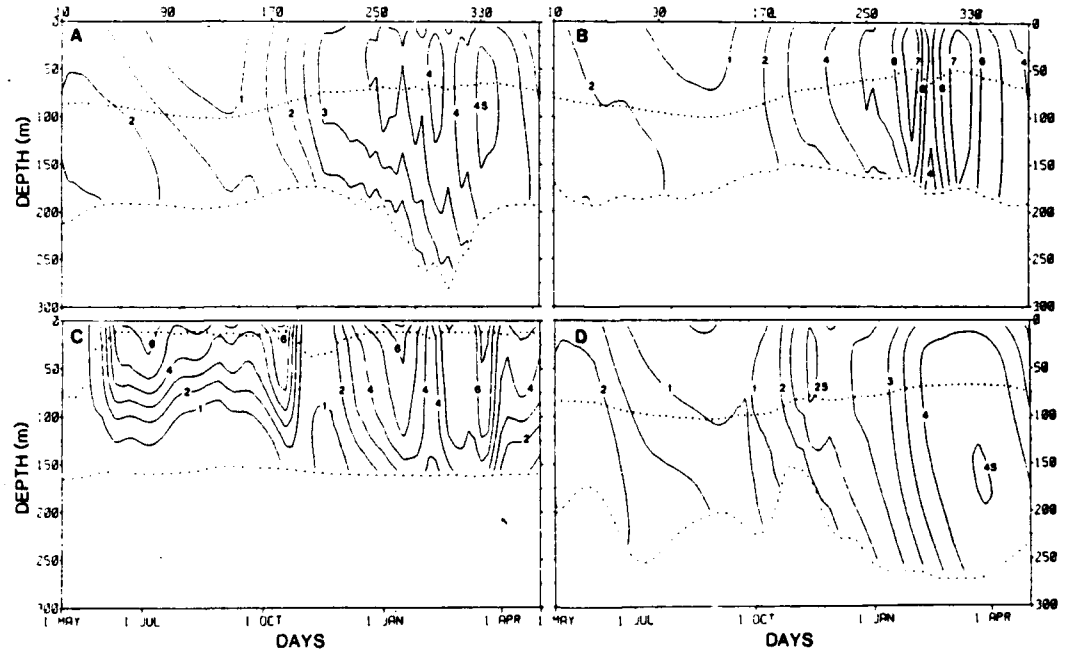

FIG.22. Annual variation of subsurface chlorophyll under seasonal wind forcing (Table 2) and Mississippi River effluent in (A) the central Gulf of Mexico, and at the edge of (B) the west Florida, (C) the Louisiana, and (D) the Texas shelves.

at $m^{-2}y^{-1}$ (Table 3), somewhat larger than that derived from the case of a constant interface depth of 200m (Fig.14a), should have led to a mean chlorophyll content of 51.6mg chl m^{-2} and a "new" primary production of 26.6g C $m^{-2}y^{-1}$ (Case A of Table 3).

Instead, chlorophyll abundances of 122mg chl m^{-2} were found within the 174m upper layer above the southwest Florida shelf-break on days 280 and 315 (Fig.22b), after the maximum southward excursion of the Mississippi River-derived plume on day 260 (Fig.19c). About 700km southeast of the mouth of the Mississippi River at 25°8'N, 84°8'W, the mean algal standing crop was 58.8mg chl m^{-2}, with an associated "new" primary production of 27.7g C $m^{-2}y^{-1}$ and an export of 350.7mg chl $m^{-2}y^{-1}$ (Case B of Table 3). At 29°8'N, 88°23'W on the southeast Louisiana slope within 50km of the mouth of the Mississippi River (Fig.1), and thus much closer to this estuarine source of nutrients (Fig.21c), the phytoplankton biomass accordingly increases tenfold (Fig.22c). Note that the contour interval is 1.0μg chl ℓ^{-1} in Figure 22c and 0.1μg chl ℓ^{-1} in Figure 22b, and .05 μg chl ℓ^{-1} in Figures a and d.

Upwelling at the Louisiana shelf-break (Fig.11) would input 188.4mg-at $NO_3 m^{-2}y^{-1}$ in the absence of river discharge (Case A of Table 3). The interface depth remains at 159m, but in sharp contrast to the southwest Florida slope (Fig.21b), about 1μg-at NO_3 ℓ^{-1} is at times left above the 1% light depth of 19m near the mouth of the Mississippi River (Fig.21c). The combined anthropogenic and natural nutrient input yields a mean chlorophyll content of 479.9mg chl m^{-2}, with an associated "new" primary production of 332.4g C $m^{-2}y^{-1}$ and an export at the interface of 1497mg chl $m^{-2}y^{-1}$ (Table 3). As a result of remineralization of plankton grown on anthropogenic nitrogen sources in the upper layer, more nitrate is added to the upper layer from nitrification (522.4mg-at $NO_3 m^{-2}y^{-1}$) than from upwelling (176.9mg-at $NO_3 m^{-2}y^{-1}$). Assuming a maximum f ratio of 0.83, a total production of 400.5g C $m^{-2}y^{-1}$ is inferred.

At 2 stations near the 420m isobath of the southwest Louisiana slope (Location F of Fig.1), i.e. outside the Mississippi River plume (Fig.19), mean *in situ* concentrations of nitrate were 0.79μg-at NO_3 ℓ^{-1} and of chlorophyll were 0.74μg chl ℓ^{-1} over the upper 100m of the 8-9 December 1982 water column (M. DAGG, personal communication). With southward movement of the algal plume on the southeast Louisiana slope on day 170 (Figs.19b, 20b), the simulated nitrate (Fig.21c) and chlorophyll (Fig.22c) concentrations at 29°8'N, 88°23'W during days 180-230, i.e. October 18 to December 7, matched the observations at 28°33'N, 89°53'W (DAGG, ORTNER and AL-YAMANI, 1987). Similarly over an annual cycle, observed total primary production of 250-350 g C $m^{-2}y^{-1}$ within 50km of the Mississippi River (THOMAS and SIMMONS, 1960; FUCIK, 1974) suggests that our coupled models accurately depict some of the consequences of eutrophication in the northern Gulf of Mexico.

Farther to the west at 27°38'N, 95°38'W on the Texas shelf-break, the depth of the interface remains below 200m for 125 days (Fig.21d), as a result of downwelling within anticyclonic eddies, shed by the Loop Current. Consequently, the annual nutrient input of 119.3mg-at NO_3 $m^{-2}y^{-1}$ allows a mean algal biomass of only 55.5mg m^{-2}, with annual "new" production of 15.6g C $m^{-2}y^{-1}$ and export of 247.4mg chl $m^{-2}y^{-1}$ (Table 3). On days 35 and 205, chlorophyll stocks increase to 0.25mg chl m^{-3} (Fig.22d) in response to upwelling at the edge of the eddies (Figs.11,20), but the seasonal mixing signal dominates the annual cycle beyond day 230 in this region of the Gulf of Mexico. Like the central part of the Gulf, the computed export at the interface depth here is the smallest on the continental margin of the basin (Figs 23a,c).

In the absence of Mississippi River discharge, the largest input of organic matter to the sediments occurs off Tampa Bay at the west Florida shelf-break. A flux of 0.40g chl $m^{-2}y^{-1}$ occurs at the interface depth (Fig.23a) and 0.1g chl $m^{-2}y^{-1}$ arrives at the slope bottom (Fig.23c). Advection of organic matter to the southeast from the Louisiana shelf leads to a doubling of the

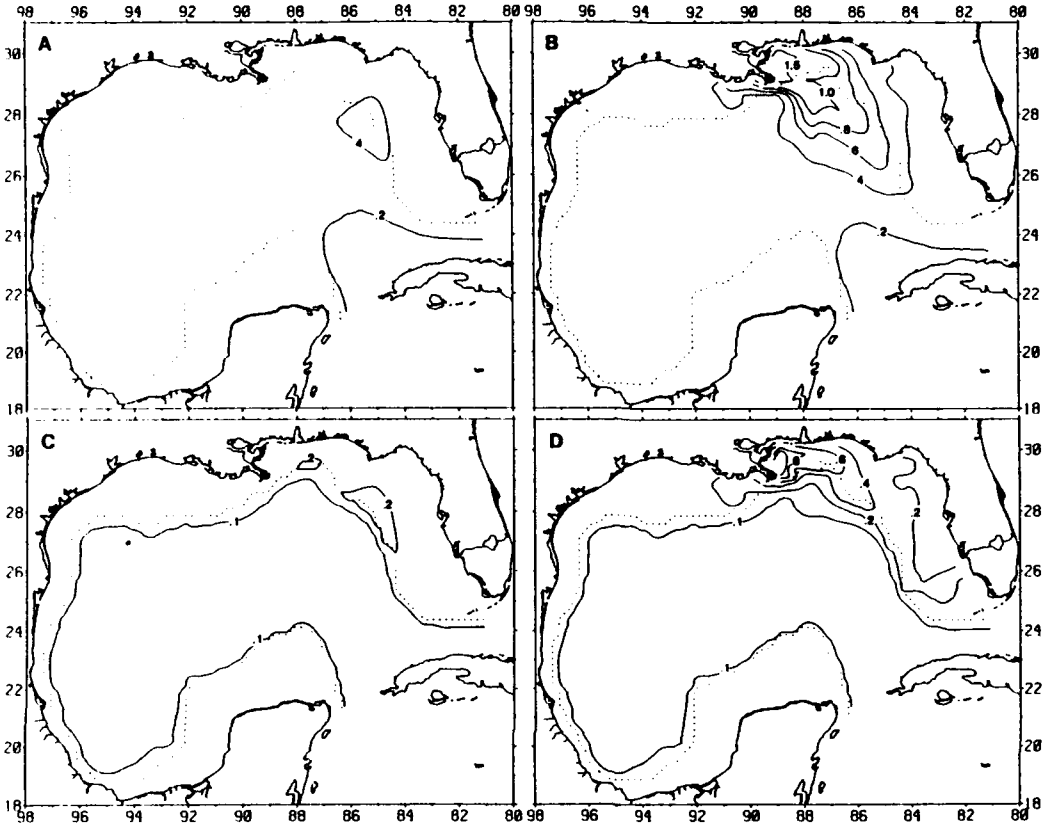

FIG.23. Annual input of chlorophyll to the surficial sediments of the Gulf of Mexico from the upper (A,B) and lower (C,D) layers of the circulation model, with nutrient loading from oceanic (A,C) and additional terrestrial (B,D) sources.

detrital loading in this depocenter, i.e. 0.8g chl $m^{-2}y^{-1}$ at the interface and 0.2g chl $m^{-2}y^{-1}$ at the bottom (Figs.23b,d). Assuming again a C/chl ratio of 50/1-100/1 for phytodetritus (STEELE, 1964), the full range of carbon input from the water column west of Tampa Bay becomes 20-80g C $m^{-2}y^{-1}$ at the interface depth and 5-20g C $m^{-2}y^{-1}$ at the slope bottom.

In contrast, our previous range of estimates of carbon accumulation within the Gulf of Mexico sediments (Fig.8) from eq.(1) was 0.4-7.8g C $m^{-2}y^{-1}$. Since our minimum bottom depth (D) in the model, was 500m, the changing depths of the interface from 160m to 280m (Figs.21,22) more realistically represent the bottom topography of the outer shelf, where the >1.0%dw carbon deposits are found (Fig.8). A depth-weighted composite of Figures 23a and 23c, or Figures 23b and 23d, may then be a more reasonable estimate of carbon input to the bottom. At a depth range of 160-280m, for example, an input of 20-80g C $m^{-2}y^{-1}$ to the bottom, together with a survival rate of 10% for phytodetritus within the outer shelf benthic community (WALSH, BISCAYE and CSANADY, 1988b), yields a maximum accumulation rate of 8g C $m^{-2}y^{-1}$. This estimate coincides with our previous calculation of 7.8g C $m^{-2}y^{-1}$ for the 1.5%dw carbon sediments.

Within deeper regions, at bottom depths of 1600-2800m where >0.5% carbon deposits are found (Fig.8), an input of 5-20g C $m^{-2}y^{-1}$ and a 10% survival rate on the bottom implies a minimum accumulation rate of 0.5g C $m^{-2}y^{-1}$. This agrees with our previous calculation of 0.4g C $m^{-2}y^{-1}$ for 0.75%dw carbon sediments, where lower sedimentation rates were assumed. Higher sinking rates of 30-300m d^{-1}, resulting from seasonal aggregation processes, instead of 3m d^{-1} used in the model, could yield a larger input of carbon to the continental margins of the Gulf of Mexico, if these settling velocities prevailed throughout the year.

4. CONCLUSIONS

Seasonal succession of phytoplankton species and possible aggregation processes, leading to the rapid sinking of diatoms (LAMPITT, 1985) and picoplankton (LOCHTE and TURLEY, 1988), are beyond the scope of our present physical and biological models of the Gulf of Mexico. Without a realistic depiction of mesoscale plankton dynamics at the species level, we may thus have underestimated the nitrogen burial and evasion losses in the Gulf. Furthermore, if wind-induced upwelling contributes additional supplies of "new" nitrogen, beyond that parameterized by Loop Current-induced upwelling, we may have underestimated the "new" production and again the sinking losses out of the water column.

Oceanic forcing, in the form of a western boundary current, has been a major focus of this study. This forcing may be responsible for some of the longshore currents on the outer West Florida shelf (STURGES and EVANS, 1983). Local wind forcing is highly coherent with flows over bottom depths <45m on the West Florida (MITCHUM and STURGES, 1982) and Texas-Louisiana (COCHRANE and KELLY, 1986) shelves, however, and may lead to local regions of intensified upwelling in the Gulf of Mexico (WALLCRAFT, 1986). Although we used seasonal changes of wind stress to calculate both the depth of the surface mixed layer and the vertical eddy viscosity (Table 2) of the biological model, the circulation model was, of course, unable to replicate either the wind-induced upwelling, or the westward advection of Mississippi and Atchafalaya River effluent (COCHRANE and KELLY, 1986; DINNEL and WISEMAN, 1986).

Coupling of a local shelf model, with increased vertical resolution of the circulation, description of the wind response, and inclusion of phytoplankton species succession, to our present basin-scale calculations is the goal of our future research. We do not expect burial of organic matter in shallow shelf waters (<50m) to have an important impact, however, on our conclusions from a nitrogen budget for the larger Gulf of Mexico. An underestimate of the burial loss would again be the consequence of poorly resolved coastal regions. The nitrogen budget of Table 4 attempts to address these deficiencies by consideration of various scenarios of increased burial rather than remineralization losses.

The simulated fluxes of nitrate in through Yucatan Strait and out via Florida Strait (Fig.24) have a weak time dependency related to the penetration cycle of the Loop Current. On day 170, when the Loop Current has reached 27°N (Fig.16b), the depth of the interface on the cyclonic side of the Current is ~10m deeper in Yucatan Strait (Fig.24a) and ~5m deeper in Florida Strait (Fig.24b) than on day 330 (Figs.24c,d). More upwelling occurs within these Straits on day 330, when the Loop Current retreated to 25°N (Fig.18b), similar to nitrate sections in January 1952 (Fig.3) and October 1977 (Fig.4) rather than during November 1976 (Fig.5).

As a result of less biological utilization, however, the 0.5μg-at l^{-1} isopleth of nitrate is ~5m higher in the water column on day 170 than 330 within both Yucatan and Florida Straits (Fig.24), such that the flux differences are minimal. During deep penetration of the Loop Current, the

Table 4. Annual nitrogen budget of surface waters of the Gulf of Mexico

Eutrophication				
Nitrogen sources ($x10^{10}$kg N y^{-1})			Nitrogen sinks ($x10^{10}$kg N y^{-1})	
Yucatan dissolved		1.16	Florida dissolved	1.13
Yucatan particulate		0.09	Florida particulate	0.12
Mississippi effluent		0.12	Sinking detritus	
Upwelling/diffusive		0.32	after remineralization	0.45
	Total	1.69	Total	1.70
Natural case				
Nitrogen sources ($x10^{10}$kg N y^{-1})			Nitrogen sinks ($x10^{10}$kg N y^{-1})	
Yucatan dissolved		1.16	Florida dissolved	1.13
Yucatan particulate		0.09	Florida particulate	0.11
Upwelling/diffusive		0.32	Sinking detritus	0.37
	Total	1.57	Total	1.61

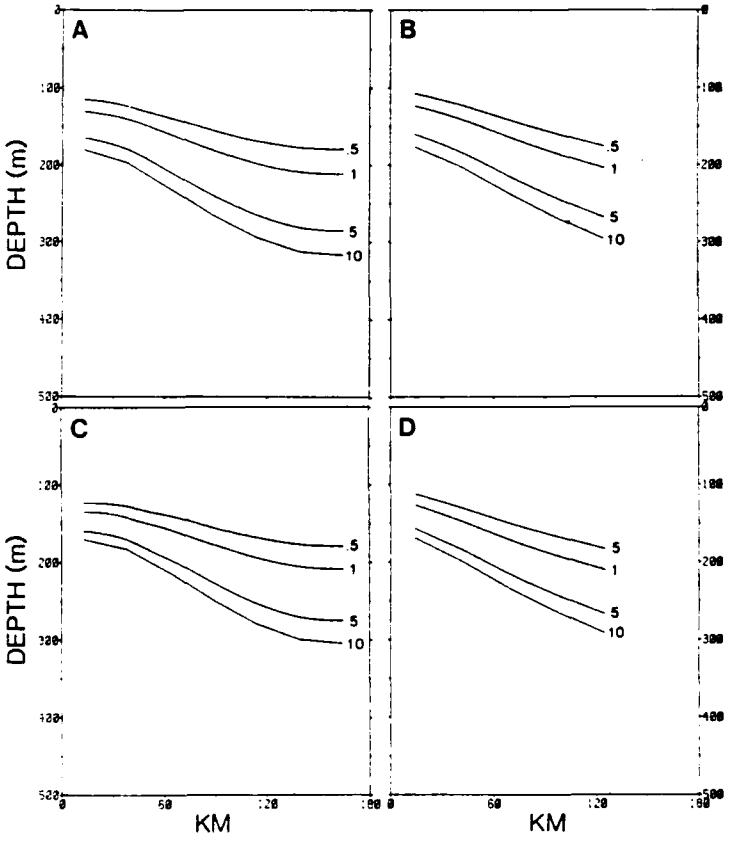

FIG.24. The simulated distribution of nitrate across Yucatan Strait (A,C) and Florida Strait (B,D) on days 170 and 330 under seasonal wind forcing and Mississippi River effluent.

influx of nitrogen in the upper layer across Yucatan Strait was actually 373.8kg NO_3-N s^{-1} on day 170, compared to 372.1kg NO_3-N s^{-1} on day 330. Similarly, the efflux of nitrogen across Florida Strait was 365.7kg NO_3-N s^{-1} on day 170, instead of 363.2kg NO_3-N s^{-1} on day 330.

On both days, more dissolved nitrogen entered the Gulf of Mexico in the upper layer across Yucatan Strait than departed via Florida Strait (Fig.24). On an annual basis, 1.16 x 10^{10}kg NO_3-N, or 368.7kg NO_3-N s^{-1}, entered Yucatan Strait above a mean interface depth of 248.1m. Continued upwelling led to a mean interface depth of 236.1m within Florida Strait, but an efflux of only 1.13 x 10^{10}kg NO_3-N y^{-1}, or 359.2kg NO_3-N s^{-1}, occurred (Table 4). A comparable average of January 1952 and October 1977 observations for the 1-10μg-at NO_3 ℓ^{-1} layers is 440kg NO_3-N s^{-1} within Yucatan Strait and 435kg NO_3-N s^{-1} within Florida Strait (Table 1). Addition of the particulate nitrogen influx through Yucatan Strait in the form of chlorophyll (0.09 x 10^{10}kg chl-N y^{-1}) and its outflux through Florida Strait (0.12 x 10^{10}kg chl-N y^{-1}) to the annual nitrogen budget of Table 4 yields a balanced total of ~1.25 x 10^{10}kg N y^{-1}.

After one year of simulated time, the model solutions are not quite those at equilibrium, such that in the natural case of Table 4, the detrital loss of particulate nitrogen is somewhat larger (3%) than the upwelled/diffusive input of nitrate. The 0.05 x 10^{10}kg chl-N y^{-1} additional sink of particulate nitrogen is derived from initial nitrate stocks in the water column. Addition of anthropogenic nitrogen to the surface waters of the model allows a faster approach to equilibrium solutions, with only a 0.01 x 10^{10}kg chl-N y^{-1} discrepancy between supply and loss of nitrogen in surface waters. The additional nitrogen inputs of the Mississippi River effluent (0.12 x 10^{10}kg N y^{-1}) and vertical exchange from the lower layer (0.32 x 10^{10}kg NO_3-N y^{-1}) are now converted into sinking detrital nitrogen (0.45 x 10^{10}kg chl-N y^{-1}), with only a small export of particulate matter still derived from the initial nitrate stocks.

At the equilibrium state of the eutrophication case, the particulate export will be just maintained by an input of 0.12 x 10^{10}kg NO_3-N y^{-1} from the Mississippi River and of 0.32 x 10^{10}kg NO_3-N y^{-1} from the lower layer of the Loop Current and its anticyclonic rings. In the absence of eutrophication and upwelling at the cyclonic edges of these western boundary currents in the Gulf of Mexico basin, however, only 0.11-0.21 x 10^{10}kg NO_3-N y^{-1} would have instead entered the upper layers of the coupled models, i.e. with constant interface depths of respectively 400 and 200m in the biological model (Fig.14). The "total" nitrogen production and carbon fixation of the Gulf, other than cyanobacteria, would then be a function of the operant f ratio at a particular depth and time.

Assuming a tempo-spatial average f ratio of 0.06 over the mean 1% light depth of 80m, where the nitrate content was 0.09μg-at NO_3 ℓ^{-1} for case A, i.e. seasonal wind mixing and no Mississippi discharge, the total nitrogen uptake would be 5.3 x 10^{10}kg N y^{-1} as a result of Loop Current-induced upwelling. The total uptake would be only 1.8-3.5 x 10^{10}kg N y^{-1} in its absence, i.e. constant interface depths of 400 and 200m. With a C/N ratio of 6/1, the higher total primary production of 32 x 10^{10}kg C y^{-1}, spread over a basin of 1.53 x 10^6km^2 extent, yields an annual average of 209g C m^{-2}, instead of 72-137g C $m^{-2}y^{-1}$ in the absence of upwelling.

Inclusion of either clouds to reduce the incident radiation, or greater sinking rates to reflect aggregates, would have reduced the algal biomass and the amount of "new" production, with an increase of nitrate stocks left behind in the water column. Consequently the f ratio would increase, yielding lower total primary production. Over the 0.1% light depth of 119m in Case A, for example, the average nitrate content was 0.23μg-at NO_3 ℓ^{-1} and the mean f ratio was instead 0.12. An f ratio of 0.12 over the deeper water column would imply a mean annual production of 105g C $m^{-2}y^{-1}$ in the absence of Mississippi River effluent.

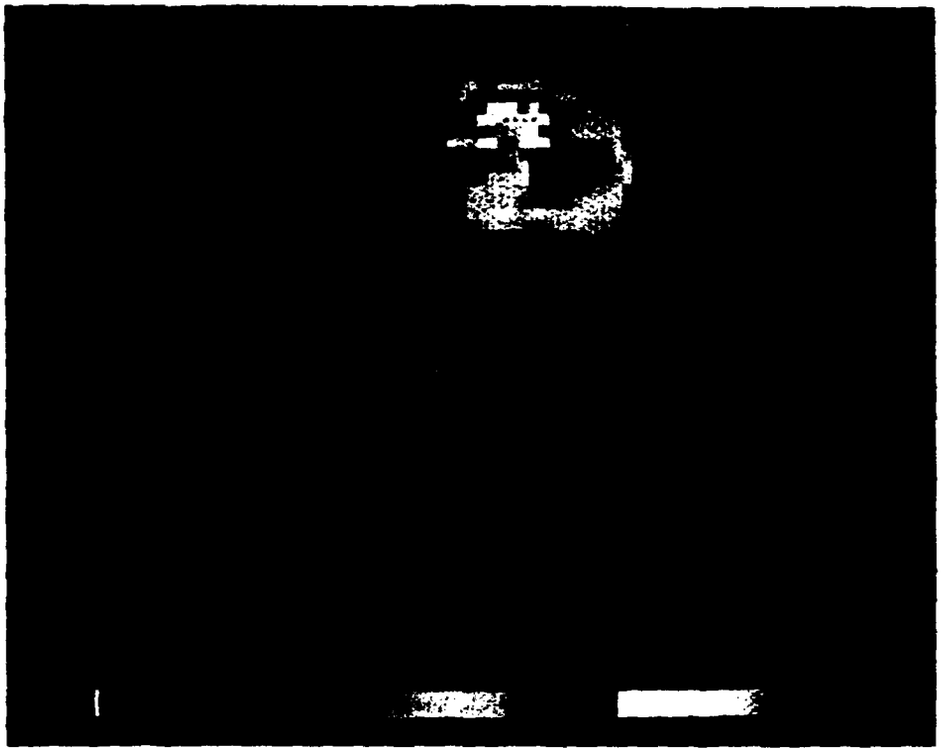

FIG.25. Color enhancement of the distribution of surface chlorophyll within the Gulf of Mexico on day 170 under seasonal wind forcing and Mississippi effluent - see Fig. 19b.

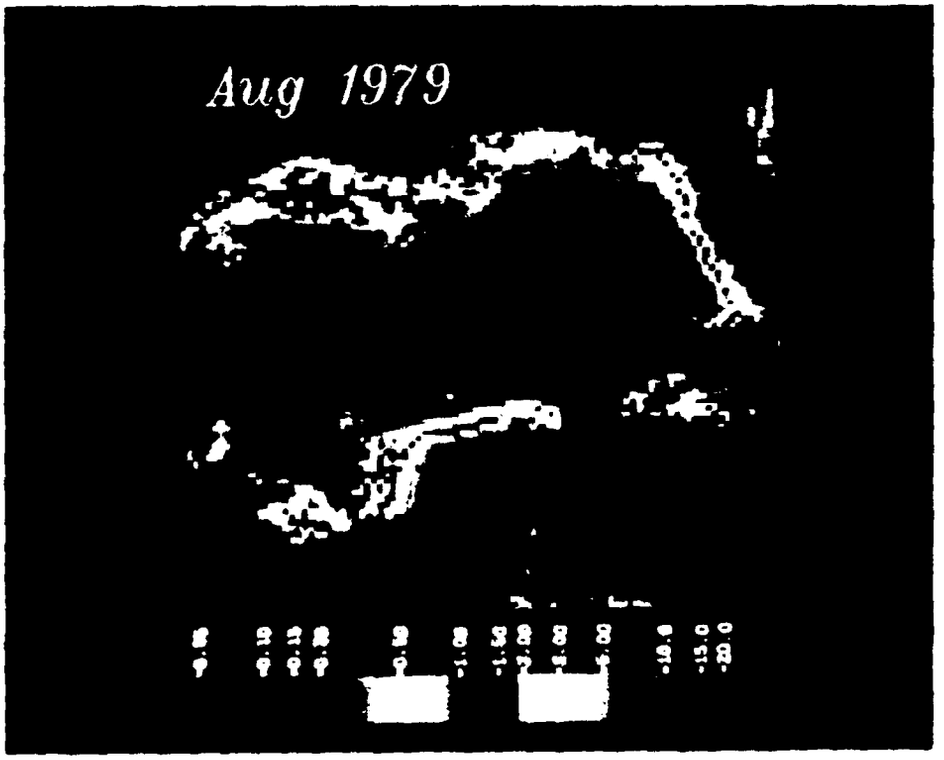

FIG.26. A monthly composite of the distribution of surface chlorophyll within the Gulf of Mexico during August 1979, using the same color bar as Fig. 25.

With few *in situ* estimates of primary production, the validity of the model's results can be tested with preliminary satellite time series (MÜLLER-KARGER *et al.*, 1988). Figure 25 of the model output of Case B (with the Mississippi River discharge) on day 170 is a color-enhanced version of the surface chlorophyll field depicted in Figure 19b. Note that the 0.05 and 0.10μg chl ℓ^{-1} isopleths of algal biomass are now represented by the purple and dark blue hues of Figure 25; >5μg chl ℓ^{-1} is simulated as the orange color off the mouth of the Mississippi River. Using the same color bar, a similar spatial pattern and amount of low chlorophyll was seen by the CZCS sensor during August 1979 (Fig.26) within both the Loop Current in the eastern Gulf and a previously-shed anticyclonic eddy in the western half; extensive regions of apparent algal biomass >5μg chl ℓ^{-1} were observed on the Florida, Mississippi, Louisana, Texas, and Campeche shelves. Monthly composites of satellite-sensed algal biomass, e.g. Figure 26, were used to construct the 4 year time series of Figure 27.

In Case A of the model with no Mississippi discharge, for example, the simulated chlorophyll mean over the whole basin of the Gulf of Mexico underestimates the satellite estimate of the same spatial domain, containing eutrophic coastal waters (Fig.26), for most of the time during 1979-1982 (Fig.27a). This comparison implies an underestimate of the f ratio and total production by the model as well. Within subregion H in the middle of the western Gulf (Fig.27c), however, the model overestimates the seasonal maxima of the CZCS pigment concentration by threefold each year - see Figure 1 for locations of the pigment time series G and H.

Within the Loop Current subregion G of the eastern Gulf, greater interannual variability of algal biomass evidently occurs, such that the model exactly reproduced the maximum amount of the seasonal satellite signal in 1981, but not in other years (Fig.27b). Note that both the satellite data and the model overestimate by threefold (Fig.27b) the shipboard observations of 0.11-0.13μg chl ℓ^{-1} within surface waters of the Loop Current during early February 1981 (ORTNER *et al*, 1984). However, only the satellite data coincide with shipboard observations of 0.05-0.07μg chl ℓ^{-1} in surface waters of the Loop Current during late February 1980 (EL-SAYED and TREES, 1980). The model apparently overestimates by fivefold (Fig.27b) the observed 1980 chlorophyll biomass in the region of the Loop Current, but only by twofold (Fig.27c) the 0.2-0.3μg chl ℓ^{-1} measured in the western area during February 1980 (EL-SAYED and TREES, 1980).

Pending future resolution of the quality of these data sets, it appears that the model may either equal or overestimate by at least two- to threefold the chlorophyll content and ensuing "new" production in most of the Gulf of Mexico. The total primary production, depending on concomitant changes in f ratios, may thus be as much as 70-210g C $m^{-2}y^{-1}$ in the oligotrophic parts of the basin, in contrast to prior estimates of ~25g C $m^{-2}y^{-1}$ (EL-SAYED, 1972). The mean of the equivalent carbon fixation of the "new" production of Case A (Table 3) at the 4 representative time series (21.9g C $m^{-2}y^{-1}$) actually includes some recycled production, since it is based on both upwelled nitrate and local remineralized nitrate.

The remineralization rate of $0.005d^{-1}$ in the model results in nitrification values of 0.001 to 0.010mg-at N $m^{-3}d^{-1}$ over the upper 264m of the simulated water column (Table 3). They are somewhat lower than those observed (0.016-0.068mg-at N $m^{-3}d^{-1}$) within eutrophic waters off southern California (WARD, OLSEN and PERRY, 1982) and in the nitrite maximum layer of the equatorial North Pacific (WADA and HATTORI, 1972). The model's results are comparable to those computed at 100m for open waters (0.003-0.023mg-at N $m^{-3}d^{-1}$) off the North Pacific (MARTIN *et al.*, 1987), however, suggesting that our estimates of bacterial decomposition of particulate matter in the upper layer are reasonable.

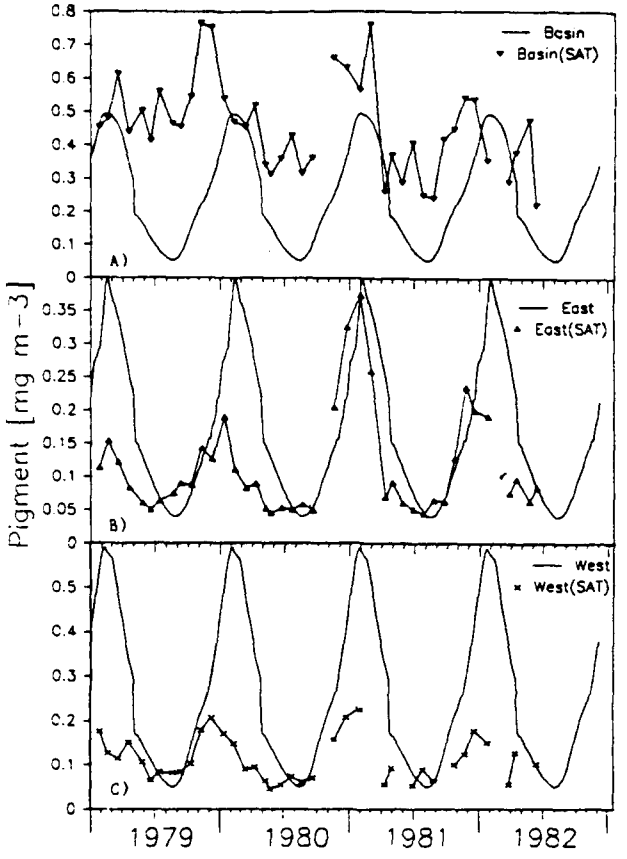

FIG.27. Annual variation of simulated surface chlorophyll under only seasonal wind forcing, with respect to 1979-82 CZCS estimates of pigment (A) over the whole basin, (B) within the eastern Gulf of Mexico, and (C) within the western Gulf - see Fig.1 for locations of the aggregated satellite and model time series.

With no further decomposition, 45 x 10^8kg chl-N y^{-1} of detrital nitrogen would arrive on the bottom of the Gulf of Mexico, compared to 6 x 10^8kg N y^{-1} required from our previous estimates of burial and denitrification. Application of the smaller decomposition rate of 0.0025d $^{-1}$ within the lower layer of the model results in a nitrification of 9 x 10^8kg N_3-N y^{-1} beneath the interface and a particle flux of 15 x 10^8kg chl-N y^{-1} to the bottom sediments.

Increasing the dissolved nitrogen flux across the interface by 50% to 0.47 x 10^{10}kg NO_3-N y^{-1} in the January mixing case, i.e. simulating additional upwelling by local winds, yields sinking fluxes of 58 x 10^8kg chl-N y^{-1} at the interface and 22 x 10^8kg chl-N y^{-1} at the bottom. Removal of the Mississippi River input from Table 4 results in decreased remineralization rates as well, with sinking fluxes of 37 x 10^8kg chl-N y^{-1} at the interface and 12 x 10^8kg chl-N y^{-1} at the bottom, i.e. similar to the eutrophication case of 15 x 10^8kg chl-N y^{-1} at the sediment interface. In all of these situations, the input of particulate nitrogen to the sea floor (12-22 x 10^8kg chl-N y^{-1}) exceeds the estimated burial flux of 3.5 x 10^8kg N y^{-1}, allowing loss of nitrogen as both N_2 and reduced nitrogen compounds.

Within the uncertainties of the assumptions in our physical and biological models, we are pleased that the budgets of Table 4 are in fair agreement after one year of simulated time. Additional *in situ* and satellite data, together with inclusion of second-order processes in another simulation model, will advance our understanding of the way carbon and nitrogen are cycled on the margins of the ocean. For example, arguments about unbalanced global nitrogen budgets have been advanced in the past (McElroy, 1983) and hinge on uncertainties about the amount of both sinks and sources (Fogg, 1982; Walsh, 1984), particularly nitrogen fixation, which we have neglected.

In a first-order approximation, however, it would appear that less than 25% of man's accelerated inputs of nitrogen are possibly stored in bottom sediments on the continental margin. The remainder may be dispersed in dissolved form, after initial uptake in the euphotic zone and remineralization beneath the pycnocline. On a relative basis, the presence of a western boundary current in the Gulf of Mexico may increase the "new" and total production by two- to threefold that of the other oligotrophic regions in the ocean. As concomitant ocean color and thermal data from satellite imagery continue to become available, we will refine the above calculations to both extend the spatial domain of these models to regions of open boundary conditions, and to resolve apparent interannual temporal variations of primary production. The fate of this fixed carbon and the nature of the organisms involved await the next generation of coupled physical/biological models.

5. ACKNOWLEDGEMENTS

This research was supported by the Office of Naval Research under grant N00014-87-G-0218, by the National Aeronautics and Space Administration under grant NAGW-678, and by the Department of Energy under grant DE-FG05-85ER60285. We thank George Berberian, Mike Dagg, Otis Brown and Bob Evans for the unpublished data used in this analysis.

6. REFERENCES

Alexander, J.E., J.H. Steele and E.F. Corcoran (1962) The seasonal cycle of chlorophyll in Florida Straits. *Proceedings Annual Gulf Caribbean Fisheries Institute*, 14, 63-67.

Angel, M. (1989) Does mesopelagic biology affect the vertical flux? In: *Productivity of the ocean: past and present*, W.H. Berger, V. Smetacek and G. Weper, editors, John Wiley & Sons, New York, 155-173.

Armstrong, D.W. (1974) *Some dynamics of carbon, nitrogen and phosphorous in the marine shelf environment of the Mississippi Fan*. Masters thesis, Texas A&M University, College Station, 1-79.

Atkinson, L.P. and D. Wallace (1975) The source of unusually low surface salinities in the Gulf Stream off Georgia. *Deep-Sea Research*, 22, 913-916.

Atkinson, L.P., D.W. Menzel and K.A. Bush, (1985) Oceanography of the southeastern US continental shelf. *Coastal and Estuarine Science*, 2, American Geophysical Union, Washington, 1-156.

Auer, S.J. (1987) Five-year climatological study of the Gulf Stream system and its associated rings. *Journal of Geophysical Research*, 92, 11709-11726.

Azam, F., T. Fenchel, J.G. Field, J.S. Gray, L.A. Meyer-Reed and F. Thingstad (1983) The ecological role of water-column microbes in the sea. *Marine Ecology: Progress Series*, 10, 257-263.

Bane, J.M. and W.K. Dewar (1988) Gulf Stream bimodality and variability downstream of the Charleston Bump. *Journal of Geophysical Research*, 93, 6695-6710.

Bannister, T.T. and A.D. Weidemann (1984) The maximum quantum yield of phytoplankton photosynthesis *in situ*. *Journal of Plankton Research*, 6, 275-294.

Berberian, G.A. and R.B. Starr (1978) The circulation between the Cayman Sea and the Gulf of Mexico as deduced from nutrient distributions. In: *Cooperative investigations of the Caribbean and adjacent regions*, H.B. Stewart, editor, FAO Fisheries Report, 200, Rome, 255-266.

Berger, W.H., K. Fischer, G. Lai and G. Wu (1987) Ocean productivity and organic carbon flux. *SIO Reference 87-30*, University of California, San Diego, 1-67.

Berryhill, H.L. (1977) *Environmental studies, South Texas Outer Continental Shelf, 1975: An atlas and integrated*

study. Prepared for the Bureau of Land Management, Contract 08550-MU5-20, p.240.

BIENFANG, P.K., J. SZYPER and E. LAWS (1983) Sinking rate and pigment responses to light limitation of a marine diatom: implications to dynamics of chlorophyll maximum layers. *Oceanologica Acta*, 6, 55-62.

BLUMBERG, A.F. and G.L. MELLOR (1983) Diagnostic and prognostic numerical evaluation studies of the South Atlantic Bight. *Journal of Geophysical Research*, 88, 4579-4592.

BLUMBERG, A.F. and G.L. MELLOR (1985) A simulation of the circulation in the Gulf of Mexico. *Israel Journal of Earth Science*, 34, 122-144.

BROOKS, I.H. and P.P. NIILER (1975) The Florida Current at Key West: summer 1972. *Journal of Marine Research*, 33, 83-92.

BRYAN, K. and M.D. COX (1972) The circulation of the world ocean: a numerical study. 1. A homogeneous model. *Journal of Physical Oceanography*, 2, 319-335.

CAPONE, D.G. and E.J. CARPENTER (1982) Nitrogen fixation in the marine environment. *Science*, 217, 1140-1142.

CHRISTENSEN, J.P. (1981) *Oxygen consumption, denitrification, and sulfate reduction in coastal marine sediments*. Doctoral dissertation, University of Washington, Seattle, 1-231.

COCHRANE, J.D. and F.J. KELLY (1986) Low-frequency circulation on the Texas - Louisiana continental shelf. *Journal of Geophysical Research*, 91, 10645-10659.

COX, M.D. (1975) A baroclinic numerical model of the world ocean. In: *Numerical models of ocean circulation*, National Academy of Science, Washington, 107-120.

CSANADY, G.T. (1976) Mean circulation in shallow seas. *Journal of Geophysical Research*, 81, 5389-5399.

CSANADY, G.T. (1986) Mass transfer to and from small particles in the sea. *Limnology and Oceanography*, 31, 237-248.

CSANADY, G.T. and P. HAMILTON (1988) Circulation of slopewater. *Continental Shelf Research*, 8, 565-624.

CULLEN, J.J. and R.R. EPPLEY (1981) Chlorophyll maximum layers of the southern California Bight and possible mechanisms of their formation and maintenance. *Oceanologica Acta*, 4, 23-32.

DAGG, M.J., P.B. ORTNER and F. AL-YAMANI (1987) Winter-time distribution and abundance of copepod nauplii in the northern Gulf of Mexico. *Fisheries Bulletin*, 86, 319-330.

DINNEL, S.P. and W.J. WISEMAN (1986) Fresh water on the Louisiana and Texas shelf. *Continental Shelf Research*, 6, 765-784.

ELLIOTT, B.A. (1982) Anticyclonic rings in the Gulf of Mexico. *Journal of Physical Oceanography*, 12, 1291-1309.

EL-SAYED, S.Z. (1972) Primary productivity and standing crop of phytoplankton. In: *Chemistry, primary productivity, and benthic algae of the Gulf of Mexico*, V.C. BUSHNELL, editor, Serial Atlas of the Marine Environment, American Geographical Society, 22, 8-13.

EL-SAYED, S.Z. and C.C. TREES (1980) Ecological studies of phytoplankton in the Gulf of Mexico during NOAA/NMFS Oregon II Cruise. *Texas A&M Technical Report*, 80-8-T, 1-53.

EPPLEY, R.W. (1972) Temperature and phytoplankton growth in the sea. *Fisheries Bulletin*, 70, 1063-1085.

EPPLEY, R.W., E.H. RENGER and W.G. HARRISON (1979) Nitrate and phytoplankton production in southern California coastal waters. *Limnology and Oceanography*, 24, 483-494.

EPPLEY, R.W. and B.J. PETERSON (1979) Particulate organic matter flux and planktonic new production in the deep ocean. *Nature*, 282, 677-680.

ESE and LGL (1985) Southwest Florida shelf benthic communities study. *Year 4 annual report submitted by Environmental Science and Engineering, Inc., and LGL Ecological Research Associates Inc. to Marine Minerals Service*, Metairie, Louisiana. Contract No. 14-12-0001-30071, p.94.

ETTER, .P.C. (1983) Heat and freshwater budgets in the Gulf of Mexico. *Journal of Physical Oceanography*, 13, 2058-2069.

FASHAM, M.J., T. PLATT, B. IRWIN and K. JONES (1985) Factors affecting the spatial pattern of the deep chlorophyll maximum in the region of the Azores Front. *Progress in Oceanography*, 14, 129-165.

FOGG, G.E. (1982) Nitrogen cycling in sea water. *Philosophical Transactions of the Royal Society of London*, B 296, 511-570.

FRANKS, P.J., J.S. WROBLEWSKI and G.R. FLIERL (1986) Prediction of phytoplankton growth in response to the frictional decay of a warm-core ring. *Journal of Geophysical Research*, 91, 7603-7610.

FUCIK, K.W. (1974) *The effect of petroleum operations on the phytoplankton ecology of the Louisiana coastal waters*. Masters thesis, Texas A&M, College Station, 1-82.

FURNAS, M.J. and T.J. SMAYDA (1987) Inputs of subthermocline waters and nitrate onto the Campeche Bank. *Continental Shelf Research*, 7, 161-175.

GEARING, P.J. (1975) *Stable carbon isotope ratios of continental margin sediments*. Doctoral dissertation, University of Texas, Austin, 1-154.

GEARING, P., J.N. GEARING, T.F. LYTLE and J.S. LYTLE (1976) Hydrocarbons in 60 northeast Gulf of Mexico shelf sediments: a preliminary survey. *Geochimica et Cosmochimica Acta*, 40, 1005-1017.

GEARING, P., F.E. PLUCKER and P.L. PARKER (1977) Organic carbon stable isotope ratios of continental margin sediments. *Marine Chemistry*, 5, 251-266.

GEIDER, R.J. and B.A. OSBORNE (1986) Light absorption, photosynthesis, and growth of *Nannochloris atomus* in nutrient-saturated cultures. *Marine Biology*, 93, 351-360.

GOLDMAN, J.C., J.J. MCCARTHY and D.G. PEAVEY (1979) Growth rate influence on the chemical composition of phytoplankton in oceanic waters. *Nature*, 279, 210-215.

GORDON, A.L. (1967) Circulation of the Caribbean Sea. *Journal of Geophysical Research*, 77, 62-73.

GORDON, H.R., O.B. BROWN, R.H. EVANS, J.W. BROWN, R.C. SMITH, K.S. BAKER and D.K. CLARKE (1988) A semianalytic radiance model of ocean color. *Journal of Geophysical Research*, 93, 10909-10924.

HAINES, J.R., R.M. ATLAS, R.P. GRIFFITHS and R.Y. MORITA (1981) Denitrification and nitrogen fixation in Alaska continental shelf sediments. *Applied and Environmental Microbiology*, 41, 412-421.

HALTINER, G.J. (1971) *Numerical weather predictions*, J. Wiley and Sons, New York, 1-317.

HAMILTON, P. and M. RATTRAY (1978) A numerical model of the depth dependent, wind driven circulation on a continental shelf. *Journal of Physical Oceanography*, 8, 437-457.

HANSEN, D.V. and R.L. MOLINARI (1979) Deep currents in the Yucatan Strait. *Journal of Geophysical Research*, 84, 359-362.

HATHAWAY, J.C. (1971) WHOI data file, Continental Margin program, Atlantic coast of the United States. *WHOI Technical Report*, 77-15.

HEDGES, J.I. and P.L. PARKER (1976) Land-derived organic matter in surface sediments from the Gulf of Mexico. *Geochimica et Cosmochimica Acta*, 40, 1019-1029.

HINGA, K.R., J.M. SIEBURTH and G.R. HEATH (1979) The supply and use of organic matter at the deep-sea floor. *Journal of Marine Research*, 37, 557-579.

HOFMANN, E.E. and S.J. WORLEY (1986) An investigation of the circulation of the Gulf of Mexico. *Journal of Geophysical Research*, 91, 14221-14236.

HOLLAND, W.R. and A.D. HIRSCHMAN (1972) A numerical calculation of the circulation of the North Atlantic Ocean. *Journal of Physical Oceanography*, 5, 642-669.

HOLLAND, W.R. and L.B. LIN (1975) On the origin of mesoscale eddies and their contribution to the general circulation of the ocean. I. A preliminary numerical experiment. *Journal of Physical Oceanography*, 5, 642-657.

HULBURT, H.E. and J.D. THOMPSON (1980) A numerical study of Loop Current intrusions and eddy shedding. *Journal of Physical Oceanography*, 10, 1611-1651.

JASSBY, A.D. and T. PLATT (1976) Mathematical formulation of the relationship between photosynthesis and light for phytoplankton. *Limnology and Oceanography*, 21, 540-547.

JENKINS, W.J. (1988) Nitrate flux into the euphotic zone near Bermuda. *Nature*, 331, 521-523..

KING, F.D. and A.H. DEVOL (1979) Estimates of vertical eddy diffusion through the thermocline from phytoplankton uptake rates in the mixed layer of the eastern tropical Pacific. *Limnology and Oceanography*, 24, 645-651.

KIRK, J.T.O. (1983) *Light and Photosynthesis in aquatic environments*, Cambridge University Press, 399pp.

KIRWAN, A.D., J.K. LEWIS, A.W. INDEST, P. REINERSMAN and I QUINTERO (1988) Observed and simulated kinematic properties of Loop Current rings. *Journal of Geophysical Research*, 93, 1189-1198.

KULLENBERG, G.E. (1976) On vertical mixing and the energy transfer from the wind to the water. *Tellus*, 28, 159-165.

LAMPITT, R.S. (1985) Evidence for seasonal deposition of detritus to the deep-sea floor and its subsequent resuspension. *Deep-Sea Research*, 32, 885-898.

LEE, T.N., L.P. ATKINSON and R. LEGECKIS (1981) Observation of a Gulf Stream frontal eddy on the Georgia continental shelf, April 1977. *Deep-Sea Research*, 28, 347-378.

LEIPPER, D.F. (1970) A sequence of current patterns in the Gulf of Mexico. *Journal of Geophysical Research*, 75, 637-657.

LEVITUS, S. (1982) Climatological atlas of the world ocean. *NOAA Professional Paper*, No.13, 1-173.

LEWIS, M.R., W.G. HARRISON, N.S. OAKEY, D. HEBERT and T. PLATT (1986) Vertical nitrate fluxes in the oligotrophic ocean. *Science*, 234, 870-873.

LGL ECOLOGICAL RESEARCH ASSOCIATES (1986) *Gulf of Mexico continental slope study annual report: year 2*. Submitted to Marine Minerals Management Service, Metairie, Louisiana, Contract No. 14-12-0001-30212, pp.B10-B19.

LOCHTE, K. and C.M. TURLEY (1988) Bacteria and cyanobacteria associated with phytodetritus in the deep sea. *Nature*, 33, 67-69.

MALONE, T.C. and P.J. NEALE (1981) Parameters of light-dependent photosynthesis for phytoplankton size fractions in temperate estuarine and coastal environments. *Marine Biology*, 61, 289-297.

MARTIN, J.H., G.A. KNAUER, D.M. KARL and W.M. BROENKOW (1987) VERTEX: Carbon cycling in the northeast Pacific. *Deep-Sea Research*, 34, 267-285.

MAUL, G.A. (1977) The annual cycle of the Gulf Loop. Part I. Observations during a one-year time series. *Journal of Marine Research*, 35, 219-247.

MAUL, G.A. (1978) The 1972-73 cycle of the Gulf Loop Current. Part II: Mass and salt balances of the basin. In: *Cooperative investigations of the Caribbean and adjacent regions*, H.B. STEWART, editor, FAO Fisheries Report 200, Rome, 597-619.

MAUL, G.A., G.C. THOMAS and T.A. NELSEN (1979) Hydrographic data from the NOAA ship *Researcher* during the October 1977 ocean color and circulation cruise in the Gulf of Mexico. *NOAA Data Report ERL AOML-1*, Miami, 1-31.

MCELROY, M.B. (1983) Marine biological controls in atmospheric CO_2 and climate. *Nature*, 302, 328-329.

MELLOR, G.L. and T. YAMADA (1974) A hierarchy of turbulence closure models for planetary boundary layers. *Journal of Atmospheric Science*, 31, 1791-1806.

MERRELL, W.J., J.M. MORRISON, W.D. NOWLIN, R.L. MOLINARI, I.H. BROOKS and R. YAGER (1978) A description of the circulation observed in the eastern Gulf of Mexico during CICAR survey month II, May 1972. In: *Cooperative Investigations of the Caribbean and Adjacent Regions*, H.B. STEWART, editor, FAO Fisheries Report 200, Rome, 51-61.

MITCHUM, C.T. and W. STURGES (1982) Wind-driven currents on the West Florida shelf. *Journal of Physical Oceanography*, 12, 1310-1317.

MOLINARI, R.L. and R.E. YAGER (1977) Upper layer hydrographic conditions at the Yucatan Strait during May 1972. *Journal of Marine Research*, 35, 11-20.

MONTGOMERY, R. (1941) Transport of the Florida Current off Habana. *Journal of Marine Research*, 4, 198-220.

MOREL, A. and R.C. SMITH (1974) Relation between total quanta and total energy for aquatic photosynthesis. *Limnology and Oceanography*, 19, 591-600.

MORRISON, J.M. and W.D. NOWLIN (1977) Repeated nutrient, oxygen, and density sections through the Loop Current. *Journal of Marine Research*, 35, 105-126.

MULLER, P.J. and E. SUESS (1979) Productivity, sedimentation rate, and sedimentary organic matter in the ocean. I. Organic carbon preservation. *Deep-Sea Research*, 26, 1347-1362.

MÜLLER-KARGER, F.E., J.J. WALSH, D.A. DIETERLE and R.H. EVANS (1988) The seasonal cycle of the circulation in the western North Atlantic: the interplay between the open ocean, the Caribbean Sea, and the Gulf of Mexico. *EOS*, 69, 1113.

MUNK, W.H. (1950) On the wind-driven ocean circulation. *Journal of Meteorology*, 7, 79-93.

MUNK, W.H. and E.R. ANDERSON (1948) Notes on a theory of the thermocline. *Journal of Marine Research*, 7, 277-295.

MURPHY, E.B., K.A. STEIDINGER, B.S. ROBERTS, J. WILLIAMS and J.W. JOLLEY (1975) An explanation for the Florida east coast *Gymnodinium breve* red tide of November 1972. *Limnology and Oceanography*, 20, 481-486.

NIILER, P.P. (1975) Deepening of the wind-mixed layer. *Journal of Marine Research*, 33, 405-422.

NIILER, P.P. and W.S. RICHARDSON (1973) Seasonal variability of the Florida Current. *Journal of Marine Research*, 31, 144-167.

NOWLIN, W.D. and H.J. MCLELLAN (1967) A characterization of the Gulf of Mexico waters in winter. *Journal of Marine Research*, 25, 24-59.

NOWLIN, W.D. and J.M. HUBERTZ (1972) Contrasting summer circulation patterns for the eastern Gulf Loop Current versus anticyclonic ring. *Texas A&M University Oceanographic Study 2*, L.R. CAPURRO and R.O. REID, editors, Gulf Publishing Co., Houston, 119-138.

O'BRIEN, J.J. (1971) A two-dimensional model of the wind-driven North Pacific. *Investigacion Pesquera*, 35, 331-349.

O'BRIEN, J.J. (1986) The hyperbolic problem. In: *Advanced physical oceanographic numerical modelling*. J.J. O'BRIEN, editor, Reidel, Dordrecht, 165-186.

O'BRIEN, J.J. and H.E. HULBURT (1972) A numerical model of coastal upwelling. *Journal of Physical Oceanography*, 2, 14-26.

O'BRIEN, J.J. and G.W. HEBURN (1983) The state-of-the-art in coastal ocean modelling: a numerical model of coastal upwelling off Peru — including mixed layer dynamics. In: *Coastal ocean modelling*, H.G. GADE, A. EDWARDS and H. SVENDSEN, editors, Plenum, New York, 113-164.

ORTNER, P.B., R.L. FERGUSON, S.R. PIOTROWICZ, L. CHESAL, G.A. BERBERIAN and A.V. PALUMBO (1984) Biological consequences of hydrographic and atmospheric advection within the Gulf Loop Intrusion. *Deep-Sea Research*, 31, 1101-1120.

PARKER, R.A. (1977) *Radiocarbon dating of marine sediments*. Doctoral dissertation, Texas A&M University, College Station, 1-128.

PASKAUSKY, D.F. and R.O. REID (1972) A barotropic prognostic numerical circulation model. In: *Contributions on the physical oceanography of the Gulf of Mexico, Volume II*, L.R. CAPURRO and R.O. REID, editors, Gulf Publishing Company, Houston, 163-176.

PLATT, T. and A.D. JASSBY (1976) The relationship between photosynthesis and light for natural assemblages of coastal marine phytoplankton. *Journal of Phycology*, 12, 421-430.

PLATT, T. and W.G. HARRISON (1985) Biogenic fluxes of carbon and nitrogen in the ocean. *Nature*, 318, 55-58.

REED, R.K. (1977) On estimating insolation over the ocean. *Journal of Physical Oceanography*, 7, 482-485.

ROWE, G.T. and D.W. MENZEL (1971) Quantitative benthic samples from the deep Gulf of Mexico. *Bulletin of Marine Science*, 21, 556-566.

SCHOLL, D.W. (1963) Sedimentation in modern coastal swamps, southwestern Florida. *American Association of Petrologists and Geologists Bulletin*, 47, 1581-1603.

SCHROEDER, W.W., S.P. DINNEL, W.J. WISEMAN and W.J. MERRELL (1987) Circulation patterns inferred from the movement of detached buoys in the eastern Gulf of Mexico. *Continental Shelf Research*, 7, 883-894.

SHOKES, R.F. (1976) *Rate-dependent distribution of lead-210 and interstitial sulfate in sediments of the Mississippi River Delta*. Doctoral dissertation, Texas A&M University, College Station, 1-123.

SMETACEK, V.S. (1985) Role of sinking in diatom life-history cycles: ecological, evolutionary, and geological significance. *Marine Biology*, 84, 239-251.

SMOLARKIEWICZ, P.K. (1983) A simple positive definite advection scheme with small implicit diffusion. *Monthly Weather Review*, 111, 479-486.

STEELE, J.H. (1964) A study of production in the Gulf of Mexico, *Journal of Marine Research*, 22, 211-222.

STETSON, H.C. and P.D. TRASK (1953) The sedimentation of the western Gulf of Mexico. *Papers in Physical Oceanography and Meteorology*, 12, 1-46.

STOMMEL, H. (1965) *The Gulf Stream*, University of California Press, Berkeley, 1-248.

STOMMEL, H. (1987) *A view of the sea*, Princeton University Press, Princeton, 1-165.

STURGES, W. and J.C. EVANS (1983) On the variability of the Loop Current in the Gulf of Mexico. *Journal of Marine Research*, 41, 639-653.

SUGIMOTO, T. and T. ICHIYE (1988) On seasonal and year-to-year variations of the Loop Current and eddy formation in the Gulf of Mexico based on rotating model experiments. *Deep-Sea Research*, 35, 569-594.

SUSIO (1977) *Baseline monitoring studies, Mississippi, Alabama, Florida, outer continental shelf, 1975-76. Volume III. Results*. Compiled by the State University System of Florida Institute of Oceanography, St. Petersburg, for the Bureau of Land Management. Contract No. 08550-CTS-30. US Document PB-282 803, Springfield, pp.361.

SVERDRUP, H.U., M.W. JOHNSON and R.H. FLEMING (1942) *The oceans*, Prentice-Hall, Englewood Cliffs, 1-1060.

THOMAS, W.H. and G. SIMMONS (1960) Phytoplankton production in the Mississippi Delta. In: *Recent sediments, northwest Gulf of Mexico*, F.P. SHEPARD, F.B. PHLEGER and T.H. VAN ANDEL, editors, American Association of Petrologists and Geologists, Tulsa, 103-116.

THOMPSON, J.D. (1974) *The coastal upwelling cycle on a beta-plane. Hydrodynamics and thermodynamics*. Doctoral dissertation, Florida State University, Tallahassee, 1-141.

TRASK, P.D. (1953) The sediments of the western Gulf of Mexico, Part II. Chemical studies of sediments in the western Gulf of Mexico. *Papers in Physical Oceanography and Meteorology*, 12, 47-120.

TREES, C.C. (1985) *Remote sensing of ocean color in the northern Gulf of Mexico*. Doctoral dissertation, Texas A&M University, College Station, 1-258.

UPSHAW, C.F., W.B. CREATH and F.L. BROOKS (1966) Sediments and microfauna off the coasts of Mississippi and adjacent states. *Mississippi Geological, Economic and Topographic Survey, Bulletin*, 106, 1-127.

VASILEV, G.D. and Y.A. TORIN (1969) Oceanographic and fishing-biological characteristics of the Gulf of Mexico and the Caribbean Sea. In: *Soviet-Cuban fishery research*, A.S. BOGDANOV, editor, Israel Programs for Scientific Translation, Jerusalem, 225-250.

VUKOVICH, F.M. and G.A. MAUL (1985) Cyclonic eddies in the eastern Gulf of Mexico. *Journal of Physical Oceanography*, 15, 105-117.

VUKOVICH, F.M., B.W. CRISSMAN, M. BUSHNELL and W.J. KING (1979) Some aspects of the oceanography of the Gulf of Mexico using satellite and *in situ* data. *Journal of Geophysical Research*, 84, 7749-7768.

WADA, E. and A. HATTORI (1972) Nitrite distribution and nitrate reduction in deep sea waters. *Deep-Sea Research*, 19, 123-132.

WALLCRAFT, A. (1986) *Gulf of Mexico circulation modelling study*. Progress report by JAYCOR to Minerals Management Service, Metairie, Louisiana. Contract No. 14-12-0001-30073, pp.1-94.

WALSH, J.J. (1983) Death in the sea: enigmatic phytoplankton losses. *Progress in Oceanography*, 12, 1-86.

WALSH, J.J. (1984) The role of the ocean biota in accelerated ecological cycles: a temporal view. *Bioscience*, 34, 499-507.

WALSH, J.J. (1988) *On the nature of continental shelves*, Academic Press, New York, 1-520.

WALSH, J.J., G.T. ROWE, R.L. IVERSON and C.P. MCROY (1981) Biological export of shelf carbon is a neglected sink of the global CO_2 cycle. *Nature*, 291, 196-201.

WALSH, J.J., E.T. PREMUZIC, J.S. GAFFNEY, G.T. ROWE, G. HARBOTTLE, R.W. STOENNER, W.L. BALSAM, P.R. BETZER and S.A. MACKO (1985) Organic storage of CO_2 on the continental slope off the mid-Atlantic bight, the southeastern Bering Sea, and the Peru coast. *Deep-Sea Research*, 32, 853-883.

WALSH, J.J., D.A. DIETERLE and M.B. MEYERS (1988a) A simulation analysis of the fate of phytoplankton within the Mid-Atlantic Bight. *Continental Shelf Research*, 8, 757-788.

WALSH, J.J., P.E. BISCAYE and G.T. CSANADY (1988b) The 1983-84 Shelf Edge Exchange Processes (SEEP)-I experiment: hypotheses and highlights. *Continental Shelf Research*, 8, 435-456.

WARD, B.B., R.J. OLSEN and M.J. PERRY (1982) Microbial nitrification rates in the primary nitrite maximum off southern California. *Deep-Sea Research*, 29, 247-255.

WENNEKENS, M.P. (1959) Water mass properties of the Straits of Florida and related waters. *Bulletin of Marine Science*, 9, 1-52.

WOODS, J.D. (1988) Mesoscale upwelling and primary production. In: *Towards a theory of biological-physical interaction in the world ocean*, B.J. ROTHSCHILD, editor, D. Reidel, Dordrecht, 95-125.

WROBLEWSKI, J.S. and J.G. RICHMAN (1987) The nonlinear response of plankton to wind mixing events — implications for larval fish survival. *Journal of Plankton Research*, 9, 103-123.

WUST, G. (1964) *Stratification and circulation in the Antillean-Caribbean basins*, Columbia University Press, New York, 1-201.

Reprinted from Nature, Vol. 350, No. 6313, pp. 53–55, 7th March, 1991

Importance of continental margins in the marine biogeochemical cycling of carbon and nitrogen

John J. Walsh

Department of Marine Science, University of South Florida, 140 Seventh Avenue South, St Petersburg, Florida 33701, USA

THE continental margins occupy less than 20% of the surface area of the world ocean, and it is widely assumed that they do not play a significant part in the oceanic biogeochemical cycles of carbon and nitrogen. Data from 32 sediment-trap moorings, 16 in the deep sea and 16 on the continental slope[1], suggest that at an average depth of 2,650 m on the slope, the combined rain of surviving shelf and slope particles yields a mean carbon flux of 6.9 g C m^{-2} yr^{-1}—about ten times that at the same average depth in the deep sea (0.8 g C m^{-2} yr^{-1}). Because the area of the deep sea is about ten times greater than that of the continental slopes, using the sediment-trap data and assuming a carbon/nitrogen ratio of 5:1, the equivalent total particulate offshore nitrogen loss is 0.5×10^{14} g N yr^{-1} at 2,650 m. If these trap observations are generally representative of the oceans and continental margins, then the supply of dissolved nitrate to the overlying euphotic zones should also be similar. Here I provide an independent estimate of the annual supply of onwelling nitrate from the deep sea to the shelves and find that it may balance the offshore flux of carbon, suggesting that the continental margins and deep sea are equally important in the carbon and nitrogen biogeochemical cycles.

The mass flux of particulate matter caught with sediment traps increases with depth on the continental slope[2–4], implying a lateral transport from the adjacent shelf. If losses of dissolved organic nitrogen back to the slope, the burial of organic matter within the shelf sediments, and evasion of gaseous nitrogen (N_2, N_2O) to the atmosphere are all small, then the export flux of particulate nitrogen at the shelf break can be estimated from the exogenous dissolved nitrogen input and the phytoplankton uptake, and is equivalent to 'new' production[5]. Here I ignore fixation of atmospheric N_2 by cyanobacteria and rainfall, as well as freshwater supplies of organic matter. I have also ignored shelf nitrification because it is an endogenous source of nitrate, similar to recycling of ammonium, urea and amino acids within the shelf ecosystem. First I estimate the onwelling flux of dissolved nitrate to continental shelves from the deep sea.

A shelf area of 2.6×10^7 km^2 and an average width of 85 km yield a mean length of $\sim 3.1 \times 10^5$ km. In an attempt to account for the spatial inhomogeneity of nutrient exchange, I have partitioned shelf regions into those of coastal upwelling in eastern boundary currents, those of cyclonic eddy upwelling in western boundary currents, and those of estuarine-induced exchange (Table 1). The effect of both coastal and eddy-induced upwelling is to transport nitrate from deeper levels of slope waters to shallower depths, for example, to the 100-m isobath at the shelf break. Knowledge of the nitrate stocks at a depth of 100 m along the shelf break and the lateral flows onto the outer shelf yields the advective onshore flux of nitrate to these types of shelves (Table 2). This may be an underestimate, because I have ignored horizontal mixing in these calculations.

When coastal upwelling prevails in eastern boundary currents, the nitrate contents are 30 μmol NO_3 l^{-1} at 100 m off Oregon[6], 25 μmol NO_3 l^{-1} at this depth off Baja California[6] and southwest Africa[7], 25–30 μmol NO_3 l^{-1} off Peru[8], >20 μmol NO_3 l^{-1} off Somalia[9], and 15 μmol NO_3 l^{-1} off northwest Africa[10]. During 2–3 months of upwelling off Oregon and Peru, the onshore flow past the 100-m isobath is 1–5 cm s^{-1} over the lower half of the water column[11]. The thickness of the benthic boundary layer in these two shelves is calculated to be 10–13 m, when stratification of the water column is considered[11].

Coastal upwelling is, however, seasonal; for example, the nitrate content at the 60-m isobath off Oregon is >20 μmol NO_3 l^{-1} during only six months of the year[12]. Over 12 months, the mean onshore flow within the benthic boundary layer at the 100-m isobath of coastal upwelling regions might be only ~2.5 cm s^{-1} with a mean nitrate stock of 20 μmol NO_3 l^{-1}. Over the coastal upwelling region of 8.6×10^7 m length (Table 1), a daily onshore flux of 2.5×10^3 m day^{-1} (20 mmol NO_3 m^{-3}) within a 10-m depth interval yields an annual nitrogen input of 2.2×10^{14} g N yr^{-1} (Table 2).

When cyclonic eddies are present in western boundary currents, the nitrate content at 100 m is 15–20 μmol NO_3 l^{-1} in the Florida[13], Kuroshio[14] and Loop[15] currents. At other times, the content at this depth is at least 10 μmol NO_3 l^{-1} in the Brazil current[16], suggesting a mean content of ~15 μmol NO_3 l^{-1} (Table 2). Eddy-induced upwelling[13] is a sporadic process, however, which introduces nutrients to the shelf break only in the lower 20–30 m of the water column. Mean onshore flows of 0.5–1.1 cm s^{-1} have been observed at 3 m above the 40-m and 75-m isobaths over a four-month period in the South Atlantic Bight[17]. At mid-depth on the 75-m isobath, mean onshore flows of 3.0 cm s^{-1} have also been observed here. Assuming again an onshore flow of 2.5 cm s^{-1} in a 10-m-thick layer with a nitrate content of 15 μmol NO_3 l^{-1} yields an onwelling flux of 1.3×10^{14} g N yr^{-1} for eddy upwelling (Table 2).

In contrast to the upwelling ecosystems, the nitrate content at 100 m off estuarine-influenced shelves in the North Sea[18], the South China Sea[19], the Beaufort Sea[20] and the Mid-Atlantic Bight[21] is 10 μmol NO_3 l^{-1}. The diabathic circulation of these regions is more complex, with onshore flows at intermediate depth, rather than in a benthic boundary layer. Long-term moorings at the shelf break on the 198-m isobath south of Martha's Vineyard[22] show mean onshore flows of 1.0–2.3 cm s^{-1} at depths of 88–118 m. With a boundary condition of 10 μmol NO_3 l^{-1}, the shoreward influx of nitrate to estuarine-influenced shelves at 2.5 cm s^{-1} over a 10-m-thick layer is estimated to be 2.1×10^{14} g N yr^{-1} (Table 2).

The total input of deep-sea nitrate across the shelf break is 5.6×10^{14} g N yr^{-1}, compared to a terrestrial flux of perhaps 0.6×10^{14} g N yr^{-1} across the shoreline (Fig. 1) from dissolved inorganic nitrogen (DIN) in present river runoff and sewage discharge[12]. An estimated terrestrial dissolved-organic-carbon (DOC) loading[23] of 0.8×10^{15} g C yr^{-1} and a higher-plant carbon/nitrogen ratio of at least 16:1 suggest a similar freshwater

TABLE 1 Partitioning of shelf-break length into regions

Shelf-break length (km)	Coastal upwelling	Eddy upwelling	Estuarine exchange*
Northern Hemisphere (0–60°)	36,400	30,000	65,200
Arctic (>60°)	—	—	46,400
Southern Hemisphere (0–60°)	50,000	35,600	14,800
Antarctic (>60°)	—	—	36,000
Total	86,400	65,600	162,400

* The regions of estuarine dispersion are determined by the extent of the 33.0-p.s.u. isopleth of surface salinity, which is similar to ~2.0-p.s.u. deviations from average latitudinal salinities[38].

TABLE 2 Nitrate flux onto continental shelves from the deep sea

	Coastal upwelling	Eddy upwelling	Estuarine exchange
Nitrate content, N, at 100 m (μmol NO_3 l^{-1})	20	15	10
Advective flux, uN* (10^5 g N m^{-2} yr^{-1})	2.5	1.9	1.3
Shelf-break exchange area, A (10^8 m^2)	8.6	6.6	16.2
Nitrate input, uNA (10^{14} g N yr^{-1})	2.2	1.3	2.1

* where u is a mean onshore flow of 2.5 cm s^{-1}.

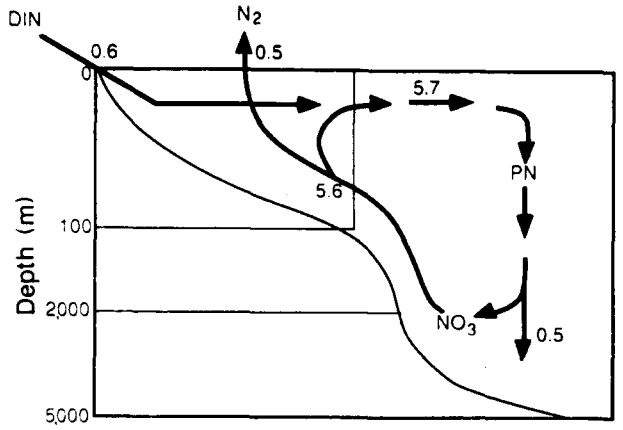

FIG. 1 Estimated fluxes (10^{14} g N yr^{-1}) of riverine dissolved inorganic nitrogen (DIN), deep-sea nitrate (NO_3), particulate nitrogen (PN), and gaseous nitrogen (N_2) in the continental margins.

input of dissolved organic nitrogen (DON) of 0.5×10^{14} g N yr^{-1}. The fate of terrestrial DON is presumably oxidation on or near the continental margins, but the lability of these compounds is unknown and I have therefore ignored them.

Before the Industrial Revolution, inputs of DIN from the land may have been ten times less than they are today[24]. Similarly, anthropogenic inputs of atmospheric nitrogen may now be affecting the nitrogen/phosphorus ratios of offshore waters[25], but rainfall is still considered a small source of nitrogen to either the coastal zone[25] or the deep sea[26]. I have also ignored burial of organic nitrogen on the shelf in this budget. Finally, previous estimates of denitrification[27,28], with evasion mainly of N_2 (perhaps 8% is N_2O) from the shelves, are similar at a maximum of 0.5×10^{14} g N yr^{-1} (Fig. 1), although recent measurements raise the possibility of a tenfold larger flux[29].

The present anthropogenic DIN loading of 0.6×10^{14} g N yr^{-1} may offset a denitrification loss of 0.5×10^{14} g N yr^{-1}, so that 5.7×10^{14} g N yr^{-1} may be available for 'new' production and export (Fig. 1) if the onwelled nitrate is efficiently converted to particulate or dissolved organic nitrogen. With a mean shelf depth of 50 m, the average residence time of onwelled nitrate would be 167 days, over which light limitation could be significant on shelves at mid-latitudes. With a phytoplankton carbon/nitrogen ratio of 5:1, this dissolved nitrogen import thus allows a maximum carbon export of 2.9×10^{15} g C yr^{-1} from the shelves in the form of particles and dissolved organic matter.

A mean DOC excretion rate[12] by shelf phytoplankton of 17% of the total photosynthesis of 5.2×10^{15} g C yr^{-1} suggests that 0.9×10^{15} g C yr^{-1}, or 1.8×10^{14} g N yr^{-1}, might be exported in dissolved form. Perhaps a third of this marine DON loss is replaced by the terrestrial DON import, but the residence time of the two nitrogen pools may differ[30]. Some unused deep-sea nitrate may exit as well, depending on the season and depth of exodus; after phytoplankton blooms, however, shelf surface waters[12] usually contain less than 1 μmol NO_3 l^{-1}.

A total particle rain of 2.2×10^{14} g C yr^{-1} trapped at 2,650 m (spread over a slope area of 3.2×10^7 km^2) and a particulate export of 2.0×10^{15} g C yr^{-1} at the 100-m shelf break imply that perhaps 10% of the detritus escapes oxidation to dissolved CO_2 during the 2,550-m descent in slope waters. Within 300 km of the shelf break, however, bottom metabolism of margin sediments[31], where half of the ocean's degradable organic carbon is stored[32], suggests that sediment traps may underestimate the influx of detritus by 200–300%, missing the lateral contribution of near-bottom suspended matter. As much as 20–30% of shelf export may thus be stored, or degraded, in slope sediments.

A total primary production of 200 g C m^{-2} yr^{-1} over all shelves (requiring 10.4×10^{14} g N yr^{-1}) and full utilization of the onwelled nitrate suggest an *f* ratio (new/total production) of 0.54. In contrast, the same new production of 5.7×10^{14} g N yr^{-1} over the deep sea (3.1×10^8 km^2), a total primary production of 20×10^{15} g C yr^{-1} here[24], and a carbon/nitrogen ratio of 5:1 suggest an *f* ratio of 0.14 for the oceanic ecosystem. These *f* ratios are consistent with tight coupling betwen primary producers, herbivores and saprovores in the deep sea, where large DOC excretion rates prevail. Here, export occurs mainly as fast-sinking (>100 m day^{-1}) faecal pellets, compared to phytodetrital export at similar setting velocities[33] from uncoupled shelf food webs.

Furthermore, a mean nitrate stock of 3.0 μmol NO_3 l^{-1} at a depth of 100 m in the deep sea[6,34] and a unit vertical influx of 1.84 g N m^{-2} yr^{-1} up the sharp oceanic gradient of nutrient (nutricline) yield an upwelling velocity of 43.8 m yr^{-1} beneath the euphotic zone (nominally 100 m). Over a similar 100-m interval of the nutricline, such an upwelling velocity is equivalent to a vertical eddy diffusivity K_z of 1.2 cm^2 s^{-1}. Field studies of nitrogen uptake by phytoplankton and vertical gradients of nitrate indeed suggest an independent estimate of K_z of ~1 cm^2 s^{-1} across the oceanic nutricline[35,36].

Marine phytoplankton are usually limited by the availability of nitrogen in the euphotic zone, not by the CO_2 concentration. Anthropogenic nitrogen loading has increased about tenfold in estuaries, where eutrophication is worldwide[24], for example, and it may be inducing phosphate limitation within the deep sea through rainfall[25]. If future 'greenhouse' warmings lead to greater evaporation in the global hydrological cycle, such that the estuarine onwelling of nitrate increases as a consequence of larger freshwater runoff, we might expect another increment of the detrital carbon sink at the margins (provided that the annually averaged partial pressure of CO_2 in these waters is held below that of the atmosphere by the enhanced photosynthesis). Furthermore, coastal upwelling may increase under intensified along-shore wind stress associated with such a global warming[37], leading to additional carbon extraction from the atmosphere. How accurate, however, are the above onwelling and denitrification estimates? Extensive studies of continental margins, where half of the ocean biogeochemical fluxes may occur, are required. □

Received 9 May 1990; accepted 14 January 1991

1 Walsh, J. J., Dieterle, D. A. & Pribble, J. R. *Deep Sea Res.* (in the press)
2 Biscaye, P. E., Anderson, R. F. & Deck, R. L. *Cont. Shelf Res.* **8**, 885–904 (1988)
3 Jackson, G. A. *et al. Eos* **70**, 146–155 (1989)
4 Honjo, S., Manganini, S. J. & Cole, J. J. *Deep Sea Res.* **29**, 609–625 (1982)
5 Eppley, R. W. & Peterson, B. J. *Nature* **282**, 677–680 (1979)
6 Walsh, J. J. *Limnol. Oceanogr.* **21**, 1–13 (1976)
7 Bailey, G. W. & Chapman, P. in *South African Ocean Colour and Upwelling Experiment* (ed. Shannon, L. W.) 125–146 (Sea Fish. Res. Inst., Cape Town, 1985)
8 Walsh, J. J. *et al. Deep Sea Res.* **27**, 1–27 (1980)
9 McGill, D. A. in *The Biology of the Indian Ocean* (Ed. Zeitzschel, B.) 53–102 (Springer, Berlin, 1973)
10 Codispoti, L. A. & Friederich, G. E. *Deep Sea Res.* **25**, 751–770 (1978)
11 Smith, R. L. in *Coastal Upwelling* (ed. Richards, F. A.) 107–118 (American Geophysical Union, Washington, DC, 1980)
12 Walsh, J. J. *On the Nature of Continental Shelves* (Academic, New York, 1988)
13 Lee, T. N., Atkinson, L. P. & Legeckis, R. *Deep Sea Res.* **28**, 347–378 (1981)
14 Hogetsu, K. & Taga, N. in *Productivity of Biocenoses in Coastal Regimes of Japan* (eds Hogetsu, K., Hatanaka, M., Hanaoka, T. & Kawamura, T.) 31–172 (University of Tokyo, 1977)
15 Walsh, J. J., Dieterle, D. A., Meyers, M. B. & Muller-Karger, F. E. *Prog. Oceanogr.* **23**, 245–301 (1989)
16 Eisma, D. & Van Bennekom, A. J. *Hydrol. Newsl. Spec. Publ.* **6**, 25–48 (1971)
17 Lee, T. N. & Pietrafesa, L. J. *Prog. Oceanogr.* **19**, 267–312 (1987)
18 Brockman, U., Billen, G. & Gieskes, W. W. in *Pollution of the North Sea* (eds Salomons, W., Bayne, B. L., Duursma, E. K. & Forstner, U.) 348–389 (Springer, Berlin, 1988)
19 Takahashi, M. & Hori, T. *Mar. Biol.* **79**, 177–186 (1984)
20 Aagaard, K., Pease, C. H. & Salo, S. A. *NOAA Tech. Mem. ERL PMEL-82* 1, 171 (1988)
21 Walsh, J. J. *et al. Limnol. Oceanogr.* **23**, 659–683 (1978)
22 Beardsley, R. C., Chapman, D. C., Brink, K. H., Ramp, S. R. & Schlitz, R. *J. phys. Oceanogr.* **15**, 713–771 (1985)
23 Richey, J. E., Brock, J. T., Naiman, R. J., Wissmar, R. C. & Stallard, R. F. *Science* **207**, 1348–1351 (1980)
24 Walsh, J. J., Rowe, G. T., Iverson, R. L. & McRoy, C. P. *Nature* **281**, 196–201 (1981)
25 Fanning, K. A. *Nature* **339**, 460–463 (1989)
26 Knap, A., Jickells, T., Pszenny, A. & Galloway, J. *Nature* **320**, 158–160 (1986)
27 Walsh, J. J. *Bioscience* **34**, 499–507 (1984)
28 Christensen, J. P., Murray, J. W., Devol, A. H. & Codispoti, L. A. *Global biogeochem. Cycles* **1**, 97–116 (1987)
29 Devol, A. H. *Nature* **349**, 319–321 (1991)
30 Suzuki, Y. & Tanoue, E. in *Ocean Margin Processes in Global Change* (eds Mantoura, R. F., Martin, J. M. & Wollast, R. F.) (Wiley, New York, in the press)

31. Jahnke, R. A., Reimers, C. E. & Craven, D. B. *Nature* **348**, 50-54 (1990).
32. Emerson, S. *et al. Nature* **329**, 51-53 (1987).
33. Alldredge, A. L. & Gotschalk, C. C. *Deep Sea Res.* **36**, 159-171 (1989).
34. Wroblewski, J. S., Sarmiento, J. L. & Flierl, G. R. *Global biogeochem. Cycles* **2**, 199-218 (1988).
35. Eppley, R. W., Renger, E. H. & Harrison, W. G. *Limnol. Oceanogr.* **24**, 483-494 (1979).
36. King, F. D. & Devol, A. H. *Limnol. Oceanogr.* **24**, 645-651 (1979)
37. Bakun, A. *Science* **247**, 198-201 (1990).
38. Dietrich, G. *General Oceanography* Chart 4 (Wiley, New York, 1963).

ACKNOWLEDGEMENTS. This analysis was funded by the Department of Energy, NASA, the Office of Naval Research and the NSF.

Deep-Sea Research, Vol. 38, No. 7, pp. 805–828, 1991.
Printed in Great Britain.

0198-0149/91 $3.00 + 0.00

Organic debris on the continental margins: a simulation analysis of source and fate

JOHN J. WALSH,* DWIGHT A. DIETERLE* and J. RAYMOND PRIBBLE*

(*Received* 19 *January* 1990; *in revised form* 31 *December* 1990; *accepted* 7 *January* 1991)

Abstract—A fine-mesh (0.5 km, 2.5 m) two-dimensional model of particle transport and decomposition in the aphotic zone (>150 m) is used to analyse time series (April–August) of element fluxes caught by sediment traps, moored in a transect from the upper slope (500 m) to the continental rise (2750 m) of the Mid-Atlantic Bight. Inclusion of a benthic boundary layer within generally quiescent offshore flows of ~1 cm s^{-1} in the model allows replication of the time phasing and amount of organic carbon sampled by the traps at 50 m above bottom. Over the lower 75 m of the water column on the upper slope, the survival of shelf diatom chains (sinking at 10 m day^{-1}), as well as slope picoplankton (1 m day^{-1}) and zooplankton fecal pellets (100 m day^{-1}), provides most of the model's fidelity after the demise of the spring bloom. On the lower slope, however, the slow settling classes of detritus (<10 m day^{-1}) do not survive the descent, with fluxes of shelf macroaggregates (also sinking at 100 m day^{-1}) and fecal pellets required instead to match observations of particle rain. Downslope resuspension, near-bottom transport, and particle disaggregation may introduce more organic matter to sediments of the continental margins than previously estimated with traps.

INTRODUCTION

OVER the last decade, 16 sediment traps moored on the continental margins, ranging from depths of 450 to 3791 m within ~250 km of the coast, yield a mean organic carbon flux of 6.89 g C m^{-2} y^{-1} at an average depth of 2265 m (Table 1). Another 16 sediment traps moored at depths of 635–3800 m in the deep sea indicate a mean particulate flux of only 0.84 g C m^{-2} y^{-1} at the same average depth of 2257 m (Table 1). Since the area of the continental slopes is ten-fold less than that of the deep sea, the total organic carbon loading at ~2260 m above the margins and within the deep sea may be equivalent. The subsequent fate of organic matter in the deep sea is different, with particles falling and decomposing over another 3000 m before arrival on the sea bottom. Consequently, half of the degradable organic carbon within the surface layer of ocean sediments is located on the continental margins (EMERSON *et al.*, 1987), while 50% of the benthic oxygen consumption may occur within 500 km of the coast (JAHNKE and JACKSON, 1987).

The higher local flux of particulate matter on the continental margins is attributed both to greater primary production of the overlying water column, and lateral import of detritus from the adjacent shelves, since the total mass flux increases with depth in the water column (HONJO *et al.*, 1982; BISCAYE *et al.*, 1988; JACKSON *et al.*, 1989). Zooplankton fecal

*Department of Marine Science, University of South Florida, St Petersburg, FL 33701, U.S.A.

Table 1. *Organic carbon fluxes* ($g\ C\ m^{-2}\ y^{-1}$) *at long-term* (2–12 *months*) *and short-term** (<1 *month*) *moorings on the continental margin and in the deep sea*

	Continental margin			Deep sea			
Region	Trap depth	Flux	Source	Region	Trap depth	Flux	Source
76°N	1700	2.9	WEFER (1989)	65–78°N	2442	0.4	WEFER (1989)
38–40°N	450	11.3	BISCAYE *et al.* (1988)	65–78°N	2823	0.4	WEFER (1989)
38–40°N	975	15.5	BISCAYE *et al.* (1988)	65–78°N	2749	0.5	WEFER (1989)
38–40°N	1200	5.1	BISCAYE *et al.* (1988)	65–78°N	2761	1.4	WEFER (1989)
38–40°N	2250	2.2	BISCAYE *et al.* (1988)	65–78°N	2630	0.6	WEFER (1989)
38–40°N	2700	2.2	BISCAYE *et al.* (1988)	50°N	3800	1.1	HONJO (1984)
38–40°N	2160	6.5*	ROWE and GARDNER (1979)	32°N	3200	0.7	DEUSER (1986)
38–40°N	2800	3.5*	ROWE and GARDNER (1979)	31°N	976	0.9	HONJO (1978)
38–40°N	3500	5.4*	ROWE and GARDNER (1979)	31°N	3694	0.3	HONJO (1978)
38–40°N	3520	3.8*	HINGA *et al.* (1979)	14–36°N	1500	1.8*	MARTIN *et al.* (1987)
34°N	1350	10.8*	HINGA *et al.* (1981)	15°N	2778	0.4	HONJO (1980)
36°N	1500	25.9*	KNAUER and MARTIN (1981)	13°N	988	1.4	HONJO (1980)
13°N	3200	0.7–2.1†	DEUSER *et al.* (1988)	11°N	635	0.9	FISCHER (1984)
5°N	3560	4.9	HONJO (1982)	11°N	1565	1.3	FISCHER (1984)
5°N	3791	3.8	HONJO (1982)	11°N	2700	1.3	FISCHER (1984)
62°S	1588	4.3	WEFER (1989)	62°S	863	0.03	WEFER (1989)
Mean: $n = 16$	2265	6.89		$n = 16$	2257	0.84	

†Assuming organic carbon is 4.5% of total particle flux.

pellets constitute less than 14% of the total organic carbon flux in the Panama Basin (PILSKAN and HONJO, 1987) and less than 17% in the Santa Monica Basin (JACKSON *et al.*, 1989), such that most of the fast sinking (~100–150 m day^{-1}) organic matter is presumably aggregated phytodetritus (ALLDREDGE, 1979; BILLET *et al.*, 1983; LAMPITT, 1985; ALLDREDGE and GOTSCHALK, 1989). Seasonal variation of the type of primary producers and associated phytodetritus, e.g. diatoms, coccolithophores, dinoflagellates or picoplankton, may significantly alter the sinking rate, the residence time and thus the pelagic oxidation loss of these sources of organic matter to the benthic communities on the continental margins.

Statistical attempts to relate different particle fluxes in the sea to changes of primary production have focused on power functions of varying complexity to represent linear decomposition of organic matter with depth (SUESS, 1980), nonlinear effects of increased productivity on export and new production (BETZER *et al.*, 1984; PACE *et al.*, 1987), i.e. food web changes, and organic fractions of decreasing resistance to decay (BERGER *et al.*, 1987). These simple power functions may overestimate destruction of organic matter below 1000 m (JAHNKE and JACKSON, 1987). A variant on this theme is to ignore primary production, and use the particle export at the bottom of the euphotic zone and a power function to calculate fluxes at other depths (MARTIN *et al.*, 1987), thereby reducing the variance in such estimates (BISHOP, 1989). After a 25-year hiatus (WYRTKI, 1962), one-dimensional causal formulations of particle decomposition have been advanced again

(CSANADY, 1986; MARTIN *et al.*, 1987; BANSE, 1990) despite observations of increased particle fluxes with depth, implying horizontal transport (PACE *et al.*, 1987).

In an attempt to distinguish between different sources of phytodetritus and subsequent fates in the water column and sediments, we have constructed a two-dimensional, time-dependent model of carbon fluxes within the aphotic zone on the continental margin of the Mid-Atlantic Bight. The state variables of the model are detrital carbon stocks of picoplankton, nanoplankton, diatoms, macroaggregates and zooplankton fecal pellets. The fate of the different types of particulate organic carbon (P_i) over a period of 6 months above the continental slope can be simply described by

$$\frac{\partial P_i}{\partial t} = K_x \frac{\partial^2 P_i}{\partial x^2} + \frac{\partial}{\partial z}\left(K_z \frac{\partial P_i}{\partial z}\right) - \frac{\partial u P_i}{\partial x} - \frac{\partial w P_i}{\partial z} - w_s \frac{\partial P_i}{\partial z} - \lambda P_i, \quad (1)$$

where x is the positive offshore coordinate, z the positive upward coordinate, and $i = 1$–5 are the detrital forms of three phytoplankton size classes, of zooplankton fecal pellets and of macroaggregates.

The first four terms on the right-hand side of equation (1) are the diffusive and advective transports of each type of detritus, w_s is their different sinking velocities (m day^{-1}), and λ is their decomposition rate (day^{-1}). Unlike our previous model of seasonal particle export in the Gulf of Mexico (WALSH *et al.*, 1989), there is no term in equation (1) for photosynthetic production of organic carbon within the overlying water column, since this analysis focuses on the aphotic zone (>150 m), from the shelf-break (150 m) to the continental rise (2750 m). We need only specify the (1) boundary fluxes of each source of organic carbon from shelf and slope surface waters, and (2) values of the variables K_z, K_x, u, w, w_s and λ to obtain numerical solutions of equation (1). Independent validation data consist of fluxes of total organic carbon caught in sediment traps (Table 2), moored on the slope and rise of the Mid-Atlantic Bight along 71°W (BISCAYE *et al.*, 1988). The relative locations of moorings Nos 4–7 are shown in Fig. 1.

METHODS

At a depth of 150 m in the water column above the continental slope and rise, the model has two boundary sources of detritus: (1) a vertical flux from the euphotic zone of slope/rise waters; and (2) a horizontal flux at the shelf-break from residues of the shelf euphotic zone. These fluxes are denoted respectively as (A) and (B) in Fig. 1, where seaward export to the deep sea is schematically depicted as (C) across the oceanic boundary of the model. The time-invariant vertical boundary flux A consists of both picoplankton and fecal pellet detritus. The horizontal boundary flux B is instead time-dependent (Table 3), mimicking species succession of phytoplankton in shelf waters. Details of these boundary assumptions, the steady-state transport model, the internal decomposition processes, and numerical techniques are discussed below.

1. *Vertical fluxes*

A depth-averaged biomass (g C m^{-3}), sampled by bottles, and a sinking rate (m day^{-1}) yield an estimate of the vertical flux (g C m^{-2} day^{-1}) of mainly phytodetritus at the top of the aphotic zone (<150 m depth), since fast sinking, larger fecal material would be undersampled. An annual mean of 19.6 mg C m^{-3} over the upper 100 m of Mid-Atlantic slope and rise waters (GORDON, 1977) and a w_s of ~1 m day^{-1} thus yield a time-invariant

Table 2. Organic carbon fluxes (mg C m^{-2} day^{-1}) *within slope waters of the Mid-Atlantic Bight during April–September* 1984 (*after* BISCAYE et al., 1988)

Sta.	Bottom depth (m)/distance from the 150-m isobath (km)	Sediment trap depth (m)	Month (1984) A	M	J	J	A	S	Mean
4	500/20	150	20	32	11	25	9	6	17.2
		450	86	73	34	42	16	22	45.3
5	1250/33	150	38	73	26	34	7	6	30.7
		450	35	43	46	13	5	—	28.4
		850	32	37	32	12	9	8	21.7
		1200	30	36	20	10	12	8	19.3
6	2300/55	150	19	40	24	14	8	2	17.8
		450	8	27	27	4	8	7	13.5
		850	18	22	31	6	17	8	17.0
		1750	17	21	15	2	6	6	11.2
		2250	12	14	11	3	2	4	7.7
7	2750/107	150	21	37	15	13	11	3	16.7
		450	4	5	10	6	4	3	5.3
		850	7	8	14	2	6	4	6.8
		1750	3	7	5	1	2	3	3.5
		2250	9	11	7	3	3	4	6.3
		2700	7	15	7	4	2	3	6.2

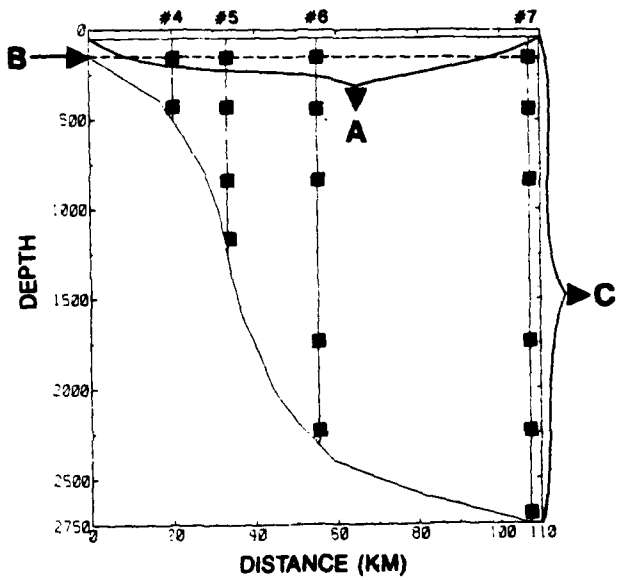

Fig. 1. The spatial domain of a fine-mesh (0.5 km, 2.5 m), x–z model of detrital fate in the aphotic zone of the Mid-Atlantic Bight, with respect to the location of the SEEP-I sediment trap arrays (■) of BISCAYE *et al.* (1988), of the vertical boundary flux A from slope waters, of lateral shelf flux B and of oceanic flux C.

Table 3. Biological parameters at a depth of ~150 m

	Source	Sinking rate (m day^{-1})	Decomposition rate (day^{-1})	Input flux (g C m^{-2} day^{-1})	Duration of input (days)	Total input* (g C m^{-1})
Macroaggregates	Shelf	100	0.01	160	30 (March)	4.8×10^4
Diatoms	Shelf	10	0.01	90	30 (April)	2.7×10^4
Nanoplankton	Shelf	1	0.01	20	120 (May–August)	2.4×10^4
Fecal pellets	Slope	100	0.01	4×10^{-3}	180 (March–August)	7.7×10^4
Picoplankton	Slope	1	0.01	20×10^{-3}	180 (March–August)	3.9×10^5

*Depth of shelf-break input = 10 m. Length of slope input = 107.5 km.

boundary flux of phytodetritus from the offshore euphotic zone of ~20 mg C m^{-2} day^{-1} (Table 3). A 2-year sediment trap study of the sinking fluxes at 100 m in the Sargasso Sea (ALTABET, 1989), together with the particulate matter in this euphotic zone, suggest a mean (n = 12) settling rate of 1.8 m day^{-1}, similar to our assumed sinking rate of 1 m day^{-1} for slope picoplankton.

Additional rare fecal pellets have much higher fall velocities of 100 m day^{-1} (Table 3), of course. An assumed zooplankton fecal pellet flux of 4 mg C m^{-2} day^{-1} within slope waters is 17% of the total vertical boundary flux in the model, similar to observations in the Panama and Santa Monica Basins (PILSKAN and HONJO, 1987; JACKSON *et al.*, 1989). We must now derive settling rates for the different size classes of shelf detritus.

Before the spring bloom, a low February 1984 chlorophyll concentration of ~0.5 mg chl m^{-3} (WALSH *et al.*, 1988a), a C:chl ratio of 45:1 (MALONE *et al.*, 1983), and near-bottom particle fluxes of 155–243 mg C m^{-2} day^{-1} (FALKOWSKI *et al.*, 1988) imply sinking rates of at least 7–11 m day^{-1} for unaggregated populations of shelf phytoplankton. A similar unaggregated algal sinking rate of 10 m day^{-1} gave reasonable results in a previous model of the shelf food web in the Mid-Atlantic Bight (WALSH *et al.*, 1988b). In contrast, macroaggregates of diatom flocs can sink as fast as 200 m day^{-1} (ALLDREDGE and GOTSCHALK, 1989), while motile nanoplankton may sink at <1 m day^{-1}. We thus assumed that shelf nanoplankton sank at 1 m day^{-1}, while shelf diatom chains had a settling velocity of 10 m day^{-1}, and macroaggregate flocs fell at 100 m day^{-1} (Table 3).

After the lateral fluxes of shelf carbon are injected at the shelf-break boundary, it is assumed they sink within slope waters at the various settling rates for nanoplankton, diatoms, and macroaggregates (Table 3), together with the particle rain of slope origin (picoplankton and fecal pellets). The results of the model, in terms of total organic carbon fluxes, are thus the sum at each time step and grid point of the five types of detritus.

2. *Lateral boundary fluxes*

At the model's shelf-break, a ten-fold change in the daily lateral flux of carbon simulates the spring bloom and species succession (Table 3). For example, a mean particulate carbon concentration of 24 mg C m^{-3} was found on the Scotian shelf during 22 January–6 February 1973 (GORDON, 1977), quite similar to the 22.5 mg C m^{-3} estimated above for February 1984 on the Mid-Atlantic shelf. At a near-bottom, seaward flow of 1.15 cm s^{-1} (BEARDSLEY *et al.*, 1985; AIKMAN *et al.*, 1988), or 1000 m day^{-1}, a lateral boundary flux of 22–24 g C m^{-2} day^{-1} may occur during pre-bloom conditions.

Table 4. Physical parameters of 107.5 km × 2700 m *domain*

	Horizontal diffusivity (10^4 cm^2 s^{-1})	Vertical diffusivity (cm^2 s^{-1})	Offshore advection (cm s^{-1})
Case 1	2.5	equation (4) if $z \leqq h$*	equation (2) if $z \leqq h$
		1 if $z > h$	0 if $z > h$
Case 2	2.5	Same	0
Case 3	2.5	Same	0 if $z \leqq 1900$ m
			10 if $z > 1900$ m

*h is the depth of the benthic boundary layer = 15 m.

After initiation of the spring bloom, the average offshore chlorophyll flux from near-bottom current meter and fluorometer time series at the 80-m isobath was 2.2 ng chl cm^{-2} s^{-1} between 18 February and 8 April 1984 (WALSH *et al.*, 1988a). This amounts to a mean of 85 g C m^{-2} day^{-1} with a constant C:chl ratio of 45. At a peak April algal biomass of 3.5 mg chl m^{-3}, the offshore export flux might then have been as high as 158 g C m^{-2} day^{-1}. To mimic the decline of the spring bloom, we first assumed a lateral flux of 160 g C m^{-2} day^{-1} for the first 30 days of the simulations and then an input of 90 g C m^{-2} day^{-1} over the next 30 days (Table 3).

A seasonal decline of near-bottom chlorophyll concentrations to 0.5 mg chl m^{-3} by 16 July 1983 at another fluorometer on the 110-m isobath (WALSH *et al.*, 1987) and the same mean flow and C:chl ratio yield a possible export of 22.5 g C m^{-2} day^{-1} during summer conditions, similar to the pre-bloom situation. To mimic the seasonal species succession from diatom netplankton to flagellate nanoplankton in the Mid-Atlantic Bight (MALONE *et al.*, 1983), we assumed a lateral boundary flux of 20 g C m^{-2} day^{-1} for the remaining 120 days of the simulation (Table 3).

Over what vertical depth interval of the model do these lateral flux estimates apply? The depth increment of our two-dimensional grid (Fig. 1) is 2.5 m, to resolve a bottom boundary layer of at least 7 m extent (BUTMAN, 1988); the bottom nepheloid layer may be only 10-m thick on the shelf (FALKOWSKI *et al.*, 1988; GARDNER, 1989), but possibly ~50 m thick at depths of 400–600 m on the upper slope (GARDNER, 1989). We allowed a bottom boundary layer thickness of 10 m at the shelf-break for the lateral particle input B at depths of 140–150 m (Fig. 1).

3. *Transport processes*

Plumes of fine-grain suspended matter, observed by profiling transmissometers, disperse offshore into deeper slope waters of the Mid-Atlantic Bight from bottom depths of 400–600 and 1000–1200 m (GARDNER, 1989). Their source may be resuspension of both terrigenous and marine detritus, since near-bottom current speeds of >7 cm s^{-1} resuspend spring phytodetritus at 4000 m in the northeast Atlantic Ocean (LAMPITT, 1985). Within the weak diabathic flow field (<1 cm s^{-1}) above the Mid-Atlantic continental slope, dispersal of particulate matter may be described adequately by turbulent mixing, with a horizontal eddy diffusivity, K_x, of 2.5 × 10^4 cm^2 s^{-1} at a grid scale of 0.5 km (Table 4), but

resuspension within the bottom Ekman layer requires additional parameterization of along-slope advective processes.

Since the surface mixed layer of the ocean during April–September at 40°N is shallower than 150 m (LEVITUS, 1982), we assume a nominal vertical eddy diffusivity, K_z, of 1 cm^2 s^{-1}, over most of the aphotic zone (Table 4). Near the bottom, however, both u and K_z vary as a function of depth (Fig. 2) within an elementary Ekman boundary layer (POND and PICKARD, 1983), in the presence of a parabathic, geostrophic current to the west and south of approximately 3 cm s^{-1} (CSANADY *et al.*, 1988).

Accordingly, the offshore diabathic component of this flow, u, is prescribed as a steady-state function of the distance from the bottom, z, by

$$u = -v\, e^{-z/D} \sin(z/D), \tag{2}$$

where $D = (2\bar{K}_z/f)^{1/2}$, in which K_z is a constant eddy viscosity, f is the Coriolis parameter and v is the geostrophic current. For example, as shown in Fig. 2, with a mean $\bar{K}_z = 10\ cm^2\ s^{-1}$, $f = 10^{-4}\ s^{-1}$ and $v = -3\ cm\ s^{-1}$, u reaches a value of about 0.9 cm s^{-1} within the lower 10 m of the benthic boundary layer. In this situation, the thickness of the boundary layer is estimated (POND and PICKARD, 1983) by

$$h = \pi\sqrt{2K_z/f}, \tag{3}$$

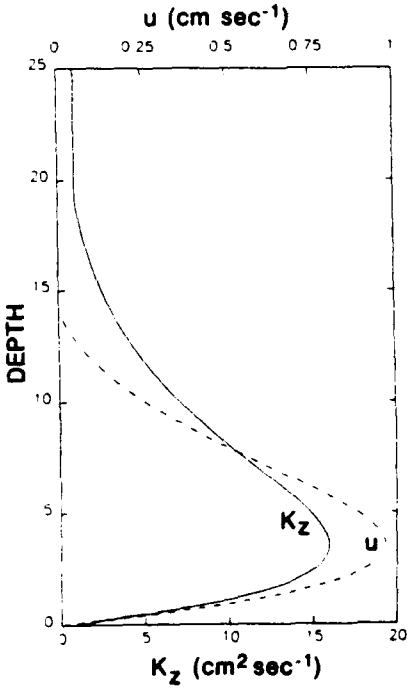

Fig. 2. The vertical structure of horizontal velocity, u, and vertical eddy diffusivity, K_z, within a benthic boundary layer of ~15 m thickness.

yielding 14.0 m. Within the bottom flow regime, the vertical velocity, w, was then calculated to satisfy continuity; it did not exceed 12 m day^{-1}.

The influence of vertical mixing is not uniform, however, if we resolve the mean $\bar{K}_z$ as a depth-dependent parameter, i.e.

$$\bar{K}_z = \frac{1}{h}\int_0^h K_z \mathrm{d}z.$$

Within the benthic boundary layer, for example, mean near-bottom speeds of 7 cm s^{-1} over the mid-slope and rise lead to a maximum K_z of approximately 15 cm^2 s^{-1} within the first 10 m of the layer (Fig. 2). The depth dependence of vertical mixing (SHIR, 1973) is derived from

$$K_z = 0.4(\tau/\rho)^{1/2} z e^{-4z/h}, \tag{4}$$

where τ is the bottom stress, ρ is the density, h is the depth of the boundary layer and z is again the distance above the bottom.

To solve equation (4), we must obtain the depth of the boundary layer, h, from another equation (5). Using a drag coefficient, c, of 2×10^{-3} (RICHARDS, 1982) in the quadratic law for bottom stress ($\tau = c\rho s^2$), and a near-bottom speed, s, of 7 cm s^{-1}, yields a value for the bottom friction velocity, $u^* = (\tau/\rho)^{1/2}$, of 0.31 cm s^{-1}. The thickness of the bottom boundary layer, h, can then be estimated (SHIR, 1973) by

$$h = 0.46u^*/f, \tag{5}$$

where f is once more the Coriolis parameter, yielding a second estimate of 14.3 m for h. This is similar to our previous estimate with a constant K_z.

If any type of detritus escapes decomposition in the upper water column to arrive within the bottom boundary layer, its apparent vertical displacement could accelerate to as much as ~100 m day^{-1} on the steep parts of the slope. Over a Mid-Atlantic continental slope inclination of 10%, a downslope flow of 1 cm s^{-1} is equivalent to a depth change of about 100 m day^{-1} (BUTMAN, 1988). At 7 m above bottom on the 500- and 1100-m isobaths, the mean observed downslope flow was 1.6 cm s^{-1} during October 1983 to November 1984, south of Nantucket Island.

Within Case 1 of our model this increased export to depth is achieved with the offshore and vertical components of the boundary layer flow, u and w respectively, rather than by w_s. Thus no discrimination is made between particles of shelf or slope origin. As a result, even slope picoplankton can descend to the 1000-m isobath, by sinking at the shelf-break and being entrained in the benthic boundary layer within Case 1. Case 3 has instead a strong flow field within just the upper 800 m of the water column, while Case 2 represents a purely diffusive habitat (Table 4).

4. *Decomposition rate*

Advective–diffusive models (WYRTKI, 1962), enzyme assays (PACKARD and WILLIAMS, 1981; GARFIELD *et al.*, 1983), radioactive tracers (JENKINS, 1982), hydrographic data (JENKINS and GOLDMAN, 1985), and sediment traps (MARTIN *et al.*, 1987; I. D. WALSH *et al.*, 1988a) have all been used to estimate decomposition rates of organic matter over the upper 2000 m of the water column. More recent enzyme measurements in upper slope and

oceanic waters of the Mid-Atlantic Bight show exponential depth profiles of oxygen utilization (PACKARD *et al.*, 1988), analogous to the depth profile of bulk organic carbon here (GORDON, 1970), implying perhaps a simple relationship. The composition and sinking rates of organic matter instead vary with depth (ITTEKOT *et al.*, 1984; LEE and CRONIN, 1984; WAKEHAM *et al.*, 1984), of course.

Calculation of oxygen utilization, or the decomposition rate, λ, depends critically on the assumed sinking rate and lability of the organic matter (BERGER *et al.*, 1987). Using a settling velocity of 100 m day^{-1}, for example, λ was estimated to be 6.5% day^{-1} between depths of 505 and 1895 m, compared to 2.2% day^{-1} at greater depths of 1465–3495 m, in the Equatorial Pacific (I. D. WALSH *et al.*, 1988a). Within a previous model of the Gulf of Mexico (WALSH *et al.*, 1989), with a sinking velocity of 3 m day^{-1}, values of λ were instead taken to be 0.5% day^{-1} in a surface layer of labile carbon stocks and 0.25% day^{-1} within a subsurface layer of more refractory carbon.

Since the sinking rates of the various detritus ranged from 1 to 100 m day^{-1} in our model, we chose a constant λ of 1.0% day^{-1} for all detritus (Table 3), reflecting temperatures of <10°C (BANSE, 1990) in the slope aphotic zone. In this model, we do not consider burial or benthic metabolism, but allow the surviving detritus to slowly sink out of the bottom 15 m of the simulated water column. Eventual respiration or offshore transport are thus the fates of all organic matter in the benthic boundary layer.

5. *Numerical techniques*

The bottom relief of the model approximates the SEEP-I transect of the Mid-Atlantic slope along 71°W (WALSH *et al.*, 1988c), between the 150- and 2750-m isobaths over a distance of ~110 km (Fig. 1). The slope is steepest at about the 1200-m isobath, where the gradient is about 10%. However, we used a model aspect ratio of 2.5 m:500 m here, rather than 50 m:500 m, to both resolve the benthic boundary layer and solve mass storage constraints.

The grid arrangement consists of uniform increments in the x and z dimensions. The solid wall boundaries in both x and z along the continental slope and rise describe an irregular staircased pattern. The no-flux orthogonal condition at these solid walls, particularly in x, leads to perhaps anomalous results of high carbon concentration in areas of very steep topography at sediment trap array No. 5 (Fig. 1). However, increasing K_x or K_z to mitigate wall effects, i.e. increased horizontal and vertical dispersion, was deemed inappropriate, considering the implicit diffusion of the numerical methods. Similarly, a previous curvilinear conformal mapping scheme (WALSH *et al.*, 1988b) was rejected.

Within any particular grid cell, a staggered configuration is used, with u and the horizontal turbulent flux, $K_x \partial P_i/\partial x$, defined on the vertical interfaces, w, w_s, and $K_z \partial P_i/\partial z$ on the horizontal interfaces, and the mass concentrations, P_i, at the center of the cell. The advection terms of equation (1) are approximated, using a standard upstream differencing scheme (ROACHE, 1976). This first scheme contains implicit numerical diffusion, with respective K_x of $\sim 2.5 \times 10^4$ cm^2 s^{-1} and K_z of ~15 cm^2 s^{-1}, for a 1 cm s^{-1} flow in the bottom Ekman layer, a maximum 100 m day^{-1} sinking velocity, and the grid mesh of 0.5 km and 2.5 m. A second anti-viscosity scheme of SMOLARKIEWICZ (1983), in which numerical dispersion is subtracted, did not produce substantially different results for this horizontal advection; we thus used the simpler advective scheme for economy of computation time.

The turbulent diffusion terms are computed, first using adjacent values of P_i to calculate $K_x\,\partial P_i/\partial x$ and $K_z\,\partial P_i/\partial z$, and then adjacent values of these expressions for the corresponding flux divergences. Since the vertical eddy diffusivities and the biological loss rate, λ, of 1% day^{-1} were relatively small, we did not employ the semi-implicit Crank–Nicholson scheme of our previous Gulf of Mexico model (WALSH *et al.*, 1989). Time steps of 900 s are also performed using forward differences to avoid the time-splitting problems of leap-frog techniques (WALSH *et al.*, 1989).

Since picoplankton sink so slowly, we first ran the model for 180 days to obtain the initial vertical conditions of this size class at the beginning of the spring bloom. Initial conditions of the other state variables (Table 3) were set to zero. Boundary flux conditions were specified in the euphotic zone, at the sea bottom, at the shelf-break, and at the open sea.

At the top and bottom interfaces, the vertical flux condition was specified by

$$(w + w_s)P_i - K_z\left(\frac{\partial P_i}{\partial z}\right) = F_z, \tag{6}$$

where $F_z = 0$ at the bottom, i.e. no net accumulation of sediment carbon. To allow for a shelf inflow at 0–10 m above the 150-m isobath of the shelf-break, the model domain actually starts at a depth of 50 m in the slope water column (solid line of Fig. 1). Here, F_z = 50 mg C m^{-2} day^{-1} of picoplankton and 4 mg C m^{-2} day^{-1} of fecal pellets to allow, after decomposition, the vertical boundary fluxes at 150 m of Table 3.

Similarly, along the coastal wall boundaries, the lateral flux condition was

$$uP_i - K_x\left(\frac{\partial P_i}{\partial x}\right) = F_x, \tag{7}$$

where F_x is the time-dependent detrital input of Table 3 at the shelf-break, and $F_x = 0$ for solid interfaces at deeper isobaths. Along the offshore, outflow wall the boundary condition for the purely diffusive Case 2 (Table 4) was $K_x\,\partial^2 P_i/\partial x^2 = 0$. For the two other cases, in which different steady-state flow fields were prescribed, $K_x\,\partial P_i/\partial x = 0$, and the advective flux out of the model domain was then calculated from the upstream finite difference formulation of equation (1).

RESULTS

Case 1

Case 1 of the model is a physical habitat with implicit and explicit horizontal dispersion of 2.5–5.0 × 10^4 cm^{-2} s^{-1} and similar combined vertical mixing of 1–30 cm^2 s^{-1}, in which the flow field has a maximum velocity, u, of ~1 cm s^{-1} in a benthic boundary layer (Fig. 2). Even in the presence of downslope advection and varying numerical dispersion associated with the different settling velocities and near-bottom currents, the relative contribution of fast and slow sinking particles, of both shelf and slope origin, to the near-bottom detrital pool is easily distinguished. As a function of a fast settling velocity and thus less decomposition, for example, shelf macroaggregate flocs, with 100 m day^{-1} sinking rates, arrive at a bottom depth of ~1700 m after 30 days (the 0.01 mg C m^{-2} day^{-1} isopleth of Fig. 3a) of lateral injection at the shelf-break.

Smaller chains of shelf diatoms, with settling rates of 10 m day^{-1}, descend after 30 days to only ~600 m (Fig. 3b), while shelf nanoplankton, at 1 m day^{-1}, sink to a bottom depth of

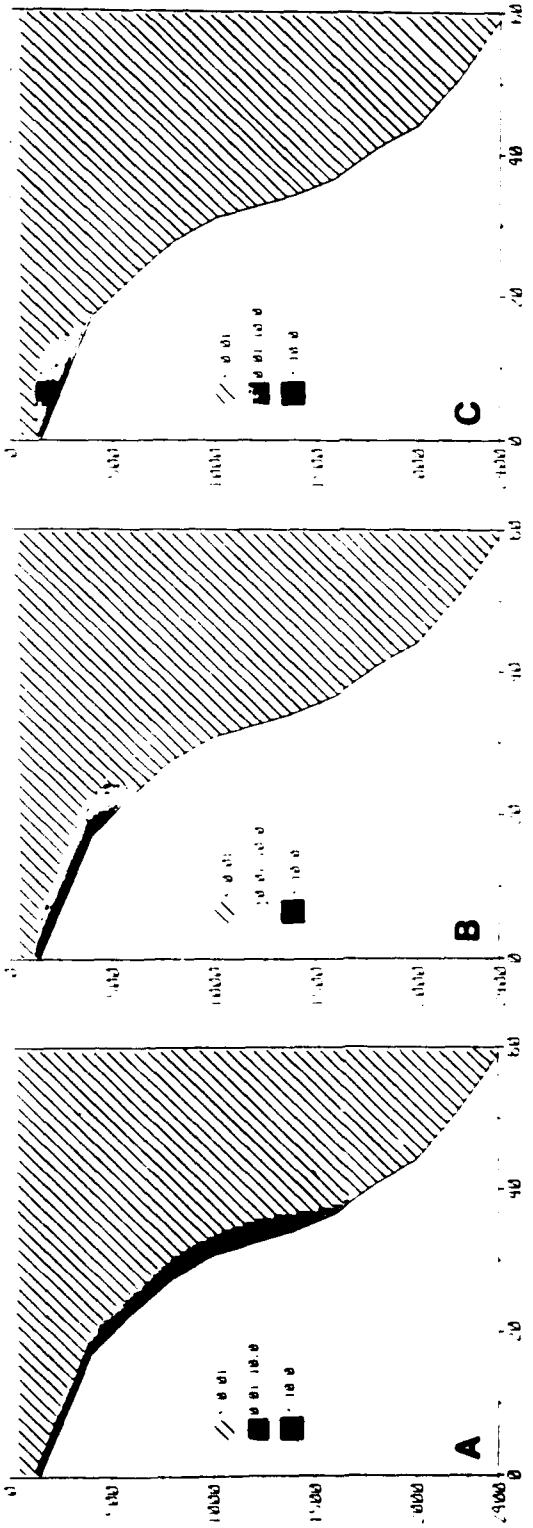

Fig. 3. The distribution of shelf (A) macroaggregate, (B) diatom and (C) nanoplankton fluxes of carbon (mg C m^{-2} day^{-1}) after 30 days of settling at 100, 10 and 1 m day^{-1} in Case 1.

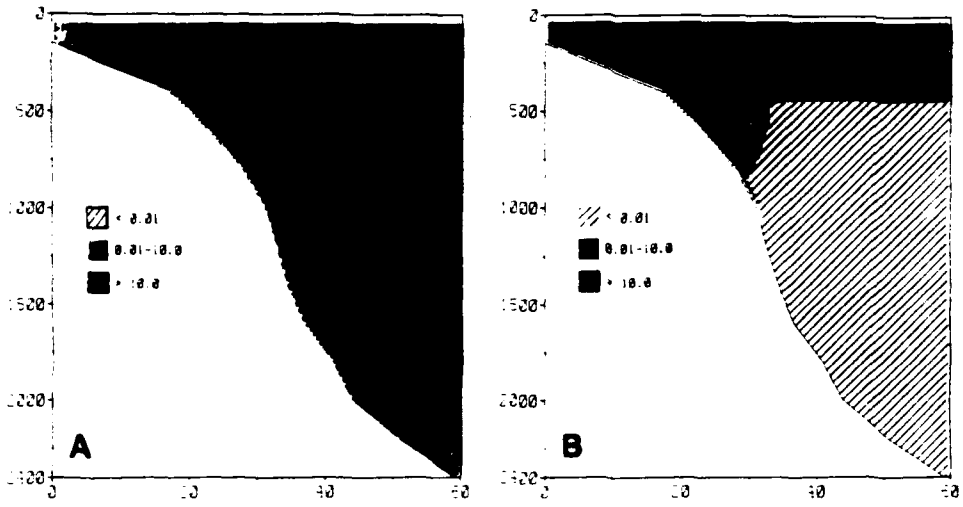

Fig. 4. The distribution of slope (A) zooplankton fecal pellet and (B) picoplankton fluxes of carbon (mg C m^{-2} day^{-1}) after 30 days of settling at 100 and 1 m day^{-1} in Case 1.

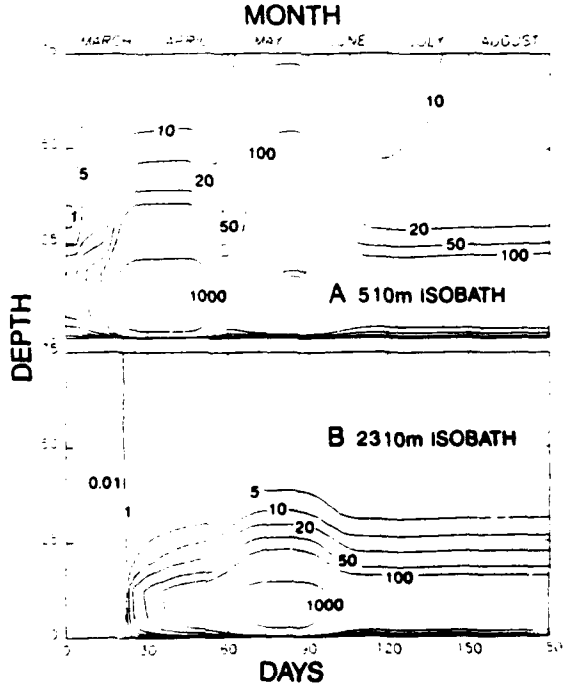

Fig. 5. A 180-day time series of total detrital carbon (mg C m^{-2} day^{-1}) fluxes of macroaggregates, diatoms, nanoplankton, fecal pellets and picoplankton over 180 days (March–August) within the lower 75 m of the water column at the (A) 510-m isobath and (B) 2310-m isobath in Case 1.

~400 m after the same time (Fig. 3c). In contrast, zooplankton fecal pellets, again falling at 100 m day^{-1}, sink to all bottom depths within 30 days, since their source is ubiquitous within the slope water column (Fig. 4a). The slope picoplankters have reached a steady state in deeper waters after settling for 210 days at 1 m day^{-1}, such that the 0.01 mg C m^{-2} day^{-1} isopleth is at ~450 m. Within ~30 km of the shelf-break, however, they penetrate to a depth of ~1000 m after entrainment in the near-bottom flow (Fig. 4b).

To condense 6 months of the simulated fate of five types of detritus at $\sim 2 \times 10^5$ grid points of the model, we concentrate on time series of total and constituent carbon fluxes within 75 m of the bottom at the 510-, 2310- and 2750-m isobaths. For example, the total detrital carbon flux at 75 m above the 510-m isobath on the upper slope of Case 1 (Fig. 5a) is dominated by zooplankton fecal pellets for only the first 14 days (Fig. 6c). Afterwards, the macroaggregates arrive, constituting >90% of the detrital flux by day 21 as the 1000 mg C m^{-2} day^{-1} isopleth of Fig. 5a. Then the shelf pulse of diatom chains (Fig. 6a) and the steady slope source of picoplankton (Fig. 6b) become significant after day 60, with export of most of the previous shelf source of macroaggregates to greater depths (Fig. 5b).

During May–June at 50–60 m above bottom of the upper slope, the total simulated flux of 50–100 mg C m^{-2} day^{-1} (Fig. 5a) approximates that of 85 and 73 mg C m^{-2} day^{-1},

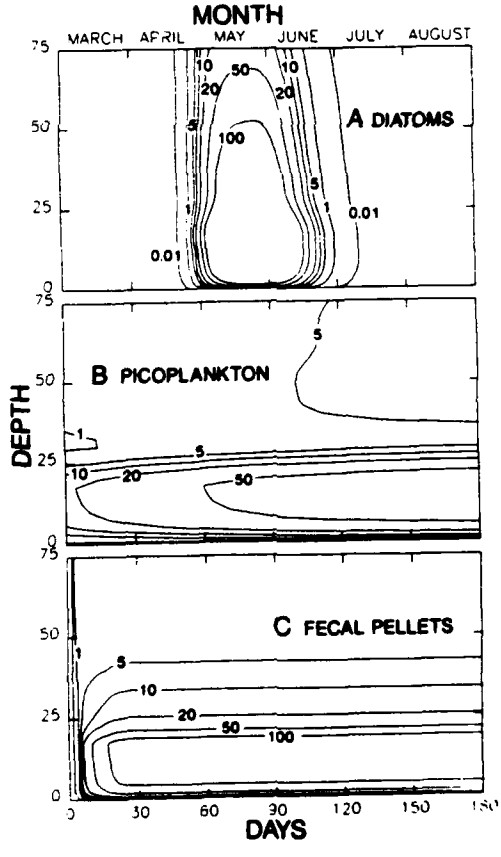

Fig. 6. A 180-day time series of (A) diatom, (B) picoplankton and (C) fecal pellet fluxes (mg C m^{-2} day^{-1}) at the 510-m isobath in Case 1.

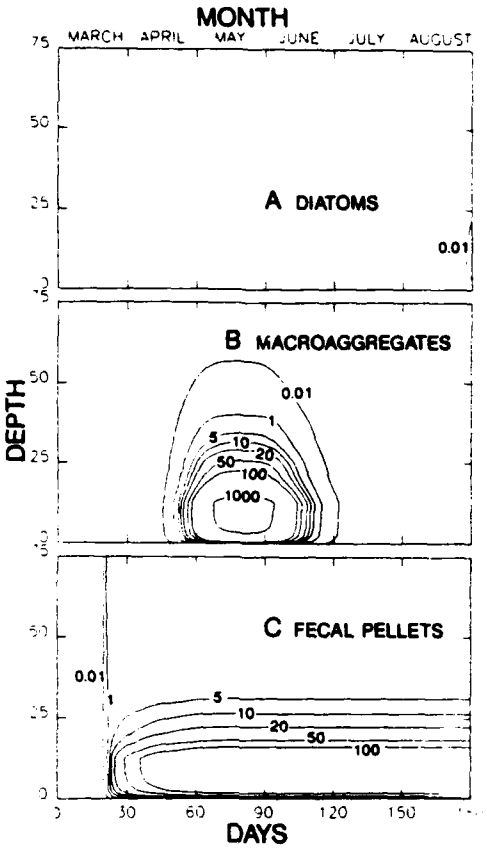

Fig. 7. A 180-day time series of (A) diatom, (B) macroaggregate and (C) fecal pellet fluxes (mg C m^{-2} day^{-1}) at the 2310-m isobath in Case 1.

measured at the same depth in April–May (Sta. 4 of Table 2). Note that 60 days before, the faster sinking macroaggregates instead yielded a ten-fold smaller particle flux at the same distance above bottom (Fig. 5a). By day 150, the total flux of the model at this depth interval has declined to 10–20 mg C m^{-2} day^{-1} (Fig. 5a), similar to the 16 mg C m^{-2} day^{-1} observed at the end of August (Table 2). Without sediment trap data in March, the short pulse of diatom phytodetritus from the shelf (Fig. 6a), as well as constant inputs of slope picoplankton (Fig. 6b) and fecal pellets (Fig. 6c), account for most of the model's fidelity between April and August at Sta. 4.

Within the benthic boundary layer at the 2310-m isobath of the lower slope, about a 40-day time-lag of shelf input is simulated, reflecting the separation distance of 35 km between Stas 4 and 6. The 1000 mg C m^{-2} day^{-1} isopleth of macroaggregates is found after day 64 (Figs 5b and 7b) rather than during day 21 (Fig. 5a). At 30–35 m above bottom on this isobath, the model mimics the observed carbon fluxes at 2250 m (Sta. 6 of Table 2) of 14 and 11 mg C m^{-2} day^{-1} at the end of May and June, as well as 2–4 mg C m^{-2} day^{-1} for the next 3 months (Fig. 5b). Neither the slope picoplankton, nor the shelf nanoplankton and diatom chains (Fig. 7a) survived the longer descent, however.

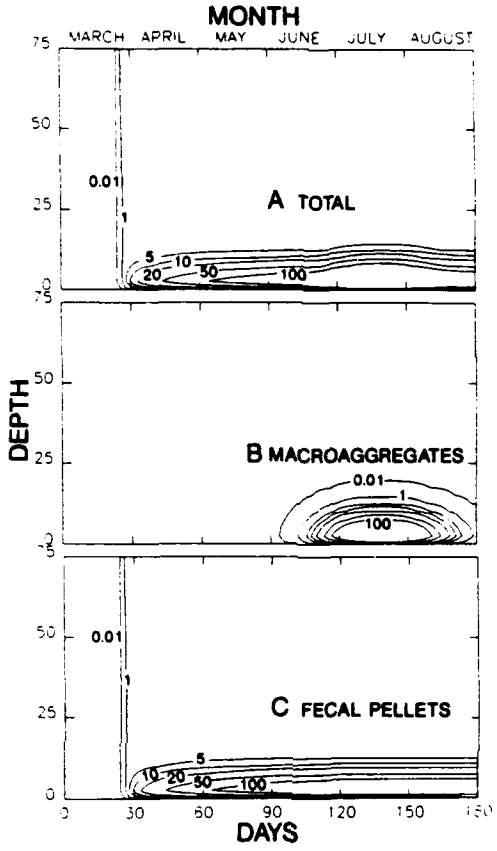

Fig. 8. A 180-day time series of (A) total detrital, (B) macroaggregate and (C) fecal pellet fluxes (mg C m^{-2} day^{-1}) at the 2750-m isobath in Case 1.

Among the two fast sinking detrital types at the 2310-m isobath, the macroaggregates constitute >90% of the total flux in the benthic boundary layer between days 65 and 100, and <1% after day 120 (Fig. 7b). With only one sediment trap at 50 m above the bottom here, insufficient validation data prevent discrimination between a fecal pellet or macroaggregate source of detritus on the lower slope. If a seasonal signal of fecal pellets, rather than macroaggregates (Table 3) had been invoked in the model, for example, the observed May pulse of carbon at a depth of 2250 m (Table 2) could also be replicated, with an accompanying ten-fold reduction of the simulated total carbon at 10 m above bottom. Twice as many fecal pellets are simulated at 25 m above bottom on the 510-m isobath (Fig. 6c) than on the 2310-m isobath (Fig. 7c), reflecting greater decomposition losses here of this detrital type as well. More observations are thus required to validate the predicted May aggregate flux of 1000 mg C m^{-2} day^{-1} at 2260 m (Fig. 7b).

At 55 km farther offshore, the shelf pulse of macroaggregates is indeed reduced ten-fold during July (Fig. 8b), with arrival of the carbon source at the 2750-m isobath delayed until day 120. The actual seasonal pulse of measured carbon fluxes at 2700 m (Sta. 7 of Table 2) coincides, however, with the simulated May buildup of fecal pellets (Fig. 8c) in the benthic boundary layer. A flux of 15 mg C m^{-2} day^{-1} is then predicted at 10 m above bottom

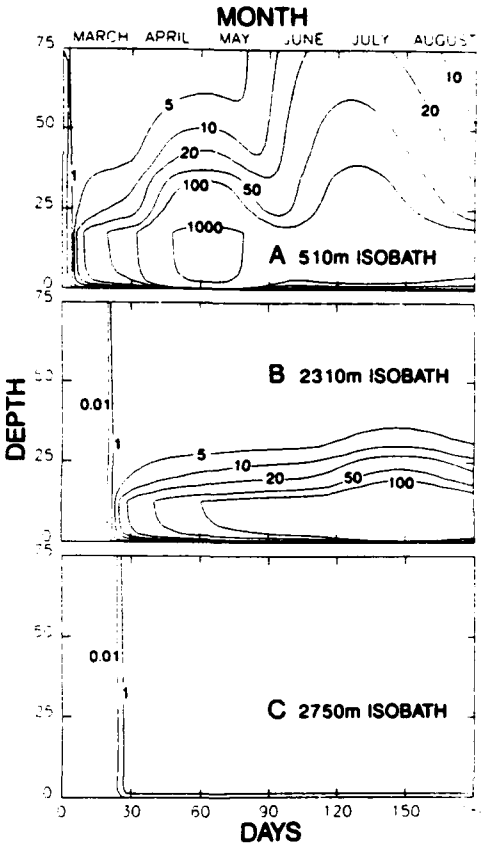

Fig. 9. A 180-day time series of total detrital carbon (mg C m^{-2} day^{-1}) fluxes of macroaggregates, diatoms, nanoplankton, fecal pellets and picoplankton over 180 days (March–August) within the lower 75 m of the water column at the (A) 510-m isobath, (B) 2310-m isobath and (C) 2750-m isobath in Case 2.

(Fig. 8a), however, not at 50 m as observed. Since the largest flux of particulate matter exited the euphotic zone at 150 m during May above this isobath as well (Table 2), a slope source of organic carbon (Fig. 8c), rather than the shelf (Fig. 8b), is the most likely origin of near-bottom detritus on the continental rise, barring disaggregation to particles of smaller settling velocities and/or strong offshore advection by a boundary current.

Case 2

At a grid spacing of 0.5 km, a horizontal eddy diffusivity of 2.5×10^4 cm^2 s^{-1} is equivalent to a flow field of only 1 cm s^{-1}. Without the explicit advection (Fig. 2) and associated numerical dispersion in the benthic boundary layer of Case 1 (Table 4), organic matter of shelf origin takes much longer to arrive at the bottom of the deep sea during Case 2 (Fig. 9). Within such a diffusive habitat, the simulated diatom pulse of detritus arrives at the 510-m isobath in July (Fig. 9a) rather than during May (Fig. 6a). In the absence of advection (u and w) within the benthic boundary layer, the 100 mg C m^{-2} day^{-1} isopleth of diatoms then also occurs at ~40 m (Fig. 9a) above bottom rather than at 55 m (Fig. 5a).

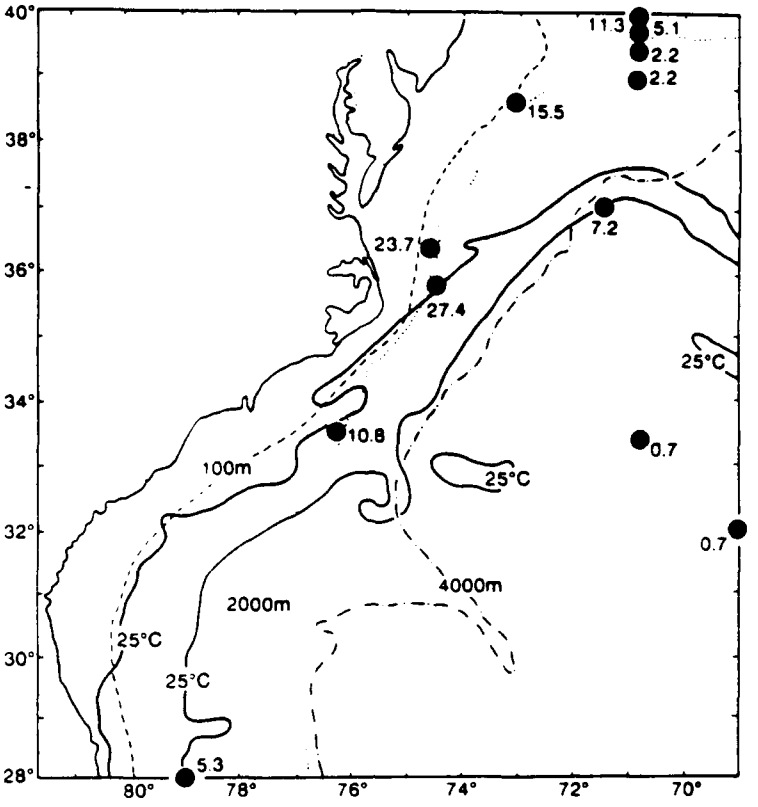

Fig. 10. The surface 25°C envelope of the Gulf Stream System, sensed by the TIROS AVHRR during June 1984, in relation to near-bottom carbon fluxes (g C m^{-2} y^{-1}) at long-term moorings (except for the observations in the Florida Current) of sediment traps on the continental margin of the western North Atlantic Ocean (after HINGA *et al.*, 1979; DEUSER, 1986; HEGGIE *et al.*, 1987; BISCAYE *et al.*, 1988; P. BISCAYE and O. BROWN, personal communication).

In this scenario, the transit time and respiratory losses are sufficiently greater than Case 1 (Fig. 5b), such that the macroaggregate pulse of 1000 mg C m^{-2} day^{-1} never reaches the 2310-m isobath (Fig. 9b). None of the phytoplankton escape respiration to arrive on the continental rise (Fig. 9c). Only a few zooplankton fecal pellets survive the descent to 2750 m in Case 2 (Fig. 9c), yielding a ten-fold lower flux than the observations at Sta. 7 (Table 2). These last results suggest that the bottom boundary layer is an important conduit for delivery of even zooplankton debris to the continental rise. Without flow in the benthic boundary layer, neither the time-phasing nor the amount of organic carbon fluxes at the near-bottom sediment traps are replicated by the model.

Case 3

An increase of the flow field to 10 cm s^{-1} within the upper 800 m (with an implicit K_z of $\sim 2.5 \times 10^5$ cm^2 s^{-1}) for Case 3 (Table 4) attempts to simulate the entrainment, at Cape Hatteras, of shelf particulate matter from the Mid-Atlantic Bight by the Gulf Stream (Fig. 10). At ten-fold higher explicit speeds within the upper water column, detritus would be

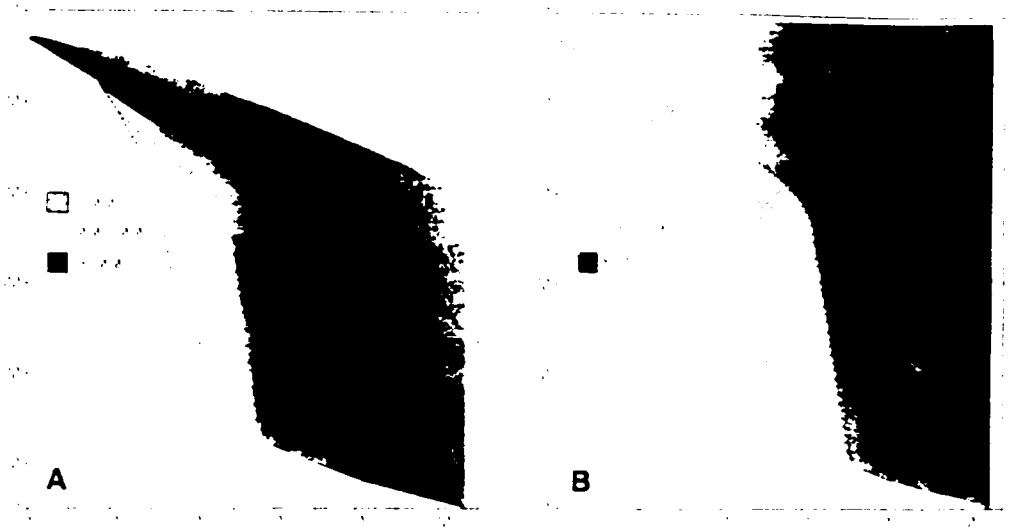

Fig. 11. The distribution of (A) shelf macroaggregate and (B) slope fecal pellet fluxes of carbon (mg C m^{-2} day^{-1}) after 30 days of settling at 100 m day^{-1} in Case 3.

swept through the 108-km offshore extent of the model in ~11 days. Such a transit time allows only the fast sinking macroaggregates (Fig. 11a) and zooplankton fecal pellets (Fig. 11b) to settle to the lower water column and thence to the bottom, which no longer has an Ekman boundary layer. Contrast these results of Case 3 with those of Figs 3a and 4a of Case 1 at different offshore length scales.

Since the macroaggregates are injected at depths of 140–150 m at the shelf-break, rather than at the 50-m depth of fecal pellet origin within slope waters, the shelf source of Case 3 dominates the particulate loading at the 510-m isobath (Fig. 12a). However, only 20 mg C m^{-2} day^{-1} of macroaggregates are simulated at 50–60 m above bottom of the upper slope. Here just 0.01 mg C m^{-2} day^{-1} of zooplankton fecal pellets are computed at 70 m above bottom, instead of ~3.5 mg C m^{-2} day^{-1} at the same depth and time in Case 1.

At 87 km farther offshore on the continental rise, the late April pulse of detrital carbon is now still ~12 mg C m^{-2} day^{-1} at 50–60 m above bottom (Fig. 12c); ten-fold more macroaggregates survive this descent than in the previous cases. The zooplankton fecal pellets constitute <10% of the April signal in this scenario; after day 90, however, the fecal pellets are again the dominant source of detritus. How representative are the Case 3 results of the model?

About 350 km offshore of Cape Hatteras, at 4163 m underneath the ~200 cm s^{-1} Gulf Stream (Fig. 10), 19.7 mg C m^{-2} day^{-1} were caught by a long-term sediment trap mooring (HEGGIE *et al.*, 1987). This is similar to the 20 mg C m^{-2} day^{-1} of macroaggregates predicted at 2500 m, ~75 km from the shelf source, within the 10 cm s^{-1} flow field of Case 3 (Fig. 11a). Such convergence of data and model scaling may be fortuitous. The different cases of the model and these sediment trap fluxes on the New England slope and beneath the Gulf Stream (Fig. 10) do nevertheless underscore the contrasting roles of weak and strong advective regimes in offshore transport of particulate matter from the continental margins.

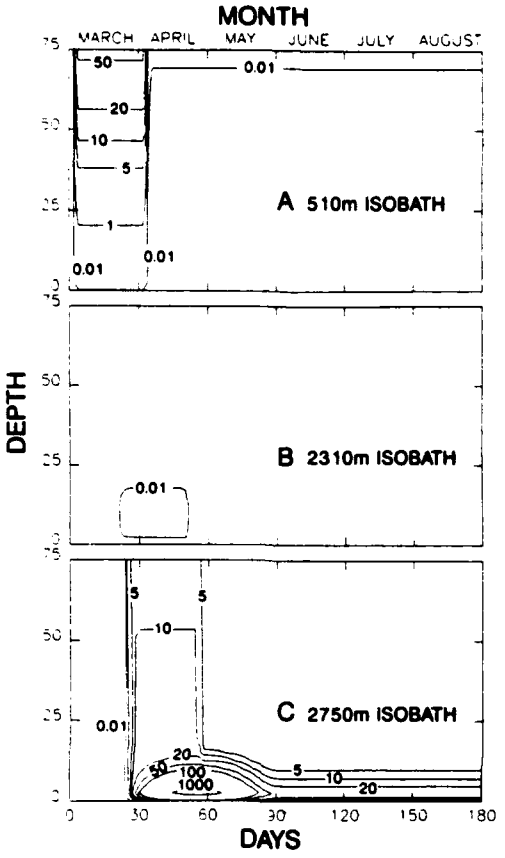

Fig. 12. A 180-day time series of total detrital carbon (mg C m^{-2} day^{-1}) fluxes of macroaggregates, diatoms, nanoplankton, fecal pellets and picoplankton over 180 days (March–August) within the lower 75 m of the water column at the (A) 510-m isobath, (B) 2310-m isobath and (C) 2750-m isobath in Case 3.

DISCUSSION

Over a year, our assumed picoplankton carbon flux of 20 mg C m^{-2} day^{-1}, at a depth of 150 m within slope regions of the model (Table 3), suggests a fallout of particulate nitrogen of 1.2 g N m^{-2} y^{-1}, with a C:N ratio of 6:1. A sinking rate of 1 m day^{-1} and a decomposition rate of 0.01 day^{-1} then imply an annual sinking flux of 2.4 g N m^{-2} y^{-1} at a depth of 100 m within simulated slope waters; 2.7 g N m^{-2} y^{-1} was observed at 100 m in the Sargasso Sea, near Bermuda, during 1986–1988 (ALTABET, 1989). If we had included a seasonal pulse of fecal pellets, measured presumably as a detrital carbon maximum of ~4 mg C m^{-2} day^{-1} in March–April at 3200 m off Bermuda by DEUSER (1986) as well, the simulated carbon at 2280 m (Fig. 7c) and 2735 m (Fig. 8c) on the continental slope and rise would have also coincided with observations (Table 2).

Similar concurrence of modelled and observed fluxes of organic matter was found during May in the upper slope waters above the 500-m isobath (Fig. 5a, Table 2). In case 1, a lateral injection of shelf diatom chains of 90 g C m^{-2} day^{-1} was added to the model at a

sinking rate of 10 m day^{-1} over the previous month of April (Table 3). This input, in addition to picoplankton and fecal pellets, provided most of the fidelity of the model on the upper slope.

Without March data (Table 2), we are unsure of the duration of the simulated macroaggregate sinking pulse on the lower slope. Of perhaps greater importance may be the resuspension of macroaggregates (LAMPITT, 1985), as particles with slower sinking rates during additional downslope transport (ASPER, 1986). At the 2310- and 2750-m isobaths of the model, for example, the same amount of total fluxes of carbon was simulated 20–40 m lower in the water column than that observed at 50 m above bottom.

A thicker benthic boundary layer, for higher resuspension of slow sinking particles, can be obtained with a modification of equation (5) to included stratification of the water column (WEATHERLY and MARTIN, 1978). For example,

$$h = 1.3u^*/f(1 + N^2/f^2)^{1/4} \quad (8)$$

is a possible scenario, where f is the Coriolis parameter, $N = (g/\rho\ \partial\rho/\partial z)^{1/2}$ is the Brunt–Vasäliä frequency, and g is the acceleration of gravity. With $N = 0$, i.e. neutral stratification, h could be 40 m, instead of the 14-m thickness employed in our model (Fig. 2). More typical, near-bottom values of N on the mid-Atlantic slope are 1.2 cycles h^{-1}, or about 2×10^{-3} radians s^{-1}, however, suggesting an h of only 7.4 m.

Thus, a more likely source of a greater carbon flux to the sediment traps (Table 2) may be resuspension of sediment at an isobath above the depth of the trap, rather than below, and offshore transport of fast (~80 m day^{-1}) and slowly settling (~1 m day^{-1}) macroaggregate particles (ASPER, 1986; GARDNER and WALSH, 1990) to the vicinity of the trap. Data on such a "rebound" process (I. D. WALSH *et al.*, 1988b) are clearly required. The conclusions of our simulation analyses on the spatial extent of shelf export may be an underestimate, if the lateral rebound process is a significant transfer mechanism. For example, bottom metabolism of sediments within 300 km of the shelf-break suggests that overlying traps underestimate the input of organic matter by as much as 200–300% (SMITH, 1987; JAHNKE *et al.*, 1990) missing lateral import of near-bottom suspended materials.

In Case 1 of the model, the diatom chain and nanoplankton size fractions of the shelf source were mostly respired within 55 km of the shelf-break (Fig. 7). Inappropriate time-phasing of the arrival of larger shelf macroaggregates was also found 107 km offshore at the 2750-m isobath (Fig. 8). Based on these results, the likely offshore impact of shelf export may be restricted to within 60 km of the shelf-break in a 1 cm s^{-1} flow regime, unless disaggregation occurs at depth (CSANADY, 1986), resulting in wider dispersal of smaller particles.

In the Case 1 habitat, picoplankton of slope water origin only penetrate the deep sea, beneath the mean pycnocline (~500 m), within 30 km of the shelf-break (Figs 4b and 6b). Instead, zooplankton fecal pellets of slope origin evidently contribute the bulk (~3.8 mg C m^{-2} day^{-1}) of settling particles above the continental rise. The pellets may also be entrained offshore within the bottom Ekman layer, since a diffusive habitat of Case 2 results in ten-fold less abundance.

Within a stronger flow regime of Case 3, slow sinking (<10 m day^{-1}) detritus of shelf or slope origin is respired above the main pycnocline, without intersecting even the upper slope. Detrital material, entrained by a boundary current near the bottom of the shelf-break water column, can instead survive the descent to the continental rise at settling velocities of 100 m day^{-1}. Respiration or burial of this organic matter, beneath the main

pycnocline, can then serve as biogenic CO_2 sinks in global carbon cycles. Uncoupled food webs with high f ratios, leading to aggregations of ungrazed phytoplankton, are the most likely biological structures, in slow or fast currents, to foster such export to the deep sea.

Without a macroaggregate pulse of ungrazed phytoplankton detritus, the only source of fast-sinking carbon to the deep sea is zooplankton fecal pellets, involving a ~10% transfer efficiency from one trophic level to the next. The flux of 7.2 g C m^{-2} y^{-1} caught in the deep sea at 4163 m underneath the Gulf Stream (Fig. 10), for example, is representative of continental margins and not included in Table 1. It is ten-fold that of 0.7 g C m^{-2} y^{-1} observed either at 4000 m on the Cape Hatteras Abyssal Plain (HEGGIE *et al.*, 1987) or at 3200 m off Bermuda (DEUSER, 1986). A fecal pellet flux of 4 mg C m^{-2} day^{-1} at 150 m, a sinking rate of 100 m day^{-1}, and λ of 0.01 day^{-1} (Table 3) instead suggest that 0.9 g C m^{-2} y^{-1} might arrive at 4000 m in the deep sea.

Note that only 2.2 g C m^{-2} y^{-1} was caught at 2250 or 2750 m in the Mid-Atlantic Bight (Table 1). At advection and oxidation rates of 1 cm s^{-1} and 1% day^{-1} within this quiescent slope sea, about 0.4 g C m^{-2} y^{-1} would survive the additional seaward distance of ~80 km between Sta. 7 (Table 2) and the 4000-m isobath to the south. The source of higher carbon flux underneath the Gulf Stream must thus be near Cape Hatteras, implying that a western boundary current transforms a deep-sea oligotrophic ecosystem of low f ratio and export to a continental margin ecosystem, with high values of f ratio and export, by extending the seaward boundary of the latter.

Within cyclonic eddies shed by the Gulf Stream in the South Atlantic Bight, new production may exceed 50% of the total primary production. Here, diatom populations of 1.8×10^6 cells l^{-1} form gelatinous colonies up to 1 mm in diameter (YODER, 1985), which may be the source of a subsurface plume of macroaggregates at Cape Hatteras (ASPER, 1986). They would have sufficient fall velocities (ALLDREDGE and GOTSCHALK, 1989) to survive a descent of 4163 m underneath the Gulf Stream (Fig. 10). A coupled three-dimensional, biophysical model is now required, however, in conjunction with appropriate field experiments, to examine the global role of western boundary currents in the exchange of dissolved nutrients (RINTOUL, 1988) and particulate matter (WALSH *et al.*, 1989) between continental margins and the deep sea.

Acknowledgements—This research was sponsored by the Department of Energy, the Office of Naval Research and the National Aeronautic and Space Administration under grants DE-FG05-85ER60285, N00014-87-J-1218 and NAGW-678.

REFERENCES

AIKMAN F., W. H. OU and R. W. HOUGHTON (1988) Current variability across the New England continental shelf-break and slope. *Continental Shelf Research*, **8**, 625–652.

ALLDREDGE A. L. (1979) The chemical composition of macroscopic aggregates in two neritic seas. *Limnology and Oceanography*, **24**, 855–866.

ALLDREDGE A. L. and C. C. GOTSCHALK (1989) Mass flocculation of diatom blooms. *Deep-Sea Research*, **36**, 159–171.

ALTABET M. A. (1989) Particulate new nitrogen fluxes in the Sargasso Sea. *Journal of Geophysical Research*, **94**, 12771–12780.

ASPER V. L. (1986) Accelerated settling of particulate matter by "marine snow" aggregates. Ph.D. Thesis, Woods Hole Oceanographic Institution, **86-12**, 189 pp.

BANSE K. (1990) New views on the degradation and disposition of organic particles as collected by sediment traps in the open sea. *Deep-Sea Research*, **37**, 1177–1195.

BEARDSLEY R. C., D. C. CHAPMAN, K. H. BRINK, S. R. RAMP and R. SCHLITZ (1985) The Nantucket Shoals Flux Experiment (NSFE 79). Part I: a basic description of the current and temperature variability. *Journal of Physical Oceanography*, **15**, 713–748.

BERGER W. H., K. FISCHER, C. LAI and G. WU (1987) Ocean productivity and organic carbon flux. Part I. Overview and maps of primary production and export production. *SIO Reference 87-30*, University of California, San Diego, pp. 1–67.

BETZER P. R., W. J. SHOWERS, E. A. LAWS, C. D. WINN, G. R DiTULLIO and P. M. KROOPNICK (1984) Primary productivity and particle fluxes on a transect of the equator at 153°W in the Pacific Ocean. *Deep-Sea Research*, **31**, 1–11.

BILLET D. S., K. S. LAMPITT, A. L. RICE and R. F. MANTOURA (1983) Seasonal sedimentation of phytoplankton to the deep-sea benthos. *Nature*, **302**, 520–522.

BISCAYE P. E., R. F. ANDERSON and R. L. DECK (1988) Fluxes of particles and constituents to the eastern United States continental slope and rise: SEEP-I. *Continental Shelf Research*, **8**, 885–904.

BISHOP J. K. (1989) Regional extremes in particulate matter composition and flux: effects on the chemistry of the ocean interior. In: *Productivity of the ocean: present and past*, W. H. BERGER, V. SMETACEK and G. WEFER, editors, J. Wiley and Sons, New York, pp. 117–138.

BUTMAN B. (1988) Downslope Eulerian mean flow associated with high-frequency current fluctuations observed on the outer continental shelf and upper slope along the northeastern United States continental margin: implications for sediment transport. *Continental Shelf Research*, **8**, 811–840.

CSANADY G. T. (1986) Mass transfer to and from small particles in the sea. *Limnology and Oceanography*, **31**, 237–248.

CSANADY G. T., J. H. CHURCHILL and B. BUTMAN (1988) Near-bottom currents over the continental slope in the Mid-Atlantic Bight. *Continental Shelf Research*, **8**, 653–671.

DEUSER W. G. (1986) Seasonal and interannual variations in deep-water particle fluxes in the Sargasso Sea and their relation to surface hydrography. *Deep-Sea Research*, **33**, 225–246.

DEUSER W. G., F. E. MÜLLER-KARGER and C. HEMLEBEN (1988) Temporal variations of particle fluxes in the deep subtropical and tropical North Atlantic: Eulerian versus Langrangian effects. *Journal of Geophysical Research*, **93**, 6857–6862.

EMERSON S., C. STUMP, P. M. GROOTES, M. STUIVER, G. W. FARWELL and F. H. SCHMIDT (1987) Estimates of degradable organic carbon in deep-sea surface sediments from ^{14}C concentrations. *Nature*, **329**, 51–53.

FALKOWSKI P. G., C. N. FLAGG, G. T. ROWE, S. L. SMITH, T. E. WHITLEDGE and C. D. WIRICK (1988) The fate of a spring phytoplankton bloom: export or oxidation? *Continental Shelf Research*, **8**, 457–484.

FISCHER K. (1984) Particle fluxes in the eastern tropical Pacific Ocean—sources and processes. Ph.D. Thesis, Oregon State University, Corvallis, 225 pp.

GARDNER W. D. (1989) Baltimore Canyon as a modern conduit of sediment to the deep sea. *Deep-Sea Research*, **36**, 323–358.

GARDNER W. D. and I. D. WALSH (1990) Distribution of macroaggregates and fine-grained particles across a continental margin and their potential role in fluxes. *Deep-Sea Research*, **37**, 401–412.

GARFIELD P. C., T. T. PACKARD, G. E. FRIEDERICH and L. A. CODISPOTI (1983) A subsurface particle maximum layer and enhanced microbial activity in the secondary nitrite maximum of the northeastern tropical Pacific Ocean. *Journal of Marine Research*, **41**, 747–768.

GORDON D. C. (1970) Some studies on the distribution and composition of particulate organic carbon in the North Atlantic Ocean. *Deep-Sea Research*, **17**, 233–244.

GORDON D. C. (1977) Variability of particulate organic carbon and nitrogen along the Halifax–Bermuda section. *Deep-Sea Research*, **24**, 257–270.

HEGGIE D., C. MARIS, A. HUDSON, J. DYMOND, R. BEACH and J. CULLEN (1987) Organic carbon oxidation and preservation in NW Atlantic continental margin sediments. In: *Geology and geochemistry of abyssal plains*, P. P. E. WEAVER and J. THOMPSON, editors, Geological Society Special Publication No. 31, pp. 215–236.

HINGA K. R., J. M. SIEBURTH and G. R. HEATH (1979) The supply and use of organic material at the deep-sea floor. *Journal of Marine Research*, **37**, 557–579.

HONJO S. (1978) Sedimentation of materials in the Sargasso Sea at a 5637 m deep station. *Journal of Marine Research*, **36**, 469–492.

HONJO S. (1980) Material fluxes and modes of sedimentation in the mesopelagic and bathypelagic zones. *Journal of Marine Research*, **38**, 53–97.

HONJO S. (1982) Seasonality and interaction of biogenic and lithogenic particulate flux at the Panama Basin. *Science*, **218**, 883–884.

HONJO S. (1984) Study of ocean fluxes in time and space by bottom-tethered sediment trap arrays: a recommendation. In: *Global Ocean Flux Study*, National Academy of Sciences Press, Washington, D.C., pp. 306–324.

HONJO S., S. J. MANGANINI and J. J. COLE (1982) Sedimentation of biogenic matter in the deep ocean. *Deep-Sea Research*, **26**, 609–625.

ITTEKOT V., W. G. DEUSER and E. T. DEGENS (1984) Seasonality in the fluxes of sugars, amino acids, and amino sugars to the deep ocean: Sargasso Sea. *Deep-Sea Research*, **31**, 1057–1069.

JACKSON G. A., F. AZAM, A. F. CARLUCCI, R. W. EPPLEY, B. FINNEY, D. S. GORSLINE, B. HICKEY, C.-A. HUH, R. A. JAHNKE, I. R. KAPLAN, M. R. LANDRY, L. F. SMALL, M. I. VENKATESAN, P. M. WILLIAMS and K. M. WONG (1989) Elemental cycling and fluxes off the coast of southern California. *EOS*, **70**, 146–155.

JAHNKE R. A. and G. A. JACKSON (1987) Role of sea floor organisms in oxygen consumption in the deep North Pacific Ocean. *Nature*, **329**, 621–623.

JAHNKE R. A., C. E. REIMERS and D. B. CRAVEN (1990) Intensification of recycling of organic matter at the sea floor near ocean margins. *Nature*, **348**, 50–54.

JENKINS W. J. (1982) Oxygen utilization rates in the North Atlantic subtropical gyre and primary production in oligotrophic systems. *Nature*, **300**, 246–248.

JENKINS W. J. and J. C. GOLDMAN (1985) Seasonal oxygen cycling and primary production in the Sargasso Sea. *Journal of Marine Research*, **43**, 465–491.

KNAUER G. A. and J. H. MARTIN (1981) Primary production and carbon–nitrogen fluxes in the upper 1500 m of the northeast Pacific. *Limnology and Oceanography*, **26**, 181–186.

LAMPITT R. S. (1985) Evidence for the seasonal deposition of detritus to the deep-sea floor and its subsequent resuspension. *Deep-Sea Research*, **32**, 885–898.

LEE C. and C. CRONIN (1984) Particulate amino acids in the sea: effects of primary productivity and biological decomposition. *Journal of Marine Research*, **42**, 1075–1097.

LEVITUS S. (1982) *Climatological atlas of the world ocean*. NOAA Professional Paper No. 13, 1–173.

MALONE T. C., T. S. HOPKINS, P. G. FALKOWSKI and T. E. WHITLEDGE (1983) Production and transport of phytoplankton biomass over the continental shelf of the New York Bight. *Continental Shelf Research*, **1**, 305–337.

MARTIN J. H., G. A. KNAUER, D. M. KARL and W. W. BROENKOW (1987) VERTEX: carbon cycling in the northeast Pacific. *Deep-Sea Research*, **34**, 267–286.

PACE M. L., G. A. KNAUER, D. H. KARL and J. M. MARTIN (1987) Primary production, new production, and vertical flux in the eastern Pacific Ocean. *Nature*, **325**, 803–804.

PACKARD T. T., M. DENIS, M. RODIER and P. GARFIELD (1988) Deep-ocean metabolic CO_2 production: calculations from ETS activity. *Deep-Sea Research*, **35**, 371–382.

PACKARD T. T. and P. J. WILLIAMS (1981) Rates of respiratory oxygen consumption and electron transport in surface seawater from the northwest Atlantic Ocean. *Oceanological Acta*, **4**, 351–358.

PILSKAN C. H. and S. HONJO (1987) The fecal pellet fraction of biogeochemical particle fluxes to the deep sea. *Global Biogeochemical Cycles*, **1**, 31–48.

POND S. and G. L. PICARD (1983) *Introductory physical oceanography*. Pergamon Press, Oxford, 329 pp.

RICHARDS K. J. (1982) Modeling the benthic boundary layer. *Journal of Physical Oceanography*, **12**, 428–439.

RINTOUL S. R. (1988) Mass, heat, and nutrient fluxes in the Atlantic Ocean determined by inverse methods. Ph.D. Dissertation, Woods Hole Oceanographic Institution/Massachusetts Institute of Technology, Cambridge, MA, 287 pp.

ROACHE P. J. (1976) *Computational fluid dynamics*. Hermosa Publications, Albuquerque, New Mexico, 446 pp.

ROWE G. T. and W. D. GARDNER (1979) Sedimentation rates in the slope water of the northwest Atlantic Ocean measured directly with sediment traps. *Journal of Marine Research*, **37**, 581–600.

SHIR C. C. (1973) A preliminary numerical study of atmospheric turbulent flows in the idealized planetary boundary layer. *Journal of Atmospheric Science*, **30**, 1327–1339.

SMOLARKIEWICZ P. K. (1983) A simple, positive definite scheme with small implicit diffusion. *Monthly Weather Review*, **111**, 479–486.

SMITH K. L. (1987) Food energy supply and demand: a discrepancy between particulate organic carbon flux and sediment community oxygen consumption in the deep ocean. *Limnology and Oceanography*, **32**, 201–230.

SUESS E. (1980) Particulate organic carbon flux in the oceans—surface productivity and oxygen utilization. *Nature*, **288**, 260–263.

WAKEHAM G. G., C. LEE, J. W. FARRINGTON and R. B. GARGOSIAN (1984) Biogeochemistry of particulate organic matter in the ocean: results from sediment trap experiments. *Deep-Sea Research*, **31**, 509–528.

WALSH I. D., J. DYMOND and R. COLLIER (1988a) Rates of recycling of biogenic components of settling particles in the ocean derived from sediment trap experiments. *Deep-Sea Research*, **35**, 43–58.

WALSH I. D., K. FISCHER, D. MURRAY and J. DYMOND (1988b) Evidence for resuspension of rebound particles from near-bottom sediment traps. *Deep-Sea Research*, **35**, 59–70.

WALSH J. J., D. A. DIETERLE and W. E. ESAIAS (1987) Satellite detection of phytoplankton export from the mid-Atlantic Bight during the 1979 spring bloom. *Deep-Sea Research*, **34**, 675–703.

WALSH J. J., C. D. WIRICK, L. J. PIETRAFESA, T. E. WHITLEDGE, F. E. HOGE and R. N. SWIFT (1988a) High frequency sampling of the 1984 spring bloom within the Mid-Atlantic Bight: synoptic shipboard, aircraft, and *in situ* perspectives of the SEEP-I experiment. *Continental Shelf Research*, **8**, 529–563.

WALSH J. J., D. A. DIETERLE and M. B. MEYERS (1988b) A simulation analysis of the fate of phytoplankton within the Mid-Atlantic Bight. *Continental Shelf Research*, **8**, 757–787.

WALSH J. J., P. E. BISCAYE and G. T. CSANADY (1988c) The 1983–84 Shelf Edge Exchange Processes (SEEP)-I experiment: hypotheses and highlights. *Continental Shelf Research*, **8**, 435–456.

WALSH J. J., D. A. DIETERLE, M. B. MEYERS and F. E. MÜLLER-KARGER (1989) Nitrogen exchange at the continental margin: a numerical study of the Gulf of Mexico. *Progress in Oceanography*, **23**, 245–301.

WEATHERLY G. L. and P. J. MARTIN (1978) On the structure and dynamics of the oceanic bottom boundary layer. *Journal of Physical Oceanography*, **8**, 557–570.

WEFER G. (1989) Particle flux in the ocean: effects of episodic production. In: *Productivity of the ocean: present and past*, W. H. BERGER, V. SMETACEK and G. WEFER, editors, J. Wiley and Sons, New York, pp. 139–154.

WYRTKI K. (1962) The oxygen minima in relation to ocean circulation. *Deep-Sea Research*, **9**, 11–23.

YODER J. A. (1985) Environmental control of phytoplankton production on the U.S. southeastern continental shelf. In: *Oceanography of the southeastern U.S. continental shelf*, L. P. ATKINSON, D. W. MENZEL and K. A. BUSH, editors, American Geophysical Union, Washington, D.C., pp. 93–103.

JOURNAL OF GEOPHYSICAL RESEARCH, VOL. 96, NO. C7, PAGES 12,645–12,665, JULY 15, 1991

On the Seasonal Phytoplankton Concentration and Sea Surface Temperature Cycles of the Gulf of Mexico as Determined by Satellites

FRANK E. MÜLLER-KARGER AND JOHN J. WALSH

Department of Marine Science, University of South Florida, St. Petersburg

ROBERT H. EVANS

Rosenstiel School of Marine and Atmospheric Science, University of Miami, Miami, Florida

MARK B. MEYERS

Department of Marine Science, University of South Florida, St. Petersburg

Monthly climatologies of near-surface phytoplankton pigment concentration and sea surface temperature (SST) were derived for the Gulf of Mexico from multiyear series of coastal zone color scanner (CZCS) (November 1978 to November 1985) and advanced very high resolution radiometer (AVHRR) (January 1983 to December 1987) images. We complement these series with SST from the comprehensive ocean-atmosphere data set (1946–1987) and Climate Analysis Center (1982–1990), and hydrographic profile data from the NOAA National Oceanographic Data Center (1914–1985). The CZCS ocean color satellite data provide the first climatological time series of phytoplankton concentration for the region. The CZCS images show that seasonal variation in pigment concentration seaward of the shelf is synchronous throughout the gulf, with highest values (>0.18 mg m^{-3}) in December to February and lowest values (~0.06 mg m^{-3}) in May to July. Variation in SST is also synchronous throughout the gulf, with maxima in July to September and minima in February to March. The amplitude of the SST variation in the western gulf is about twice that observed in the eastern gulf, and SST maxima and minima persist longer in the west. Larger amplitudes in SST variation are also observed toward the margins. While annual cycles of SST and pigment concentrations are out of phase relative to each other, the phases of mixed layer depth change and pigment concentration change are similar. Model simulations suggest that the single most important factor controlling the seasonal cycle in surface pigment concentration is the depth of the mixed layer. The combined use of ocean color and infrared images permits year-round observation of spatial structure of the surface circulation in the gulf and the pattern of dispersal of the Mississippi River plume. Infrared images are most useful between November and mid-May, when strong SST gradients occur. During this time, pigment concentrations are high and can be horizontally homogeneous. In contrast, between late May and October, SST fields are uniform, but the Loop Current and large anticyclonic eddies could be traced with the CZCS. Three anticyclonic eddies were observed in 1979, and at least two were observed in 1980. No eddies were observed during summers of subsequent years in the CZCS time series, but this may be a result of the dramatic decrease in the satellite sampling rate. The series of color images showed that small parcels of Mississippi River water were frequently (2–4 times a year) entrained in the cyclonic edge of the Loop Current, stretched along the Current, and carried to the southeast along the western Florida shelf. However, most of the Mississippi River water flowed to the west, following the Louisiana-Texas coast as far south as the Mexico–United States border. Here, a persistent cyclone may reside, exporting shelf constituents to deeper regions of the gulf.

INTRODUCTION

The Gulf of Mexico (Figure 1) has been the focus of extensive physical oceanographic field and modeling studies [*Austin*, 1955; *Nowlin et al.*, 1968; *Nowlin*, 1972; *Nowlin and Hubertz*, 1972; *Wert and Reid*, 1972; *Robinson*, 1973; *Schroeder et al.*, 1974; *Sturges and Blaha*, 1976; *Paluszkiewicz et al.*, 1983; *Blumberg and Mellor*, 1985; *Hofmann and Worley*, 1986; *Pechmann et al.*, 1986; *Kirwan et al.*, 1988]. The main attractions have been the warm Loop Current and the large (100- to 200-km diameter) anticyclonic rings repeatedly shed by this current [*Vukovich et al.*, 1979; *Vukovich and Maul*, 1985; *Vukovich*, 1986, 1988*a*; *Elliott*, 1982; *Auer*, 1987; *Kirwan et al.*, 1984*a*, *b*; *Lewis and Kirwan*, 1987]. However, compared to the knowledge that has accumulated about physical processes in the gulf, very little is known about the biological oceanography of the region.

Most biological oceanographic studies in the Gulf of Mexico have been geographically restricted [e.g., *Ortner et al.*, 1984; *Biggs et al.*, 1984, 1991], and only one attempt to carry out a synoptic ship survey of the phytoplankton distribution in the gulf has been made [*El-Sayed and Trees*, 1980]. It took 30 days to complete the latter survey (February 25 to March 27, 1980), and the extreme eastern and southeastern gulf were not sampled. *Trees* [1985] produced a contoured map of chlorophyll *a* from this survey, but no clear patterns emerged. Furthermore, he found no apparent relationship between the contoured data and pigment con-

Paper number 91JC00787.
0148-0227/91/91JC-00787$05.00

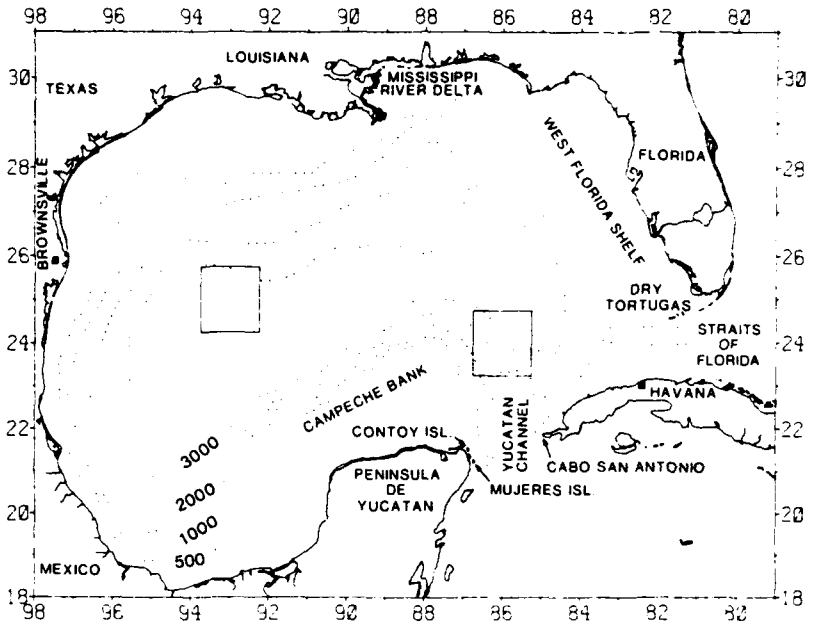

Fig. 1. Schematic map of the Gulf of Mexico showing areas for which time series of pigment concentration and sea surface temperature were extracted: entire basin, eastern gulf (Loop Current waters, 200 × 200-km^2 box, centered at 24°N, 86°W), and western gulf (modified Gulf of Mexico waters, 200 × 200-km^2 box, centered at 25°N, 93°W).

centration fields inferred from four single coastal zone color scanner (CZCS) satellite images collected during the survey. *Maul et al.* [1984] also attempted to use CZCS data (among other remotely sensed information) in an effort to compare spatial patterns of catch per unit effort for Atlantic bluefin tuna in the Gulf of Mexico with spatial patterns in oceanographic variables but he could not use any of the data covering the sampled fishery periods on account of cloudiness or location.

Walsh et al. [1989] reviewed the available phytoplankton and nutrient data in an effort to validate a coupled physical-biological numerical model for the Gulf of Mexico. In their model of the biological response to eddy shedding and nutrient injection by the Loop Current, incident light and vertical mixing varied seasonally. The simulated phytoplankton concentrations also followed a well-defined seasonal cycle. *Walsh et al.* [1989], however, found that historical in situ data were scarce and insufficient to validate the model results. Nevertheless, carbon deposition patterns observed in sediments of the Gulf of Mexico as well as more recent surface chlorophyll concentration distribution patterns, observed in a preliminary time series of CZCS images at 20-km resolution, were reproduced by the model.

This is a companion paper to the numerical simulation of the Gulf of Mexico by *Walsh et al.* [1989]. Our primary goals in this study were to (1) derive the climatological seasonal cycle of pigment concentration in the gulf, needed for basic validation of numerical simulations; (2) examine the spatial and temporal variability of the surface distribution of phytoplankton in the region; (3) determine the main factor(s) controlling the observed spatial and temporal changes in pigment concentration in the interior of the gulf; (4) derive a climatology of sea surface temperature (SST) based on infrared satellite data and validate it using historical in situ information; (5) show that a combination of infrared and ocean color space-based sensors can provide year-round observations on the spatial structure of the surface circulation in the region; and (6) trace the general pattern of dispersal of the Mississippi River plume.

METHODS

Pigment Concentrations

Synoptic estimates of the concentration of pigments in surface waters of the Gulf of Mexico were derived using the CZCS, launched by NASA on the Nimbus 7 satellite in October 1978. The CZCS was an experimental sensor that provided an estimate of the water-leaving radiance originating in the first optical depth. The average phytoplankton concentration in this layer has been empirically related to the water-leaving radiance, and thus at low concentrations (0.04–0.5 mg pigment m^{-3}) the CZCS-derived pigments represent the optically weighted average algae biomass within a surface layer of approximately 1- to 10-m depth.

The CZCS data were screened with the BROWSE quick-look facility developed at the Goddard Space Flight Center by G. Feldman and N. Kuring. Only scenes which covered at least some portion of the Gulf of Mexico containing patches of valid data greater than approximately 200 × 200 km were selected. Pigment concentrations were obtained at a spatial resolution of approximately 4 km by subsampling the original CZCS images to 1/16 of their original resolution at NASA's Goddard Space Flight Center (GSFC), Greenbelt, Maryland [see *Feldman et al.*, 1989]. Concentrations were derived from ratios of the blue (443 nm) or blue-green (520 nm) water-leaving radiances to the green radiance (550 nm), using the atmospheric correction and bio-optical algorithms of *Gordon et al.* [1983*a*] (also see *Gordon et al.* [1983*b*] and *Gordon et al.* [1988]). Clouds were masked using a simple threshold test on the 750-nm band (channel 5). The threshold was selected as the value where the CZCS visible

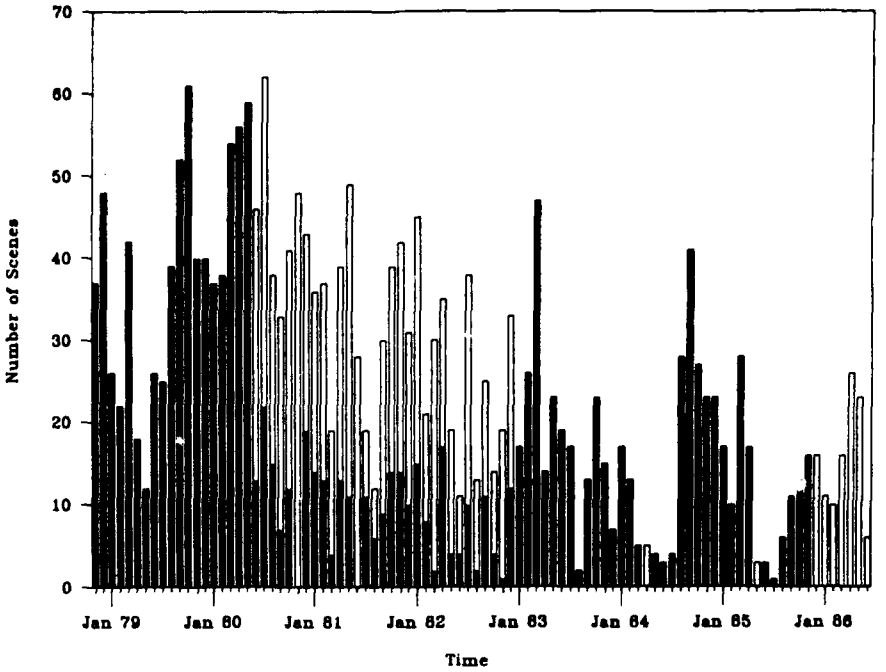

Fig. 2. Temporal coverage of the Gulf of Mexico realized during the lifetime of the CZCS (November 1978 to June 1986, open bars), as well as temporal coverage of data used for this study (November 1978 to November 1985, solid bar overlays). The CZCS data were screened with the BROWSE quick-look facility developed at the Goddard Space Flight Center by G. Feldman and N. Kuring. Only scenes which covered at least some portion of the Gulf of Mexico containing patches of valid data greater than approximately 200 × 200 km were selected. Consecutive 2-min segments from one satellite pass were counted as separate scenes. Data used in this study were binned into monthly means as described in the text (see Plate 1).

channels, particularly the 670-nm band (channel 4), begins to saturate, a point at which atmospheric correction is no longer possible. The processed CZCS data also include a mask for Sun glint.

Coherent spatial patterns of pigment concentration in the gulf could not be discerned using individual CZCS images or even weekly composites owing to extensive cloud cover or lack of programed coverage (see, for example, *Trees* [1985]). Therefore we binned the data into monthly composites. All images were first mapped to congruent cylindrical equidistant projections. Binning used all available cloud-free pixels for a month, generating fields with sum X, sum X^2, and N for each pixel. Daily fields were converted into fields representing arithmetic average pigment concentration, standard deviation, and number of scenes available within the given time interval (see below). Valid pixels were those having pigment concentrations between 0.04 and 7.0 mg m^{-3}; i.e., we excluded missing data, clouds, and extremely high pigment values. The resulting composite images had the same spatial resolution as the input images. Clearly, locations affected by clouds or missing data in successive images resulted in smaller temporal bins relative to locations with valid data.

Composites for November 1978 through May 1980 represent calendar monthly means. These data were binned at spatial resolutions of 4 km. Subsequent composites through December 1981 were based on the first 10 days of consecutive 30-day periods, which clearly represents only a fraction of the available data (see Figure 2). We binned these data into 20-km × 20-km squares prior to deriving composites. From January 1982 through December 1985, composites represent 30-day means of all CZCS data collected during that time. The resolution of this latter set was further reduced to approximately 36 km × 30 km per pixel. The reduction of spatial and of temporal resolution as described was arbitrary and was done to help alleviate computer mass storage restrictions. We believe that this scheme still provides first-order estimates of the monthly means.

To examine time variation in the concentration of phytoplankton, we obtained arithmetic means for the three areas shown in Figure 1:

Entire Gulf of Mexico. This area included all waters within the gulf to a line across the Yucatan Channel (between Isla Mujeres off Yucatan and Cabo San Antonio, Cuba) and a line across the Straits of Florida (extending along 81°W). Three means were derived for each month: a mean including continental shelf waters, a mean based only on waters deeper than the continental shelf and a shelf mean. A shelf mask for waters shallower than 200 m was obtained from a digital, 0.5-min resolution bathymetric data set from the Naval Ocean Research and Development Activity (NORDA) in Stennis Space Center, Mississippi.

Eastern gulf. This area included a box 200 × 200 km^2 centered at 24°N, 86°W, containing Loop Current water.

Western gulf. This area included a box 200 × 200 km^2 centered at 25°N, 93°W, containing modified Gulf of Mexico water.

From these series we further derived a 7-year monthly climatology for each region by averaging by month across years.

To test the effects of spatial resolution on the regional means derived from the CZCS data, we compared monthly composites derived in four different ways for the period

November 1978 through May 1980. This period was chosen because it was the only one for which we had a complete 4-km resolution data set at the time of the study. Specifically, we computed four versions of the monthly mean concentration for the 200 × 200-km box located in the eastern Gulf of Mexico (Figure 1), as follows: (1) Regional means were computed directly from the 20-km resolution CZCS monthly composites of the North Atlantic generated by G. Feldman (NASA GSFC) and described by *McClain et al.* [1990]. (2) Regional means were computed directly from the 4-km resolution CZCS monthly composites of the Gulf of Mexico. (3) Using the daily 4-km resolution CZCS images of the Gulf of Mexico, the monthly means were computed by averaging the series of daily regional means. (4) Using the daily 4-km resolution CZCS images of the Gulf of Mexico, the monthly means were computed by weighting the daily regional means by the number of valid pixels in each daily image (valid pixels are those with valid data).

We found that there were no significant differences between these series using a simple t test on month-to-month differences between any pair of series. The null hypothesis tested was that the population of differences had an average value of 0. The test criterion was that of significance at the 0.1% level or better. In summary, all versions provided the same result regardless of how they were derived.

There may be problems in applying simple statistical tests, such as the t test used here, to satellite images of geophysical data. This is because such data are frequently spatially correlated (and therefore not independent). It is also hard to estimate degrees of freedom and standard errors. The t test is not statistically rigorous for the comparisons attempted here because phytoplankton biomass does not follow a normal distribution in space but rather follows a lognormal distribution [see *Campbell and O'Reilly*, 1988]. Also, sample size of the populations of means was different for each of the series just compared, simply as a result of the way in which the means were derived. Nevertheless, such comparisons suggest that differences in the series for the deep waters of the Gulf of Mexico, derived in radically different ways, are small.

This differs from the conclusion of *Müller-Karger et al.* [1989], who in a study of the Caribbean Sea found that the most robust series of means was obtained using the weighted daily means. The reason that this method did not provide different results for the Gulf of Mexico is that the areas examined by *Müller-Karger et al.* [1989] were very large ($>10^5$ km^2) relative to the 200 × 200-km boxes used here, and within those areas of the Caribbean examined, patches of high concentrations occurred periodically as a result of the dispersal of river plumes or upwelling. Under such conditions, partial coverage of the sampling areas by the CZCS led to biases in the regional means, and weighting reduced the impact of the outlying values on the mean.

On the other hand, the use of imagery of varying resolution may not provide equivalent results for studies of small-scale processes, i.e., over scales much smaller than the 200 × 200-km boxes used here. At such small scales it is best to use full resolution imagery (1-km pixels in the case of the CZCS and the advanced very high resolution radiometer (AVHRR)). Subsampling of the original data by factors of 16 or more, as was done here, with subsequent grouping into bins of 20 km or larger, aliases (or filters) small-scale features from the data.

It is clear that the nature of the data set used has to be well understood. It is not uncommon to find low-resolution data sets, such as global CZCS images with a nominal pixel resolution of 18–20 km (i.e., 2048 × 1024 pixel images), further degraded by a factor of 8 for digital display on 512 × 512 pixel screens, being used as if they had not been subsampled. Such data are inadequate to study local, small-scale phenomena.

In terms of the accuracy of the concentrations derived, previous results suggest that in low-pigment waters (0.08–1.5 mg m^{-3}), retrieved pigment concentrations are within 30–40% of in situ concentrations [*Gordon et al.*, 1980, 1982, 1983*a*]. The deep Gulf of Mexico falls in this category, with waters of case I type [see *Morel and Prieur*, 1977]. However, the accuracy of derived values is questionable over shelf waters and in areas of river plume dispersal [see *Müller-Karger et al.*, 1989; *Carder et al.*, 1989], even though CZCS pigment values in areas affected by rivers may be realistic [*Yoder et al.*, 1987; *Barale et al.*, 1986; *Gordon et al.*, 1983*a*]. Such areas have been broadly classified as being case II by *Morel and Prieur* [1977], to indicate that there may be a large concentration of gelbstoffe (yellow dissolved organic matter) as well as other marine or terrigenous constituents which do not covary with phytoplankton.

The presence of additional colored constituents can lead to an overestimate of phytoplankton concentration [see *Baker and Smith*, 1982; *Carder et al.*, 1986]. The degree of correlation among phytoplankton, suspended matter, and gelbstoffe near the Mississippi River delta or the nearshore environment of the Gulf of Mexico is unclear, and in such environments it is difficult to quantify chlorophyll concentration based on a simplistic blue-green ratio of CZCS radiances [e.g., *Fisher et al.*, 1986]. The algorithms used here did not compensate for the presence of these additional constituents. It is important that future studies refine our present ocean color algorithms using extensive direct ground information [e.g., *Carder et al.*, 1986, 1989; also R. R. Bidigare et al. (Influence of the Orinoco River outflow on distributions of algal pigments in the Caribbean Sea, submitted to *Journal of Geophysical Research*, 1991)] and indirect mass balance models [e.g., *Müller-Karger et al.*, 1989] in order to accurately quantify carbon pools and concentrations of other optical constituents.

An additional source of error in the CZCS data is a "ringing" (sensor overshoot) effect caused by a lag in the adjustment of the CZCS amplifiers to large changes in target brightness off the eastern and northeastern boundaries (downscan side) of some clouds [see *Mueller*, 1988]. Ringing effects were minimized in our 20-km spatial resolution products by masking of affected areas prior to the spatial binning process. Mask generation relied both on the properties of the CZCS and the behavior of the normalized water-leaving radiance at 520 nm (band 2). The nominal value of normalized water-leaving radiance at 520 nm is 0.48 mW cm^{-2} μm^{-1} sr^{-1}. This decreases with increasing chlorophyll concentration (see, for example, Figure 2 of *Gordon et al.* [1988]). The 520-nm CZCS channel exhibited the lowest instrument noise of any of the CZCS bands but suffered a large overshoot response. A threshold of 0.7 mW cm^{-2} μm^{-1} sr^{-1} was chosen to allow for in-water scattering and residual aerosol radiance. Once the atmospherically corrected 520-nm radiances decreased below 0.7, a subsequent test required the pixel-to-pixel radiance difference to be less

than 0.10 mW cm^{-2} μm^{-1} sr^{-1} (approximately two instrument counts). A distance limit restricted the test to pixels within 40 original resolution pixels of the cloud edge determined with the 750-nm band as was explained above.

Note that we corrected the sensor overshoot artifacts when deriving the 20-km spatially binned data but for comparison purposes did not apply this correction to the 4-km CZCS products discussed below. Similar to what was found by *Müller-Karger et al.* [1990], the geographical area affected by ringing in the Gulf of Mexico was small relative to our area of study, affecting a band of the order of 10 km or less on the downscan side of clouds. Below we show that there were no statistical differences between the regional means derived using the 20- or the 4-km data sets, in spite of the different masks applied.

Sea Surface Temperature

To complement the pigment time series, we examined SST fields derived from the NOAA operational multichannel sea surface temperature (MCSST) product archived at the University of Miami [*Olson et al.*, 1988]. The SST values are derived from AVHRR data and distributed by NOAA (global retrieval tapes). The NOAA product consists in lists of latitude, longitude, time, and MCSST. MCSST techniques are described by *Walton* [1988], *Strong and McClain* [1984], and *McClain et al.* [1983]. The algorithms used were those of *McClain et al.* [1985]. These include a series of tests, using radiance thresholds for visible channels and differences of brightness temperatures for the infrared channels, to detect cloud-contaminated pixels. The data were sorted by time and grouped into 2-week bins for 1982–1986 and into 1-week bins starting in 1987. Subsequently, data points were geographically binned into pixels of a 2048 × 1024 matrix covering the globe (cylindrical equidistant projection). A Laplacian interpolation was used to fill gaps, with the condition that one valid retrieval exist within nine pixels of the pixel being evaluated. For purposes of this work we focused on the Gulf of Mexico and the northwestern Caribbean Sea. We derived SST climatologies for the subregions shown in Figure 1 by binning data by month across years.

We also examined multiyear series of SST extracted from the comprehensive ocean-atmosphere data set (COADS) and the Climate Analysis Center (CAC) data set. Both of these data sets are archived and described in the on-line NASA climate data system (NCDS) of the NASA Space Science Data Center (NSSDC) at NASA GSFC.

The COADS is described by *Woodruff et al.* [1987]. It contains monthly averaged marine observations for the years 1854 through 1987 on a 2° × 2° geographical grid. We used the SST subset for the years 1946–1987. The COADS is derived from weather observations taken near the ocean's surface, primarily from merchant ships, and is supplemented by data from buoys, surface level bathythermographs, the global telecommunication system (GTS), and ocean station vessel observations. We used COADS to derive an additional SST climatology for the interior of the Gulf of Mexico by binning monthly data across the years.

The CAC SST was derived from in situ (ship-of-opportunity and fixed buoy) data and radiance data collected from the AVHRR. The AVHRR retrievals were derived by the multichannel technique referred to by *Reynolds* [1988]. The CAC SST data set [*Reynolds*, 1988; *Reynolds and Roberts*, 1987] contains gridded (2° × 2°) SSTs and corresponding quality parameters, indicating whether the data is only from in situ or from blended SST observations (in situ SSTs blended with AVHRR-derived SSTs). Here, we used the blended analysis grids, which are available from January 1982 to December 1990. The CAC data have been subjected to objective quality controls as described by *Reynolds* [1988]. The global monthly average bias error is less than 0.1°C. The global monthly average rms error is less than 0.8°C. However, errors at individual grid points could be larger.

Finally, we derived mean monthly climatological profiles of temperature, salinity, and density (σ_t) in the Gulf of Mexico using all standard depth NOAA National Oceanographic Data Center (NODC) station cast data for bottom depths >50 m available for the gulf (period 1914–1985). The NODC data have limitations in terms of the spatial distribution of observations in the Gulf of Mexico. The highest density of observations is found in the Yucatan Channel and Straits of Florida along the west Florida shelf, and immediately east of the Mississippi delta. The rest of the gulf is more or less uniformly covered, with at least one station within 20 km of any other stations. The lowest density of stations is found in the southwestern quadrant of the gulf. We attempted deriving a climatology of nutrient concentration profiles, but the data archived for the gulf were so few and unreliable that it was not possible to interpret the results in a meaningful way.

RESULTS

Data Distribution

We derived a total of 81 composite CZCS images representing a series of monthly mean pigment fields in the Gulf of Mexico from November 1978 through November 1985. This time series included 1562 individual scenes collected between November 1978 and November 1985 (the CZCS collected over 2500 scenes of the gulf over its lifetime: see Figure 2).

Figure 2 summarizes the temporal coverage of the Gulf of Mexico realized during the lifetime of the CZCS (November 1978 to June 1986), as well as the temporal coverage used for this study (November 1978 to November 1985). The total number of scenes included in a composite (Figure 2) is frequently slightly larger than the number of monthly CZCS passes that provided useful data. This occurs because CZCS data are archived in 2-min segments, and two or three consecutive segments collected during a single orbital pass were counted as separate scenes. Also, the total number of scenes used per binning period (Figure 2) is typically larger than the largest number of scenes included per pixel (N) in a composite. This also is a consequence of scheduling and satellite position as well as variability in cloud cover.

The best sequence of images spanned 1979 and the first half of 1980, the period over which 41% of the data examined were collected (Figure 2). Over 50% of the pixels in each of these monthly composites had a sample size larger than 2, and on occasion, average sample sizes over the Gulf of Mexico and adjacent Cayman Sea exceeded five images per month per pixel (e.g., August, September, and October 1979 and March, April, and May 1980). In contrast, our temporal sampling scheme (10 days per month) for June 1980 through

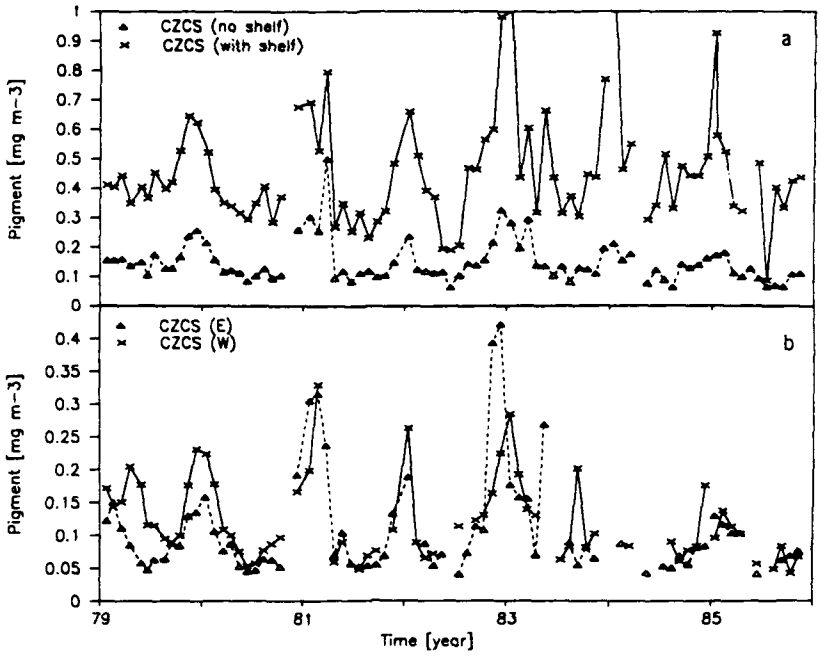

Fig. 3. Time series of regional monthly mean pigment concentration values in the Gulf of Mexico (milligrams per cubic meter). (*a*) Means derived for the entire basin: the solid curve shows the series which includes the continental shelf region; the dashed curve shows values obtained excluding the shelf. (*b*) Means derived for 200 × 200-km^2 subregions shown in Figure 1: the solid curve represents the western box; the dashed curve shows the eastern box.

December 1982 resulted in markedly decreased coverage relative to the number of scenes available (Figure 2). Complete lack of coverage using the described sampling scheme occurred in November 1980, June 1981, April 1984, and May 1985.

It has been pointed out that cloud cover can alias time series of pigment fields [e.g., *Abbott and Zion*, 1987]. Clouds would preclude coverage of large portions of the Gulf of Mexico during periods of atmospheric front passage or during storm periods. Any transients of the near-surface pigment concentration resulting from storm activity may thus remain undetected by the CZCS. AVHRR-derived SST products would experience similar aliasing problem.

However, while we expected a strong seasonal pattern in the availability of CZCS data due to meteorological problems, the CZCS collected as many good data over the gulf during summers as during winters (e.g., Figure 2). In particular, the second half of 1979 and the first half of 1980 showed exceptionally good coverage of the gulf. It seems that more than cloud cover the reason for lack of coverage of the gulf was scheduling. In general, sample scheduling appears to have provided more frequent coverage of the eastern margin of the gulf: the dense coverage of the west Florida shelf is primarily the result of scheduling for data collection of the East Coast of the United States, with concomitant cover of this portion of the gulf.

A discussion of the distribution of clouds or cloud-free pixels in space or over time, and the aliasing effect of such variability on variations in ocean color, phytoplankton concentration, and sea surface temperature, is beyond the scope of the current study. This would require continuous coverage of the region and processing of the entire data set. Currently, it is difficult to separate the confounding factors of lack of data due to scheduling, geographical coverage during various orbital passes, data drops due to temporary sensor failure, and cloud cover.

Phytoplankton Pigment Concentration Series

Figure 3 shows the four time series of regional pigment means derived from the CZCS composites. Figure 3*a* shows that there is an offset of 0.30 mg pigment m^{-3} between the basin mean including the continental shelf (mean = 0.45 mg pigment m^{-3}, SE = 0.18, n = 80 means) and the mean excluding the shelf (mean = 0.15 mg pigment m^{-3}, SE = 0.07, n = 81 means). Also, there clearly are higher values of algal biomass every boreal winter relative to the summer concentrations. Figure 3 also suggests that temporal variability over the shelf increased during 1983 and that the high winter concentrations in other regions of the gulf were attenuated after 1982. There is also a general lack of spatial and temporal pattern in the series of images starting in 1983. It is important to note that these time series are robust only up to about 1982, since afterward artifacts may have been introduced by the decrease in CZCS sampling. Furthermore, the calibration of the CZCS sensors after 1982 remains unknown. The climatologies derived here include the latter part of the record as well.

Figure 3*b* shows the time series of monthly mean pigment concentrations within the two 200- × 200-km subregions of the gulf outlined in Figure 1. These subregions were chosen to examine the contrast between an offshore area directly influenced by the Loop Current and one that is not. Note that the eastern box is not necessarily always in the Loop Current. In particular, when anticyclonic eddies are shed, the Loop Current flows directly from Yucatan Channel through the Straits of Florida, i.e., south of the box. Accordingly, we expected variables measured in this box to show

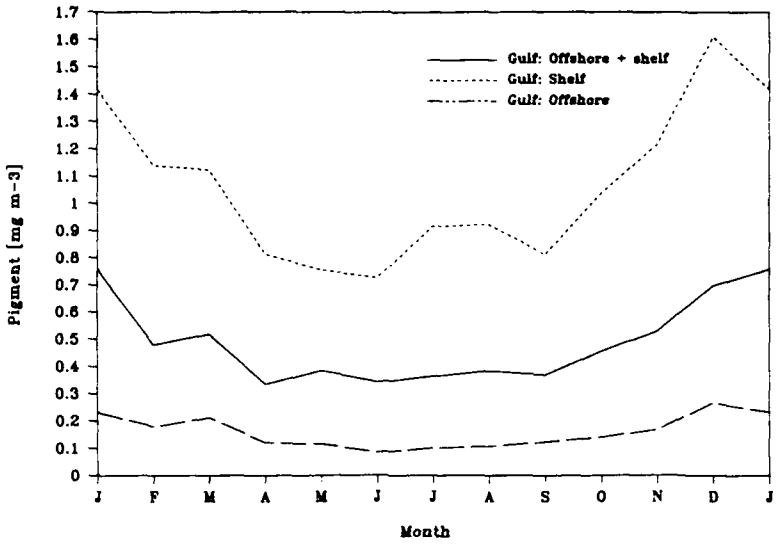

Fig. 4. Monthly climatology of pigment concentration (milligrams per cubic meter) in the Gulf of Mexico based on 7 years of CZCS data (1979–1985).

wide variability. In spite of this the eastern and western time series of algal biomass were very similar. Except for 1979 and late 1982 the subregion series tracked each other, showing that pigment variability in offshore waters is generally synchronous throughout the gulf at seasonal time scales.

Figure 4 shows the climatological seasonal cycle of pigment concentration in the Gulf of Mexico. The seasonal cycle for the continental shelf (waters shallower than 200 m) was obtained by masking waters deeper than 200 m. There is a seasonal cycle, both offshore and over the shelf, but it is clearly more pronounced over the shelf.

The climatological seasonal cycles of phytoplankton concentration in the two subregions of the Gulf of Mexico are shown in Figure 5. In both subregions, consistently low

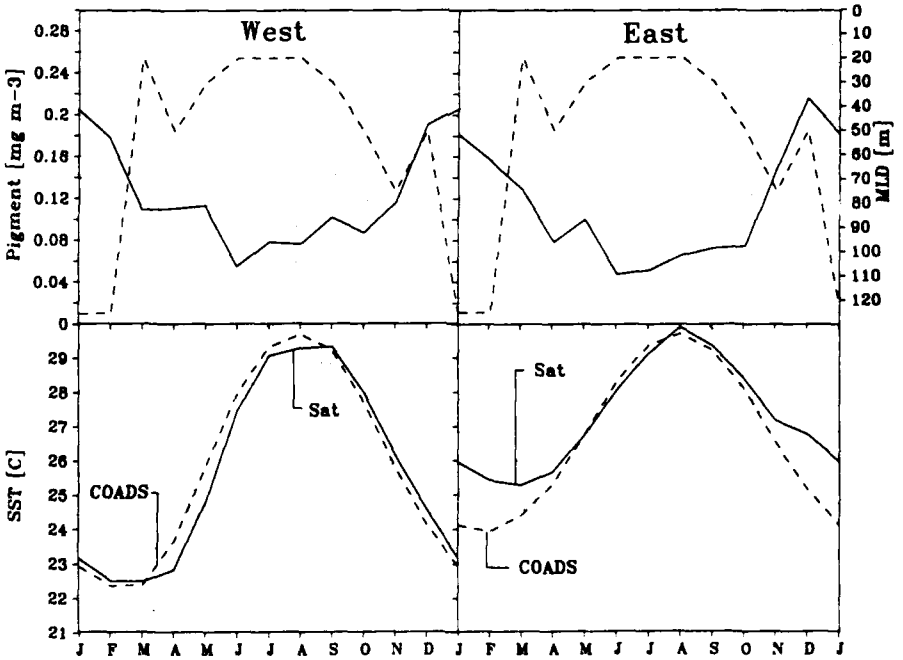

Fig. 5. Monthly climatology of pigment concentration (milligrams pigment per cubic meter) and sea surface temperature (degrees Celsius) within the two 200 × 200 km^2 subregions of the Gulf of Mexico shown in Figure 1. (Top) The solid curves represent a monthly pigment concentration climatology based on 7 years of CZCS data (1979–1985), and the dotted curves represent the standard error envelope of the series. The dashed curve overlay represents the climatological mixed layer depth, estimated from all historical NODC σ_t data in the gulf (bottom depth > 50 m; see text). (Bottom) Solid curves show monthly mean SST estimated from 5 years of AVHRR data (1983–1987), and the dotted curves represent the standard error envelope of the series. The dashed curves represent monthly mean SST values obtained from the COADS data set (1946–1987) for the 2° × 2° boxes closest to the center of the subregions of interest.

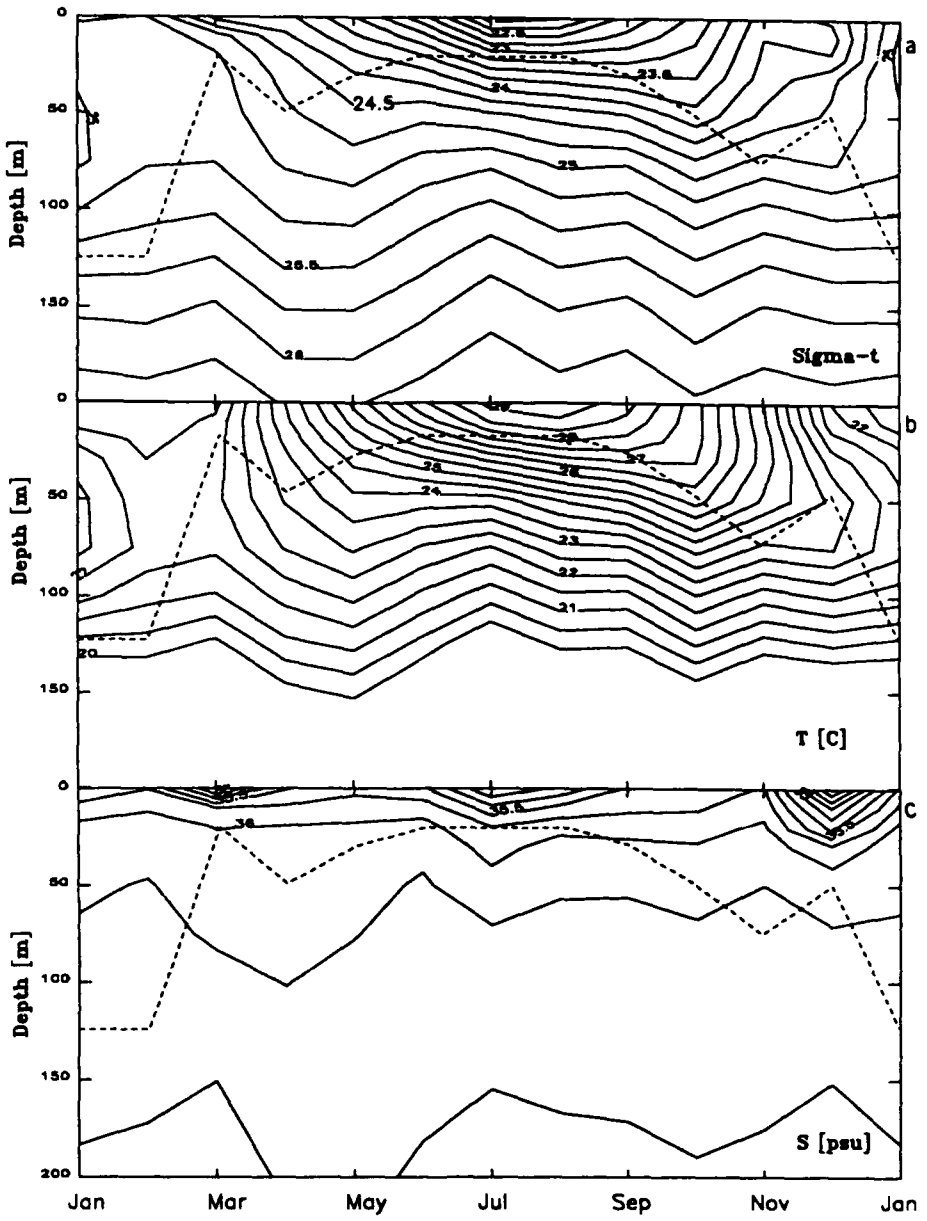

Fig. 6. The seasonal cycle of water column properties and mixed layer depth offshore in the Gulf of Mexico. The monthly climatology was derived from all the available NODC station data for the region with recorded water depths greater than 50 m: (*a*) σ_t, (*b*) temperature, and (*c*) salinity. The MLD (dashed curve overlay) was derived from the monthly climatological σ_t profiles and defined as the first depth at which a change in σ_t larger than 0.5 occurred relative to the mean density within the upper 10 m.

pigment values occurred during summer (about 0.06 mg m^{-3} or less) and high values occurred during winter (>0.18 mg m^{-3}). As was mentioned above, the cycles in both subregions are very similar. The eastern subregion, however, which is directly affected by the Loop Current, showed larger variability during late fall (November to December) than the western subregion. This appears to be the result of interannual variation in the chlorophyll concentration of waters flowing into the Gulf of Mexico from the Cayman Sea.

Mixed Layer Depth and SST Series

Figure 6 summarizes the seasonal cycle of water column properties in the offshore Gulf of Mexico. Monthly climatological σ_t values (Figure 6*a*), temperature (Figure 6*b*), and salinity (Figure 6*c*) were derived at standard depths from all the available NODC station data for the region with recorded water depths greater than 50 m (years included: 1914–1985). The mixed layer depth (MLD) (shown in Figures 5 and 6) was defined as the first depth at which a change in σ_t larger than 0.5 occurred relative to the mean density within the upper 10 m, using the monthly climatological σ_t profiles. Clearly, density in the upper 100 m undergoes a strong seasonal cycle which leads to shallow (<20 m) mixed layers during boreal summers. The density changes are largely the result of temperature changes.

Figure 7 shows the COADS and satellite-derived SST time series derived for the eastern and western subregions for the

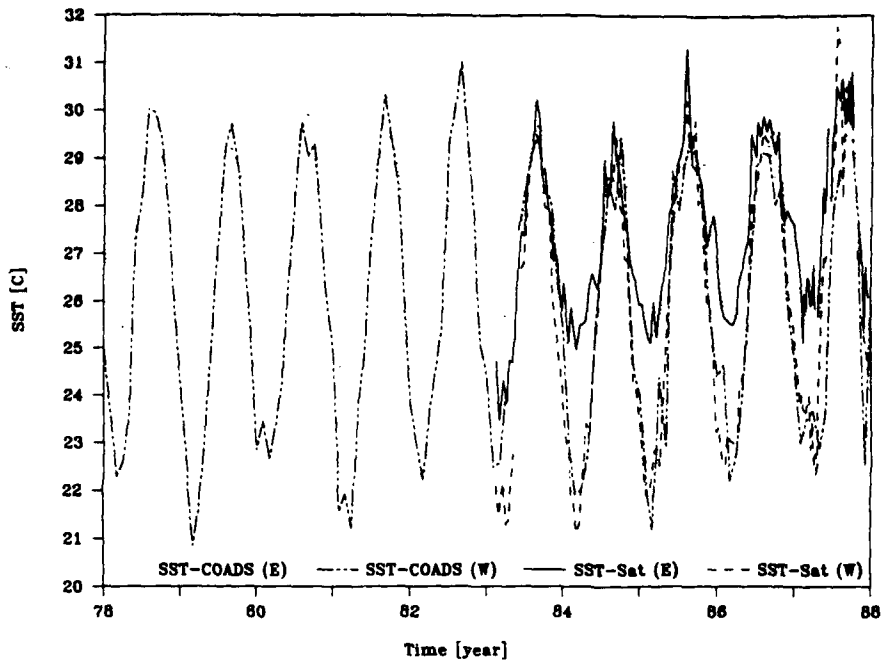

Fig. 7. Time series of SST (°C) within the two 200 × 200-km² subregions of the Gulf of Mexico shown in Figure 1. The series were derived from 5 years of AVHRR data (1983–1987) and from a subset (1978–1988) of the COADS data set for the 2° × 2° boxes closest to the center of the subregions of interest.

period 1978–1988. In general, the COADS observations (1946–1987) suggested that interannual variation within the gulf is relatively small. This is also reflected in the narrow envelope of deviations from the monthly climatological SST means for the subregions (Figure 5) estimated both from the COADS (1946–1987) and from the AVHRR (1983–1987) data sets.

SST changes in the east and in the west were synchronous, but the amplitude of the seasonal variation was larger in the west (Figures 5 and 7). While between July and September both regions had relatively similar SSTs (>29°C), from December through April the western subregion showed SSTs as much as 4°C lower than the eastern region. On the average, the mean SST range was about 7°C in the west, compared with about 5°C in the east. Also, SST maxima and minima in the west persisted for longer periods than maxima and minima in the east. The dampening of the seasonal variation in the east is caused by the influx of warm Caribbean water into the gulf via the Loop Current during winters; this water is warmer than western gulf waters. Even larger amplitudes of temperature occur closer to the Texas-Louisiana coast, away from the influence of the warm Loop Current and anticyclonic eddies shed by it.

A month-by-month comparison of the AVHRR-derived SSTs and the COADS SSTs for the period of overlapping observations (1983–1987) resulted in rms differences of 1.22°C for the western subregion (n = 58 months) and 0.92°C for the eastern subregion (n = 60 months). A similar comparison between the AVHRR-derived SSTs and the CAC SSTs for the same period resulted in rms differences of 0.90°C for the western subregion (n = 60 months) and 0.82°C for the eastern subregion (n = 60 months). The difference between monthly COADS SST and the satellite SST (COADS-satellite SST), as well as the difference between monthly CAC SST and the satellite SST (CAC-satellite SST), showed a negative slope when regressed against time (slope significantly different from 0 at the 0.001 level within both subregions). There also seems to be a small phase lag between the climatological monthly values obtained from these data sets, leading to cyclic departures from a 1:1 relationship on a seasonal basis (Figure 8).

The causes for the differences among the COADS, CAC, and AVHRR SST data sets are difficult to assess. Such peculiarities may be due to effects derived from time of day at which AVHRR measurements are made (daytime passes in this case). There is also an uncertainty in the estimates associated with the fact that the AVHRR "sees" skin SST [*Schluessel et al.*, 1990], while SST measured in situ may reflect the bulk temperature. From a climatological point of view it is possible that the Loop Current developed a more persistent intrusion into the northern gulf during the winters of 1983–1987 (years of AVHRR data) relative to previous years (COADS spanned 1946–1987), thus leading to higher winter temperatures in the eastern sector (see Figure 8).

Clearly, there is considerable scatter between pigment concentration and SST throughout the Gulf of Mexico at seasonal time scales (Figure 9). This scatter is a result of the phase difference between these variables and is evidence that algal biomass is not directly related to temperature of the water. Figure 9 emphasizes the difference in the SST range between the eastern and western subregions, while showing that pigment values in both subregions are similar during any one month. It is also clear from Figure 9 that widely different levels of algal biomass may be found at any one temperature within the SST cycle of the Gulf of Mexico. The spread in pigment values within a region is much larger during the boreal winter than during the summer.

In addition to the temporal variability observed in the surface pigment concentration, SST, and hydrographic profile series, dramatic changes in the spatial structure were

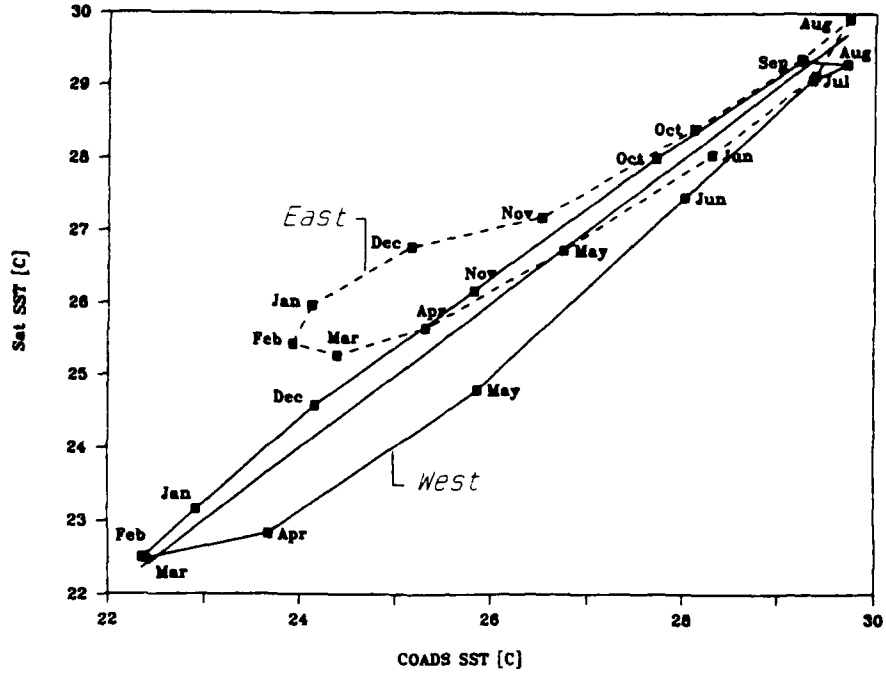

Fig. 8. Phase relation between climatological, monthly mean SST values derived from ship observations (COADS) and from the AVHRR. The two elliptical paths were obtained by comparing AVHRR-derived SST values from the subregions (Figure 1) to COADS SST values retrieved from the 2° × 2° boxes closest to the center of the subregion of interest.

observed in the CZCS images. The series of images showed that during summer there was marked spatial structure in the pigment fields associated with the Loop Current and anticyclonic eddies (see sequences for both 1979 and 1980, Plate 1). The eastern Gulf was dominated by the clear water intrusion of the summer Loop Current, while the western side contained patches of clear water. In winter, concentrations increased simultaneously throughout the gulf, and offshore pigment fields became homogeneous between about December and February. Homogeneous fields can occur early, as was observed in late October 1979. Spatial structure did not develop again until at least February, when a tongue of low values (<0.1 mg m^{-3}) extended into the gulf from Yucatan Channel (for example, see March to M 1979 or 1980 in Plate 1). This is also an indication of reduce nination of wind mixing and marks the low-pigment r signature of the Loop Current.

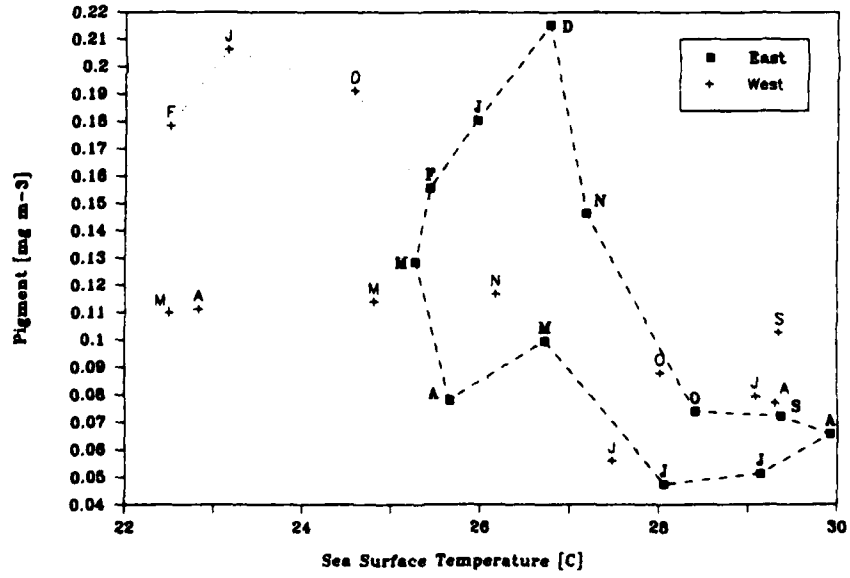

Fig. 9. Phase diagram showing the scatter in the relationship between pigment concentration and satellite-derived SST (MCSST, degrees Celsius) within two subregions of the Gulf of Mexico (see Figure 1). The dashed curve represents the seasonal cycle in the eastern Gulf of Mexico, and the dotted curve represents the variation in the western gulf. Letters represent month of the year.

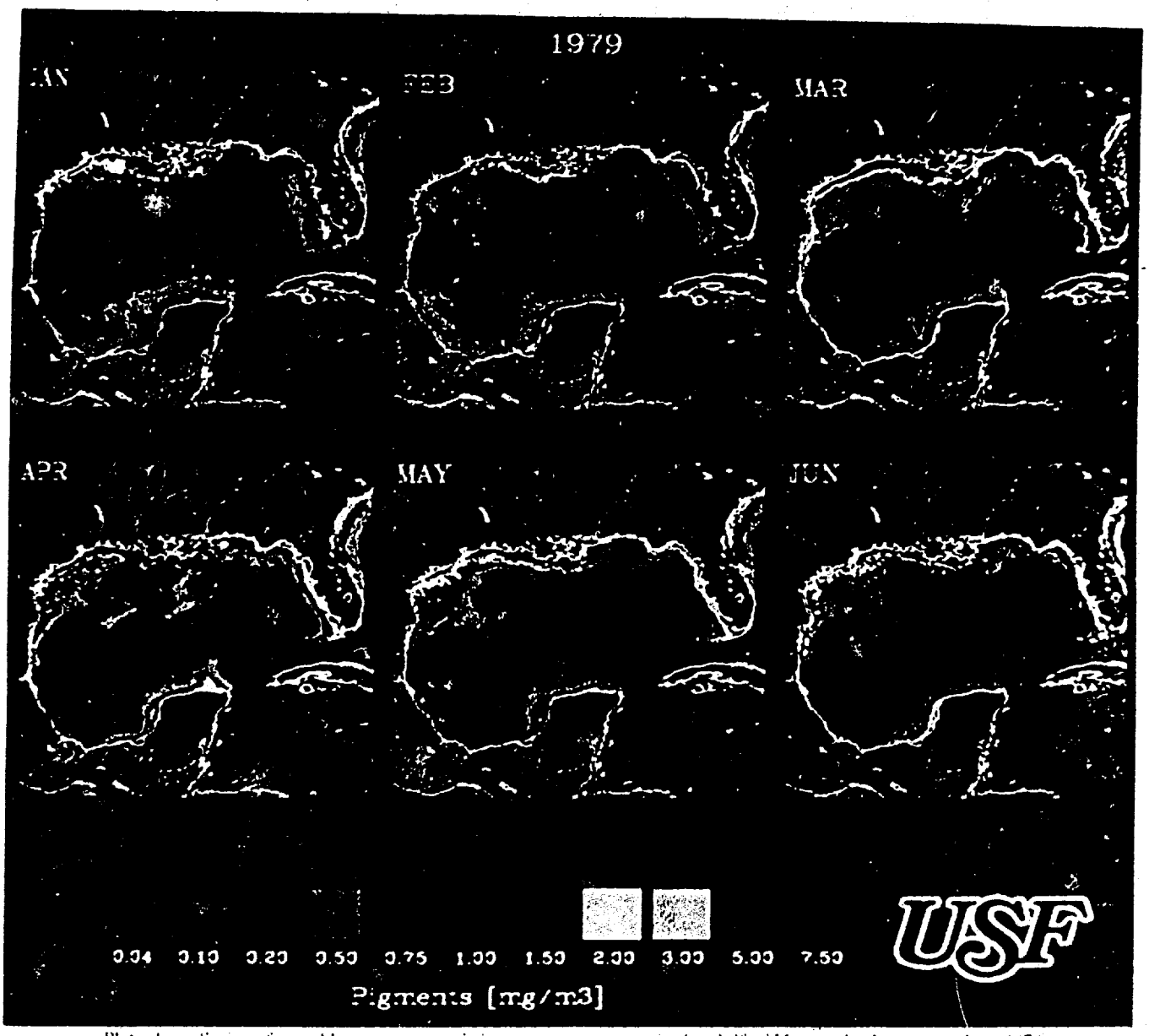

Plate 1*a*. Series of monthly composites of pigment concentration in the Gulf of Mexico for January to June 1979. Concentrations (milligrams per cubic meter) were color coded, with purple and blue representing low pigment concentrations (note that the lowest concentrations have been overemphasized to enhance spatial patterns using violet with a reddish tint). Yellow and red indicate higher concentrations. Land is masked grey, the coastline, white; and clouds and missing data black. Rivers affecting the region have been drawn in blue as part of the land mask for information purposes. All rivers have been drawn with the same line width, and therefore these lines do not contain information on discharge rates nor on the size of the rivers.

Discussion

Because of the large scale of the Loop Current and its anticyclonic rings and because of the variability in the occurrence, shape, and location of these features, ships alone provide inadequate definition of the circulation and biogeochemical cycling within the Gulf of Mexico. New approaches have combined models, satellites, drifters, and hydrographic and expendable bathythermograph (XBT) data to map the details of the physical environment [cf. *Paskausky and Reid*, 1972; *Hulburt and Thompson*, 1980; *Science Applications International Corporation (SAIC)*, 1986, 1988]. In particular, infrared satellite images have provided synoptic maps of the Loop Current and its eddies since the 1970s, something that was not possible previously even after extensive ship surveys [*Lewis and Kirwan*, 1987; *Vukovich*, 1986, 1988*a*; *Vukovich and Maul*, 1985; *Maul et al.*, 1985; *Paluszkiewicz et al.*, 1983; *Elliott*, 1982; *Maul*, 1981; *Vukovich et al.*, 1979; *Hall et al.*, 1978, 1981]. However, infrared satellite images provide information on the spatial structure of the circulation in the Gulf only during a 7-month period (late October through mid-May). During the rest of the year, SST gradients are small throughout the Gulf rendering infrared imagery useless for identifying the summer Loop Current or other surface circulation features.

The possibilities of using remotely sensed ocean color data as a complement to infrared imagery for year-round study of surface circulation patterns in the Gulf of Mexico was first examined by *Maul and Gordon* [1975] and *Maul* [1977]. Maul and Gordon tested this concept using in situ data and images from the Earth Resources Technology Satellite ERTS-1 (the

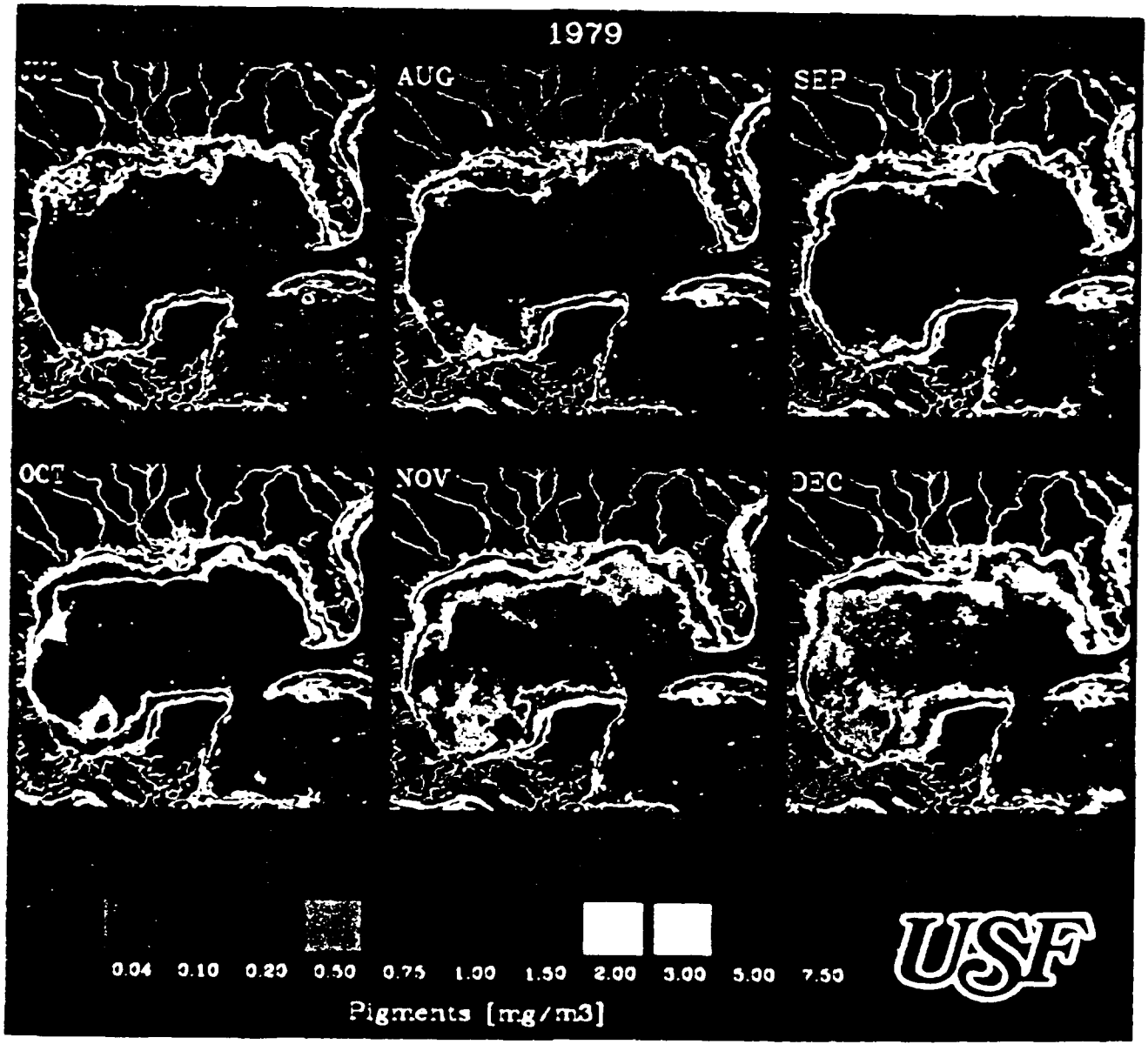
1979
JUL
AUG
SEP
OCT
NOV
DEC
0.04 0.10 0.20 0.50 0.75 1.00 1.50 2.00 3.00 5.00 7.50
Pigments [mg/m3]
USF

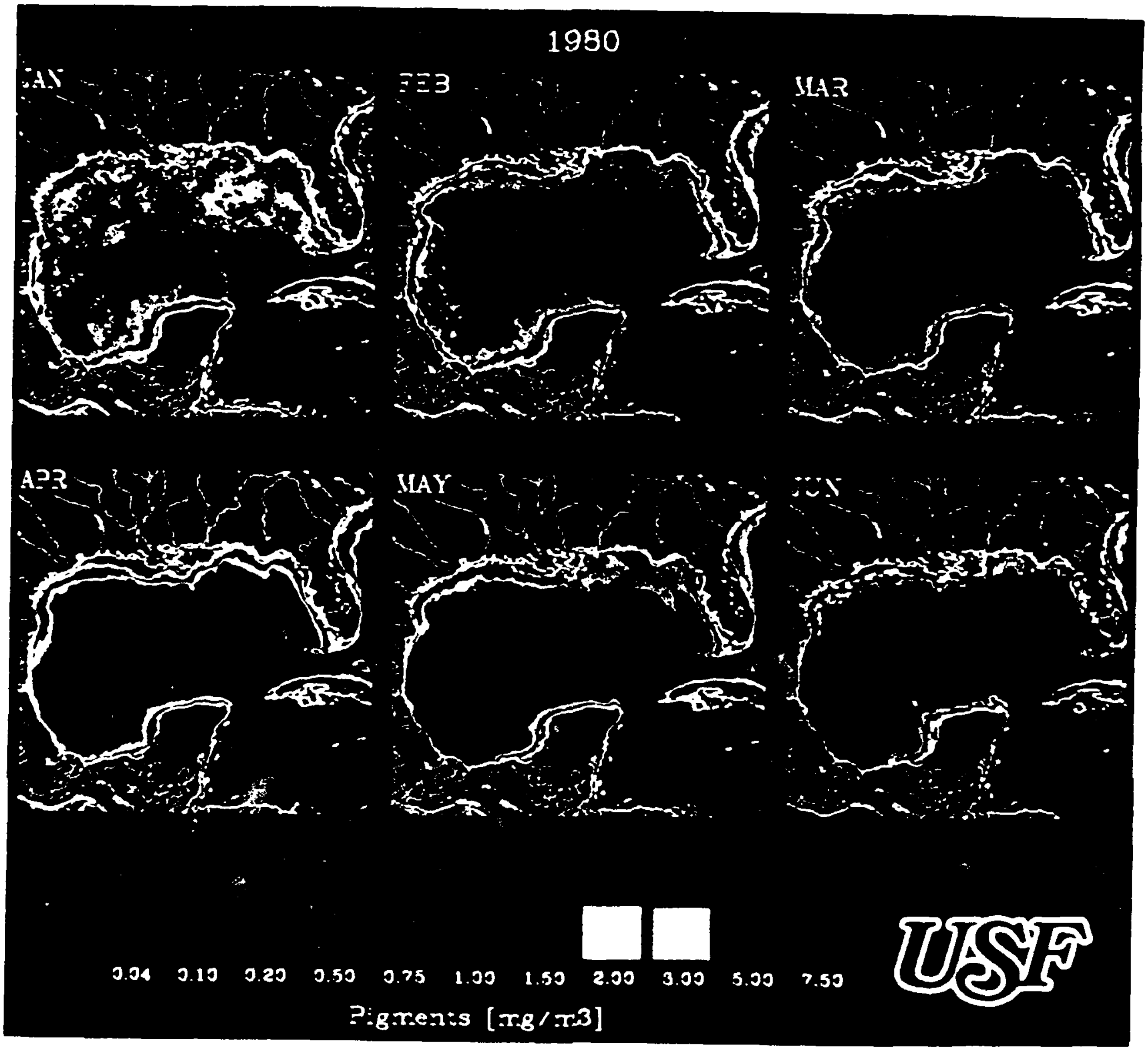

Plate 1. Series of monthly composites of pigment concentration in the Gulf of Mexico for January to June 1980.

Using historical data, it is possible to establish which factors control such a cycle of phytoplankton concentration. While there is a long-term exchange of properties between incoming water of the Caribbean Sea and those resident in the Gulf of Mexico [*Walsh et al.*, 1989; *Kawamura et al.*, 1984a; [illegible], 1979], a comparison between long time series of physical and biological variables in the gulf suggests that on the average, the local physical processes dominate the productivity of the upper water column over the course of 1 year. In particular, the seasonal cycles of algal biomass left behind in the surface water of the eastern and western gulf (see Figure 7) are similar regardless of the presence or absence of anticyclonic eddies and the Loop Current, as is indicated by a 3–4°C temperature contrast between the two regions (Figure 7).

Another important result from our comparison of the climatological SST and pigment time series is that the pigment concentrations are out of phase relative to the SST [illegible] (Figures 5 and 6). Minima of algal biomass occur 2 to 3 months before the SST maxima. Similarly, the highest pigments occur 2 to 3 months prior to the coldest SSTs, while chlorophyll concentrations begin to decrease before SST minima occur. This lack of agreement shows not only that there is little direct impact of a 5°–7°C temperature range on phytoplankton growth but that SST cannot be used to predict phytoplankton concentrations with a simple statistical model of negative correlations.

In contrast, pigment concentrations and mixed layer depth have matching phases (Figure 5). *Walsh et al.* [1989], using a complex coupled physical-biological numerical model, determined that the single most important factor controlling the seasonal variation of chlorophyll concentrations in offshore waters of the Gulf of Mexico was the depth of the mixed layer embodying both light limitation and nutrient availability. While downwelling, grazing, and sinking are important processes, they play a smaller role in controlling the seasonal abundance of phytoplankton stimulated by new supplies of nitrogen, i.e., nitrate. In the Gulf of Mexico there is adequate illumination in the mixed layer on a year-round basis. Since algal biomass is highest when the surface mixed

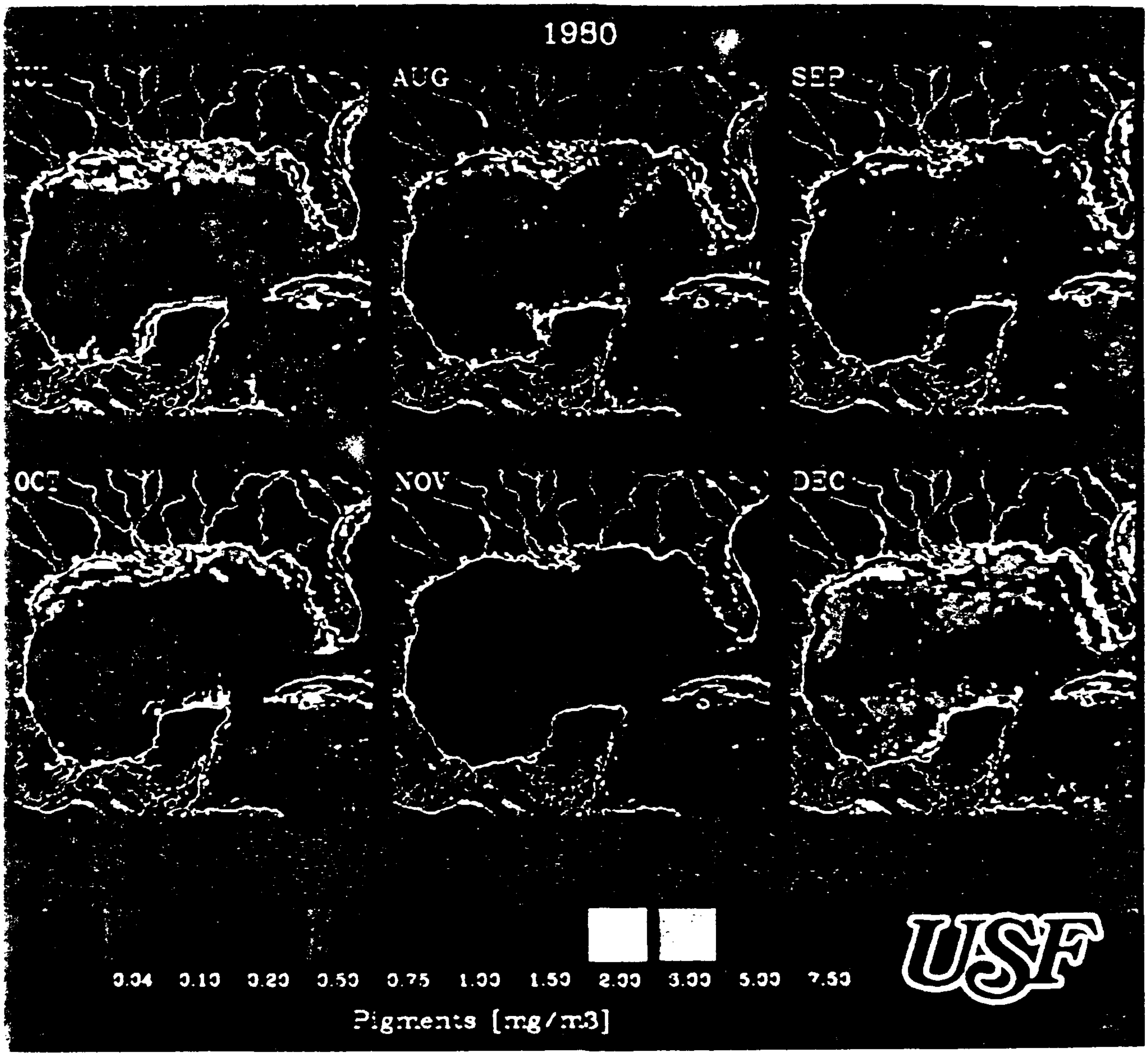

[illegible] Series of monthly composites of pigment concentration [illegible] Mexico [illegible] 1980.

[illegible] deepest. This is strong evidence that primary production in this region is controlled by variations in upward [illegible] flux. This is similar to the process observed in the Sargasso Sea [illegible] *Dickey et al.* [1990], *Ryther and Menzel* [illegible] and *Menzel and Ryther* [1961]. Conversely, flux [illegible] when stratification ensues during summers [illegible] primary production is small. Further north, for example [illegible] a more important role in regulating the [illegible] of phytoplankton [illegible] similar conclusions to those reached by *M*[illegible] in their study of temporal changes of phytoplankton concentration in the Sargasso Sea.

[illegible] mixed layer depth was specified on a monthly [illegible] using modified climatological [illegible] 1982] at [illegible] N [illegible] W in the Atlantic [illegible] a climatological hydrographic profile for [illegible] confirms the phase and general validity of the [illegible] concentrations were highest when [illegible] deepest [illegible] and reached a minimum [illegible] the shallowest mixed layer [illegible] derived pigment concentrations did not [illegible] crease [illegible] until the mixed layer [illegible] deeper than about [illegible] in August or September [illegible] Figure 7.

When [illegible] processes of wind mixing do not dominate [illegible] [illegible] can be used [illegible] of the Gulf of Mexico [illegible] time series of pigment images shows [illegible] associated with the Loop Current and [illegible] see differences for both 1979 and 1980 in Plate [illegible] eastern Gulf [illegible] dominated by the clear water [illegible] of the summer Loop Current, while the western [illegible] associated with [illegible]

Such structure of the pigment field disappeared [illegible]

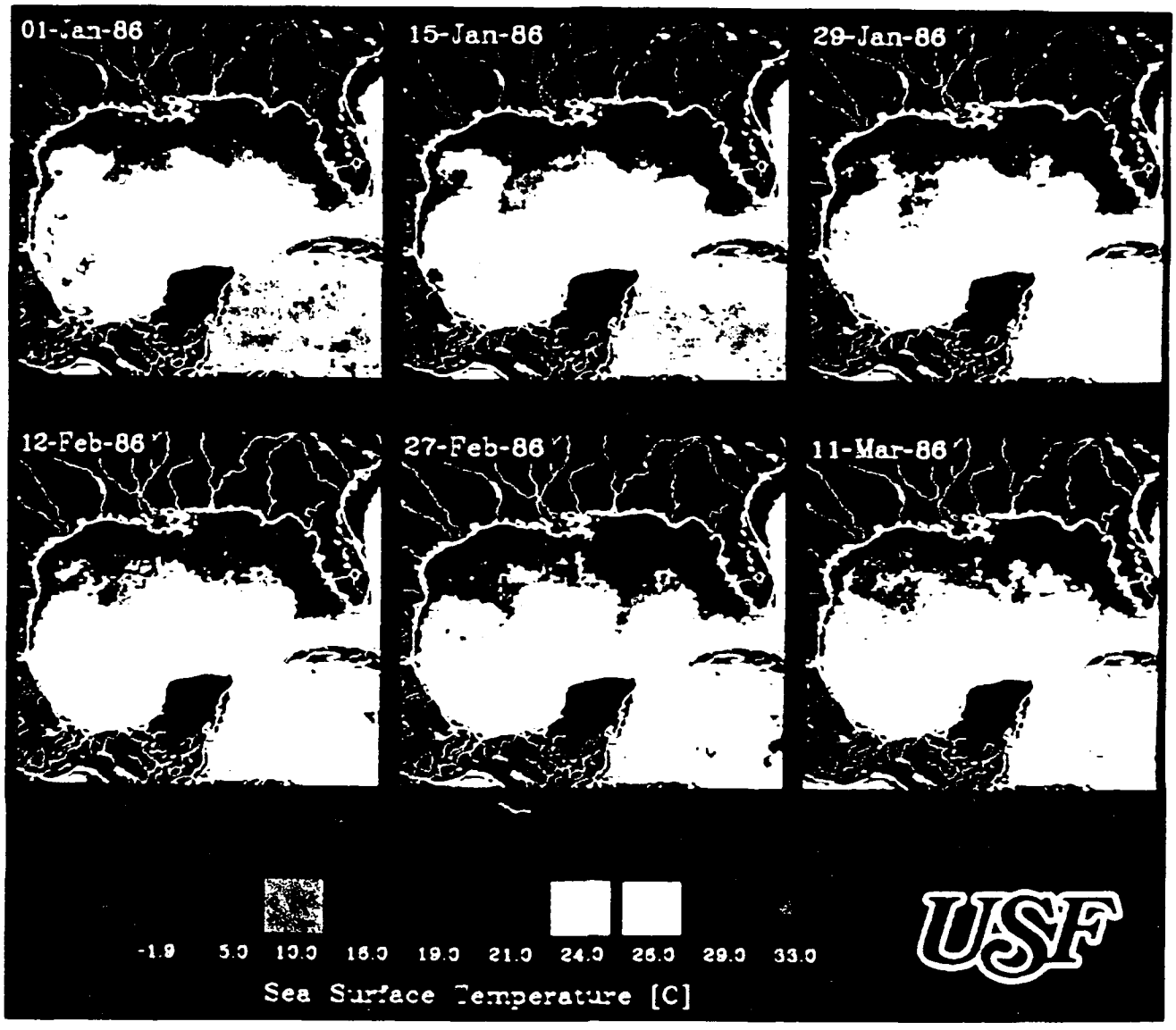

Plate 2. Sequence of 2-week mean AVHRR-derived SST fields showing both anticyclonic and cyclonic rings in winter of 1986. Land is masked grey, the coastline, white, and clouds and missing data black. Rivers affecting the region have been drawn in blue as part of the land mask for information purposes.

however, as concentrations increased simultaneously throughout the gulf (Plate 1). Offshore pigment fields became homogeneous as early as late October and did not develop spatial structure again until about February of the following year. The first indication of the development of summer patchiness occurred when a tongue of low values (< 0.1 mg m^{-3}) extended into the gulf from Yucatan Channel (for example, see March to May 1979 or 1980 in Plate 1), marking the position of the Loop Current.

In contrast, spatial structure in AVHRR images was poorly developed during summer (mid-May through October) but very well developed in winter (November through mid-May). We show examples in Plate 2 of winter SST from 1986. Clearly, AVHRR data delineate the winter circulation patterns of the Loop Current or eddies when a sufficient SST gradient occurs. Both winter and summer AVHRR-derived SST values are comparable to the COADS estimates (Figures 5, 7, and 8), showing that in fact the AVHRR provides a reasonable estimate of SST year-round. Further tests of this nature are necessary to decrease the rms difference between satellite and in situ SST data.

The CZCS data show marked differences between the pigment concentrations offshore in the gulf and those over the continental shelf. In general, concentrations over the shelf were always high (> 0.5 mg m^{-3}) relative to values offshore (0.2 mg m^{-3} or less), with extremes occurring in restricted areas along the coast (> 5 mg m^{-3}). Furthermore, high concentrations of algal biomass are persistent (1) off Florida, (2) off Mississippi, Louisiana, and Texas, and (3) over Campeche Bank. Clearly, much of the shelf area of the Gulf of Mexico falls under the case II water type of *Morel and Prieur* [1977].

The biological productivity of the shelf is strongly affected by (1) the effluent of the Mississippi River [*Walsh*, 1988], (2) outflow from coastal lagoons and smaller rivers, (3) cyclonic eddies which develop along the continental margin (e.g., *Biggs et al.*, 1984, 1991], and (4) wind-driven upwelling. Unfortunately, because of a dearth of nutrient and primary

productivity observations at this stage, it is impossible to improve upon our prior estimate of the relative contribution of these nutrient supply mechanisms [*Walsh et al.*, 1989].

The Mississippi River discharges, on the average, about 1.7×10^4 m^3 s^{-1}, with a range of 0.81×10^4 m^3 s^{-1} in September to 2.81×10^4 m^3 s^{-1} in April. The northern Gulf of Mexico shelf receives, in addition, the discharge of the Mobile River, at an average of 1670 m^3 s^{-1}, or the equivalent of 10% of the Mississippi, via Mobile Bay [*Morisawa*, 1968]. The Mobile River shows large variability in its discharge, and in 1980 its flood was the second largest in 20 years (R. Stumpf, U.S. Geological Survey, personal communication, 1991).

The Mississippi River discharges an average of 2.1×10^8 tons sediments per year [*Milliman and Meade*, 1983], which generally settle out of the water column, since a primary production of >250 g C m^{-2} y^{-1} occurs at the mouth of the river [*Thomas and Simmons*, 1960]. As a result, we are able to use riverine-induced growth of phytoplankton as a tracer of freshwater discharge on the Texas-Louisiana shelves, similar to previous studies of the plumes of the Amazon and Orinoco rivers [*Muller-Karger et al.*, 1988, 1989].

The CZCS data clearly show that a large amount of colored material enters the Gulf of Mexico via the Mississippi delta and Mobile Bay. Furthermore, the series of CZCS images was useful for following this material and tracing the dispersal of the discharge. This was important especially because the simulated Mississippi plume dispersed toward the east in our model, a result of not being able to apply local wind forcing to the Lagrangian circulation scheme. On the basis of a few studies of the shelf in the northern gulf it has been inferred instead that the Mississippi River outflow usually spreads to the west of the delta over the continental shelf [*Nowlin*, 1972; *Smith*, 1980; *Dinnel and Wiseman*, 1986; *Cochrane and Kelly*, 1986]. As a consequence, the surface salinity fields of the Louisiana-Texas shelves exhibit a strong seasonal signal, with 15-psu (practical salinity units) water found off the mouth of the river and 28 psu near Brownsville, Texas, during May 1964, in contrast to 30 and 33 psu, respectively, in November 1964 [*Cochrane and Kelly*, 1986].

Dispersal of fresh water to the east of the Mississippi delta also occurs, however. *Maul* [1977], for example, during a study of the annual cycle of the Loop Current using in situ and Landsat satellite data, found a narrow band of low-salinity water off western Florida (24 psu) and in the Straits of Florida (30 psu). He inferred that this was Mississippi River water entrained along the cyclonic edge of the Loop Current when the current penetrated northward to the vicinity of the delta. Low-salinity waters (34.5 psu), presumably of Mississippi origin, were reported as far north as Georgia during this period [*Atkinson and Wallace*, 1975].

Our time series of CZCS images confirmed both the predominant westward dispersal and occasional eastward transport of combined Mississippi and Mobile river water. Also, the CZCS data showed definite patterns in the variability of the width and length of the plume. We examined the series of daily CZCS images for the period November 1978 to May 1980 to obtain a general perception of the frequency of eastward transport of plume water. We found that eastward dispersal was sporadic and short-lived and that it covered a small area. Typically, the surface area occupied by strongly discolored water (e.g., pigment concentrations >1 mg m^{-3}) derived from such events was a small fraction (typically 1–5%) of the surface area of similarly discolored plume waters flowing westward. Eastward dispersal occurred either as a very thin (~5–10 km) band near the coast, as diffuse dispersal within 50 km of the coast, or as a large event in which a bolus of discolored water, over 50 km in diameter, moved eastward. Two such large events were detected. In each of these, water moved along the coast past Cape San Blas (Florida) and subsequently flowed south, offshore along the western Florida shelf. The first event took place in mid-March 1979, the second in late April 1980. In both cases the cycle of eastward plume transport, full extension to the Florida keys, and dissipation lasted 20–30 days.

In addition to eastward transport along the coast, small parcels of river water were also frequently observed being entrained in the cyclonic edge of the Loop Current and dispersed offshore. For example, during September to October 1979, southeastward dispersal of Mississippi water in a narrow (20–80 km) but long (>900 km) band occurred along the cyclonic edge of the Loop Current. This band could clearly be seen extending to the Dry Tortugas and being swept into the Straits of Florida on images taken on October 9 and 19, 1979. By October 24 this plume, clearly defined by concentrations of ~0.2–0.4 mg pigment m^{-3}, flowed past Miami within a 26-km band along the coast of southern Florida. However, by then this patch had severed from the main body of the plume near the Mississippi delta. Note that the eastward flowing feature is not clearly visible in the October 1979 monthly composite except as a faint trace of a wider (~70 km), diffuse band of ~0.2 mg pigment m^{-3} along the eastern edge of the Loop Current (Plate 1). In images from mid-November 1979, mid-December 1979, and mid-January 1980, new streamers of river water could be seen entrained in the eastern cyclonic edge of the Loop Current. These were short-lived and did not exceed about 500 km in length. By mid-May 1980, however, another streamer had been carried to the Straits of Florida.

It is possible that in addition to entrainment in the edge of the Loop Current during periods of northward intrusions, which may occur at any time during a year, eastward dispersal of river water is facilitated by prevailing wind patterns over the northern gulf during the first half of the year. *Pechmann et al.* [1986] computed the monthly wind-driven transport for the Gulf of Mexico for the period 1977–1985 based on the National Weather Service limited area, fine mesh model II (LFM II) results. They show that the monthly mean wind-driven transport in the northeastern gulf is weakly north-northwestward for January through March, nil in June through September, and strongly west-northwestward in October through December. It is conceivable that during the period of weak transport, northward wind events or northward intrusions of the Loop Current facilitate eastward movement of river water parcels. It appears that only on very rare occasions do small amounts of river water move east during the second half of the year.

Typically, however, the Mississippi-Mobile plume appeared as a massive band of high pigments extending west of Mobile Bay and the Mississippi delta along the coast. The width of the Mississippi River plume seemed to vary with seasonal changes in discharge rate: a wider plume was observed during the months of high discharge. Furthermore,

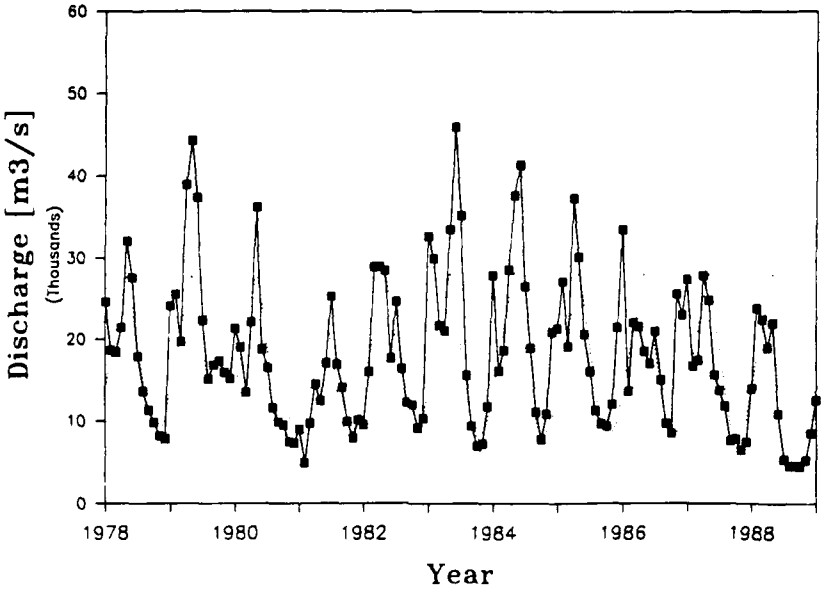

Fig. 10. Time series of monthly mean discharge (cubic meters per second) values for the Mississippi River at Vicksburg (Mississippi). The solid curve represents actual monthly mean discharge estimates. The dotted curve shows a climatology based on monthly mean discharge between 1929 and 1989.

changes in the length of the plume seemed to follow major changes in the total annual discharge.

The total annual discharge rate for the Mississippi may vary by a factor of 3 or more between years; clearly, part of the variance was embedded in our time series. For example, in 1978 and 1980 the Mississippi River flow closely followed the long-term hydrograph (Figure 10). The monthly CZCS composites for 1978 (November and December, not shown) and for 1980 (Plate 1) show that most of the discharge was carried west in a band following the coast and extending at least as far as Tampico, Mexico. The band was broadest over the shelf off Louisiana and Texas, exhibiting a cross-shelf gradient in pigments. Values >2 mg m^{-3} occurred within 5 km of the coast, rapidly decreasing to values around 0.5 mg m^{-3} about 30 km off the coast and decreasing to about 0.1 mg m^{-3} roughly 100 km from the coast. Off Brownsville, Texas, the band was less than 60 km wide.

The annual average discharge in 1979 was about 1.6 times larger than that estimated for 1978 or 1980 (Figure 10). In fact, discharge during the second half of 1979 was nearly twice that experienced during the second semester of 1980. This was the result of at least five cyclonic storms which occurred in the gulf between July and September 1979 [*Halper and Schroeder*, 1990]. The higher discharge led to a longer, wider, and more persistent coastal band containing pigment values >2 mg m^{-3} relative to the plume seen in 1980 (Plate 1).

The plume dispersal patterns in 1979 showed additional peculiarities. In contrast to the patterns seen in 1980, a large portion of the chlorophyll plume was carried offshore near the southern border of Texas starting approximately in April. The offshore movement of this plume in April to June may have been due to cyclonic eddy motions near the edge of the continental shelf. Note the cyclonic eddy depicted by the AVHRR in this region during January 15–29, 1986 (Plate 2). Similar cyclonic eddies are seen within thermal images of at least February 1984 and January 1987 (not shown here).

In addition to an offshore movement effected by a cyclonic eddy, during July to August 1979 the plume was affected by hurricane activity in the northern Gulf of Mexico. In particular, Hurricane Bob (July 9–11) formed in the southwestern Gulf of Mexico and made landfall in Louisiana, east of the Atchafalaya River mouth [*Halper and Schroeder*, 1990]. The Texas and Louisiana coasts were for the most part on the trailing edge (left-hand side) of the hurricane, which would have led to the offshore dispersal of coastal waters. Very high pigment concentrations are indeed seen moving offshore in this area in the July 1979 CZCS composite. Tropical storms Claudette (July 21–24) and Elena (August 29 to September 1) further helped disperse the plume offshore. Hurricane Frederic (September 10–12) then followed a track [see *Halper and Schroeder*, 1990] which caused a tongue of Mississippi water to wrap around the cyclonic edge of an anticyclonic eddy pinched off from the Loop Current (see below). Again in this case, the Mississippi plume was located on the trailing edge of the hurricane.

A persistent cyclone in the western Gulf of Mexico would agree with the general pattern of offshore recirculation described by *Cochrane and Kelly* [1986] and *Dinnel and Wiseman* [1986], who concluded that the fresh water from the Mississippi and Atchafalaya rivers is carried offshore off central-south Texas and then is carried back east along the shelf break. There is ample evidence for offshore flow near the Mexico–United States border: *Elliott* [1979] suggests that there is an eastward flow from the coast of Texas resulting from the confluence of the coastal currents moving south along Texas and north along Mexico, while *Merrel and Morrison* [1981] suggest that this eastward jet maintains (or is maintained by) an anticyclone/cyclone eddy pair in the western gulf. Such patterns can be related to westward motion of an anticyclone, shed by the Loop Current in the eastern gulf [*Walsh et al.*, 1989]. The cyclonic eddies appear as the large anticyclone dissipates by friction as it interacts with the continental margin.

As was mentioned above, the CZCS provided the first summer pictures of the Loop Current and the anticyclonic eddies it periodically sheds. These eddies are shed sometime after the Loop Current reaches its maximum northern extreme. However, the timing of penetration by the Loop Current is variable [*Maul*, 1977]. Also, the extent of penetration varies. For example, *Nowlin and Hubertz* [1972] found the northernmost extreme of the current at 28°N, and *Huh et al.* [1978] found it entering De Soto Canyon and coming within 8 km of Pensacola Beach, Florida, on February 11, 1977. A CZCS image obtained on June 1, 1985, also clearly shows the Loop Current extending into De Soto Canyon, but most images show penetration only to less than 27°–28°N.

The best images of anticyclones were obtained in 1979 and 1980 (Plate 1). However, the pattern of eddy formation, movement, and dispersal in 1979 was totally different from that seen in 1980. It is unclear what effect hurricanes may have on anticyclonic eddies shed by the Loop Current, but the erratic behavior of two eddies shed during the second half of 1979 (see below) may have been a direct consequence of the unusual 1979 hurricane activity.

In the 1979 series of composites the Loop Current can be first seen in March 1979 extending to approximately 26.9°N. Even though this feature is barely distinguished from other Gulf of Mexico waters in Plate 1, there was a difference of more than 0.05 mg pigment m^{-3} between the interior of the Loop Current and other gulf waters. By April, a band of slightly elevated pigment concentration (>0.1 mg m^{-3}) extended from Campeche Bank toward the Florida keys, thus severing the northern portion of the intrusion. This showed the first anticyclonic eddy of the pigment series. High-pigment waters originating from Campeche Bank also outlined the western edge of the eddy, which was approximately 400 km in diameter. The fate of this eddy is not clear from the CZCS data. There is a hint of lower concentrations north of Campeche Bank and west of the Loop Current in the following composite (May 1979), but it is unclear if this represents a remnant of the eddy.

The Loop Current can be seen penetrating northward again in May and June (up to 27.5°N), flanked on its western side by a band of higher concentrations extending NNW from Campeche Bank for at least 500 km. In July 1979 another eddy can be seen breaking off the northern half of the Loop Current (N-S diameter, 240 km; E-W diameter, 380 km). This eddy, however, appears to have been reabsorbed into the Loop Current, since the August composite shows a well-defined and fully extended Loop Current.

The August composite also shows that there is a constriction at the base of the Loop Current near 23.4°N. This constriction leads to another shedding event, with an eddy of ~320-km diameter seen in the September composite. In this composite the Loop Current can be seen flowing directly from Yucatan Channel to the Straits of Florida, hugging Cuba. This eddy also seems to have been reabsorbed into the Loop Current, causing a sinuous circulation pattern which extended from Yucatan Channel to 27.9°N in October. The Loop Current and other circulation patterns were then obscured in subsequent images of the gulf, as gradients in pigment abundance weakened.

While each of these eddies seems to have been shed and subsequently reabsorbed by the Loop Current, it is possible that only one ring was shed and that this ring continually interacted with the current without reabsorption. It is possible that mixing of near-surface waters obscured the separation zone, therefore rendering the ring indistinguishable from the Loop Current in the CZCS imagery.

During 1980 the Loop Current first became distinguishable in the March composite. By June (the first of a series of 10-day composites), much of the gulf showed extremely low concentrations (<0.05 mg m^{-3}). This possibly was a result of widespread nutrient depletion in surface waters by phytoplankton uptake under conditions of strong water column stratification and was perhaps accentuated by westward penetration of anticyclonic eddies carrying clear water shed by the Loop Current. An anticyclonic ring shed during this period will become associated with a cyclone in a fall eddy pair off the Texas coast. In July the Loop Current was well defined, extending farther north to 27.1°N, compared to the May position. The intrusion was then flanked to the west by a band of higher concentrations extending from Campeche to the NNW.

The Loop Current then shed another anticyclonic eddy, visible in the August 1980 composite. The eddy entrained high-pigment water from the shelf off Florida and carried it seaward to distances over 500 km offshore. The September and October 1980 composites show that the eddy drifted toward the WSW, growing in size as it was displaced. The approximate size of this second eddy and the approximate location of its center were as follows: August, 350 km N-S diameter, 160 km E-W diameter, centered at 25.9°N, 88°W, with its northernmost extension at 27.5°N; September, 330 km N-S diameter, 235 km E-W diameter, centered at 25.3°N, 89.4°W, or approximately 160 km from the August position; and October, 350 km N-S diameter, 375 km E-W diameter, centered at 24.7°N, 90.4°W, or approximately 120 km from the September position.

This gives an approximate speed of 5 km d^{-1} over a period of 60 days, similar to translation velocities of other observed [*Vukovich and Crissman*, 1986; *Kirwan et al.*, 1988] and simulated [*Walsh et al.*, 1989] anticyclonic eddies in the Gulf of Mexico.

Note also in the October 1980 composite (Plate 1) that the cyclonic feature causing eastward export of a algal biomass from the Texas shelf is present again, similar to April 1979, but the first anticyclone of the eddy pair can now be seen to the southeast of the cyclone. Unfortunately, there were no data available for the first 10 days of November to follow the progress of either the cyclone or the two anticyclones. By December 1980 neither the Loop Current nor the eddies could be identified in the CZCS imagery because of the high uniform concentrations throughout the region. Presumably, thermal infrared satellite data would have been helpful in continuing to monitor the evolution of these features. However, we had no access to infrared data for this period.

Several oceanographers have tried to define the frequency of anticyclonic eddy shedding by the Loop Current. The general conclusion is that eddy shedding is variable. Numerical models tend to shed anticyclonic eddies at a frequency of one every 300 days, namely, at the natural frequency of the Loop Current under constant boundary conditions [see *Hulburt and Thompson*, 1980; *Walsh et al.*, 1989]. *Vukovich* [1988*b*] concludes that the average eddy-shedding frequency is 10.9 months, and *Behringer et al.* [1977] suggested that one eddy occurs per year. The most complete eddy census was carried out by *Elliott* [1979, 1982], who concluded that

there are years in which no eddies occur, but that up to three eddies may occur in any 1 year (as between October 1966 and June 1967). The CZCS data presented here tend to support the idea that the frequency of eddy shedding is variable. We look forward to future launches of a color sensor, providing contemporary and real-time satellite pigment and SST fields, to successfully monitor interannual cycles of Loop Current penetration and eddy shedding within the Gulf of Mexico.

CONCLUSIONS

Pigment concentration in the Gulf of Mexico undergoes a well-defined seasonal cycle which is generally synchronous throughout the region. Highest concentrations (>0.18 mg m^{-3}) occur between December and February, and lowest values (~0.06 mg m^{-3}) occur between May and July. SST variation is also synchronous throughout the gulf, with maxima between July and September and minima in February and March. While annual cycles of algal biomass were out of phase relative to the seasonal SST cycle, the mixed layer depth and pigment concentrations showed similar phases. Model simulations show that the single most important factor controlling the seasonal cycle in surface pigment concentration is the depth of the mixed layer.

The combined use of ocean color and infrared images promises year-round observation of the spatial structure of the near-surface circulation in the Gulf of Mexico. Infrared images are most useful between November and mid-May, when strong temperature gradients occur. During this time, pigment concentrations are relatively high and typically horizontally homogeneous. Between late May and October, SST fields are uniform, however, while surface circulation features, including the Loop Current and large anticyclonic eddies, can be traced with CZCS data as very clear water bodies (<0.05 mg pigment m^{-3}) within more turbid waters of the Gulf of Mexico. Three anticyclonic eddies were observed in summer of 1979, and at least two were observed in summer of 1980.

The monthly mean ocean color images show that most of the water discharged by the Mississippi and Mobile rivers flows to the west, following the Louisiana-Texas coast and at times reaching south of the Mexico–United States border. There were some single (daily) images showing that parcels of plume water can be carried east of the Mississippi delta and flow south along the western Florida shelf break. From limited data it appeared that such events have higher probability of occurring during the January to June period. On very rare occasions, small amounts of river water can move east also during the second half of the year. There were large interannual differences in the size (length and width) of the plume extending to the west consistent with variations in volume discharge.

During April 1979 and October 1980 in CZCS imagery, as well as during February 1984, January 1986, and February 1987 in AVHRR imagery, a cyclonic ring can be seen off the Texas coast, exporting high-chlorophyll and low-temperature water to the continental slope. Similar cyclonic features are found here in shipboard surveys [*Biggs et al.*, 1991] as well as numerical models [*Walsh et al.*, 1989]. We are presently investigating the role of cyclonic eddies in enhanced primary production within western boundary currents, where tenfold higher carbon fixation occurs, compared to the ambient oligotrophic water [e.g., *Yoder*, 1985]. Validation of complex, coupled physical-biological models requires synoptic and frequent data sets, spanning the time scales (days to years) of dominant processes.

In spite of the number of physical oceanographic studies that have been conducted in the gulf, for example, the physical processes that control ring and eddy formation [*Vukovich and Maul*, 1985] are still not fully understood. Similarly, the frequency of eddy shedding [*Elliott*, 1982; *Auer*, 1987] remains ill defined, and it is not clear whether the maximum northward penetration of the Loop Current is a seasonal phenomenon [*Leipper*, 1970; *Vukovich et al.*, 1979; *Maul*, 1977; *Sturges and Evans*, 1983]. Acceptance of an eastern gulf forcing as a major source of variance in the physical habitat of the western gulf is a result of the last decade of satellite observations, field experiments, and numerical models. However, at this point the in situ oceanographic data set for the Gulf of Mexico is still insufficient to address questions on processes affecting the distribution of biological and chemical properties.

The next decade must provide similar data for nutrient concentrations, rates of phytoplankton and zooplankton processes, and detailed regional multidisciplinary studies. Failure to build up environmental data bases will impair progress toward understanding of the temporal and spatial variability of phytoplankton distribution in this basin and the inherent biogeochemical cycles they mediate.

Acknowledgments. We thank Gene Feldman at the Goddard Space Flight Center (NASA, Greenbelt, Maryland) for providing the data for the regional CZCS archive. We also thank Lola Olsen and Roy Jenne at the NASA Space Science Data Center (NSSDC), (Goddard Space Flight Center, Greenbelt, Maryland) for their help in accessing the COADS and CAC data sets and descriptions. We appreciate the thorough and helpful comments provided by two anonymous reviewers. Processing of the data was largely carried out on the software environment "dsp," developed at RSMAS, University of Miami, and implemented at the University of South Florida. Postprocessing and final analyses were carried out using software developed at the University of South Florida. This work was supported by the National Aeronautics and Space Administration under grant NAGW-678, by the Office of Naval Research under grant N00014-87-J-1218, and by the Department of Energy under grant OE-F605-85ER60285.

REFERENCES

Abbott, M. R., and P. M. Zion, Spatial and temporal variability of phytoplankton pigment off northern California during Coastal Ocean Dynamics Experiment 1, *J. Geophys. Res.*, *92*(C2), 1745–1755, 1987.

Atkinson, L. P., and D. Wallace, The source of unusually low surface salinities in the Gulf Stream off Georgia, *Deep Sea Res.*, *23*, 913–916, 1975.

Auer, S. J., Five-year climatological survey of the Gulf Stream system and its associated rings, *J. Geophys. Res.*, *92*(C11), 11,709–11,726, 1987.

Austin, G. B., Jr., Some recent oceanographic surveys of the Gulf of Mexico, *Eos. Trans. AGU*, *36*(5), 885–892, 1955.

Austin, R. W., Gulf of Mexico, ocean color surface-truth measurements, *Boundary Layer Meteorol.*, *18*, 269–285, 1980.

Austin, R. W., and T. J. Petzold, The determination of the diffuse attenuation coefficient of sea water using the coastal zone color scanner, in *Oceanography From Space, Proceedings of the COSPAR/SCOR/IUCRM Symposium*, edited by J. F. R. Gower, pp. 239–256, Plenum, New York, 1981.

Baker, K. S., and R. C. Smith, Bio-optical classification and model of natural waters, *Limnol. Oceanogr.*, *27*, 500–509, 1982.

Barale, V., C. R. McClain, and P. Malanotte-Rizzoli, Space and

time variability of the surface color field in the northern Adriatic Sea, *J. Geophys. Res.*, *91*(C11), 12,957–12,974, 1986.

Behringer, D. W., R. L. Molinari, and J. F. Festa, The variability of anticyclonic current patterns in the Gulf of Mexico, *J. Geophys. Res.*, *82*(34), 5469–5476, 1977.

Biggs, D. C., D. E. Smith, R. R. Bidigare, and M. A. Johnson, In situ estimation of the population density of gelatinous planktivores in Gulf of Mexico surface waters, in *Divers, Submersibles, and Marine Science, Occas. Pap. Biol.*, no. 9, edited by N. C. Fleming, pp. 17–34, Memorial University of Newfoundland, St. John's, Canada, 1984.

Biggs, D. C., A. C. Vastano, R. A. Ossinger, A. G. Zurita, and A. P. Franco, Multidisciplinary study of warm- and cold-core rings in the Gulf of Mexico, in *The Role of Fishing and Aquaculture in the Development of Rural Areas of the Caribbean*, edited by J. Buitriago and R. Margalef, La Salle Foundation, Caracas, Venezuela, in press, 1991.

Blumberg, A. F., and G. L. Mellor, A simulation of the circulation in the Gulf of Mexico, *Isr. J. Earth Sci.*, *34*, 122–144, 1985.

Campbell, J. W., and J. E. O'Reilly, Role of satellites in estimating primary productivity on the Northwest Atlantic continental shelf, *Cont. Shelf Res.*, *8*, 179–204, 1988.

Carder, K. L., R. G. Steward, J. H. Paul, and G. A. Vargo, Relationships between chlorophyll and ocean color constituents as they affect remote-sensing reflectance models, *Limnol. Oceanogr.*, *31*(2), 403–413, 1986.

Carder, K. L., R. G. Steward, G. R. Harvey, and P. B. Ortner, Marine humic and fulvic acids: Their effects on remote sensing of ocean chlorophyll, *Limnol. Oceanogr.*, *34*(1), 68–81, 1989.

Clark, D. K., Phytoplankton pigment algorithms for the Nimbus-7 CZCS, in *Oceanography From Space, Proceedings of the COSPAR/SCOR/IUCRM Symposium*, edited by J. F. R. Gower, pp. 227–237, Plenum, New York, 1981.

Cochrane, J. D., and F. J. Kelly, Low-frequency circulation on the Texas-Louisiana continental shelf, *J. Geophys. Res.*, *91*(C9), 10,645–10,659, 1986.

Deuser, W. G., F. E. Müller-Karger, R. H. Evans, O. B. Brown, W. E. Esaias, and G. C. Feldman, Surface-ocean color and deep-ocean carbon flux: How close a connection?, *Deep Sea Res.*, *37*(8), 1331–1343, 1990.

Dinnel, S. P., and W. J. Wiseman, Jr., Fresh water on the Louisiana and Texas shelf, *Cont. Shelf Res.*, *6*, 765–784, 1986.

Elliott, B. A., Anticyclonic rings and the energetics of the circulation in the Gulf of Mexico, Ph.D. dissertation, Tex. A&M Univ., College Station, 1979.

Elliott, B. A., Anticyclonic rings in the Gulf of Mexico, *J. Phys. Oceanogr.*, *12*, 1291–1309, 1982.

El-Sayed, S. Z., and C. C. Trees, Ecological studies of phytoplankton in the Gulf of Mexico during NOAA/NMFS *Oregon II* cruise, *Tech. Rep.*, *80-8-T*, 53 pp., Tex. A&M Univ., College Station, 1980.

Feldman, G., et al., Ocean color, availability of the global data set, *Eos Trans. AGU*, *70*(23), 634, 1989.

Fisher, J., R. Doerffer, and H. Grassl, Factor analysis of multispectral radiances over coastal and open ocean water based on radiative transfer calculations, *Appl. Opt.*, *25*(3), 446–456, 1986.

Gordon, H. R., D. K. Clark, J. L. Mueller, and W. A. Hovis, Phytoplankton pigments derived from the Nimbus-7 CZCS: Comparison with surface measurements, *Science*, *210*, 63–66, 1980.

Gordon, H. R., D. K. Clark, J. W. Brown, O. B. Brown, and R. H. Evans, Satellite measurement of the phytoplankton pigment concentration in the surface waters of a warm core Gulf Stream ring, *J. Mar. Res.*, *40*(2), 491–502, 1982.

Gordon, H. R., D. K. Clark, J. W. Brown, O. B. Brown, R. H. Evans, and W. W. Broenkow, Phytoplankton pigment concentrations in the Middle Atlantic Bight: Comparison of ship determinations and CZCS estimates, *Appl. Opt.*, *22*, 20–35, 1983*a*.

Gordon, H. R., J. W. Brown, O. B. Brown, R. H. Evans, and D. K. Clark, Nimbus 7 CZCS: Reduction of its radiometric sensitivity with time, *Appl. Opt.*, *22*, 3929–3931, 1983*b*.

Gordon, H. R., O. B. Brown, R. H. Evans, J. W. Brown, R. C. Smith, K. S. Baker, and D. K. Clark, A semianalytic radiance model of ocean color, *J. Geophys. Res.*, *93*(D9), 10,909–10,924, 1988.

Halper, F. B., and W. W. Schroeder, The response of shelf waters to the passage of tropical cyclones—Observations from the Gulf of Mexico, *Cont. Shelf Res.*, *10*, 8, 777–793, 1990.

Hofmann, E. E., and S. J. Worley, An investigation of the circulation of the Gulf of Mexico, *J. Geophys. Res.*, *91*, 14,221–14,236, 1986.

Huh, O. K., W. J. Wiseman, and L. J. Rouse, Jr., Winter cycle of sea surface thermal patterns, northeastern Gulf of Mexico, *J. Geophys. Res.*, *83*, 4523–4529, 1978.

Huh, O. K., W. J. Wiseman, and L. J. Rouse, Jr., Intrusion of Loop Current waters onto the west Florida continental shelf, *J. Geophys. Res.*, *86*, 4186–4192, 1981.

Hulburt, H. E., and J. D. Thompson, A numerical study of Loop Current intrusions and eddy shredding, *J. Phys. Oceanogr.*, *10*, 1611–1651, 1980.

Kirwan, A. D., Jr., W. J. Merrell, Jr., J. K. Lewis, and R. E. Whitaker, Lagrangian observations of an anticyclonic eddy in the western Gulf of Mexico, *J. Geophys. Res.*, *89*(C3), 3417–3424, 1984*a*.

Kirwan, A. D., Jr., W. J. Merrell, Jr., J. K. Lewis, R. E. Whitaker, and R. Legeckis, A model for the analysis of drifter data with an application to a warm core eddy in the Gulf of Mexico, *J. Geophys. Res.*, *89*(C3), 3425–3438, 1984*b*.

Kirwan, A. D., J. K. Lewis, A. W. Indest, P. Reinersman, and I. Quintero, Observed and simulated kinematic properties of Loop Current rings, *J. Geophys. Res.*, *93*(C2), 1189–1198, 1988.

Leipper, D., A sequence of current patterns in the Gulf of Mexico, *J. Geophys. Res.*, *75*(3), 637–657, 1970.

Levitus, S., Climatological atlas of the world ocean, *NOAA Prof. Pap. 13*, 173 pp., U.S. Dep Comm., Rockville, Md., 1982.

Lewis, J. K., and A. D. Kirwan, Jr., Genesis of a Gulf of Mexico ring as determined from kinematic analyses, *J. Geophys. Res.*, *92*(C11), 11,727–11,740, 1987.

Marra, J., R. R. Bidigare, and T. D. Dickey, Nutrients and mixing, chlorophyll and phytoplankton growth, *Deep Sea Res.*, *37*(1), 127–143, 1990.

Maul, G. A., The annual cycle of the Gulf Loop Current, I, Observations during a one-year time series, *J. Mar. Res.*, *35*(1), 29–47, 1977.

Maul, G. A., Application of GOES visible-infrared data to quantifying mesoscale ocean surface temperatures, *J. Geophys. Res.*, *86*(C9), 8077–8021, 1981.

Maul, G. A., and H. R. Gordon, On the use of the Earth Resources Technology Satellite (Landsat-1) in optical oceanography, *Remote Sens. Environ.*, *4*, 95–128, 1975.

Maul, G. A., F. Williams, M. Roffer, and F. M. Sousa, Remotely sensed oceanography patterns and variability of bluefin tuna catch in the Gulf of Mexico, *Oceanol. Acta*, *7*(4), 469–479, 1984.

Maul, G. A., D. A. Mayer, and S. R. Baig, Comparisons between a continuous 3-year current-meter observation at the sill of the Yucatan Strait, satellite measurements of gulf Loop Current area, and regional sea level, *J. Geophys. Res.*, *90*(C5), 9089–9096, 1985.

McClain, C. R., W. E. Esaias, G. C. Feldman, J. Elrod, D. Endres, J. Firestone, M. Darzi, R. Evans, and J. Brown, Physical and biological processes in the North Atlantic during the First GARP Global Experiment, *J. Geophys. Res.*, *95*(C10), 18,027–18,048, 1990.

McClain, E. P., W. G. Pichel, C. C. Walton, Z. Ahmad, and J. Sutton, Multi-channel improvements to satellite-derived global sea-surface temperatures, *Adv. Space Res.*, *2*(6), 43–47, 1983.

McClain, E. P., W. G. Pichel, and C. C. Walton, Comparative performance of AVHRR-based multichannel sea surface temperatures, *J. Geophys. Res.*, *90*(C6), 11,587–11,601, 1985.

Menzel, D. W., and J. H. Ryther, Annual variations in primary production of the Sargasso Sea off Bermuda, *Deep Sea Res.*, *7*, 282–288, 1961.

Merrel, W. J., and J. M. Morrison, On the circulation of the western Gulf of Mexico with observations from April 1978, *J. Geophys. Res.*, *86*(C5), 4181–4185, 1981.

Milliman, J. D., and R. H. Meade, World-delivery of river sediment to the oceans, *J. Geol.*, *91*(1), 1–21, 1983.

Morel, A., and L. Prieur, Analysis of variations in ocean color, *Limnol. Oceanogr.*, *22*, 709–722, 1977.

Morisawa, M., *Streams, Their Dynamics, and Morphology*, 175 pp., McGraw-Hill, New York, 1968.

Mueller, J. L., Nimbus-7 CZCS: Electronic overshoot due to cloud reflectance, *Appl. Opt.*, *27*, 438–440, 1988.

Müller-Karger, F. E., C. R. McClain, and P. L. Richardson, The dispersal of the Amazon's water, *Nature*, *333*, 56–59, 1988.

Müller-Karger, F. E., C. R. McClain, T. R. Fisher, W. E. Esaias, and R. Varela, Pigment distribution in the Caribbean Sea: Observations from space, *Prog. Oceanogr.*, *23*, 23–69, 1989.

Müller-Karger, F. E., C. R. McClain, R. N. Sambrotto, and C. G. Ray, Measurements of phytoplankton distribution in the southeastern Bering Sea using the CZCS: A note of caution, *J. Geophys. Res.*, *95*(C7), 11,483–11,499, 1990.

Nowlin, W. D., Jr., Winter circulation patterns and property distributions, in *Contributions on the Physical Oceanography of the Gulf of Mexico, Tex. A&M Univ. Oceanogr. Stud.*, vol. 2, edited by L. R. A. Capurro and J. L. Reid, chap. 1, pp. 3–51, Gulf, Houston, Tex., 1972.

Nowlin, W. D., Jr., and J. M. Hubertz, Contrasting summer circulation patterns for the eastern gulf, in *Contributions on the Physical Oceanography of the Gulf of Mexico, Tex. A&M Univ. Oceanogr. Stud.*, vol. 2, edited by L. R. A. Capurro and J. L. Reid, chap. 6, pp. 119–137, Gulf, Houston, Tex., 1972.

Nowlin, W. D., Jr., J. M. Hubertz, and R. O. Reid, A detached eddy in the Gulf of Mexico, *J. Mar. Res.*, *26*(2), 185–186, 1968.

Olson, D. G., G. P. Podesta, R. H. Evans, and O. B. Brown, Temporal variations in the separation of Brazil and Malvinas currents, *J. Geophys. Res.*, *35*(12), 1971–1990, 1988.

Ortner, P. B., R. L. Ferguson, S. R. Piotrowicz, L. Chesal, G. A. Berberian, and A. V. Palumbo, Biological consequences of hydrographic and atmospheric advection within the Gulf Loop Intrusion, *Deep Sea Res.*, *31*, 1101–1120, 1984.

Paluszkiewicz, T., L. P. Atkinson, E. S. Posmentier, and C. R. McClain, Observations of a Loop Current frontal eddy intrusion onto the west Florida shelf, *J. Geophys. Res.*, *88*(C14), 9639–9651, 1983.

Paskausky, D. F., and R. O. Reid, A barotropic prognostic numerical circulation model, in *Contributions on the Physical Oceanography of the Gulf of Mexico, Tex. A&M Univ. Oceanogr. Stud.*, vol. 2, edited by L. R. A. Capurro and J. L. Reid, chap. 10, pp. 163–176, Gulf, Houston, Tex., 1972.

Pechmann, K. B., J. O. Ellis, F. G. Everdale, S. Z. Green, I. C. Sheifer, and M. K. Stern, *Marine Environmental Assessment, Gulf of Mexico 1985 Annual Summary*, pp. 49–55, U.S. Department of Commerce, Washington, D. C., 1986.

Reynolds, R. W., A real-time global sea surface temperature analysis, *J. Clim.*, *1*, 75–86, 1988.

Reynolds, R. W., and L. Roberts, Global sea-surface temperature climatology from in-situ, satellite, and ice data, *Trop. Ocean-Atmos. Newsl.*, *37*, 15–17, 1987.

Robinson, M. K., Atlas of monthly mean sea surface and subsurface temperature and depth of the top of the thermocline: Gulf of Mexico and Caribbean Sea, *Ref. 73-8*, 105 pp., Scripps Inst. of Oceanogr., La Jolla, Calif., 1973.

Ryther, J. H., and D. W. Menzel, The seasonal and geographical range of primary production in the western Sargasso Sea, *Deep Sea Res.*, *6*, 235–238, 1960.

Schluessel, P., W. J. Emery, H. Grassl, and T. Mammen, On the bulk-skin temperature difference and its impact on satellite remote sensing of sea surface temperature, *J. Geophys. Res.*, *95*(C8), 13,341–13,356, 1990.

Schroeder, W. W., L. Berner, Jr., and W. D. Nowlin, Jr., The oceanic waters of the Gulf of Mexico and Yucatan Strait during July 1969, *Bull. Mar. Sci.*, *24*, 1–19, 1974.

Science Applications International Corporation (SAIC), Gulf of Mexico physical oceanography program, final report: Years 1 and 2, vol. II, *OCS Rep. MMS 85-0094*, 378 pp., Gulf of Mex. Reg. Off., Miner. Manage. Serv., U.S. Dep. of the Inter., New Orleans, La., 1986.

Science Applications International Corporation (SAIC), Gulf of Mexico physical oceanography program, final report: Year 3, vol. II, *OCS Rep. MMS 88-0046*, 241 pp., Gulf of Mex. Reg. Off., Miner. Manage. Serv., U.S. Dep. of the Interior, New Orleans, La., 1988.

Smith, N. P., On the hydrography of shelf waters off the central Texas Gulf Coast, *J. Phys. Oceanogr.*, *10*, 806–813, 1980.

Strong, A. E., and E. P. McClain, Improved ocean surface temperatures from space, Comparisons with drifting buoys, *Bull. Am. Meteorol. Soc.*, *65*(2), 138–142, 1984.

Sturges, W., and J. P. Blaha, A western boundary current in the Gulf of Mexico, *Science*, *192*, 367–369, 1976.

Sturges, W., and J. C. Evans, On the variability of the Loop Current in the Gulf of Mexico, *J. Mar. Res.*, *41*(4), 639–653, 1983.

Sverdrup, H. U., On conditions for the vernal blooming of phytoplankton, *J. Cons. Int. Explor. Mer.*, *18*, 287–295, 1953.

Thomas, W. H., and G. Simmons, Phytoplankton production in the Mississippi delta, in *Recent Sediments, Northwest Gulf of Mexico*, edited by F. P. Shepard, F. B. Phleger, and T. H. van Andel, pp. 103–116, American Association of Petroleum Geologists, Tulsa, Okla., 1960.

Trees, C. C., Remote sensing of ocean color in the northern Gulf of Mexico, Ph.D. dissertation, 258 pp., Tex. A&M Univ., College Station, 1985.

Vukovich, F. M., Aspects of the behavior of cold perturbations in the eastern Gulf of Mexico: A case study, *J. Phys. Oceanogr.*, *18*, 1051–1059, 1986.

Vukovich, F. M., On the formation of elongated cold perturbations off the Dry Tortugas, *J. Phys. Oceanogr.*, *18*, 1051–1059, 1988*a*.

Vukovich, F. M., Loop Current boundary variations, *J. Geophys. Res.*, *93*(C12), 15,585–15,591, 1988*b*.

Vukovich, F. M., and B. W. Crissman, Aspects of warm rings in the Gulf of Mexico, *J. Geophys. Res.*, *91*(C2), 2645–2660, 1986.

Vukovich, F. M., and G. A. Maul, Cyclonic eddies in the eastern Gulf of Mexico, *J. Phys. Oceanogr.*, *15*, 105–117, 1985.

Vukovich, F. M., B. W. Crissman, M. Bushnell, and W. J. King, Some aspects of the oceanography of the Gulf of Mexico using satellite and in situ data, *J. Geophys. Res.*, *84*(C12), 7749–7768, 1979.

Walsh, J. J., *On the Nature of Continental Shelves*, 508 pp., Academic, San Diego, Calif., 1988.

Walsh, J. J., D. A. Dieterle, M. B. Meyers, and F. E. Müller-Karger, Nitrogen exchange at the continental margin: A numerical study of the Gulf of Mexico, *Prog. Oceanogr.*, *23*, 248–301, 1989.

Walton, C. C., Nonlinear multichannel algorithms for estimating sea surface temperature with AVHRR satellite data, *J. Appl. Meteorol.*, *27*, 115–127, 1988.

Wert, R. T., and R. O. Reid, A baroclinic prognostic numerical circulation model, in *Contributions on the Physical Oceanography of the Gulf of Mexico, Tex. A&M Univ. Oceanogr. Stud.*, vol. 2, edited by L. R. A. Capurro and J. L. Reid, chap. 11, pp. 177–209, Gulf, Houston, Tex., 1972.

Woodruff, S. D., R. J. Slutz, R. L. Jenne, and P. M. Steurer, A comprehensive ocean-atmosphere data set, *Bull. Am. Meteorol. Soc.*, *68*, 1239–1250, 1987.

Yoder, J. A., Environmental control of phytoplankton production in the southeastern U.S. continental shelf, in *Oceanography of the Southeastern U.S. Continental Shelf*, Coastal Estuarine Sci., vol. 2, edited by L. P. Atkinson, D. W. Menzel, and K. A. Bush, pp. 93–103, AGU, Washington, D. C., 1985.

Yoder, J. A., C. R. McClain, J. O. Blanton, and L.-Y. Oey, Spatial scales in CZCS-chlorophyll imagery of the southeastern U.S. continental shelf, *Limnol. Oceanogr.*, *32*(4), 929–941, 1987.

R. H. Evans, Rosenstiel School of Marine and Atmospheric Science, University of Miami, 4600 Rickenbacker Causeway, Miami, FL 33149.

M. B. Meyers, F. E. Müller-Karger, and J. J. Walsh, Department of Marine Science, University of South Florida, 140 Seventh Avenue South, St. Petersburg, FL 33701.

(Received November 13, 1990;
accepted December 12, 1990.)

Journal of Marine Systems, 3 (1992) 141–161
Elsevier Science Publishers B.V., Amsterdam

A time-dependent depth-integrated barotropic physical model of the Bering/Chukchi Seas for use in ecosystem analysis

Paul G. Shuert and John J. Walsh

Department of Marine Science, University of South Florida, St. Petersburg, FL 33701, USA

(Received September 4, 1990; revised version accepted April 15, 1991)

ABSTRACT

Shuert, P.G. and Walsh, J.J., 1992. A time-dependent depth-integrated barotropic physical model of the Bering/Chukchi Seas for use in ecosystem analysis. J. Mar. Syst., 3: 141–161.

A time-dependent depth-integrated barotropic physical model was constructed to simulate the gross features of the circulation of the northern Bering and southern Chukchi seas during 1985. The model uses a linear form of the Navier-Stokes and continuity equations to obtain the horizontal velocities in the x and y directions. Current meters at the upstream boundary provided a time-dependent inflow. An open boundary condition was used at the downstream end ot the model to allow only outward energy flux. Additional current meters in the interior were used for validation of the model. Two types of wind stress specification and one case of no wind forcing were applied. Biochemical tracers are added to the model in the form of dissolved nutrients and phytoplankton chlorophyll to explore the implications of short-term fluctuations in the flow field.

Introduction

Transport into the Bering Sea from the Pacific Ocean is estimated to be 11.0 Sv, of which most (~ 10.0 Sv) leaves as the East Kamchatka Current (Fig. 1). A generally cyclonic circulation in the Aleutian Basin has been recognized by many authors (Dodimead et al., 1963; Favorite, 1966 and Arsen'ev, 1967). Current velocities in the basin are sluggish, usually only 1–3 cm s^{-1}, except for areas along the continental slope, where velocities can reach 10–15 cm s^{-1}.

The Bering Slope Current flows northwest along the eastern edge of the Aleutian Basin from the Aleutian Islands to near Cape Navarin. Here most of the flow (4.0–4.5 Sv) turns south along the Siberian coast, where it contributes to the East Kamchatka Current. The remainder of the Bering Slope Current (0.5–1.0 Sv) crosses the shelf-break at Cape Navarin to flow north along the Siberian Coast as the Anadyr Current.

The Anadyr current encounters shoaling depths, such that the vorticity induced by topographic change (f/H) is at least an order of magnitude greater than the change in planetary vorticity (β). The flow concentrates as a topographic boundary current (Kinder et al., 1986) with intensification to the left when facing up slope. Once across the shelf break, the Anadyr Current continues around the Gulf of Anadyr through Anadyr Strait (Fig. 1), providing some of the source water to the ISHTAR study area (Walsh et al., 1989).

The physical features of the southeastern Bering shelf have been characterized during PROBES by Coachman (1986). He proposed three distinct domains based on water mass properties and physical processes. An outer domain, adjacent to the shelfbreak, is dominated by a general northwest advection at 1–5 cm s^{-1}, with a cross-shelf exchange on the order of 1 cm s^{-1} (Kinder and Schumacher, 1981; Coachman, 1986). An inner (coastal) domain receives freshwater discharge of $\sim 4 \times 10^3$ m^3 s^{-1} during summer

and also exhibits a distinct northward flow, somewhat slower than the outer domain, with a flushing time of approximately 6 months (compared to 4 months for the outer domain). The central domain, between the outer and coastal domains, is extremely sluggish in terms of flushing, and diffusive fluxes are of primary importance to its exchange with water masses on either side.

The ISHTAR study region was bounded at the southern edge by St. Lawrence Island in the Bering Sea and extends north through Bering Strait to approximately 71° N in the Chukchi Sea (Fig. 2). About 65% ot the summer northward transport in Bering Strait enters through the ~ 75 km wide, 45 m deep Anadyr Strait on the western side of St. Hxawrence Island, while the remainder fluxes through the wider (~ 190 km) and shallower (~ 30) Shpanberg Strait on the eastern side. Most of the water transiting Anadyr Strait is relatively cold (1–2° C) and saline (> 33 ‰) with an origin farther south as part of the Bering Slope Current. The Anadyr Current mixes slightly in the Gulf of Anadyr with central shelf water (Coachman, 1986), before it is finally advected through Anadyr Strait with an average summer velocity of 15 cm s^{-1}.

Two other water masses flow through mainly Shpanberg Strait. A low salinity (< 31.8 ‰) and warm (~ 4° C) coastal water mass, termed Alaskan Coastal Water, has its origin as coastal domain water in the southeastern Bering Sea (Coachman, 1986). It usually flows through the eastern side of the Strait. This water mass is further modified by freshwater input from the Yukon River, with a mean summer discharge of approximately 1.5×10^5 m^3 s^{-1}. The second water mass, Bering Shelf Water, has its origin as central and outer domain water that has resided

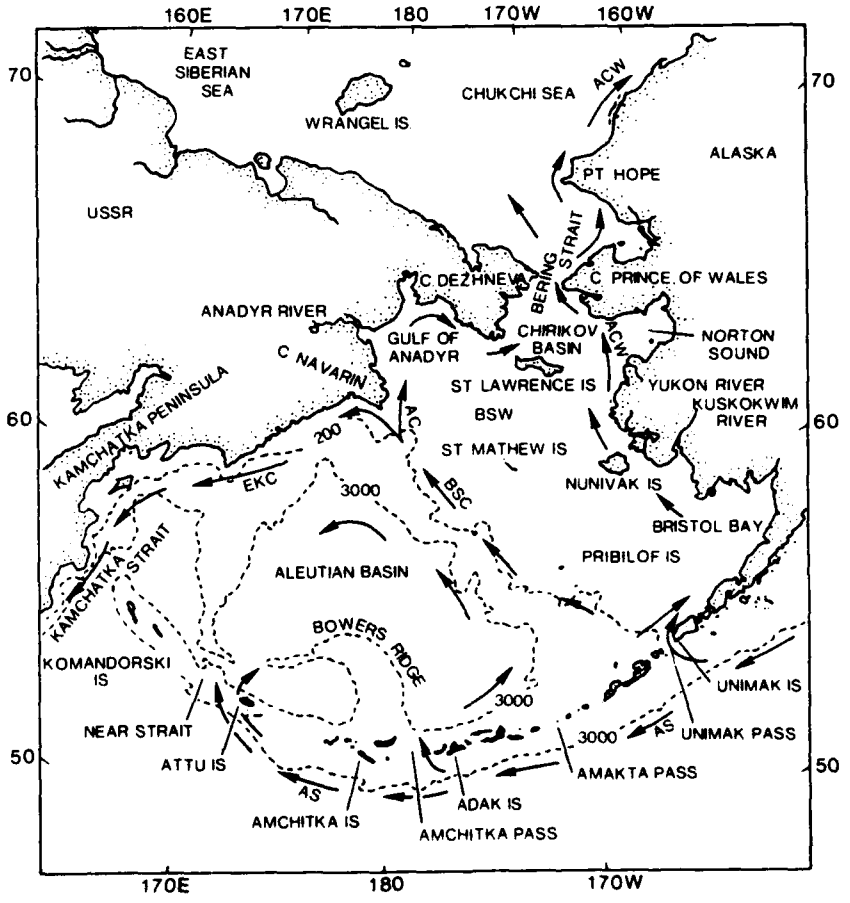

Fig. 1. Major currents of the Bering and Chukchi Seas. *ACW* is Alaskan Coastal Water, *AS* is the Alaskan Stream, *EKW* is the East Kamchatka Current, *BSC* is the Bering Slope Current and *AC* is the Anadyr Current.

for some time south of St. Lawrence Island. It flows north primarily through the western side of Shpanberg Strait, although at times it occupies the eastermost side of Anadyr Strait.

The principal driving mechanism of the northward transport through the Bering Strait is a downward sea surface slope towards the north. It is of steric origin (Coachman et al., 1975), with a mean sea level difference of 0.65 m between the North Pacific and Atlantic Oceans (Reid, 1961; Stigebrandt, 1984). About 0.50 m of this pressure gradient is between the Pacific and Arctic Oceans. Annual mean transport estimates for the Bering Strait have varied from 0.56 Sv (Aagaard et al., 1985) to 0.95 Sv (Fedorova and Yankina, 1964).

Recently Coachman and Aagaard (1988) revised the mean transport estimate to be 0.78 Sv over a 40 yr surrogate time span in Bering Strait. Periodicities of transport are evident at mesoscale intervals of 6–8 and 14–20 yr, in addition to shorter 1–2yr variations. Such variance is thought to be associated with long term global climatic changes that effect the steric difference between the North Pacific and Atlantic Oceans. There

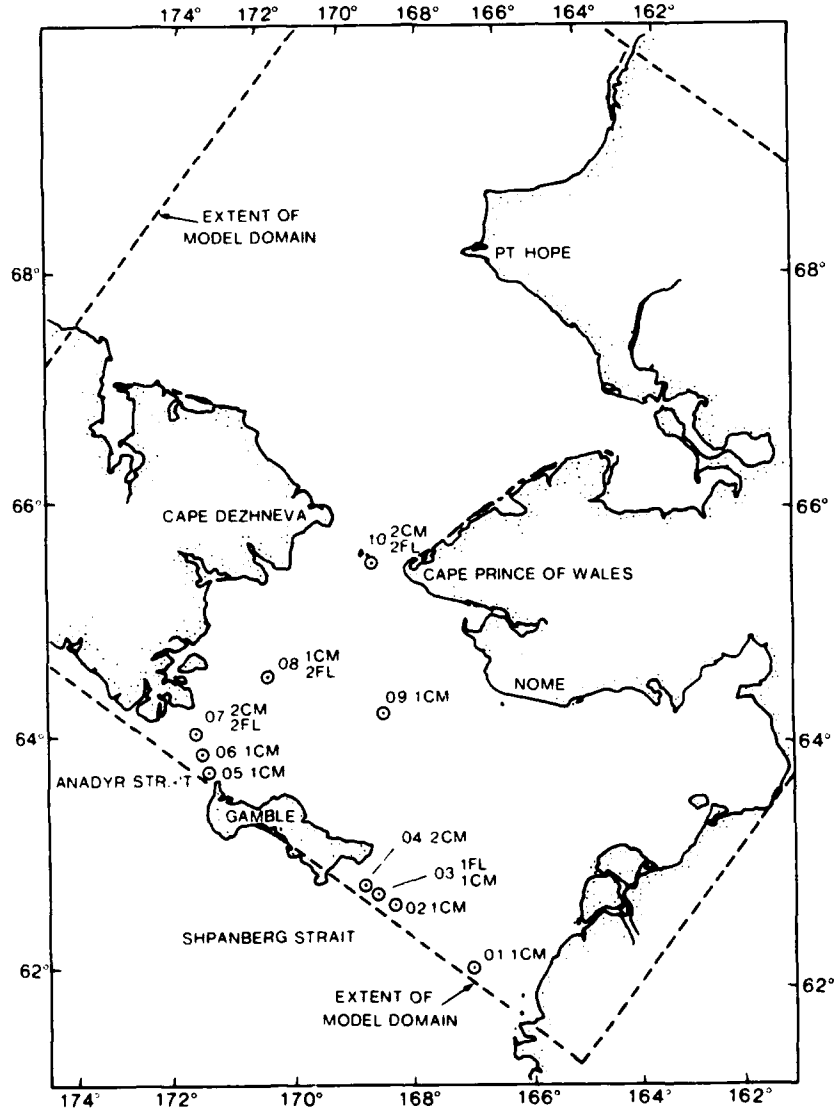

Fig. 2. Mooring locations during the 1985 ISHTAR field experiment with respect to the model domain. *CM* designate currentmeters, *FL* designate fluorometers.

are, of course, seasonal fluctuations of transport as well.

Although a hydraulic head drives the long term transport, the regional wind forcing is a primary source of the short term variability of water motion. For example, there is a reasonable correlation ($r^2 = 0.49$) between northward transport through the Bering Strait and the east–west atmospheric pressure gradient (Coachman and Aagaard, 1981). The orientation and magnitude of this pressure gradient is determined by the positions of the Siberian High and the Alaskan Low pressure cell. Generally, when atmospheric pressure is higher on the west side of the Bering Strait, air flow and water transport are towards the south.

Changes in the wind field can reverse the transport within Bering Strait, from 1–2 Sv northward to more than 3 Sv southward (Coachman and Aagaard, 1981); these changes can occur on time scales as short as 3–5 days (Coachman and Aagaard, 1988). These events can have major consequences for the spatial displacement of the lateral water mass boundaries. For example, if only the currents within Bering and Shpanberg Straits reverse, nutrient rich water of the cold, salty Anadyr Current will penetrate much further to the east. Relaxation of northerly wind forcing restores the normal northward flow through Bering Strait within 4–7 days.

The goal of the physical submodel was to simulate the gross features of the time-dependent flow field as input for a biological model. This was accomplished by using estimates of the transports within Anadyr and Shpanberg Straits as boundary values for a depth-integrated, time dependent solution of the flow field. The results of the barotropic model were compared to current meter observations within the interior of the domain (Fig. 2). The physical model was then coupled to a biological model to demonstrate the utility of using physically driven biological models for ecosystem analysis (Rothschild, 1988; Walsh, 1988). For example, 95% of the nitrate flux occurs in Anadyr Strait, where only 65% of the transport is found (Walsh et al., 1989)—see Shuert and Walsh (1991) for details of the biological model.

Methods

Model domain

An 810 × 810 km grid with 10 km spacing was rotated 37.50° clockwise from a point located at 64°17.24′ N and 173°49.33′ W. This scheme allowed the maximum number of grid points across Anadyr and Shpanberg Straits, where boundary conditions of transport, nutrients , chlorophyll and zooplankton were repeatedly measure with moored instruments and shipboard sampling during the 1985 ISHTAR field experiment (Fig. 2).

The depth of the water column at each grid point used digitized bathymetry from the U.S. Department of Commerce, the Defense Mapping Agency, and the Geophysical Institute of the University of Alaska. Grid points in areas of less than 10 m depth were set to 10 m to limit mixing time in the biological model (Shuert and Walsh, 1991). The vertical resolution of this biological model, consisted of 10 layers, with the thickness of each layer calculated as $H/10$, where H is the digitized bathymetry of the physical model.

Physical equations

A depth-integrated barotropic model was constructed to simulate the flow characteristics of the physical habitat. A linear form of the Navier-Stokes and continuity equations was used such that

$$\frac{dU}{dt} = -gH\frac{\partial e}{\partial x} + F^x - B^x + fV \quad (1)$$

$$\frac{dV}{dt} = -gH\frac{\partial e}{\partial y} + F^y - B^y - fU \quad (2)$$

$$-\frac{de}{dt} = \frac{\partial U}{\partial x} + \frac{\partial V}{\partial y} \quad (3)$$

where U and V are the depth-integrated horizontal transports in the x and y direction, respectively, i.e. $U = \int_0^z u\,dz$ and $V = \int_0^z v\,dz$ H is the depth of the water column, while g is the acceleration due to gravity , e is the elevation of the sea surface and F^x and F^y are the wind stress components of the horizontal frictional force. B^x and B^y are the bottom stress components of the hori-

zontal frictional force. The f is the Coriolis parameter given by

$$f = 2\Omega \sin \phi \tag{4}$$

where Ω is the Earth's rotation rate of 0.73×10^{-4} rotations s^{-1}, and ϕ is latitude in degrees.

Initially the Coriolis parameter was calculated for each grid point in the model. However, the spatial gradient of the Coriolis parameter introduced numerical waves in the results, when boundary values at the straits were not constant. These numerical waves resembled long Rossby-like waves and generated small numerical errors in the mass balance of the model. In order to achieve a steady state solution, a more simplistic way of parameterizing the Coriolis force from a single latitude (66°00.0′ N) was subsequently employed, (i.e. an f-plane was used) such that $f = 1.4 \times 10^{-4}$ s^{-1}. This value was used for the remainder of the calculations.

At the bottom boundary, B^x and B^y were calculated using a mean linear bottom stress over two adjacent grid points such that

$$B^x_{i,j} = (2\alpha C)(H_{i,j} + H_{i,j-1})^{-1}(V_{i,j}) \tag{5}$$

$$B^y_{i,j} = (2\alpha C)(H_{i,j} + H_{i-1,j})^{-1}(U_{i,j}) \tag{6}$$

where C is a dimensionless drag coefficient of 2×10^{-3} and α is assumed to be a constant of 50 cm s^{-1}. We used a high value of α to dampen the response of the transports to the changing downstream boundary condition. Large overshoots in the values of U and V were thus eliminated.

Wind stress was incorporated in the form of the quadratic drag law such that

$$F^x = C_{10} W W_x \tag{7}$$

$$F^y = C_{10} W W_y \tag{8}$$

where F^x and F^y are the x and y components of the wind stress in cm^2 s^{-2}. W is the total wind velocity and W_x and W_y are the x and y components, respectively in m s^{-1}. C_{10} is a dimensionless drag coefficient which varies with W such that at $W \leq 7.0$ m s^{-1}, $C_{10} = 1.6 \times 10^{-3}$ and at $W \geq 10.0$ m s^{-1}, $C_{10} = 2.5 \times 10^{-3}$. At $7.0 > W < 10.0$ m s^{-1} a linear relation between C_{10} and the wind speed was assumed.

Three separate cases of wind forcing were tried in the physical model. In the first case, wind stress was taken to be spatially invariant. The 3-h observation at Nome, Alaska were averaged over a 24 hour period and entered in equations (7) and (8). A second case made use of spatially varying winds, derived from the Fleet Numerical Oceanographic Center (FNOC) weather model predictions on a 2.5° square grid (Mikoh and Kaitala, 1976). FNOC winds were averaged daily and linearly interpolated to each grid point of the circulation model. Finally a third case was run without any wind stress.

The numerical integration of eqns. (1)–(3) was carried out using a forward differencing scheme in time and space. The time step Δt satisfies the Courant–Freidricks–Lewy condition (Lax, 1967) of numerical stability for explicit time difference algorithms such that

$$\Delta t < \frac{\Delta x}{\sqrt{(2gH_{max})}} \tag{9}$$

Assuming $H_{max} = 50$ m in the Bering Sea, g is 10 m s^{-1} and Δx is 10 km, the maximum limit of Δt is 318 s. A time step of 180 s was chosen to calculate the flow, this being well within the limits of the stability criterion.

At the land boundary, a condition of $U = V = e = 0$ was assumed, with no influx of water from the Yukon River. At the downstream open boundary in the Chukchi Sea, a "sponge" with an absorbing boundary (Israeli and Orszag, 1981) was invoked, allowing only outward energy flux. Bottom friction was increased over the last ten grid points at this end of the model domain.

At the southern boundary, daily values of total transport through Anadyr and Shpanberg Straits were first calculated from time series of three current meters (nos. 3, 6, and 7 of Fig. 2), with the relations (L. Coachman, pers. commun.)

$$ANADYR\ TRANSPORT = 0.033\ v - 0.036 \tag{10}$$

$$SHPANBERG\ TRANSPORT = 0.030\ V - 0.080 \tag{11}$$

where v is the northward component of velocity. Four cross-strait surveys of profiling current meters and the moored arrays in 1985 yielded eqns.

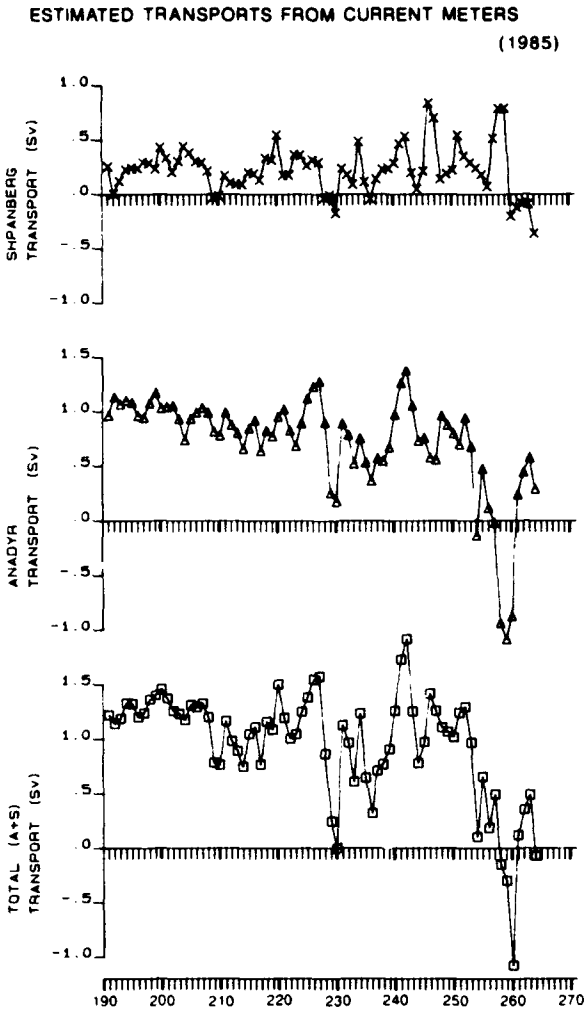

Fig. 3. Daily transports through Anadyr and Shpanberg Straits and their total during the 1985 simulation period.

(10) and (11) for the respective transports with an r^{-2} of ~ 0.85. Figure 4 shows the daily variation of estimated transport through these straits during 1985.

The proportion of the total transport at each boundary grid point was then partitioned (Fig. 4) based on the same four surveys. At times when the net transport across a strait was southward, (Fig. 3), there were still northward flows at some grid points (Fig. 4). Finally, within the time domain, this spatial partition of the daily changing transport (Fig. 3) at each boundary grid point was linearly interpolated between the four observation times of Fig. 4.

Initial conditions of flow within the model domain were achieved by running the model for 30 days with the boundary conditions for Julian day 190 (8 July 1985) in the different wind cases. Each simulation run lasted from 8 July 1985 (Julian day 190) to 26 September 1985 (Julian day 270). The results of the coupled physical/biological model in just the Nome wind case are shown as an example of the apparent biological consequences of current reversals in the ISHTAR study area.

A total of thirteen current meters were deployed at 10 locations within the Bering Sea during the 1985 ISHTAR experiment (Fig. 2). The sampling interval for all current meters was 20 min over a period of 38 to 84 days. Daily averages of the speed and direction at moorings 8, 9 and 10 are used as validation data. Moorings 7 and 10 each contained two current meters. In these cases, velocity and direction of the top and bottom current meters were also averaged. The differences between the mean velocity and direction form the top and bottom meter were small, < 5 cm s^{-1} and $< 10°$, i.e. our justification for the use of a barotropic circulation model.

A series of partial differential equations describe the temporal-spatial changes in the pools of nitrate, ammonium, chlorophyll, zooplankton

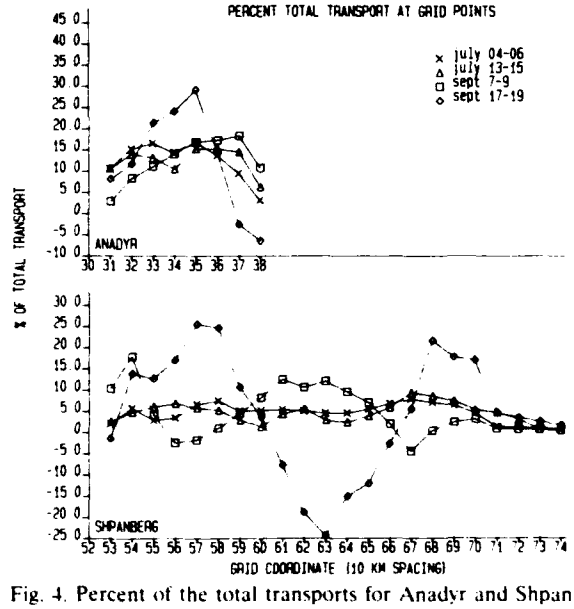

Fig. 4. Percent of the total transports for Anadyr and Shpanberg straits assigned to each grid point at the southern boundary.

and benthos. The state equation for nitrate (μg-at NO_3 l^{-1}) is,

$$\frac{\partial NO_3}{\partial t} = -u\frac{\partial NO_3}{\partial x} - v\frac{\partial NO_3}{\partial y} + K_x\frac{\partial^2 NO_3}{\partial y^2} + K_y\frac{\partial^2 NO_3}{\partial y^2} + K_z\frac{\partial^2 NO_3}{\partial z^2} - a'P_N \quad (12)$$

The state equation for ammonium (μg-at NH_4 l^{-1}) is,

$$\frac{\partial NH_4}{\partial t} = -u\frac{\partial NH_4}{\partial x} - v\frac{\partial NH_4}{\partial y} + K_x\frac{\partial^2 NH_4}{\partial x^2} + K_y\frac{\partial^2 NH_4}{\partial y^2} + K_z\frac{\partial^2 NH_4}{\partial z^2} - a''P_N + eZ + rB \quad (13)$$

The chlorophyll distribution (μg Chl l^{-1}) is described by,

$$\frac{\partial P}{\partial t} = -u\frac{\partial P}{\partial x} - v\frac{\partial P}{\beta y} + K_x\frac{\partial^2 P}{\partial y^2} + K_y\frac{\partial^2 P}{\partial y^2} + K_z\frac{\partial^2 P}{\partial z^2} + abP - gZ - s\frac{\partial P}{\partial z} \quad (14)$$

For zooplankton (μg C l^{-1}), the state equation is,

$$\frac{\partial Z}{\partial t} = -u\frac{\partial Z}{\partial x} - v\frac{\partial Z}{\partial y} + K_x\frac{\partial^2 Z}{\partial y^2} + K_y\frac{\partial^2 Z}{\partial y^2} + K_z\frac{\partial^2 Z}{\partial z^2} + gZ - eZ + GZ - fZ \quad (15)$$

And finally for the benthos (μg C l^{-1}),

$$\frac{\partial B}{\partial t} = s\frac{\partial P}{\partial z} - rB + fZ \quad (16)$$

The first four terms on the right hand side of eqns. (12)–(15) express the advection and diffusion of each state variable, where u and v are the time-dependent barotropic velocities obtained from eqns. (1)–(3), i.e. $u = U/H$ and $v = V/H$. K_x and K_y are the horizontal numerical diffusion coefficients in the x and y direction, respectively and are implicit in the model. K_z is the vertical mixing coefficient in the z direction and is derived from the local wind stress at the surface (Csanady, 1976; Shuert, 1990). The terms $a'P_N$ and $a''P_N$ in eqns. (12) and (13) describe the uptake of nitrate and ammonium as a function of phytoplankton biomass in terms of particulate nitrogen, such that the sum of the two uptakes balances with the total growth rate of phytoplankton, abP in eqn. (14)— a more detailed description can be found in Shuert, 1990. eZ is the rate of excretion of ammonium by zooplankton which is a function of zooplankton biomass. r is the regeneration rate of phytoplankton nitrogen from the benthos. r is essentially an indicator of trophic efficiently which regards the biological assemblage of the benthos as grazers of phytoplankton and fecal material. No further trophic transfer within the benthos was parameterized.

gZ is the grazing loss of phytoplankton biomass expressed as a function only of zooplankton biomass, while GZ is the predatory loss of the herbivores. The last term of eqn. (14) quantities the sinking loss of phytoplankton. The biological state equations were calculated over 10 layers, where the layer depth is defined as H/10.

In equations (15) and (16) the term fZ account for the fecal pellet production as a function of zooplankton biomass. Fecal pellets are allowed to sink to the benthos at a moderate rate (s) of 50 m day $^{-1}$. Phytoplankton and fecal pellets become an undistinguished pool of organic material on the bottom. This pool is then available to be recycled into ammonium.

The rates a' and a'' are expressed as functions of light and nutrient concentration (Steele, 1962) such that,

$$a'' = \kappa_{max}\left[\frac{I_z}{I_{sat}}\right]e^{(I_z/I_{sat})}\left[\frac{NH_4^t}{1.0 + NH_4^t}\right] \quad (17)$$

$$a' = \mu_{max}\left[\frac{I_z}{I_{sat}}\right]e^{(I_z/I_{sat})}\left[\frac{NO_3^t}{1.5 + NO_3^t}\right] \quad (18)$$

The last brackets in eqns. (17) and (18) are the usual Michaelis–Menton expressions, where NO_3 and NH_4 are the external concentrations of nitrate and ammonium at time t, 1.5 is the half-saturation constant for nitrate (Walsh, 1975 and 1.0 is the half-saturation constant for ammonium (Eppley et al., 1969). Such half-saturation constants tend to favor the uptake up ammonium. The model further forces the preferential uptake of ammonium by first assuming the maximum

nitrogen requirements of growth (bounded by μ_{max}) are met by the available ammonium.

μ_{max} in eqns. (17) and (18) is the temperature dependent maximum specific growth rate of phytoplankton. Since the model did not incorporate temperature as a state variable, an average summer temperature (3°C) for the Bering Sea was used.4pI_z in eqns. (17) and (18) is the instantaneous irradiance at depth z and is a function of the total irradiance at the surface (I_0) and chlorophyll concentration in the overlying water (Shuert, 1990). The model calculates a non-spectral irradiance (I_z).

The total irradiance at the surface (I_0) is calculated at each time step using a very high spectral resolution model (Gregg, pers. commun.). The model uses the mean extraterrestrial irradiance and accounts for Rayleigh scattering, ozone absorption, aerosol scattering and absorption and surface reflectance. The total irradiance (I_0) used in the model was integrated over the photosynthetically active portion of the spectrum (400–700 nm). The maximum daily surface incident radiation (Local Noon) decreased each day of the simulation, from a maximum of ~23 cal cm^{-2} h^{-1} at Julian day 190 to a minimum of ~11 cal cm^{-2} h^{-1} at Julian day 270. The photoperiod decreases over the same period as well, from 23.15 to 11.88 h.

The exponential expression of eqns. (17) and (18) allows photoinhibition of growth at high light intensities, such that, if I_z is greater than I_{sat}, a' and a'' become smaller, expressing an inhibition of photosynthesis. Malone (1977) found light inhibition during incubation experiments at intensities of 3.6 and 4.8 cal cm^{-2} h^{-1}. Thus, I_{sat} was set to 5.0 cal cm^{-2} h^{-1}. Daily primary production was then calculated by summing the increment of growth in phytoplankton stocks at each time step and converting to carbon, using a carbon/chlorophyll ratio of 45/1.

The terms eZ in eqn. (13) and gZ in eqn. (14) couple the grazing of zooplankton on phytoplankton with the excretion of ammonium by zooplankton, eqn. (15). The consumption rate of herbivorous zooplankton is assumed to be 10% of the zooplankton biomass per day, based on feeding studies in the southeastern Bering Sea (Dagg et al., 1982). Thus, the instantaneous feeding rate of zooplankton in units of carbon is

$$g = \Delta t \frac{0.10Z}{45.0} \tag{19}$$

where 1/45 is the conversion ratio of chlorophyll to carbon.

Assuming an intermediate assimilation efficiency of 51% for the herbivorous zooplankton, 49% of their ingestion would be unassimilated fecal pellets which are allowed to sink to the benthos at a constant rate of 50 m day^{-1}. This fecal pellet flux appears as a source term for the benthos in eqn. (16). Of the assimilated food, 60% is assumed to be devoted to daily maintenance nitrogen demands; i.e. excretion amount to ~30% of the daily ingestion, gZ.

The predation loss, GZ, was described in terms of zooplankton biomass measured during the 1985 ISHTAR experiment. A predation rate in % per day was calculated based on two estimates of zooplankton biomass,

$$G = (\ln Z_1 - \ln Z_0)(t_1 - t_0)^{-1}100 \tag{20}$$

where Z_1 and Z_0 are the biomass at times t_1 and t_0 (Vidal and Smith, 1986). With $Z_1 = 2.0$ and $Z_0 = 5.0$ g dw m^{-2} and $(t_1 - t_0) = 33$ days, we obtain a predation rate of -2.78 % day^{-1}. To allow closure on the set of equations, the term GZ in eqn. (15) represents this trophic loss.

The last term in eqns. (13) and (14) and the terms of eqn. (16) parameterize both the sinking of phytoplankton and fecal pellets to the benthos and the regeneration of ammonium and its release to the water column. It was usually assumed that, of the phytoplankton and fecal pellets that reach the benthos, 80% is returned to the water column as ammonium.

Nitrate, ammonium and zooplankton were assumed to change linearly over time at the southern boundary between the sampling dates during 1985. The fluorometer records from 3 instruments moored in the two Straits, and chlorophyll data from ship transects, were also used to construct time-dependent boundary conditions of algal biomass.

Initial conditions of the state variables in the water column were obtained by advecting the

boundary conditions at Julian Day 190 of nutrients, chlorophyll and zooplankton for 150 days, after which time the concentrations at each interior grid point were unchanging. Initial conditions of the benthos were set at zero.

Results

Figures 5–7 are stick diagrams of the vectors of the observed and simulated currents under the three wind forcing cases of the model at moorings 8, 9 and 10 (Fig. 2). These results suggest that there is little difference in both magnitude and direction of the simulated flow under the three different wind forcings. The model results at mooring 8 (Fig. 5) show the best match to the observations, with speeds of the same direction and magnitude. The model output at mooring 9 (Fig. 6) shows the same direction, but the magnitudes of the vectors are approximately one third less than the observed currents. The simulated flows at mooring 10 (Fig. 7) show instead a nearly constant difference in direction of 30–40°, shifted to the east; here the same speeds are simulated, when compared to the current meter data.

Some of the discrepancies in these comparisons may result from bottom topography. The bathymetry of the model domain is somewhat smoother, for numerical considerations, than the actual bottom topography. In general, the northern Bering Sea is shallow with a mean depth of only 50 m, such that strong bathymetric steering is expected. The knolls and shallow troughs of the area, though gentle, represents a substantial fraction of the total depth.

This relief is absent in the model's specification of bathymetry, and thus unable to contribute to fine scale steering of the flow, which may occur

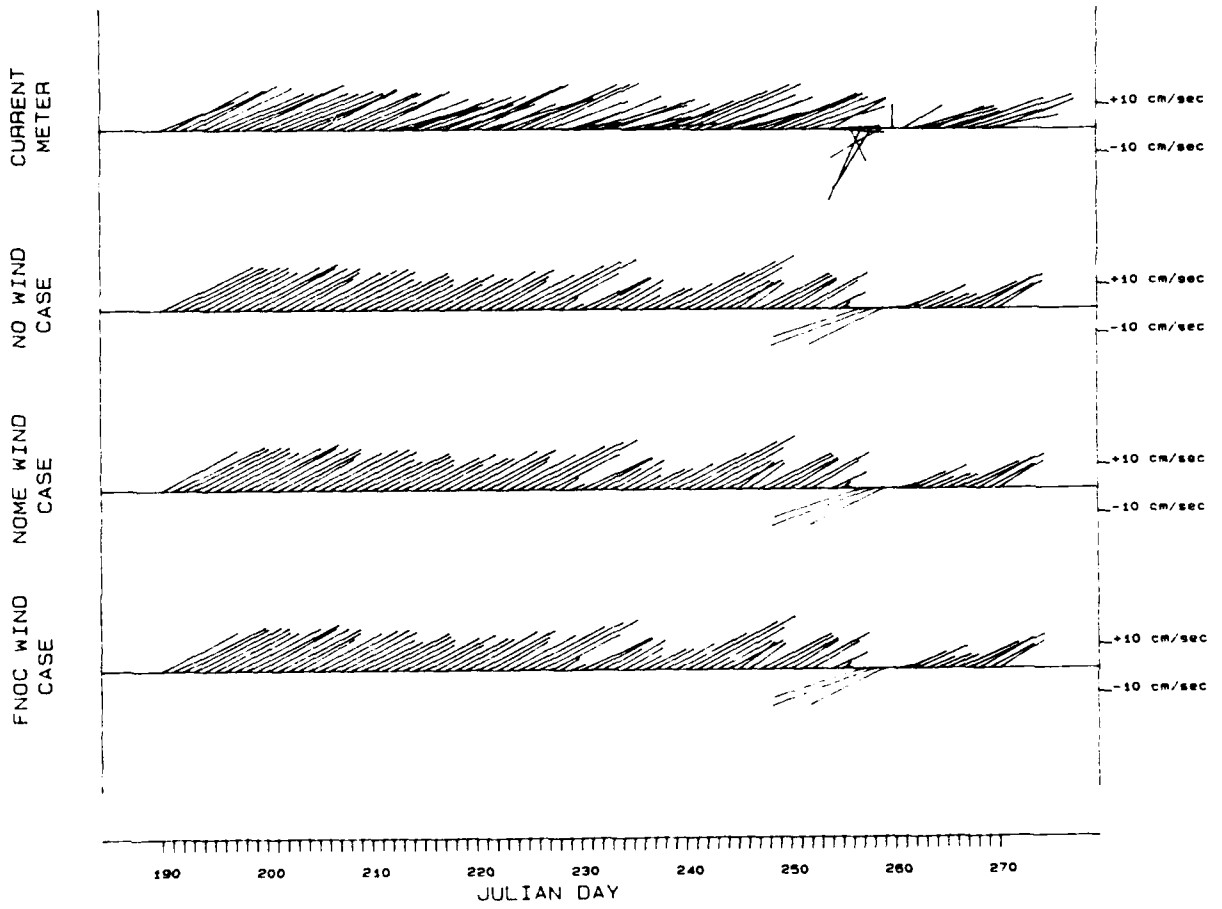

Fig. 5. Comparison of current meter data with no wind, Nome wind and FNOC wind simulations for mooring 8. (See Fig. 2).

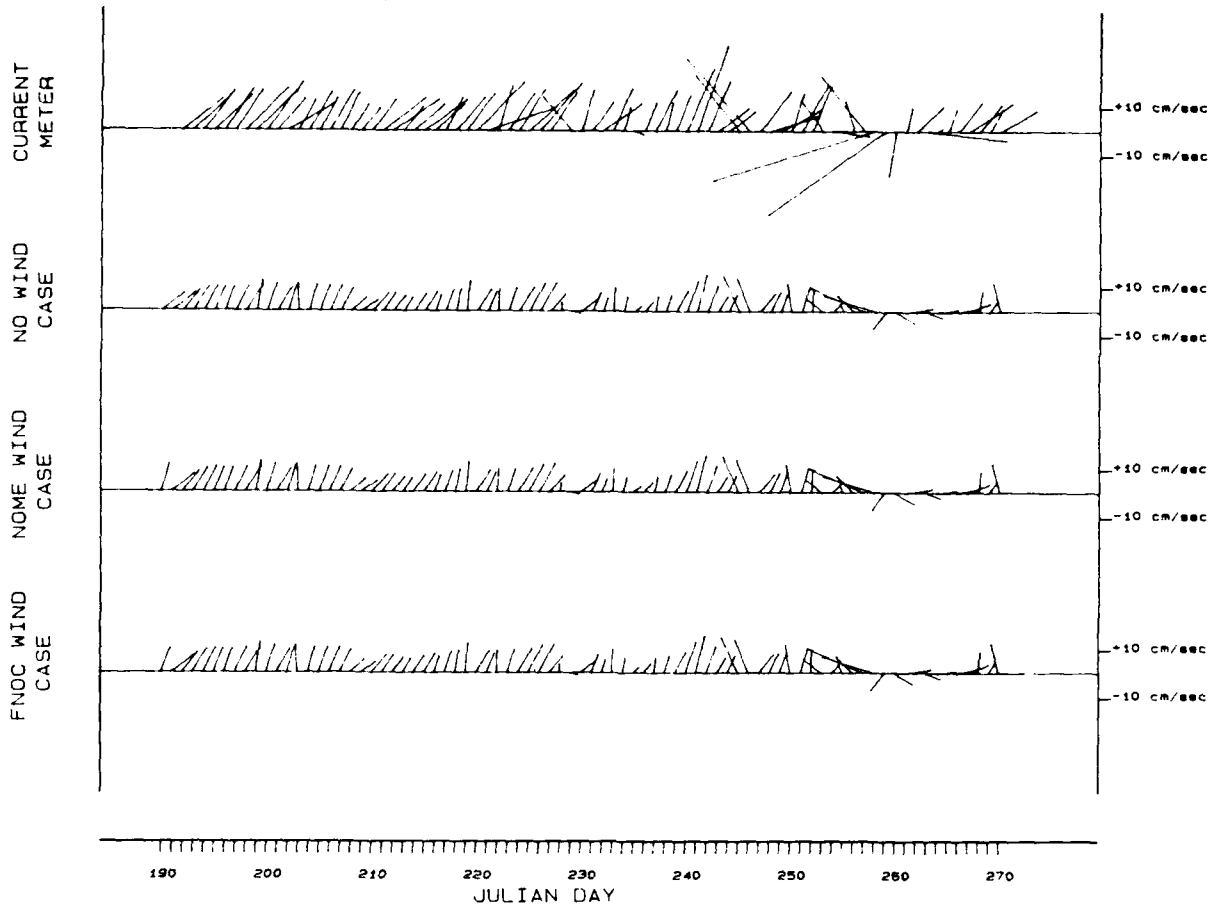

Fig. 6. Comparison of current meter data with no wind, Nome wind and FNOC wind simulations for mooring 9.

at the above moorings. A specific example is seen in Fig. 8 where the measured vs. modelled vectors at the three interior moorings for Julian days 190–195 are presented. At mooring 10, a nearly uniform ~30° offset in a direction between the measured and modelled velocities is evident. This mooring is approximately 20 km south of the Diomede Islands in Bering Strait. Actually, these islands split the Strait into two channels, whereas the model grid is too coarse to reproduce these bathymetric details.

The model vectors shown in Figs. 5–7 are most like the current meter vectors at times when Anadyr and Shpanberg Strait transports are steady, strong and northward (i.e. Julian days 190–220). A typical flow pattern is presented in Fig. 9a of the velocity field for Julian day 214 in the Nome wind case. The Bering Strait transport of 0.95 Sv then approximates the simulated 81 day mean of 0.92 Sv, i.e. representing the average summer flow pattern.

Typically, water entering Anadyr Strait of the model migrates slightly eastward in the Chirikov Basin. Bathymetric steering and the hydrostatic pressure gradient (Fig. 9b) then force the flow to turn north through Bering Strait. The Shpanberg Strait inflow follows the shallow bathymetry off the Alaskan coast before joining the Anadyr inflow at Bering Strait. Only a small transport is computed within the Norton Sound. Once through Bering Strait, flows slow with the majority of the water moving northwestward towards Wrangel Island. A small flow turns north past Pt. Hope and appears as a coastal current towards Point Barrow, Alaska.

The transport through Bering Strait can be directly related to the along axis (N–S) sea level difference (Overland and Roach, 1987). Under

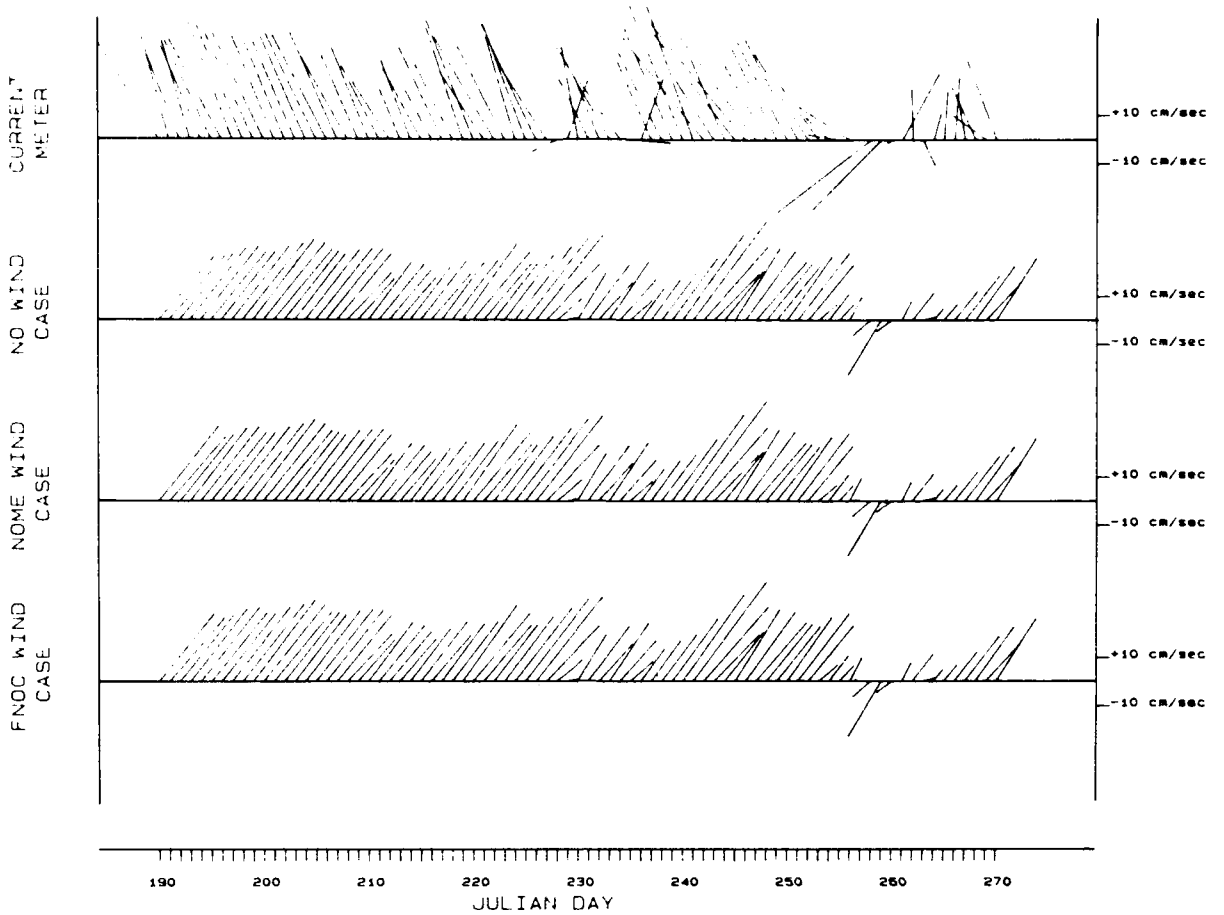

Fig. 7. Comparison of current meter data with no wind, Nome wind and FNOC wind simulations for mooring 10.

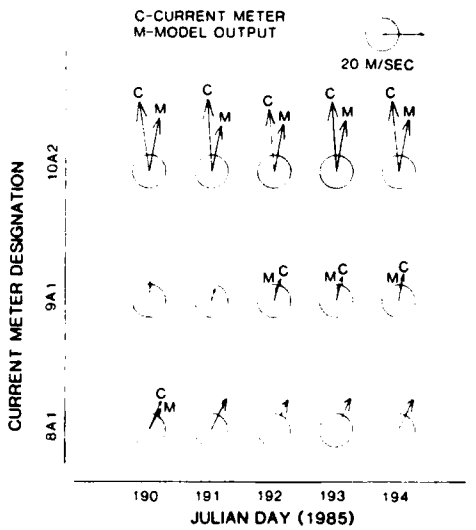

Fig. 8. Simulated and observed currents under Nome wind forcing during Julian Days 190–195 at moorings 8–10.

geostrophic control, the maximum transport is given by

$$Q = g\Delta eHf^{-1} \tag{21}$$

where Q is the transport, Δe is the along-strait sea level difference, f is the Coriolis parameter (4) and H is the average depth of the water column (Toulany and Garrett, 1984). In Fig. 10 for Julian day 241, when the maximum simulated transport through Bering Strait was obtained, the highest sea level elevation is off Cape Prince of Wales and the minimum is off Cape Dezhneva. Using eqn. (10), this along-strait sea level difference of 0.5 m (Fig. 10b) and an average depth of 50 m limits the geostrophic transport to 1.90 Sv.

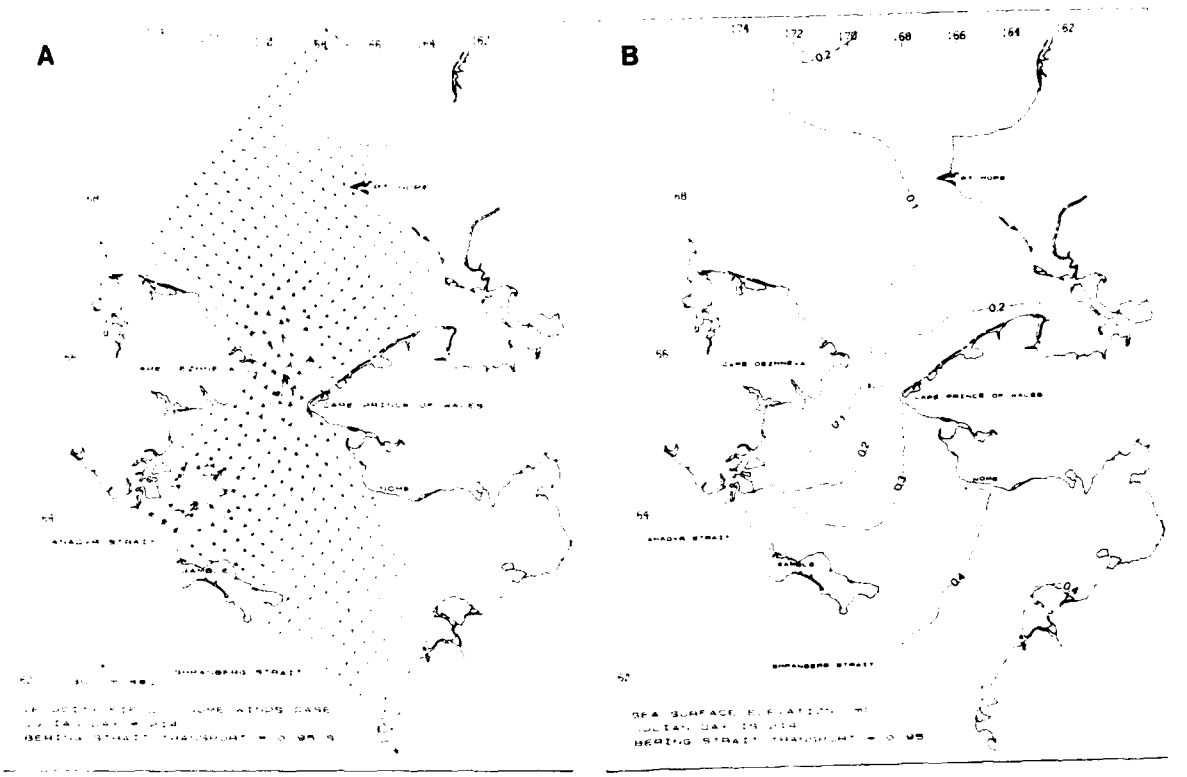

Fig. 9. The fields of (A) velocity and (B) sea surface elevation on Julian Day 214, with the Nome wind forcing.

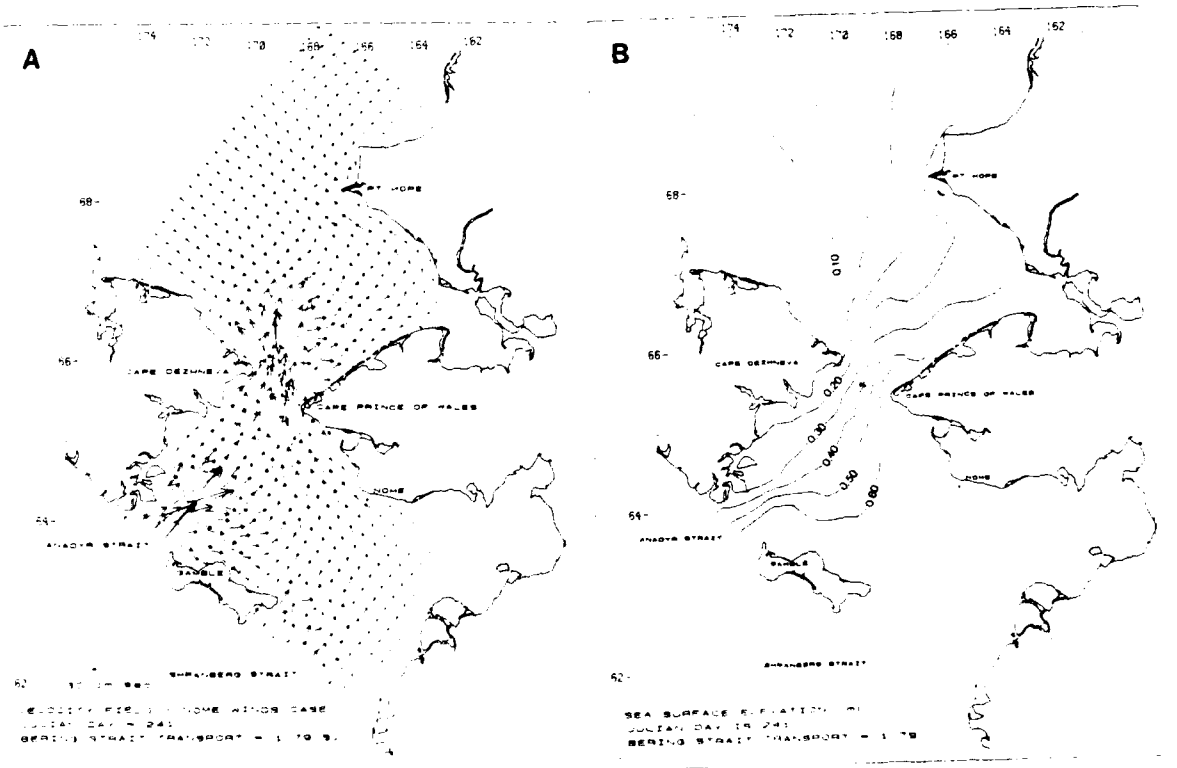

Fig. 10. The fields of (A) velocity and (B) sea surface elevation at Julian Day 241, with the Nome wind forcing.

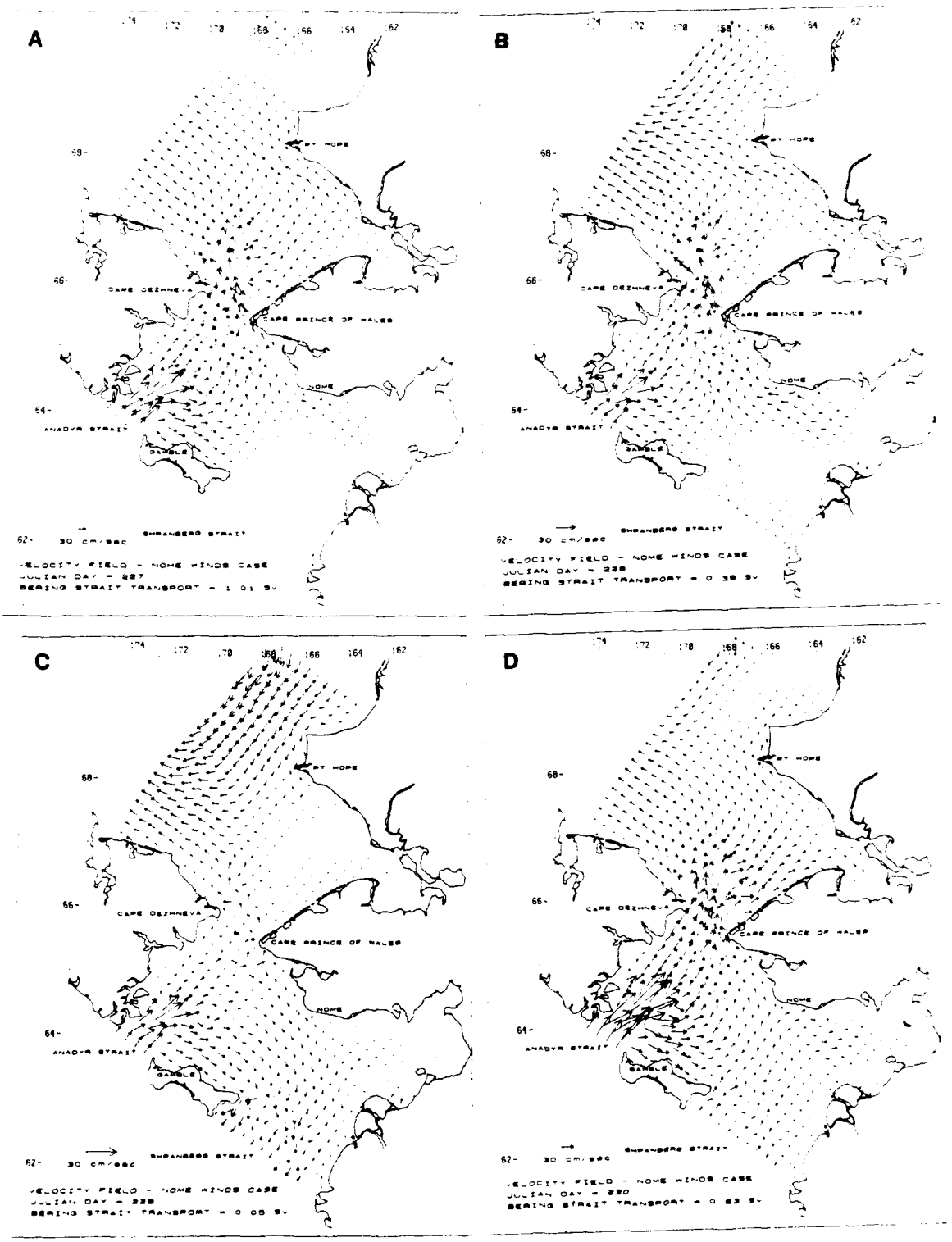

Fig. 11. The fields of velocity on Julian Days (A) 225, (B) 227, (C) 229 and (D) 231 for the Nome wind forcing.

only slightly greater than the 1.79 Sv calculated from the numerical model (Fig. 10a).

There is a normal east–west gradient of water mass properties (i.e. salinity, temperature and nitrate) as a consequence of the usual northward advection within the Chirikov Basin (Walsh et al., 1989). As seen in Figs. 9 and 10, the general northward flows tend to follow the bathymetric contours through at least Bering Strait. Water mass properties reflect this flow pattern such that the three waters masses and their different nutrient contents exhibit lateral banding across the system, with no isopleths oriented in the east–west direction (Coachman et al., 1975).

However, major changes of transport through the system can take place very rapidly, from 1 Sv northward to more than 2 Sv southward, in as short a time as 2 days (Coachman and Aagaard, 1981). These transport changes will lead to variations in the relative amounts of each water mass entering and/or leaving the system. If these transport changes are out of phase through the three straits, large scale east–west displacements of the water mass boundaries might be expected.

During summer of 1985, reversals of the flow through Shpanberg Strait were observed during Julian days 208–209, 227–229 and 235. Each of these reversals were accompanied by a reduction of the flow through Anadyr Strait and a small decline of the Bering Strait transport. Figure 11 shows the simulated velocity fields for Julian days 227 through 230.

Currents first reverse in the Chukchi Sea on Julian day 228 (Fig. 11b). The flow field between Nome and St. Lawrence Island then turns southeast by Julian day 229 (Fig. 11c). As southerly winds return and the northward transport through Shpanberg Strait is restored, stronger flows appear to flush Norton Sound on Julian day 230 (Fig. 11d), compared to Julian day 227 (Fig. 11a).

Although our physical model is not a baroclinic one, with temperature and salinity tracers (Nihoul et al., 1986), the coupled biological model does monitor the nutrient content of each water mass. Such current reversals were though to perhaps have an effect on the nutrient uptake, or primary productivity, of this ecosystem, especially further downstream of the Chirikov Basin. Slowing of the transport through the Bering Strait would increase the residence time of nutrient0-rich Anadyr Water in the Chirikov Basin, thus reducing the delivery of nutrients to the Chukchi Sea. A spatial shift in nutrient supply and utilization would also be reflected in the algal biomass left behind in the water column, if planktonic grazing were negligible.

The time-dependent boundary conditions of nutrient, zooplankton and chlorophyll at Anadyr and Shpanberg Straits were advected through the model domain, using the u and v velocities obtained from the physical model in the Nome wind case, (e.g. Figs. 9–11). Over 10 depth intervals, the biological model used a light and nutrient dependent growth rate of phytoplankton equivalent to 0.5 doublings day^{-1}, sinking rates of 1 m day^{-1} for phytoplankton and 50 m day^{-1} for fecal pellets, a benthic regeneration rate for organic matter that reached the bottom equal to 80% day^{-1}, and a vertical mixing rate dependent on the wind stress (Case 2 of Shuert and Walsh, 1991). Two forms of nitrogen (nitrate and ammonium), seasonal changes in day length and incident radiation, and weak herbivory ($< 1\%$ grazing stress) complete the description of the biological model.

The effect of flow reversals on the nutrient and chlorophyll patterns simulated by the model was less obvious than originally expected. Despite changes in the flow field (Fig. 11) on Julian days 227–230, the depth-integrated chlorophyll distributions over this week (Fig. 12), show almost no detectable change in the positions of isopleths. This situation is also evident for nitrate and ammonium distributions which are not shown here.

An examination of the flow field within the Chukchi Sea off Pt. Hope during this period indicates that speeds change from ~ 50 cm s^{-1} to the north on Julian day 226 to ~ 10 cm s^{-1} to the south on Julian day 229. These velocities suggest a net southward movement of ~ 8.6 km on Julian day 229. This small north–south movement is difficult to detect over a 10 km grid (i.e. a sub-grid scale change), let alone smaller east–west movements of the front between Anadyr and Bering Shelf Water masses.

Reversals of greater duration, which occur in

late fall and winter, would be expected to move the isopleths of nutrients and chlorophyll more towards the southeast than simulated here. Over longer time periods, the spatial patterns of the models state variables do exhibit significant changes. Patterns of nitrate utilization can be

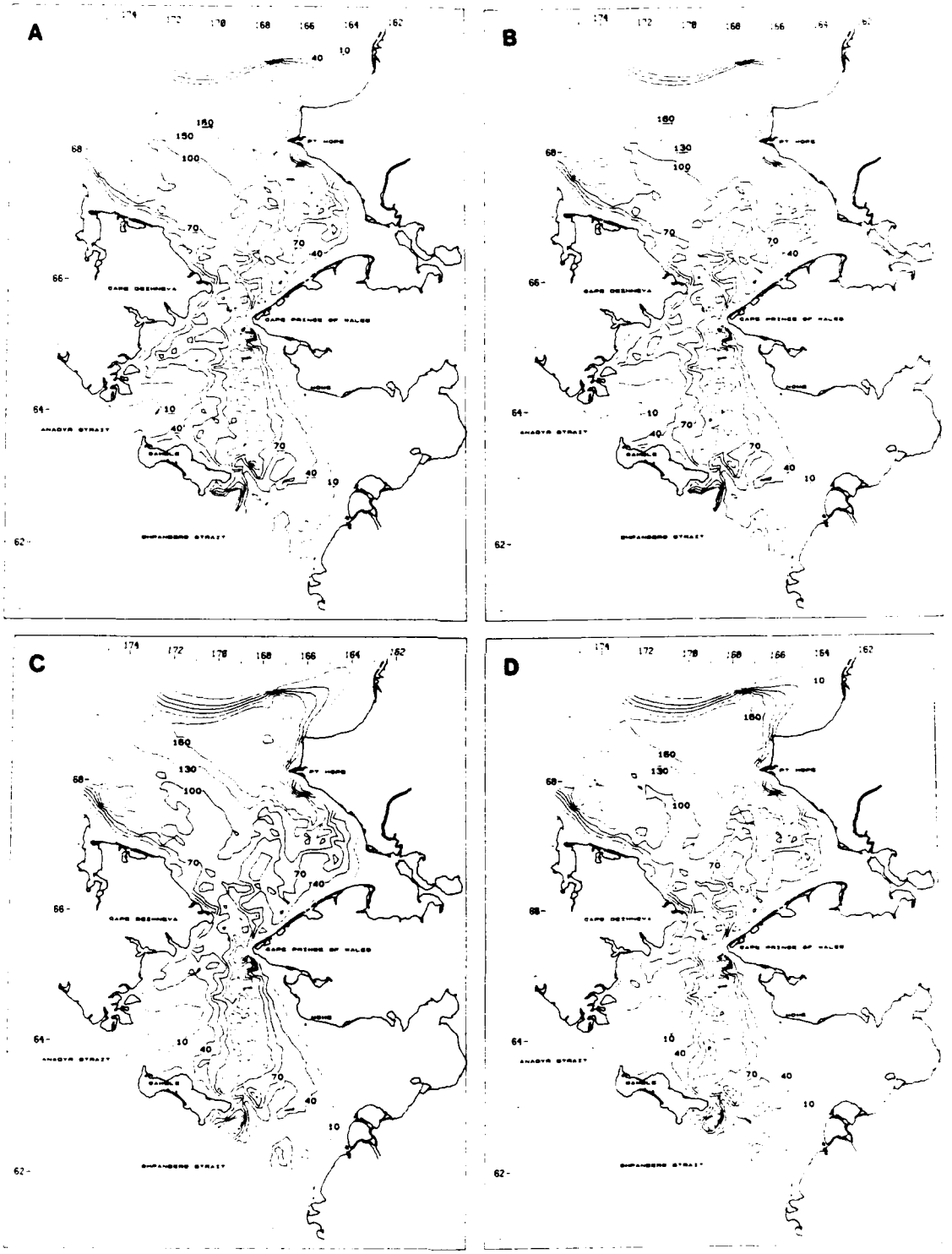

Fig. 12. The depth-integrated chlorophyll stocks (mg Chl m^{-2}) on Julian Days (A) 225, (B) 227, (C) 229 and (D) 231 for the 1985 boundary conditions.

seen in Fig. 13, for example. By Julian Day 200, (Fig. 13a), more than 450 mg-at NO_3 m^{-2} is found along the Siberian Coast, while < 45 mg-at NO_3 m^{-2} occurs in Alaskan Coastal Water on the eastern sides of both the Bering and Chukchi Seas. Nitrate depletion is observed in the Chirikov

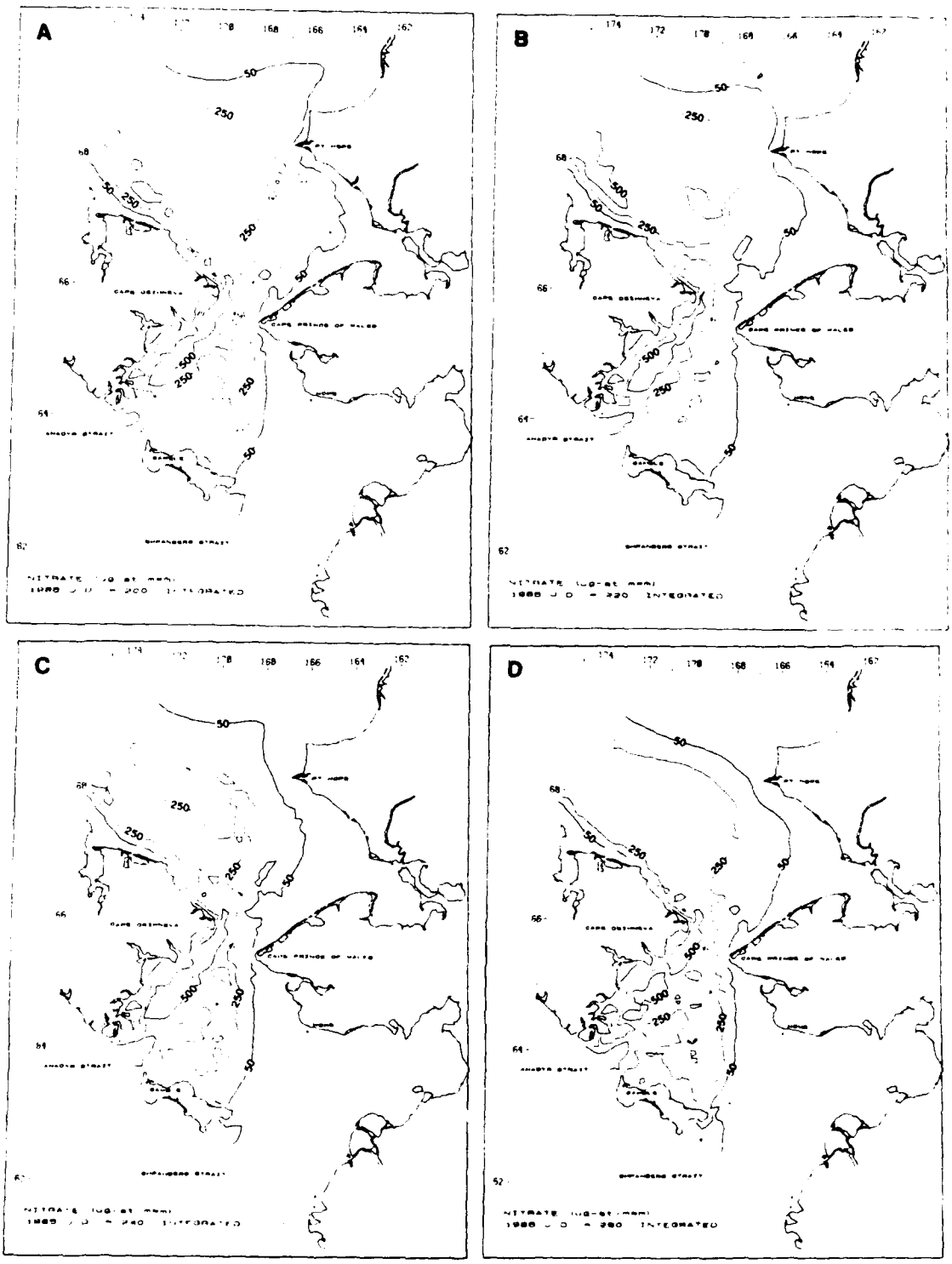

Fig. 13. The depth integrated nitrate stocks (mg-at NO_3 m^{-2}) on Julian days (A) 200, (B) 220, (C) 240 and (D) 260 for the 1985 boundary conditions.

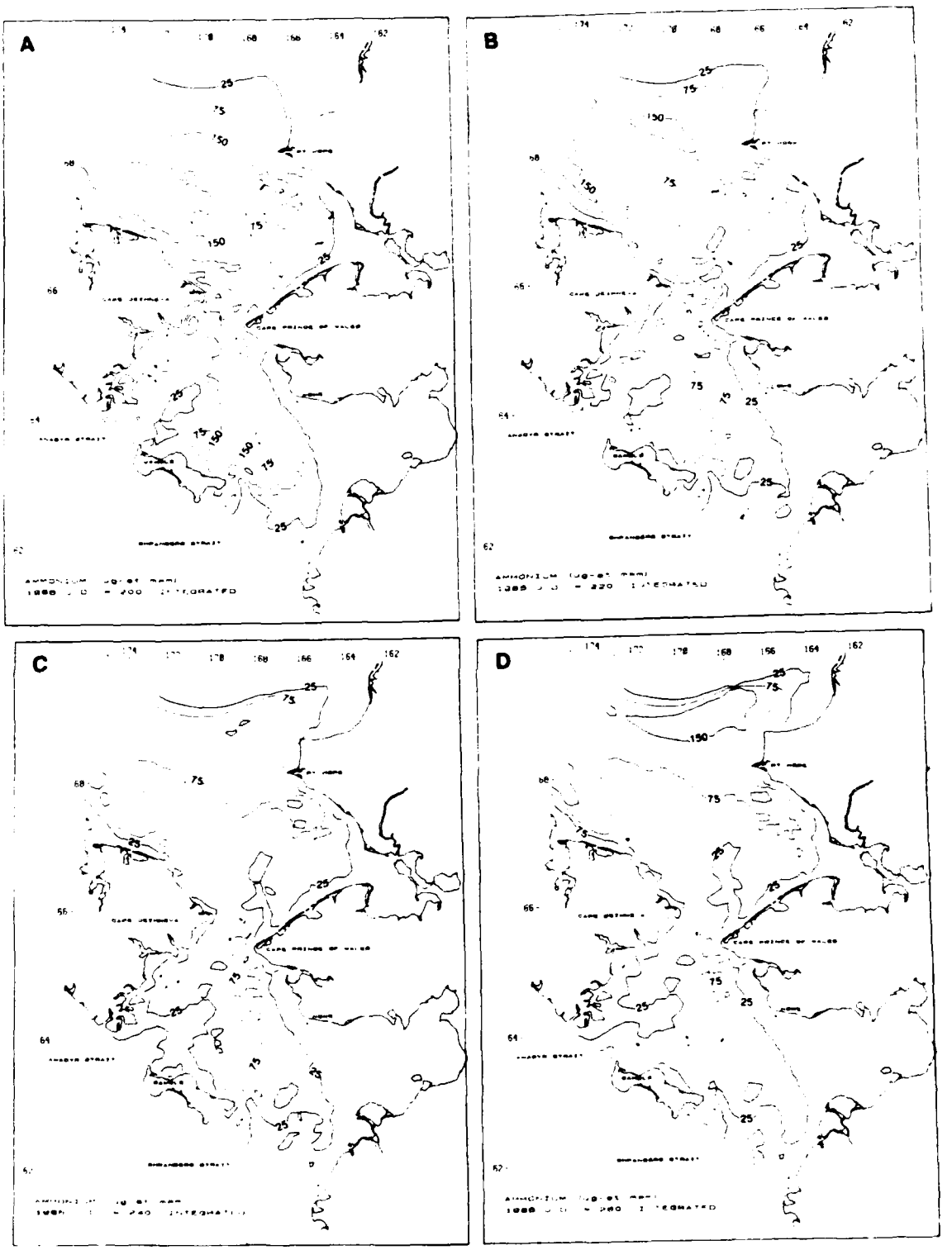

Fig. 14. The depth integrated ammonium stocks (mg-at NH_4 m^{-2}) on Julian days (A) 200, (B) 220, (C) 240 and (D) 260 for the 1985 boundary conditions.

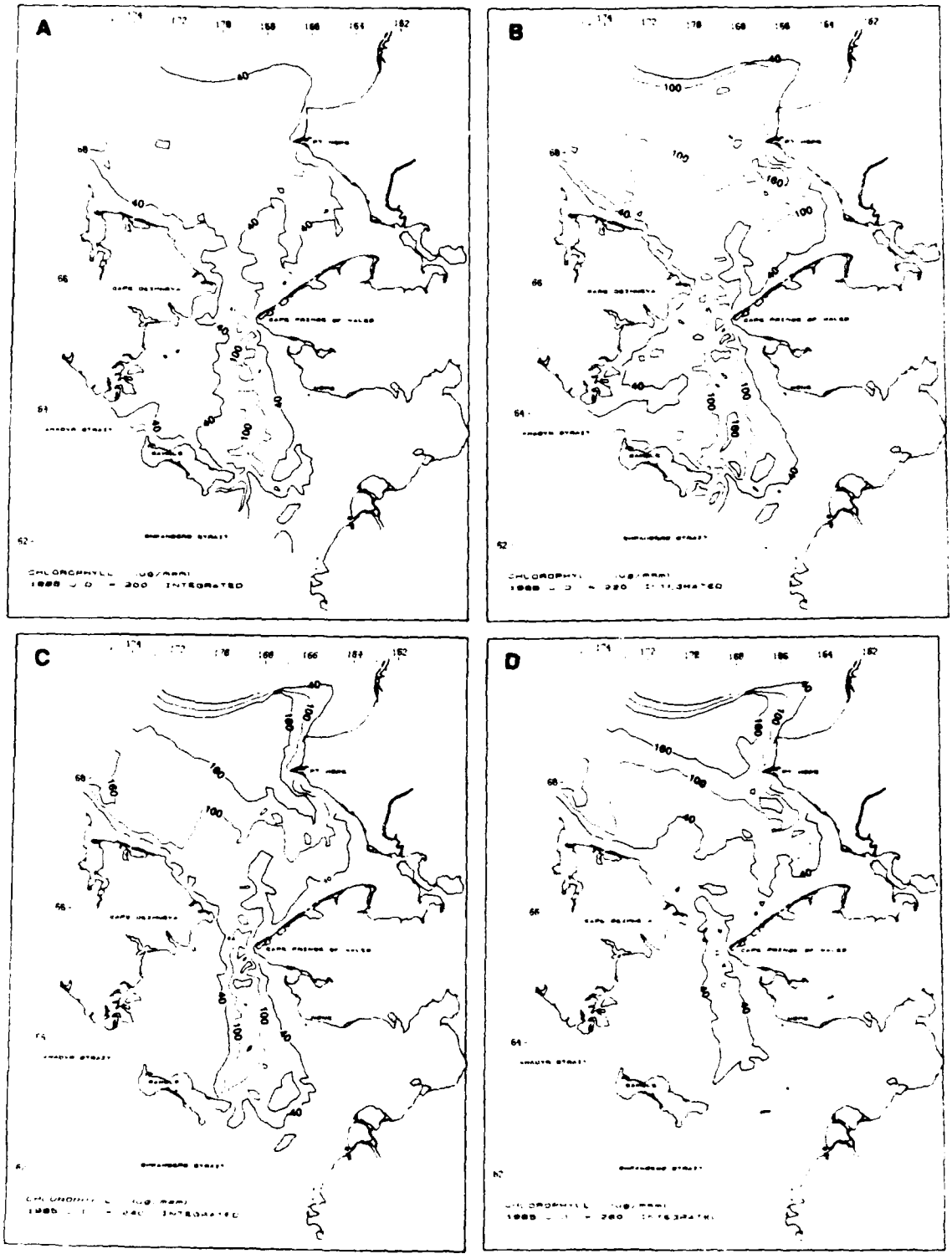

Fig. 15. The depth integrated chlorophyll stocks (mg Chl m^{-2}) on Julian days (A) 200, (B) 220, (C) 240, and (D) 260 for the 1985 boundary conditions.

Basin from the westward shift of the position of the 250 mg-at NO_3 m^{-2} isopleth on Julian day 220 (Fig. 13b), demarcating the region of enhanced production, or ergocline, running north–south from the eastern side of St. Lawrence Island to Cape Prince of Wales (Fig. 12). By Julian Day 260, declining productivity as a result of lower light conditions, and the continued northward advection of unutilized nitrate through Anadyr Strait, lead to increased stocks of nitrate both north and south of Bering Strait (Fig. 13d).

Ammonium concentrations increase dramatically in the model domain over the initial conditions of ~25 mg-at NH_4 m^{-2} at the southern end of the ergocline (Shuert and Walsh, 1991). After just 10 days, ammonium concentrations increased dramatically along the ergocline and extending into the Chukchi Sea (Fig. 14a). These high concentrations of ammonium are the result of the benthic regeneration of detrital nitrogen from the deposited phytoplankton and fecal material in the sediments; excretion by zooplankton is insignificant in the model. Ammonium concentrations decline by Julian Day 260 (Fig. 14b) both as a result of utilization by phytoplankton and a reduction in supply of detritus to the benthos.

After ten days, stocks of chlorophyll (Fig. 15a) are found along the ergocline in concentrations of > 100 mg Chl m^{-2} by Julian day 200. Despite changes in wind forcing (Fig. 11), light and even boundary conditions (Shuert and Walsh, 1991), algal biomasses remain high along the ergocline for the next 50 days (Figs. 15b, c). By Julian Day 260 (Fig. 15d), the chlorophyll stocks are lower south of Bering Strait, however, reflecting the decrease in both local photosynthesis and supply of the preferred nitrogen source, ammonium. The higher algal stocks in the Chukchi Sea also mimic greater residues of organic carbon in these sediments (Walsh et al., 1989).

Discussion

Several authors (Walsh and Dieterle, 1986; Overland and Roach, 1987; Spaulding et al., 1987) have used similar 2-dimensional, barotropic models to estimate the flow fields and transports near Bering Strait. Overland and Roach (1987) found that in the presence of winter wind stress from the northeast, a reduced sea level difference between the Pacific and Arctic Oceans of 0.4 m produced a northward transport through Bering Strait in good agreement with hydrographic estimates. Their results also indicate that the maximum flow through Bering Strait is geostrophically limited, not frictionally or inertially, similar to our calculations.

Spaulding et al., (1987) extended a similar model to compare the influence of open boundary conditions, grid sizes, bottom friction coefficients and wind forcing with current meter and sea level observations for both a winter and summer case. Both of these investigations point to the sea level difference between the Pacific and Arctic Oceans as the principal driving force of the northward transport and that the variability of the wind stress in and around Bering Strait causes variations in the transport, i.e. Fig. 11.

The model presented here, like the others, gives a representative picture of the gross features of the flow, with mean north–south sea level differences across Bering Strait of the same magnitude (0.3–0.4 m). We have added biochemical tracers to "color the water green" for our physical colleagues. It may be fortuitous that our coupled biophysical models simulate a persistent structure of high chlorophyll along a line from the southeast side of St. Lawrence Island to Cape Prince of Wales, despite changes in forcing functions and boundary conditions of the model. These same robust regions of enhanced algal biomass are seen in satellite imagery and shipboard observations (Walsh et al., 1989).

In the real world, temperature and salinity gradients extend east to west across the Chirikov basin, marking the transition of an ecotone between Anadyr and Bering Shelf water masses. These two water masses are separated by a zone of horizontal mixing, created by the interleaving of the water mass types simulated in more complex physical models (Nihoul et al., 1989). When this occurs, the water column becomes stratified, an ergocline (Legendre, et al., 1986) is created and algal growth is enhanced.

In our simple barotropic model, the magnitude of the transports through Anadyr Strait relative

to Shpanberg Strait, as well as the bathymetry, determines the east–west position to the horizontal nutricline, while the chlorophyll flux through Shpanberg Strait in 1985 provided "seed" to initiate a bloom along this nutricline (Figs. 12 and 15). When the 1988 boundary condition was used, in which the "seed" chlorophyll was instead delivered primarily through the western side of Anadyr Strait, the ergocline bloom still develops in the same relative position as with the 1985 boundary data.

When currents were reversed in these simulations, the east–west structure of the horizontal nutricline did not show a detectable change in position. Apparently the duration and magnitude of the reversals during this simulation period were not large enough to be detected at the physical model's grid scale of 10 km. Use of more complex biophysical models are required, since part of the variance in moored fluorometer records is attributed to small-scale east–west displacements (Walsh et al., 1989).

The importance of using a biological model, driven by a physical model such as the one presented here was evident in the results of the coupled models. It was determined that the distributions of chlorophyll and primary productivity in the northern Bering Sea are mainly determined by the circulation at longer time scales rather than by short-term fluctuations of the flow field. It is thus our opinion that the modelling of biological variables within an ecosystem context requires the continued use of coupled physical/biological models, e.g. Walsh (1988) and Rothschild (1988).

Acknowledgements

This research was funded by grants DPP-86-05659 from the Division of Polar Programs, National Science Foundation, NAGW-678 from the National Aeronautics and Space Administration, and N00014-87-J-1218 from the Office of Naval Research, Department of Defense. We also wish to thank L.K. Coachman and R.B. Tripp of the University of Washington for current meter data used in this research.

References

Aagaard, K., Roach, A.T. and Schumacher, J.D., 1985. On the wind-driven variability of the flow through Bering Strait. J. Geophys. Res. 90: 7213–72221.

Arsen'ev, V.S., 1967. The current and water masses of the Bering Sea. (Translated from the Russian by S. Pearson, 1968). Biological Laboratory Bureau of Commercial Fisheries, Seattle, 146 pp.

Coachman, L.K., Aagaard, K. and Tripp, R.B., 1975. Bering Strait: The Regional Physical Oceanography. Univ. Washington Press, Seattle, 172 pp.

Coachman, L.K. and Aagaard, K., 1981. Reevaluation of water transports in the vicinity of Bering Straits. In: D.W. Hood and J.A. Calder (Editor), The Eastern Bering Sea Shelf: Oceanography and Resources, Vol. I Univ. Washington Press, pp. 95–110.

Coachman, L.K., 1986. Circulation, water masses, and fluxes on the southeastern Bering Sea shelf. Cont. Shelf Res., 5: 23–108.

Coachman, L.K. and Aagaard, K., 1988. Transports through Bering Strait: Annual and interannual variability. J. Geophys. Res., 93: 15,535–15,539.

Csanady, G.T., 1976. Mean-circulation in shallow seas. J. Geophys. Res., 81: 5389–5399.

Dagg, M.J., Vidal, J. Whitledge, T.E. Iverson, R.L. and Goering, J.J., 1982. The feeding, respiration and excretion of zooplankton in the Bering Sea during a spring bloom. Deep Sea Res., 29: 45–63.

Dodimead, A.J., Favorite, F. and Hirano, T., 1963. Salmon of the North Pacific Ocean. II. Review of oceanography of the Subarctic Pacific Region. Bull. Int. North Pacific Comm., 13: 195 pp.

Eppley, R.W., Rogers, J.N. and McCarthy, J.J., 1969. Half saturation constants for the uptake of nitrate and ammonium by marine phytoplankton. Limnol. Oceanogr., 14: 912–920.

Favorite, F., 1966. Bering Sea. In: R.W. Fairbridge (Editor), The Encyclopedia of Oceanography. Reinhold New York, 1021 pp.

Fedorova, A.P. and Yakina, A.S., 1964. The passage of the Pacific Ocean water through the Bering Strait into the Chukchi Sea. Deep-Sea Res., 11: 427–434.

Israeli, M. and Orszag, S.A., 1981. Approximation of radiative boundary conditions. J. Comput. Phys., 41: 115–135.

Kinder, T.H. and Schumacher, J.D., 1981. Hydrographic structure over the continental shelf of the southeastern Bering Sea. In: D.W. Hood and J.A. Calder (Editors), Volume 1, Univ. Washington Press, Seattle, pp. 31–52.

Kinder, T.H., Chapman, D.C. and Whitehead, J.A., 1986. Westward intensification of the mean circulation on the Bering Sea shelf. J. Phys. Oceanogr., 16: 1217–1229.

Lax, P.D., 1967. Hyperbolic difference equations: A review of the Courant-Friedrichs-Lewy paper in the light of recent developments. IBM J. March 1967, pp. 235–238.

Legendre, L., Demers, S. and Lefaivre, D., 1986. Biological productivity at marine ergoclines. In: J.C.J. Nihoul (Editor), Marine Interfaces Ecohydrodynamics. Elsevier Oceanographic Series Vol. 42, Elsevier, Amsterdam, pp. 1–30.

Malone, T.C., 1977. Light-saturated photosynthesis by phytoplankton size fractions in the New York Bight, USA. Mar. Biol., 42: 281–292.

Mikoh, W.F. and Kaitala, J.E., 1976. U.S. Navy Fleet Numerical Weather Central Operational Five Level Global Fourth Order Primitive Equation Model. Mon. Weather Rev., 104: 1527–1550.

Nihoul, J.C.J., Deleersnijer, E., Djenidi, S. and Brasseur, P., 1989. Mathematical visualization of general circulation fields and frontal structures in the Northern Bering Sea. (Submitted).

Nihoul, C.J., Waleffe, F. and Djenidi, S., 1986. A 3-dimensional numerical model of the northern Bering Sea. Environ. Software, 1: 76–81.

Overland, J.E. and Roach, A.T., 1987. Northward flow in the Bering and Chukchi Seas. J. Geophys. Res., 92: 7097–7105.

Reid, J.L., 1961. On the temperature, salinity and density differences between Atlantic and Pacific Oceans in the upper kilometer. Deep-Sea Res., 7: 265–275.

Rothschild, B.J., 1988. Towards a Theory on Biological-Physical Interaction in the World Ocean. Kluwer Dordrecht, 650 pp.

Shuert, P.G., 1990. Ecosystem analysis of the Bering/Chukchi seas using a coupled time-dependent physical/biological simulation model. Diss. Dep. Sci., Univ. South Florida.

Shuert, P.G. and Walsh, J.J., 1990. A coupled physical/biological model of the Bering/Chukchi Seas. Cont. Shelf Res. (submitted).

Spaulding, M.T. Isaji, Mendelsohn, D. and Turner, A.C., 1987. Numerical simulation of the wind driven flow through the Bering Strait. J. Phys. Oceanogr., 17: 1799–1816.

Steele, J.H., 1962. Environmental control of photosynthesis in the sea. Limn. Oceanogr., 7: 137–150.

Stigebrandt, A., 1984. The North Pacific: A global scale estuary. J. Phys. Oceanogr., 14: 464–470.

Toulany, B. and Garrett, C., 1984. Geostrophic control of fluctuating barotropic flow through straits. J. Phys. Oceanogr., 14: 649–655.

Vidal, J. and Smith, S.L., 1986. Biomass, growth and development of populations of herbivorous zooplankton in the southeastern Bering Sea during summer. Deep-Sea Res., 33: 523–556.

Walsh, J.J., 1975. A spatial simulation model of the Peru upwelling ecosystem. Deep-Sea Res., 22: 201–236.

Walsh, J.J., 1988. On The Nature of Continental Shelves. Academic Press, New York, 520 pp.

Walsh, J.J. and Dieterle, D.A., 1986. Simulation analysis of plankton dynamics in the northern Bering Sea. In: J.J. Nihoul (Editor), Marine Interfaces, Ecohydrodynamics. Elsevier, Amsterdam, pp. 401–428.

Walsh, J.J., McRoy, C.P., Coachman, L.K., Goering, J.J., Nihoul, J.J., Whitledge, T.E., Blackburn, T.H., Parker, P.L >., Wirick, C.D., Shuert, P.G., Grebmeier, J.M., Springer, A.M., Tripp, R.D., Hansell, D., Djenidi, S., Deleersnijder, E., Henriksen, K., Lund, B.A., Anderson, P., Mulller-Karger, F.E. and Dean, K., 1989. Carbon and nitrogen cycling within the Bering/Chukchi Seas: source regions for organic matter effecting AOU demands of the Arctic Ocean. Prog. Oceanogr., 22: 279–361.

DISCLAIMER NOTICE

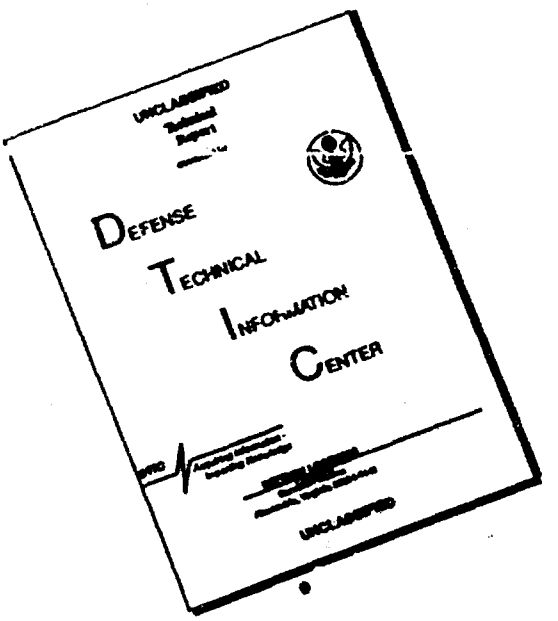

THIS DOCUMENT IS BEST QUALITY AVAILABLE. THE COPY FURNISHED TO DTIC CONTAINED A SIGNIFICANT NUMBER OF PAGES WHICH DO NOT REPRODUCE LEGIBLY.